UNIVERSITY OF CALIFORNIA,

IRVINE

Development of novel tissue engineering strategies toward the translation of articular cartilage implants

DISSERTATION

Submitted in partial satisfaction of the requirements for the degree of

DOCTOR OF PHILOSOPHY

in Biomedical Engineering

by

Gaston Andres Otarola Pezzani

Dissertation Committee:
Distinguished Professor Kyriacos A. Athanasiou, Chair
Professor Wendy F. Liu
Program Manager Jerry C. Hu

2022

To my family, my team at home.

TABLE OF CONTENTS

Acknowledgements

My time in graduate school has been everything I expected, and so much more. For that, I am grateful, and there is little I can do to express my gratitude to those who have shaped these past years. I sincerely appreciate and acknowledge the institutions that made this work possible. I thank the National Institute of Arthritis and Musculoskeletal and Skin Diseases. I also thank Becas Chile and the Fulbright program for supporting me throughout the execution of my doctoral studies. Likewise, I thank the University of California, Irvine for opening the doors to an unquantifiable number of opportunities. None of this would have been possible without their initial support and belief in me as a researcher. Chapters 2, 3, and 5 were published in the journals Tissue Engineering Part C, Journal of the Royal Society Interface, and Tissue Engineering Part A, respectively, and the Appendix was published in The American Journal of Sports Medicine. All of these journals permit republication of articles in dissertations.

I would like to thank Dr. Kyriacos Athanasiou. It is not often you get to work with one of the leaders and most recognized researchers of a given field; it is less often that person is there each day for every question, leading by example. Since our first conversation, I have felt his unconditional support, and many, many days later, he continues to do his absolute best in teaching me, no matter how many times I test his patience. Dr. Athanasiou's mentorship on critical thinking, the quality of one's work, and life are some of the most valuable teachings I have obtained from my time at UC Irvine. Gracias.

I would also like to thank my DELTAi mentors, Dr. Jerry Hu, Dr. Wendy Brown, and Dr. Heenam Kwon. Out of all the people who have accompanied me during the execution of my research, Dr. Hu is probably the one who has helped me the most during my struggles, and his guidance and advice are a fundamental part of this dissertation. Dr. Brown and Dr. Kwon have become an unlimited source of support and kindness, and I truly appreciate their dedication and

drive toward being outstanding researchers. Unknowingly, their work lifts the quality of the research of everyone around them on a daily basis.

To all the lab members of DELTAi, current and past: Trying to achieve excellence has never felt more in company. I enjoyed every second of my work with Dr. Jarret Link, Dr. Evelia Salinas, Dr. Erik Gonzalez-Leon, Dr. Ryan Donahue, Dr. Ben Bielajew, Dr. Rachel Nordberg, Dr. Gabriela Espinosa, and Dr. Nathan Castro, all of whom have directly or indirectly contributed to the findings shown here. More importantly, doing it all with a smile and sharing a laugh goes a long way, and I hope to find such an outstanding team wherever I go in the future.

My wife, Macarena Munoz Rosenberg, has been a pivotal part of my work, and it is my certainty that she deserves the doctoral distinction as much as I do. I cannot put in words how much of her I see in my work, and the team we've formed together is, to date, my biggest and proudest accomplishment.

My family, especially my mother, Paola Pezzani Schlack, and my father, Gaston Otarola Escudero, I thank for teaching me to be and do good, to look beyond, and to follow my dreams with passion. I also thank them for providing me with all the tools and preparation I needed to do it with confidence and purpose. The efforts they have made are forged into me forever.

To all my friends, the old ones and the new ones: The help you've provided is unquestionable. In particular, I would like to thank Juan Rubio and Elizabeth Clark Rubio, the first friends we made abroad, and without whom this story would be completely different; Shannon Bae, Jinwoo Bae, Joonseo Bae, and Jia Bae, who have extended their arms and received my wife and myself as one of them so that we would never feel alone; and Michael Einbund, Robin Einbund, and their gang, who will forever underestimate the value of their friendship.

Lastly, I acknowledge the good fortune I have had during the past years, which has led me to meet some of the most fantastic people in the world. The new friends I have made and the lessons learned continue to shape me and challenge me to do my best, inside and outside the lab.

Vita

Education

2022, Ph.D. in Biomedical Engineering, University of California, Irvine
2020, M.S. in Biomedical Engineering, University of California, Irvine
2014, M.S. in Biochemistry and Bioinformatics, Universidad de Concepción, Concepción, Chile
2012, B.S. in Bioengineering, Universidad de Concepción, Concepción, Chile

Appointments

September 2017 to May 2022, Graduate Student Researcher, Driving Engineering and Life-science Translational Advances at Irvine (DELTAi), University of California, Irvine, Advisor: Kyriacos Athanasiou

Field of Study

Biomedical Engineering

Publications

Espinosa, M.G.,* **Otarola, G.A.,*** Hu, J.C., Athanasiou, K.A. Cartilage assessment requires a surface characterization protocol: roughness, friction, and function. Tissue Engineering Part C; 27(4): 276-286. (*These authors contributed equally.)

Espinosa, M.G., **Otarola, G.A**., Hu, J.C., Athanasiou, K.A. Vibrometry as a noncontact alternative to dynamic and viscoelastic mechanical testing in cartilage. Journal of the Royal Society Interface 2021; 18: 20210765

Otarola, G.A., Hu, J.C., Athanasiou, K.A. Intracellular calcium and sodium modulation of self-assembled neocartilage using costal chondrocytes. Tissue Engineering Part A; 27(4): 276-286.

Oyadomari, S., Brown, W.E., Kwon, H., **Otarola, G.A**., Athanasiou, K.A., Wang, D. *In Vitro* Effects of Bupivacaine on the Viability and Mechanics of Native and Engineered Cartilage Grafts. The American Journal of Sports Medicine 2021; 49(5): 1305-1312

(Submitted): Nordberg, R.C.,* **Otarola, G.A.,*** Wang, D., Hu, J.C., Athanasiou, K.A. Translation of biologic cartilage repair products: From bench to barriers to breakthroughs. Submitted to Science Translational Medicine. (*These authors contributed equally.)

(Submitted): Salinas, E.Y.,* **Otarola, G.A.,*** Kwon, H., Wang, D., Hu, J.C., Athanasiou, K.A. Topographical characterization of the young, healthy human femoral medial condyle. Submitted to Osteoarthritis and Cartilage. (* These authors contributed equally.)

(Submitted): **Otarola, G.A**., Hu, J.C., Athanasiou, K.A. Ion modulatory treatments toward functional self-assembled neocartilage. Submitted to Acta Biomaterialia.

(In preparation for submission): **Otarola, G.A**., Kwon, H., Hu, J.C., Athanasiou, K.A. Engineering thicker scaffold-free neocartilage constructs with biomimetic properties using sequential seeding and deferoxamine.

Abstract of the Dissertation

Development of novel tissue engineering strategies toward the translation of articular cartilage implants

by

Gaston Andres Otarola Pezzani

Doctor of Philosophy in Biomedical Engineering

University of California, Irvine, 2022

Distinguished Professor Kyriacos Athanasiou, Chair

Articular cartilage diseases in the knee, initiated by age-related degenerative processes or trauma, compromise the material properties of the tissue and the function of the joint. Osteoarthritis, the most common cartilage disease, affects over 30 million people in the United States alone. Depending on the level of damage to the cartilage and/or the underlying bone, the symptoms can range from stiffness, pain, and swelling, to loss of function and disability. Current treatments aimed at treating cartilage diseases do not provide satisfactory outcomes. Osteochondral allografts are scarce, and autografts, aside from the risk of donor site morbidity, often present a mismatch to the articular surface of the recipient location. Other alternatives, including microfracture and MACI, fail to regenerate the tissue, and induce the formation of a mechanically inferior fibrocartilage repair tissue. As a result, patients eventually require revision surgeries or alternative treatments, such as synthetic implants, in as little as 5-10 years. Tissue engineering, capable of generating neocartilage constructs with properties akin to the native tissue, has emerged as a promising alternative to treating cartilage diseases. However, tissue engineering methodologies must be optimized so as to become clinically viable options; current

technologies used to generate biomimetic neocartilage constructs 1) fail to recapitulate the properties of the native tissue, 2) jeopardize the translational potential of neocartilage constructs due to high cost, low reproducibility, and high technical complexity, and 3) do not produce neotissues akin to native tissue thickness. Toward overcoming these limitations, the global objectives of this work were 1) to provide a thorough assessment of the properties of native articular cartilage to inform tissue-engineering efforts, 2) to enhance the mechanical properties of neocartilage toward native tissue levels utilizing a repeatable and cost-effective ion modulation strategy, and 3) to develop a methodology to increase the thickness of neocartilage constructs.

Toward assessing the properties of articular cartilage and providing an accurate set of data, this work first characterized the effects of storage time and temperature on the mechanical properties of juvenile bovine cartilage, a facsimile of a cartilage implant. In addition, an extensive assessment of the surface properties of cartilage was performed using conventional and novel methodologies, including non-contact vibrometry. Non-contact vibrometry was further developed as a new non-destructive measurement of the dynamic and viscoelastic mechanical properties of cartilage samples. Finally, the human medial femoral condyle, one of the knee compartments with the highest incidence of chondral degeneration, from young, healthy donors was topographically characterized using biochemical and biomechanical assays. It was determined that the articular cartilage of the human medial femoral condyle displays regional variations in the tensile and mechanical properties which may have repercussions on the injury patterns observed in the clinic; the Young's modulus, ultimate tensile strength, aggregate modulus, and shear modulus in the posterior region were 1.0-fold, 2.8-fold, 1.1-fold, and 1.0-fold less than the values in the anterior region, respectively. As opposed to other tissues and species, including bovine cartilage, the coefficient of friction in human samples does not present regional variations, ranging 0.22-0.26 throughout the condyle, and is isotropic. It was also determined that particular storage conditions can affect the properties of cartilage tissues, and that vibrometry-based viscoelastic properties not only correlate to biochemical content, but also significantly correlate with moduli from stress

relaxation and creep tests, with correlation strengths reaching up to 0.78. These findings are significant, as they not only establish a working framework for stored cartilage tissues and new non-contact testing methodologies, but also provide much needed design criteria. Moreover, the findings suggest that lower mechanical properties may predispose the tissue to chondral injuries, and propose new structure-function relationships, highlighting the importance of collagen crosslinks for the mechanical properties of cartilage.

Taking into consideration the values obtained for human articular cartilage tissues, new methods to improve the mechanical properties of neocartilage constructs were developed. Mechanotransduction and hypoxia, two well-known stimuli that promote chondrogenesis, have been used to produce neocartilage constructs. However, both stimuli require the use of bioreactors that confound production of neocartilage, increasing the costs and complexity of the process. Modulation of ions, a cost-effective pharmacological methodology of mimicking mechanotransduction and hypoxia, was examined toward improving the material properties of neocartilage. It was determined that ionomycin, a calcium ionophore, caused a 61% and 115% increase in glycosaminoglycan and pyridinoline crosslink content, which translated to a 45% increase in the aggregate modulus and a 63% increase in the tensile Young's modulus, respectively. Similarly, deferoxamine, an iron chelator, produced an 87% increase in pyridinoline crosslinks, and a 57% and 112% increases in the Young's modulus and the ultimate tensile strength (UTS) of neocartilage constructs, respectively. Importantly, the combined use of both ion modulators resulted in significant increases of 150% and 176% in the Young's modulus and UTS of neocartilage constructs, respectively. Ionomycin and deferoxamine can be used as analogs of mechanical and hypoxic stimuli, bypassing the need for bioreactors. The use of both analogs resulted in neocartilage constructs with a Young's modulus of 11.76±3.29 MPa and UTS of 4.20±1.24 MPa, the highest reported by our group thus far.

While the self-assembling process has been optimized to produce neocartilage constructs with biochemical and biomechanical properties on par to native tissue, it has been limited in its

capability to grow tissues with biomimetic thickness. The existing neocartilage constructs are several times thinner compared to the average condylar cartilage, and thus, limit its therapeutic potential. Superficial irregularities between the native tissue and the repair tissue compromise the treatment outcome; disparities induce stress concentration, delamination of the native tissue, and dislodging of the implant. Because of this, a new self-assembling methodology, using sequential seeding and deferoxamine stimulation, was developed in this work to generate constructs with increased thickness. The new methodology utilizes sequential seeding, and expanded and rejuvenated chondrocytes previously stimulated with deferoxamine. An appropriate time between separate seeding events and deferoxamine stimulation prior to the self-assembling process was determined. Constructs derived from human articular chondrocytes, the current cell type used by cell-based treatment strategies, resulted in neocartilage with a 90% increase in thickness, an 8% increase in diameter, a 33% and a 41% increase in aggregate and shear moduli, and the maintenance of the tensile properties, compared to the control group. This is the first successful attempt to produce thicker biomimetic self-assembled tissues without a tradeoff in the mechanical properties. This work demonstrates the potential of tissue-engineered neocartilage implants for the surgical treatment of cartilage diseases, and altogether, the findings of this work provide new scalable tissue-engineering strategies toward developing clinically relevant neocartilage constructs.

Introduction

Hyaline articular cartilage, the tissue found at the end of long bones, possesses mechanical properties that allow it to decrease the contact stresses in the joint and to minimize friction and wear among opposing surfaces. The function of articular cartilage, an avascular, aneural, and hypocellular tissue, is largely enabled by its unique biochemical composition; approximately 80% of its wet weight corresponds to water. Of the remaining 20%, ~60% of the dry weight corresponds to various collagens, primarily collagen type II, ~20% to proteoglycans and sulfated glycosaminoglycans, and the rest to minor proteins and chondrocytes. The resulting structure is an organized network made of crosslinked collagen fibers intertwined with negatively charged proteoglycans. Due to the charged structure, water molecules saturate the matrix, making the articular cartilage a biphasic medium: 1) a porous, permeable solid phase (the extracellular matrix) and 2) a fluid phase (water and ions). The interplay of fluid with the extracellular matrix, together with the organization of collagen fibers, among others, confers cartilage with its compressive and tensile properties.

Degradation of the articular cartilage in the knee, initiated by trauma or age-related degenerative processes, compromises the material properties of the tissue and the function of the joint. The knee cartilage can withstand cyclic loads with little to no damage. However, damage of the tissue tends to be irreversible. While the residing chondrocytes are responsible for the maintenance of the mature tissue, the tightly packed extracellular matrix, the encasement of the existing chondrocytes, and the lack of vascularization results in a tissue with virtually no turnover, and, thus, no intrinsic regeneration. Moreover, the disruption of the metabolic activity of chondrocytes can dysregulate catabolic and anabolic processes, further promoting cartilage breakdown. Osteoarthritis, the most common cartilage ailment, affects over 30 million people in the United States alone. Depending on the level of damage to the cartilage and/or the underlying bone, the symptoms range from stiffness, pain, and swelling, to loss of function and disability.

Because of the aging population and the worldwide increase in body mass, among others, it is expected that the number of people suffering from osteoarthritis will increase in the near future.

Current treatments aimed at treating cartilage diseases are limited in their capabilities and often fail to provide long-term restoration. For example, the use of osteochondral allografts provides a replacement tissue with appropriate properties, but donor tissues are scarce. Mosaicplasty, which uses autologous grafts, is associated with donor site morbidity and difficulties matching the donor tissue surface to the recipient location surface. Other alternatives, such as microfracture and matrix-induced autologous chondrocyte implantation (MACI) induce tissue repair by exploiting the healing capabilities of the subchondral bone. However, both techniques are associated with the formation of a mechanically inferior fibrocartilage repair tissue, which, compared to the hyaline articular cartilage, is prone to degeneration. In most cases, patients with cartilage degenerative diseases will eventually require a total joint replacement, which can last about 10 to 20 years. This is significant, as the number of joint-replacement surgeries has gone up among the younger population, and younger patients will most likely require a revision surgery within their lifetime. Given the impact of articular cartilage's inability to heal and the limited alternatives available in the clinic, new strategies that provide long-term restoration are needed.

Tissue engineering has emerged as a promising alternative to treating cartilage diseases. While MACI is the only cell-based tissue-engineered product approved by the Food and Drug Administration (FDA), over 10 other products are in development and going through the FDA pipeline. The majority of these products employ autologous chondrocytes, meaning they will require two surgeries, include one to three passages for cell expansion, and use some type of scaffold on which the cells are seeded. Novocart 3D, Chondrosphere, and Cartipatch, to name a few, have gone onto phase III clinical trials to determine safety and efficacy. One particular strategy that has yet to go into clinical trials is the self-assembling process, which resembles the developmental formation of cartilage formation during condensation. This scaffold-free strategy uses high-density culture within non-adherent agarose wells to form neotissues through energy

minimization, forcing cells to interact with each other and produce extracellular matrix. The resulting tissue is a hyaline-like implant. With the use of bioactive factors (e.g., transforming growth factor-beta 1 (TGF-β1), lysyl oxidase like 2 (LOXL2)) and exogenous stimuli (e.g., fluid shear, tension, hypoxia), neocartilage has been shown to achieve near native tissue properties. Despite many potential cartilage therapeutic products failing and becoming a part of the translational "valley of death," tissue engineering technologies hold promise to provide well-characterized, of-the-shelf cartilage implants on demand, with known material properties and effects, capable of restoring articular cartilage.

While on the brink of clinical translation, tissue engineered products, including self-assembled neocartilage, have certain limitations. Most cell-based strategies are limited in cell number, as chondrocytes are not abundant in the native tissue and expansion induces their dedifferentiation. The self-assembling process uses extensive expansion and aggregate rejuvenation to recapitulate the chondrogenic phenotype before seeding constructs, ensuring that the cells produce an adequate extracellular matrix (e.g., expression of collagen type II and aggrecan, no expression of collagen type I). However, the material properties of neocartilage are below native tissue values. Moreover, many of the techniques employed to improve the mechanical properties of neocartilage constructs involve the use of bioreactors that can affect reproducibility, induce user errors (e.g., contamination), and increase production cost. In addition, many cell-based products, including neocartilage generated through the self-assembling process, result in the formation of tissues that are several times thinner compared to the native cartilage, which is at least 1mm thick in the human knee. Superficial irregularities between the native tissue and the repair tissue compromise the outcome; these can induce stress concentration, delamination of the native tissue, and dislodging of the implant. Thus, work must be done to develop new tissue-engineering methodologies to improve the mechanical properties and the thickness of neocartilage constructs. When considering the translation potential and the overall production of neocartilage implants, these limitations, which involve the mechanical properties of

neocartilage and its thickness measurements, may be addressed by developing new methodologies around the self-assembling process.

Considering the desire for the translation of clinically apt tissue-engineered implants, this work aimed at developing new tissue-engineering strategies to improve the functionality of neocartilage constructs. The global objectives of this work were 1) to provide a thorough assessment of the properties of native articular cartilage to inform tissue-engineering efforts, 2) to enhance the mechanical properties of neocartilage toward native tissue levels utilizing a repeatable and cost-effective ion modulation strategy, and 3) to develop a methodology to increase the thickness of neocartilage constructs. Toward these objectives, three specific aims were investigated:

Specific Aim 1: To determine design criteria and structure-function relationships of native articular cartilage for cartilage engineering efforts. Considering the dearth of information on young, healthy human articular cartilage, this aim sought to determine various tissue properties of the medial femoral condyle from fresh, viable osteochondral allografts. These properties included histological, biochemical, tribological, tensile, and compressive data. Additionally, experiments were performed to characterize cartilage surface topography and tribology, the effects of different storage conditions, and the development of non-contact, non-destructive dynamic mechanical measurements. It was hypothesized that the lowest mechanical properties would be found in the posterior region of the medial condyle, and that tissue composition would correspond to the established structure-function relationships of cartilage. It was also hypothesized that under proper storage the properties of cartilage, including surface properties, would not be affected, and that viscoelastic properties obtained from a novel non-contact, non-destructive vibrometry-based assessment of the mechanical properties would effectively correlate with moduli, derived from stress relaxation and creep tests, providing a new method to quantify dynamic mechanical properties of cartilage.

Specific Aim 2: To improve the mechanical properties of engineered neocartilage by identifying an ion modulation regime with mechanical and hypoxic analogs. Toward addressing the need for improved mechanical properties and the cost and complexity of the strategies used to optimize the properties, this aim first examined three modulators of calcium or sodium, 1) 4α-phorbol-12,13-didecanoate (4-αPDD), an agonist of the Ca^{2+}-permeable transient receptor potential vanilloid 4 (TRPV4), 2) ouabain, an inhibitor of the Na^{+}/K^{+} pump, and 3) ionomycin, a Ca^{2+} ionophore, to enhance the maturation and mechanical properties of neocartilage constructs. In addition, the iron modulator deferoxamine, along with the glucose oxidase/catalase system, were also investigated to enhance the maturation and mechanical properties of neocartilage constructs. It was hypothesized that the ion modulators, alone or in combination, would induce a mechanotransduction-like or a hypoxia-like response that would modify the biochemical content of the neotissues, resulting in an improvement of the mechanical properties and overall superior tensile properties compared to prior literature.

Specific Aim 3: To engineer thicker neocartilage toward clinical translation. The development of a new self-assembly approach was examined, using sequential seeding. In three separate phases, the appropriate time between seeding events, the effects of deferoxamine stimulation before self-assembly, and the use of sequential seeding with deferoxamine stimulation in extensively passaged human articular chondrocytes were examined. It was hypothesized that a proper time between the two seeding events and the stimulation of chondrocytes with deferoxamine before cell seeding would result in human neocartilage constructs with increased thickness, desirable gross morphology (comparable to the control group), and mechanical properties equivalent to those of control constructs.

The three aims have been completed fully, and this dissertation describes the work toward their fulfillment. All seven chapters in the main body of this dissertation, together with the appendix, represent eight full-sized scientific publications currently published (Chapters 2, 3, 5, and Appendix A), submitted (Chapters 1, 4, 6), or to be submitted (Chapter 7).

Toward achieving Aim 1, Chapter 1 first provides a description of the process of conducting preclinical research on cell therapy products for cartilage repair and identifies the bottlenecks that must be addressed to successfully bridge the gap between basic science and clinical research. Chapters 2 and 3 then lay the foundations of working with articular cartilage grafts specimens and assess the mechanical properties focusing on surface measurements and non-contact methodologies; Chapter 2 assessed the effects of storage time and temperature on the mechanical properties of cartilage, while simultaneously characterizing the surface properties. Tribology was used to determine the coefficient of friction, and interferometry, a non-contact and non-destructive methodology, was used to determine the topography and roughness; Chapter 3 expands on non-contact measurements and utilized vibrometry to obtain viscoelastic properties significantly correlated with moduli from stress relaxation and creep tests through the resonant frequencies and bending modes, all in a fast, novel, non-destructive methodology. Finally, Chapter 4 performed a topographical characterization of the medial femoral condyle from young, healthy human specimens obtained from viable allograft specimens. This chapter not only provides design criteria for tissue-engineered implants, but also informs of new possible structure-function relationships in articular cartilage that highlight the importance of pyridinoline crosslinks to the tensile and compressive properties, and associates the lower mechanical properties of the posterior medial condyle to the predisposition of the same region to injury. The data and information compiled in Chapters 1 to 4 were used in the rest of this work so as to procure, store, test, and evaluate outcomes in the most accurate fashion.

Chapter 5 and 6 address Aim 2 by describing the development of new methodologies to improve the mechanical properties of neocartilage constructs using low-cost exogenous agents with high reproducibility and efficacy without added complexity and costs of bioreactors. Chapter 5 employed three ion modulators, 1) 4α-phorbol-12,13-didecanoate (4-αPDD), an agonist of the Ca^{2+}-permeable transient receptor potential vanilloid 4 (TRPV4), 2) ouabain, an inhibitor of the Na^{+}/K^{+} pump, and 3) ionomycin, a Ca^{2+} ionophore, as analogs of mechanical stimuli by inducing

a mechanotransduction-like response. Chapter 6 first employed deferoxamine, an iron chelator, as an analog of hypoxia. Then, it combined ionomycin-mediated calcium modulation and deferoxamine-mediated iron modulation to improve tissue maturation. From these works it was determined that ion modulation produced an increase in pyridinoline crosslinks, which was correlated to increases in the tensile properties of neocartilage. More importantly, the neotissues treated with the both ion modulators were shown to possess the highest Young's modulus and UTS thus far for self-assembled neocartilage, on par with human native tissue.

Finally, to address Aim 3, Chapter 7 established a new methodology to obtain thicker neocartilage constructs by performing self-assembly using a sequential seeding approach. In a three-phase study, the appropriate time and stimulation regime with DFO were defined. Phase I compared four different seeding times, between 1 and 4 hours, and concluded that using a 2-hour time between the first and second seeding enabled the development of constructs, derived from minipig costal chondrocytes, with a desirable gross morphology, similar to that of the control group constructs. To increase the thickness of the constructs, Phase II examined the effects of stimulating minipig costal chondrocytes with deferoxamine during aggregate rejuvenation, 24 hours before construct seeding. It was found that deferoxamine stimulation, alone and with sequential seeding, results in thicker constructs when doubling the cell number. The combined use of deferoxamine stimulation and sequential seeding, however, results in constructs with most desirable gross morphology and appropriate mechanical properties, compared to the control group. In Phase III, sequential seeding and deferoxamine stimulation were employed to produce neocartilage derived from extensively passaged (passage 7) human articular chondrocytes. It was shown that the combined treatment results in tissues with a 90% in thickness, which maintained both a desirable gross morphology toward translation and biomimetic properties.

Additional work not belonging to the main objectives of this dissertation and completed in collaboration with colleagues is included in the appendix. Appendix A provides a study on the short-term effects of bupivacaine, a local anesthetic commonly used in orthopaedic surgeries, on

the viability, biochemical properties, and mechanical properties of articular cartilage and neocartilage constructs. It was determined that a single bupivacaine exposure was chondrotoxic to both explants and neocartilage, with 0.5% bupivacaine causing a significant decrease in chondrocyte viability compared to controls. While the exposure had no significant effect on matrix content for either tissue type, the presence of abundant extracellular matrix does not appear to confer any additional resistance to the toxic effects of bupivacaine. For neocartilage constructs, there was significant weakening of the mechanical properties compared to control

In conclusion, the outcome of this work represents an important step toward the production of tissue-engineered neocartilage to treat articular cartilage defects. The new methodologies described in this work focused on using low-cost exogenous agents and reproducible techniques that can easily be scaled-up for translation in order to produce engineered tissues efficiently. Moreover, this work considered key factors in the production of neocartilage, including the model (minipig and human neocartilage), cell source (articular cartilage and costal cartilage), and cell expansion (low passage and high passage), toward the future execution of preclinical and clinical studies, FDA approval, and medical use self-assembled neocartilage implants.

CHAPTER 1: Translation of biologic cartilage repair products: From bench to barriers to breakthroughs

Abstract

Despite advances in cartilage tissue engineering, long-term clinical repair of articular cartilage remains elusive. In the past decade, only a single cartilage repair therapy classified as a "cellular and gene therapy product" has obtained FDA approval (i.e., matrix-assisted autologous chondrocyte implantation (MACI)). While multiple new strategies for cell-based cartilage repair are currently in development in laboratories around the world, translation of these technologies is impeded by challenges with 1) navigating regulatory pathways, 2) designing *in vitro* studies that support *in vivo* success, 3) selecting an appropriate animal model, 4) adapting surgical and rehabilitation strategies to animal models, and 5) determining what *in vivo* data are required to support an application to conduct clinical trials. Due to these challenges, over 200 large animal cartilage repair studies have been published and yet only one cell therapy product for cartilage repair is clinically available. Understanding the barriers to translation and developing novel solutions to address them will be critical for advancing cell therapy products for cartilage repair to clinical use.

Introduction

Despite major advances in cell and tissue research in recent decades, to date, the Food and Drug Administration (FDA) has only approved 22 cellular and gene therapy products (1). While the Agency provides guidance documents toward developing cell therapy products (2, 3), interpreting such documents can be difficult given the lack of predicate therapies. When researchers seek to obtain regulatory approval for a product, they must navigate guidance documents that apply to a

Chapter submitted as: Nordberg, R.C.,* Otarola, G.A.,* Wang, D., Hu, J.C., Athanasiou, K.A. Translation of biologic cartilage repair products: From bench to barriers to breakthroughs. Submitted to Science Translational Medicine. (*These authors contributed equally.)

broad spectrum of therapies, determine what is applicable for their specific product, and design preclinical studies to support an application for clinical trials. This task can be daunting to researchers without a regulatory background. The objective of this review is to discuss the main bottlenecks that hinder the translation of cell therapy products from basic research to clinical trials, with a specific focus on the regulatory guidance for cartilage repair therapies.

In the early 1990s when the term tissue engineering came to denote the fabrication of tissues using cells, scaffolds, and bioactive signals, it was predicted that cartilage would be one of the first tissues to be successfully regenerated (4). Twenty years later, we published a review highlighting the many challenges of regenerating cartilage despite these predictions (5). Today, nearly three decades later, only one cellular and gene therapy product is approved for cartilage repair (matrix-induced chondrocyte implantation, MACI, Vericel Corp) despite a wealth of basic science research within the field of cartilage repair and the clear clinical need for additional treatments.

Hyaline articular cartilage is a highly specialized connective tissue that facilitates joint movement by providing lubrication between bones, reducing friction, distributing forces, and preventing wear within the articulation (6). It is composed of water (70-80%), collagen type II (~20%), proteoglycans (~5%), chondrocytes (~2%), and trace amounts of minor collagen subtypes (7, 8). Articular cartilage is susceptible to injury and osteoarthritis (OA); in the United States alone, approximately 78 million adults will be diagnosed with arthritis by 2040 (9). Current treatment options for early-stage articular cartilage defects and OA include allografts, autografts, microfracture, and MACI. The use of cartilage allografts and autografts is restricted by tissue scarcity and donor-site morbidity, respectively (10–12). Microfracture induces fibrocartilage repair tissue with inadequate mechanical properties and a propensity to degenerate (13, 14). MACI, a therapy that uses expanded autologous chondrocytes seeded on a porcine collagen type I and III membrane, is limited in that it requires two surgeries and may cause donor-site morbidity (15–

18). Because these treatment options are not ideal, the development and translation of new strategies to treat cartilage ailments would have a significant impact on public health.

In this review, we will give context and perspective on the main barriers to clinical translation of articular cartilage repair products, as overviewed in Figure 1. First, the regulatory structure of the FDA in the context of cartilage repair products will be presented, followed by a description of *in vitro* evaluations to conduct before proceeding with animal studies. Next, large animal models for cartilage repair studies will be discussed, including species-specific advantages and disadvantages, key considerations for the surgical approach in these animal models, and *in vivo* experimental designs. Finally, we will provide perspective on the challenges that the field faces and steps that may be taken to increase the chances of future translation of cartilage repair products.

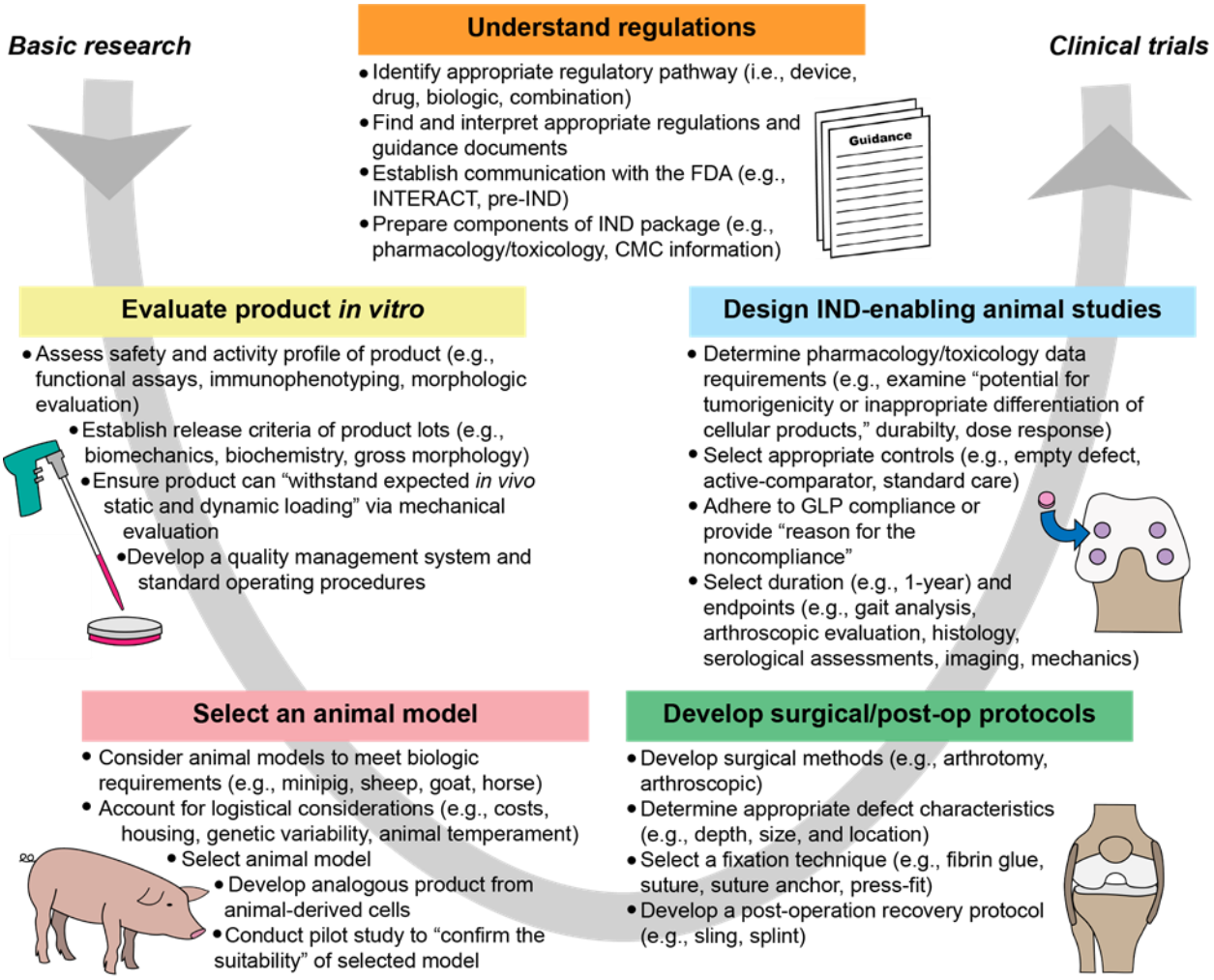

Figure 1. Bottlenecks in translating biologic cartilage repair products from basic research to clinical trials. Researchers must navigate the many challenges within this process at the stages of *in vitro* research, animal model selection, surgical development, and the conduct of IND-enabling animal studies. All stages should be conducted in accordance with appropriate regulations and guidance. This figure captures the salient aspects of this process, but for additional information guidance documents should be consulted. All quotations within this figure were taken from guidance documents (2, 3). Abbreviations: INitial Targeted Engagement for Regulatory Advice on CBER producTs (INTERACT), Chemistry, Manufacturing, and Controls (CMC), Good Laboratory Practice (GLP), Investigational New Drug (IND).

FDA regulation of cartilage repair products

FDA structure. In the United States, the FDA regulates all medical products including cartilage-repair products. Three of the FDA's centers are particularly relevant for cartilage products: the Center for Biologics Evaluation and Research (CBER), the Center for Drug Evaluation and Research (CDER), and the Center for Devices and Radiological Health (CDRH) (19). Products classified as a biologic, drug, or device will be assigned to CBER, CDER, and CDRH, respectively. If assigned to CDRH, the product will also be subject to device classifications (i.e., Class I, II, and III) that depend on the risk the device poses to the patient (20). Products may be combination products (e.g., biologic and device) in which case the primary mechanism of action will be used by the Office of Combination Products to determine assignment to a center with primary jurisdiction. Each center has a different set of applications that must be completed to obtain approval for clinical studies and commercialization, as depicted in Figure 2A. For example, a product classified as a biologic will be regulated by CBER and will require an Investigational New Drug (IND) application before clinical studies and a Biologics License Application (BLA) before market approval.

Meetings with the FDA are held at specific times along the regulatory pathway. Optional informal meetings are offered by each center, e.g., INitial Targeted Engagement for Regulatory Advice on CBER producTs (INTERACT) for CBER, to obtain initial guidance during development. The first formal meeting within the CBER and CDER pathways is the pre-IND meeting. Other key meetings within the regulatory process are depicted in Figure 2A. There are several expedited programs that can be considered when applying for biologic or drug approval: Fast Track designation, Breakthrough Therapy designation, regenerative medicine advance therapy (RMAT) designation, priority review, and accelerated review (Table 1) (21). While each expedited program has specific criteria for acceptance and varying benefits, these programs, overall, are intended to reduce the time to market and may allow for more directed guidance from the agency. Navigating the regulatory process for cellular and gene therapy products may be challenging because the

research on these products is rapidly evolving and there has been little historical precedent on this matter.

Summary of approved cellular and gene therapy products. To date, the FDA has approved 22 cellular and gene therapy products (1). Of these products, eight are allogeneic cord blood cell therapy products, six are T-cell therapy products, and three are viral therapies. Other products include Laviv (autologous fibroblasts to reduce the appearance of nasaloabial folds), Rethymic (human allogeneic thymus tissue to treat congenital athymia), Gintuit (allogeneic cultured keratinocytes and fibroblasts for treatment of mucogingival conditions), Stratagraft (allogeneic cultured keratinocytes and dermal fibroblasts for treatment of deep partial-thickness burns), and MACI. Table 2A provides details on each product and the preclinical studies performed for each product as found within their FDA documentation (note cord blood cell therapies were excluded).

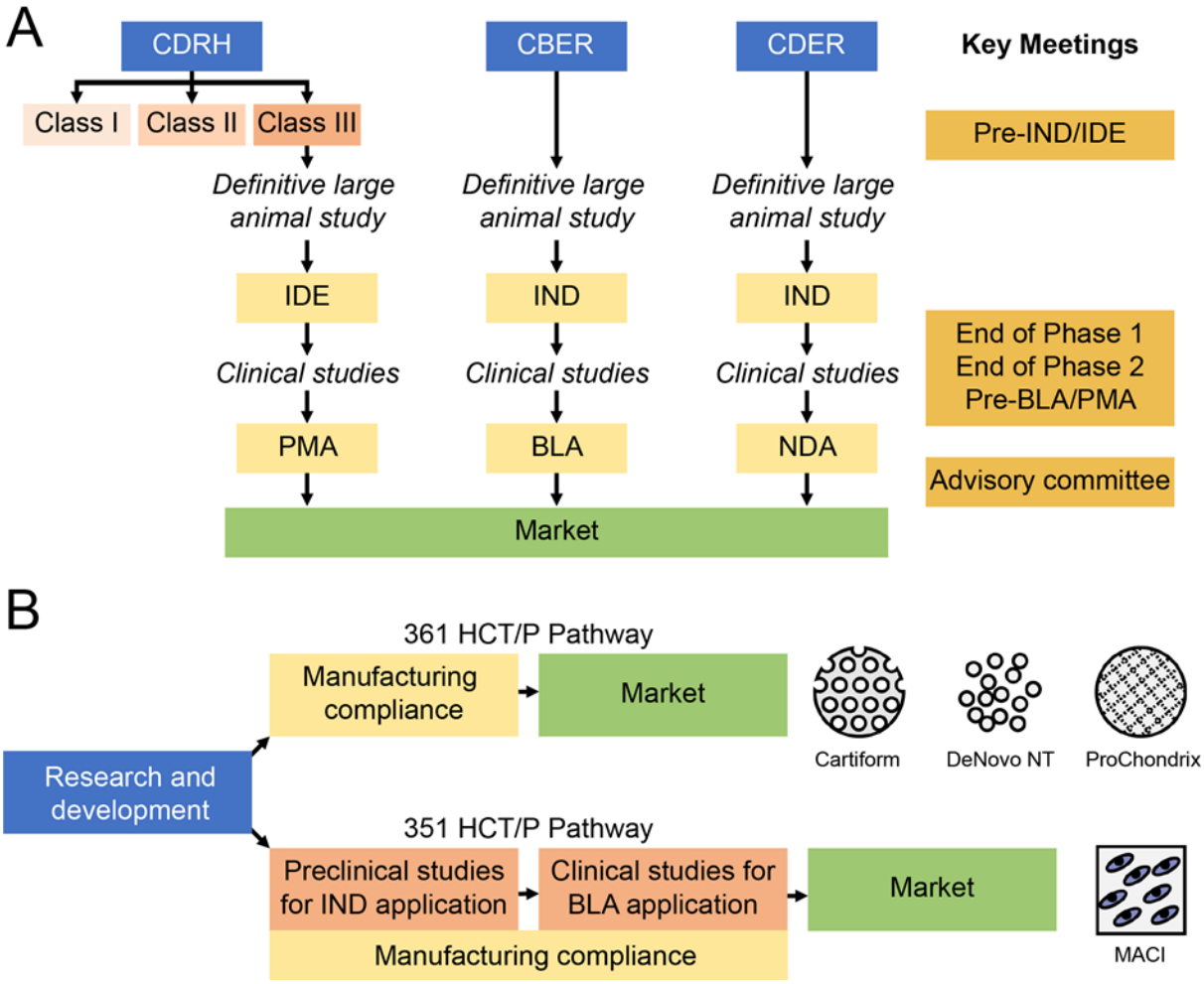

Figure 2. FDA organizational structure as it relates to biologic cartilage repair products. **A**. The sequence of studies, applications, and meetings that products proceeding through Center for Biologics Evaluation and Research (CBER), the Center for Drug Evaluation and Research (CDER), and the Center for Devices and Radiological Health (CDRH) regulatory pathways must follow. Before clinical trials, an Investigational New Drug (IND) application or Investigational Device Exemption (IDE) application must be filed. Upon completion of clinical trials and before marketing a Premarket Approval (PMA), Biologics License Application (BLA), or New Drug Application (NDA) must be filed. **B**. The two pathways of human cell, tissue, and cellular and tissue-based product (HCT/P) approval and cartilage repair products that have utilized these mechanisms.

Table 1. Expedited programs that are offered by the FDA for products classified as biologics

Program	Requirements	Benefits
Fast Track designation	1) Treats a serious or life-threatening condition 2) Addresses an unmet clinical need or provides an advantage over available therapies	• Close communication with FDA throughout development • Rolling review of BLA • Eligibility for Priority Review and Accelerated Approval of BLA
Breakthrough Therapy designation	1) Treats a serious or life-threatening condition 2) Provides substantial improvement over available therapies	• All the benefits of Fast Track designation • Intensive FDA guidance • Organizational involvement of senior management in facilitating product's development
RMAT (regenerative medicine advanced therapy) designation	1) Is a regenerative medicine therapy 2) Treats a serious or life-threatening condition 3) Preliminary clinical evidence indicates the product has potential to address unmet clinical needs	• All the benefits of Breakthrough Therapy designation
Priority review	1) Previously received Fast Track, Breakthrough, or RMAT designation 2) Treats a serious or life-threatening condition 3) Provides a significant improvement in safety or effectiveness of the treatment of a condition	• BLA application will be reviewed within 6 months
Accelerated review	1) Treats a serious or life-threatening condition 2) Provides therapeutic advantage over available therapies 3) Demonstrates effect on a surrogate endpoint or clinical endpoint that can be measured earlier than irreversible morbidity and mortality	• Approval based on surrogate endpoint

Predicate cartilage therapies. Human cell, tissue, and cellular and tissue-based products (HCT/Ps) are regulated under Section 361 of the PHS Act (for minimally manipulated,

homologous use products) and Section 351 of the PHS Act (all other products), as illustrated in Figure 2B (22, 23). The 361 HCT/P pathway is intended for minimally processed products that perform the same basic function in the recipient and donor, and these products are subject to relatively less burdensome regulation (e.g., clinical trials not required). Cartilage repair products that have utilized the 361 HCT/P pathway are DeNovo NT, ProChondrix, and Cartiform, all of which consist of minimally manipulated allograft tissue. A product that is not minimally processed must utilize the 351 HCT/P pathway, which requires clinical trials to market. MACI is the only cartilage product that has obtained approval through the 351 HCT/P pathway. It should be noted that, before its approval in 2016, MACI had already been marketed and used in the European Union. However, more stringent requirements for animal testing in the EU have been implemented in recent years (24, 25). Therefore, future products may not be able to follow the same pathway for regulatory approval as MACI. For specific details on MACI preclinical data, see Table 2B. Historically, the Office of Combination Products has determined CBER to have primary jurisdiction over cell therapy products for cartilage repair. With this precedent, future tissue-engineered cartilage repair products will likely be considered primarily as biologics under Section 351 of the PHS, and secondarily a device (Class III). A sponsor (i.e., a person or organization responsible for a clinical investigation) will need to file an IND/Investigational device exemption (IDE) application to begin clinical trials and, eventually, to file a BLA/PMA to request marketing approval. The FDA has issued guidance documents for the types of data/assays that will be required before first-in-human testing can proceed; the next section presents the salient scientific considerations for *in vitro* preclinical studies.

Scientific and ethical considerations prior to conducting large animal studies

In vitro development is the first step toward advancing through the FDA regulatory framework, and aspects of *in vitro* research will be included in the preparation of IND and BLA submissions. Before proceeding with animal studies, it is prudent to conduct a thorough *in vitro* characterization

of the product, perform initial safety evaluations, consider manufacturing requirements of a definitive (i.e., IND-enabling) animal study, and uphold the ethical principles of animal use.

***In vitro* functional characterization**. Inasmuch as FDA guidance specifically calls for the inclusion of mechanical testing data (2), it is important that tissue engineered products be mechanically evaluated. It should be noted, however, that *in vitro* mechanical testing would not be applicable to products that only consist of a cell slurry. Mechanical characterization of the product aims to determine its biomimicry and "ability to withstand the level of static and dynamic loading expected *in vivo*" (2). Guidance recommends that static mechanical behavior should be assessed (e.g., Young's modulus, aggregate modulus) as well as the dynamic properties (e.g., complex shear modulus G*) (2). Although not stated in the guidance document, tribological testing can also be considered to provide friction and lubrication (26). As acknowledged in the guidance, certain types of products such as soft scaffolds and membranes are not capable of withstanding such mechanical tests prior to implantation, for which case the characterization will have to be made at a preclinical or clinical study stage following repair tissue maturation (2). Large animal studies should be preceded with clear hypotheses on how a therapeutic agent would behave mechanically, remain in place, and persist within the *in vivo* mechanical environment.

The FDA-recommended preclinical assessments for medical devices, pharmaceuticals, and biologics are summarized in Table 3A and cartilage specific recommendations are presented in Table 3B. While not specified in FDA guidance, a functionality index (FI) can be used to combine multiple outcome measures or endpoints into a single value, as previously described (27, 28). The FI is a weighted average of salient functional outputs directly compared to native tissue properties. The closer the FI value is to 1, the closer the functional properties are to native tissue. Having an FI to distill multiple functional properties into a single value could be useful to establish release criteria for a particular implant design (in *in vitro* research) or implant batch (in large animal studies, clinical studies, and implant manufacturing upon regulatory approval).

Overall, ensuring that the implant's functional characteristics mimic those of native tissue will likely improve the durability of an implant *in vivo*.

***In vitro* safety evaluation.** Early safety assessments of the product may be obtained through *in vitro* assays (Table 3A-C). The safety profile of the product must be provided within an IDE or an IND, and products categorized as biologics may use *in vitro* assays to screen for abnormal cell differentiation, cell malignancy, or tumorigenicity (29). A karyotype analysis can determine the existence of genetic alterations, which can appear during extensive subculture or differentiation steps (30). Similarly, FACS and qRT-PCR can be used to determine the existence of abnormally differentiated cells (31). The effects of genotype alterations can also be studied using tumorigenicity assays such as the soft agar colony formation assay. Short-term degradation kinetics for the product can be evaluated *in vitro* (32), as a degradation profile should be provided for scaffold-based approaches (3). Finally, though less common and often restricted to immune therapy products, *in vitro* immunogenicity assays can test for potential adverse immune reaction based on specific cell type activation (e.g., T-cell response, secreted cytokine) or establish the type of reaction based on cell population recruitment (immunophenotyping) (33, 34). Assessing these safety considerations before proceeding with animal studies will both mitigate problems that can arise during preclinical studies and provide initial pharmacology/toxicology data.

Chemistry, Manufacturing, and Controls. As *in vitro* development of a product advances, thought should be given to the Chemistry, Manufacturing, and Controls (CMC) of a product. For a cellular therapy to be tested in animals, an analogous animal product must be developed for the animal species used for testing (3). If passaged cells are used in the generation of a cellular therapy, a cell bank system should be considered, which will also be subject to safety testing (35). Because CMC information is a required component of an IND-application, CMC should be considered early within the product development.

FDA applications require Good Laboratory Practice (GLP) or a justification for why GLP was not followed (2, 36). In the latter case, a quality assurance statement must be provided, and an independent overseer must provide a statement that Standard Operating Procedures (SOPs) were followed. Although not all *in vitro* data can or should be collected under GLP, preclinical safety and toxicology studies are governed by GLP regulations, and considering GLP implementation early on will help ease the transition to IND-enabling research (37). Variability within the product manufacturing process or the product itself will negatively affect a study's outcome and, thus, a quality management system (QMS) should be implemented (38–40). Likewise, the development of standard operating procedures (SOPs), for example, should occur before performing large animal studies to ensure reproducibility in the manufacturing process and outcome measures (41). However, GLP-level scientific rigor can be expensive due to the necessity to adapt the existing infrastructure to meet GLP standards, to prepare and maintain extensive documentation, and to provide appropriate training to all personnel (42). Interestingly, out of the 22 FDA-approved, most did not comply with GLP in most or all their preclinical data (Table 2A). Overall, considering how and when GLP will be implemented will be a crucial decision within the translation of a product.

Ethics of animal research. Before proceeding with *in vivo* experimentation, researchers should fully optimize and characterize their product *in vitro*. The "principles of the 3Rs," which focus on replacement, reduction, and refinement strategies within animal studies, were established to assess the necessity of animal research, to ensure that only the minimum number of animals is used, and to improve animal welfare (3, 43). Replacement of animal experimentation emphasizes the use of *in vitro* studies when alternatives exist or can be developed (3). Reduction and refinement focus on the model selection, reducing the number of animals used, and how the animals will be managed to minimize suffering to the fullest extent possible (44). Reduction and refinement include, for example, using a single species and a single study to collect both

pharmacological and toxicological data and using non-terminal evaluations (e.g., MRI scanning) to maximize data acquisition. Appointed Institutional Animal Care and Use Committees (IACUCs) oversee the proper use of animals in research, in accordance with the Animal Welfare Act and the Public Health Service Policy on Humane Care and Use of Laboratory Animals (45, 46). Therefore, all *in vitro* data should be evaluated critically and a careful review of supporting literature should be performed to establish a strong rationale for any proposed animal study.

Rationale for selecting preclinical animal models in cartilage repair

While the FDA recognizes "there is no perfect animal model of articular cartilage injury" (2), several models have been widely used for cartilage repair studies. The International Cartilage Repair Society (ICRS) specifically recommends the pig, horse, sheep, and goat for preclinical animal studies (47). While ICRS does not specify pig breed, minipigs (e.g., Yucatan, Göttingen) are used more commonly than farm pigs because their size is more manageable and they are temperamentally more docile (48). Small and intermediate animal models (e.g., mouse or rabbit) do not provide sufficient evidence to support translation of a cartilage-repair product due to their capacity for spontaneous cartilage healing, thin articular cartilage, and gait patterns that differ significantly from those of humans (49). When selecting an animal model, one must consider the 1) analogy of the animal model's anatomy, cartilage, and biology to the human and 2) experimental requirements and logistical considerations. An overview of characteristics of key animal models is provided in Table 4.

Analogy of the model's joint anatomy, cartilage characteristics, and biology. An animal model's cartilage, joint, and mechanism of osteochondral healing should mimic those of human cartilage to the greatest extent possible. Because the pig, horse, sheep, and goat are quadrupeds, there are inherent differences between the animal model and human that cannot be reconciled regardless of choice of animal model.

The FDA has acknowledged that range of motion and joint anatomy are important for animal model selection (50). The goat, sheep, and pig knee (stifle) joint have similar ranges of motion ranging from approximately 45° to 145° (see Table 4 for animal-specific ranges) (51–53). Because the human range of motion is 2.5° to 137.5° (51), no widely used quadrupedal animal model replicates the human range of motion. In terms of cartilage thickness, the pig and the horse most closely mimic the human (Table 4) (47, 54, 55). Joint proportions in the pig, horse, sheep, and goat are similar to humans, but ligaments may have different attachment sites than in the human (51). Knee joint anatomy does not preclude these animal models from “second look” arthroscopic evaluation (56–58). Although there are differences between quadruped models and the human, in terms of anatomy, all proposed quadrupedal large animal models are relatively comparable.

Although the mechanical properties of the cartilage should be considered when selecting an animal model, there has not been a study that directly compares the mechanical properties of knee cartilage in minipigs, sheep, goats, and horses. Previous interspecies characterization of human, cow, dog, monkey, and rabbit found that compressive stiffness of distal femur cartilage was similar between the examined species (59). Analogous studies are needed for the major translational models used for cartilage repair research. For other anatomical locations, it has been found that minipig and human cartilage have similar functional properties. For example, in the human and minipig temporomandibular joint disc, mechanical properties were reported to be comparable with a compressive 20% instantaneous modulus of 1.12 MPa in the minipig and 1.32 MPa in the human (60). In the facet joint, the aggregate modulus of minipig cartilage was reported to be similar to primate (Rhesus Macaque) cartilage (61). Similar interspecies comparisons in the stifle joint of minipigs, goats, sheep, and horses are needed.

The healing response to cartilage injury of a chosen animal model should mimic that of humans. Ovine or caprine models have a tendency to form subchondral cysts during cartilage repair studies (62), which is not representative of the human situation in which subchondral cysts are considered to be a precursor to OA (63, 64). Osteochondral grafts implanted into the sheep

have been reported to induce cystic lesion formation in the subchondral bone (65). Subchondral drilling in sheep was reported to induce subchondral bone cyst formation in 63% of cases and intralesional osteophytes in 26% of cases (66). Similarly, in the goat, cavitation of the subchondral bone, a persistent central cyst, and, ultimately, structural collapse of the underlying bone was observed after full-thickness defects were generated (67). Goats implanted with osteochondral allografts developed bone cysts, subchondral bone channels, and subchondral bone roughening, which were not present in the non-operated contralateral control joints (68). Because ovine or caprine models have a greater propensity to exhibit abnormal healing patterns, they appear to have a different healing response than that of humans, and, therefore, may not be as suitable for animal studies as other large animals.

Overall, many of the anatomic and functional characteristics of the most common quadruped models are relatively similar, with the notable exception of cyst formation in the goat and sheep. Additionally, the pig and the horse have slightly thicker cartilage layers that more accurately resemble human anatomy, and, thus, may be favorable for cartilage repair studies.

Animal model logistical considerations and experimental requirements. Logistics of conducting a definitive animal must also be taken into account including resource requirements, genetic variability, and animal temperament. Considering the significant capital investment of conducting IND-enabling animal research, costs and the availability of facilities are of great importance when designing a large animal study. Although the horse has been used in previous preclinical studies, its use has been limited due to the high costs associated with purchase, husbandry, surgery, and recovery, as compared to the other large animal models discussed above. Moreover, horses require specialized equine facilities to house, which are rare, especially in GLP settings. There are several GLP-compliant animal facilities that frequently use the minipig animal model (e.g., Absorption Systems in San Diego, CA, BioSurg in Winters, CA, Sinclair Research in Auxvasse, MO). While the size of an animal does not necessarily preclude a species

from use, the selection of a smaller animal (e.g., minipig) may reduce personnel required and housing costs, thus, reducing costs overall. Therefore, unless the sponsor resides at an institution that specializes in equine research, the minipig is considerably more feasible than the horse.

Another practical consideration when designing a study is the genetic variability of the species or herd that is chosen for the study. Of the large animal models recommended by ICRS for preclinical research, the minipig is the only model that is bred specifically for research purposes, and, thus, specific parameters can be controlled (animal number, sex, and age). It is difficult to obtain a homogenous population of horses for research purposes, limiting the interpretability of data gathered from horse studies. However, as companion animals with a propensity to develop focal cartilage defects and OA (69), horses may be useful for providing predictive proof-of-concept data to support clinical translation (70). Because goats and sheep are bred for agricultural purposes, these species also have more genetic variability than the minipig (62). Therefore, to obtain a homogenous population of animals for the completion of a proposed definitive preclinical study, the minipig may be the most accessible.

The temperament of the animals used for an *in vivo* study can dictate the success or failure of a study. In our experience, we have worked with horses (71), goats (72), sheep (73), and minipigs (58, 74), for large animal studies. We have found goats and sheep to be problematic from a behavioral standpoint because of their tendency to panic and jump upon waking from surgery, imparting super-physiological and biomechanically aberrant stresses to the joint. Similarly, immediately post-operatively the horse poses a danger to itself because of its tendency to flee. The post-surgery recovery of these animals, thus, does not replicate a human surgery where the patient can be informed of the importance of avoiding any extreme movements post-operatively to allow the implant time to integrate into the host tissue. On the other hand, minipigs are relatively docile, especially when recovered in a sling or small pen (58). We have carried out successful studies in the minipig (58, 74), and have found minipigs to have the appropriate temperament for a study of this nature.

Table 2A. Summarized preclinical data submitted by FDA-approved cellular and gene therapy products; ■, Data not disclosed or not available; †, Predominantly.

Company BLA approval date	Product description	Indication	Prior clinical use	Number of preclinical studies *in vitro*/*in vivo*	Animal model(s)	Pharmacology tests	Toxicology tests	Activity tests	Analogous animal product	Control group	Study duration	Sex	GLP	Refs
CELLULAR PRODUCTS (TISSUE ENGINEERING)														
MACI Vericel Corp. Dec. 13, 2016	Autologous cultured chondrocytes on a porcine collagen membrane	For the repair of single or multiple symptomatic, full-thickness cartilage defects of the knee with or without bone involvement	Yes	4 0/4	Rabbit Horse	No	Yes	Yes	Yes	Empty defect, ACI-Maix, micro-fracture	12-53 wks	M + F	No	*(96)*
GINTUIT Organogenesis Inc. Mar. 9, 2012	Allogeneic cultured keratinocytes and fibroblasts in bovine collagen	For topical (non-submerged) application to a surgically created vascular wound bed in the treatment of mucogingival conditions	Yes	26 ≥12/≥9	Mouse	Yes	Yes	Yes	■	■	7-28 days or 3-6 mos	■	No†	*(97)*
STRATAGRAFT Stratatech Corp	Allogeneic cultured keratinocytes and dermal fibroblasts in murine “collagen-dsat”	For the treatment of thermal burns containing intact dermal elements for which surgical intervention is clinically indicated	No	18 ≥8/≥4	Mouse	No	Yes	No	■	No controls	7-421 days	M + F	No	*(98)*

June 15, 2021		(deep partial-thickness burns)											
LAVIV Fibrocell Technologies, Inc. June 21, 2011	Autologous cellular product	For improvement of the appearance of moderate to severe nasolabial fold wrinkles	Yes	0	No preclinical studies performed due to previous human experience, the autologous nature of the product, and the lack of a proper animal model								*(109)*
RETHYMIC Enzyvant Therapeutics GmbH Oct. 8, 2021	Allogeneic processed thymus tissue	For immune reconstitution in pediatric patients with congenital athymia	No	2 1/1	Rat	Yes	No	Yes	Yes	Non-trans-planted	2-294 days	M	■	*(110)*
CELLULAR PRODUCTS (IMMUNOTHERAPY)														
ABECMA Celgene Corporation Mar. 26, 2021	B-cell maturation antigen (BCMA)-directed genetically modified autologous T cell immunotherapy	For the treatment of adult patients with relapsed or refractory multiple myeloma after four or more prior lines of therapy*	No	12 ≥6/≥6	Mouse	Yes	Yes	Yes	No	Vehicle, Positive (Borte-zomib), Negative (anti-CD19 CAR T cells)	23-85 days	F†	■	*(99)*
BREYANZI Juno Therapeutics, Inc. Feb. 5, 2021	CD19-directed genetically modified autologous T cell immunotherapy	For the treatment of patients with relapsed or refractory large B-cell lymphoma after two or more	No	28 22/6	Mouse	Yes	Yes	Yes	■	Vehicle, Mock trans-duced cells,	14-100 days	F†	No†	*(100)*

		lines of systemic therapy*							No control					
KYMRIAH Novartis Pharmaceuticals Corp. Aug. 30, 2017	CD19-directed genetically modified autologous T-cell resolution immunotherapy	For the treatment of acute lymphoblastic leukemia and relapsed or refractory large B-cell lymphoma	No	■	Mouse	Yes	Yes	Yes	■	■	■	■	■	*(111)*
PROVENGE Dendreon Corp. Apr. 29, 2010	Autologous cellular immunotherapy	For the treatment of asymptomatic or minimally symptomatic metastatic castrate resistant (hormone refractory) prostate cancer	No	6 1/5	Mouse Rat	Yes	No	Yes	Yes	■	■	M	No	*(112)*
TECARTUS Kite Pharma, Inc. Oct. 1, 2021	CD19-directed genetically modified autologous T cell immunotherapy	For the treatment of patients with relapsed or refractory mantle cell lymphoma and patients with relapsed or refractory B-cell precursor acute lymphoblastic leukemia	No	6 3/3	Mouse	Yes	No	Yes	Yes	Untreated or ■	■	■	■	*(113)*
YESCARTA Kite Pharma, Inc. Oct. 18, 2017	CD19-directed genetically modified autologous T	For the treatment of patients with relapsed or refractory large B-cell lymphoma and patients with	No	4 3/1	Mouse	Yes	No	Yes	Yes	Non-transduced T cells	■	■	■	*(114)*

	cell immunotherapy	relapsed or refractory follicular lymphoma												
GENE THERAPY PRODUCTS														
IMLYGIC Amgen, Inc. Oct. 27, 2015	Genetically modified oncolytic viral therapy	For the local treatment of unresectable cutaneous, subcutaneous, and nodal lesions in patients with recurrent melanoma	No	56 8/48	Mouse Rat Dog	Yes	Yes	Yes	Yes	■	3-85 days	M/ F†	No†	*(115)*
LUXTURNA Spark Therapeutics, Inc. Dec. 19, 2017	Adeno-associated virus vector-based gene therapy	For the treatment of patients with confirmed biallelic RPE65 mutation-associated retinal dystrophy	No	15 3/12	Mouse Dog NHP	Yes	Yes	Yes	Yes	No injection, Sham injection	≤6.5 mos	M/ F	No†	*(116)*
ZOLGENSMA Novartis Gene Therapies, Inc. May 24, 2019	Adeno-associated virus vector-based gene therapy	For the treatment of pediatric patients less than 2 years of age with spinal muscular atrophy with biallelic mutations in the survival motor neuron 1 (SMN1) gene	No	3 0/3	Mouse	Yes	Yes	Yes	No	Vehicle or ■	3-12 wks	M/ F†	Yes†	*(117)*

Table 2B. Preclinical data submitted by MACI. For other FDA-approved CGT products please refer to Supplementary table 1. *(96)*

Preclinical studies	Pharmacology assessment	Toxicology assessment	Activity assessment	Duration	Endpoints
Cellular cartilage repair product					
Four studies: Two studies in rabbits (S1 and S2); two studies in horses (S3 and S4). Experiment: implantation of analogous products (same membrane as MACI with rabbit or horse cells) in critical-size defects in the hind limbs.	Yes. The four preclinical *in vivo* studies were used to determine safety and/or activity. Pharmacokinetics assessed in S4. No mechanism of action. Please see BLA reviewer's comment below regarding only considering the horse study for overall safety and activity.	Yes, S4, plus one additional genotoxicity study (not disclosed), one additional *in vitro* toxicity study (of fibrin glue on chondrocytes, details not disclosed), and 13 additional biocompatibility studies (not disclosed). No developmental and reproductive toxicity studies and no carcinogenicity/ tumorigenicity studies were performed (due to the avascular local implantation, the terminally differentiated sate of the cells, and the lack of systemic distribution of MACI).	Yes. S1 and S2 reported an improvement in the histopathology assessment (in-house scoring system) compared to empty defect (S1) and microfracture controls (S2). S3 and S4 report a trend toward improved cartilage repair compared to empty and ACI-Maix controls. S4 further reports near native cartilage appearance, increased GAG, and improved mechanical testing outcomes of the repair tissue.	S1 and S2 (in rabbit): 12 and 24 weeks. S3 and S4 studies (in horse): 24 and 53 weeks.	For S1: Histopathology For S2: Histopathology, clinical observation, body weights. For S3: Lameness score, clinical pathology, second-look arthroscopy, synovial fluid analysis, synovial membrane histology, gross and microscopic exams, collagen type II IHC. For S4: Clinical observation, mortality, lameness, clinical pathology, synovial fluid analysis, second-look arthroscopy, and terminal assessments (gross pathology, histology, scoring of the repair tissue, GAG, and collagen content, DNA measure, and biomechanical testing).
	Comments: "*This reviewer cannot make any definitive conclusions from the study summary provided (S1). The safety and activity profile of MACI will thus be entirely based on the 53-week horse study (Study #4) and the clinical data*."				

Table 3. Recommended assessments and measurements/assays for IND applications of cartilage cellular therapy products. Part A presents general FDA guidance for medical devices, pharmaceuticals, and biologics. Part B presents guidance specific for cartilage cellular therapy products. Part C presents literature-based recommendations for cartilage cellular therapy products.

Assessment	Measurement / Assay	*In vitro*	*In vivo*	Refs
Part A. Selected preclinical assessments recommended by the FDA for medical devices, pharmaceuticals, and biologics				
CMC safety and quality testing	Per requirements of 21 CFR 610, including potency, sterility, purity, identity, stability, mycoplasma, endotoxin, and other adventitious agents	×	-	*(3, 118, 119)*
Genotoxicity	Standard genetic toxicology. Measure chromosomal aberrations using *in vitro* and *in vivo* (for mutagenic assessment) tests	×	×	*(3, 120, 121)*
Carcinogenicity	Evaluation of carcinogenic and tumorigenic potential. Early stage *in vitro* assays (e.g., cell transformation) can be performed. *In vivo* studies are recommended (e.g., rodent study)	×	×	*(3, 120, 122)*
Toxicity	Chronic toxicity testing (in rodents and non-rodents)	-	×	*(3, 120, 123)*
Toxicokinetics, systemic exposure	Generation of pharmacokinetic data to describe the systemic exposure (*in vivo*) and its relationship to dose level and the time course of the toxicity study	-	×	*(120, 124)*
Safety pharmacology	Identify, evaluate, and investigate the mechanism of any adverse pharmacodynamic effect of a therapy product (i.e. substance) that may have relevance to its human safety	×	×	*(125)*
Developmental and Reproductive toxicity (DART)	Assess the effect of a therapeutic product (i.e., pharmaceutical) on reproduction and development (if applicable). Complete life cycle (*in vivo*) studies are recommended. Alternative assays (e.g., *in vitro*, *ex vivo*) may defer or replace (in certain circumstances) conventional *in vivo* studies	×	×	*(120, 126)*
Immunotoxicity	Identify compounds which have the potential to be immunotoxic. Assays include T-cell dependent antibody response (TDAR), immunophenotyping, and cell/function activation assays	×	×	*(120, 127)*
Cytotoxicity	Agar diffusion cell culture screening	×	×	*(128)*
Degradation	*In vivo* degradation assessment recommended for absorbable therapy products		×	*(128)*
Part B. Cartilage-specific recommended assessments (from FDA and ASTM)				
Mechanical data	Address the product's ability to withstand loading, the fixation method, and the propensity to generate wear debris. Compressive testing is specifically recommended to quantify aggregate modulus (H_A), shear modulus (μ), permeability (k), dynamic modulus (G*)	×	×	*(2)*
Biological response	Biological activity, including "proof-of-concept" (treatment feasibility) and safety data	-	×	*(2)*
Durability	Length of time needed to assess repair tissue formation and wear resistance. Large animal models recommended	-	×	*(2)*
Toxicology	Assessment of local and systemic toxicity	-	×	*(2)*

Dose response	Characterization of the therapy product's components that may affect repair tissue formation. Large animal models recommended	-	×	*(2)*
Arthroscopy and/or MRI	Interim arthroscopic assessments and/or MRI evaluations in the animal studies (to reduce number of animal sacrifices at each time)	-	×	*(2)*
Tissue structure	Histological evaluation (macroscopic and microscopic analysis and scoring)	×	×	*(104)*
General biochemical characterization	Biochemical quantification of proteins and proteoglycans in repair tissue compared to native cartilage is recommended but not specified	×	×	*(104)*
Part C. Recommended assessments for cartilage cellular therapy products (from scientific literature and guidance documents)				
Compressive mechanics	Aggregate modulus, shear modulus, and permeability via creep indentation; or instantaneous modulus, relaxation modulus, and coefficient of viscosity via stress-relaxation	×	×	*(129, 130)*
Tensile mechanics	Young's modulus, ultimate tensile strength, and toughness via uniaxial tensile loading	×	×	*(131)*
Tribology	Coefficient of friction (μ) via tribometer	×	×	*(132, 133)*
Mechanics of fixation	Fixation strength via pull-apart or push-through or lap shear tests	×	-	*(134)*
Mechanics of integration	Interface strength via pull-apart or push-through tests	-	×	*(135)*
Chromosome instability and genetic alterations	Karyotype analysis of cells (for extensively passaged cells and stem cell products)	×	-	*(128, 136)*
Tumor formation and cell malignancy	Soft agar colony formation, tumor sphere assay, colony forming/clonogenic assay, immunodeficient rodent tumorigenicity assay (for stem cell products)	×	×	*(128)*
Abnormal cell differentiation	FACS, qRT-PCR (for stem cell products)	×	-	*(128)*
Tissue structure	Histological staining for general structure and integration (H&E), collagen (picrosirius red), and glycosaminoglycan (safranin-O)	×	×	*(137)*
Biochemical composition	Collagen (e.g., hydroxyproline) Glycosaminoglycan (e.g., DMMB Blyscan GAG) DNA (e.g., Picogreen) Crosslinks (e.g., mass spectrometry or HPLC-based)	×	×	*(138–141)*
Activity	Pre- and post-operative activity measurement via activity monitors	-	×	*(142)*
Repair tissue collagens	Collagen types via mass spectrometry or immunohistochemistry or ELISA (at least types I and II)	-	×	*(141)*
Midpoint assessments	Arthroscopic evaluation, synovium analysis	-	×	*(58)*
Animal observation	Lameness, behavior, and eating and drinking habits	-	×	*(74)*
Additional terminal assessments	Necropsy, gross pathology, histological evaluation and scoring, synovium analysis, immunohistochemistry of immune cells	-	×	*(74)*

Table 4. Biologic and practical considerations of common large animal models for cartilage repair.

Consideration	Sheep	Goat	Minipig	Horse
Passive ROM	40° to 147° *(51)* 72° to 145° *(52)*	45° to 146° *(51)*	42° to 144° *(51)*	30° to 160° *(53)*
Cartilage thickness	0.4 to 1.2 mm *(47, 54)*	0.7 to 1.5 mm *(47, 54)*	1.5 to 3.2 mm *(47, 54, 55)*	1.5 to 3.2 mm *(47, 54, 55)*
Subchondral cyst formation	Yes *(65) (66)*	Yes *(67) (68)*	No	No
Facilities required	Large animal facilities	Large animal facilities	Large animal facilities	Equine facilities
Purpose for breeding	Agriculture	Agriculture	Research	Companion animal
Temperament	Instinct to flee upon awaking from surgery	Instinct to flee upon awaking from surgery	Relatively docile upon awaking from surgery	Instinct to flee upon awaking from surgery

Perspectives on the minipig. The porcine species has been increasingly recognized as an important animal model for translational research due to its similarity to the human in terms of size, immunology, genome, and physiology, as recently reviewed (75). Within the context of cartilage repair, the minipig has been recognized as a “clinically-relevant large animal model” (76) and has been used in many cartilage repair studies (76–81). In 2011, the FDA released guidance for conducting cartilage repair preclinical animal studies (2). This document did not specifically list the minipig as a model although it should be noted that the FDA does not limit models to those listed and allows for investigators to provide appropriate justification for their chosen model, for example through the Animal Model Qualification Program. Despite one report suggesting that the pig’s range of motion may be inappropriate for cartilage repair studies (50), literature reports that the stifle joint of the pig is comparable to all other animal models listed within the guidance document (51). The many advantages of using the minipig described in this review elevate this animal model to, in our opinion, the foremost animal model for cartilage repair studies and should be included within a revised FDA guidance document.

Surgical approach and rehabilitation

Once an animal model has been selected, the surgical approach, defect parameters, fixation technique, and post-surgical rehabilitation and recovery protocols must be developed before IND-enabling animal studies can be conducted.

Surgical approach. The technical aspects of the surgical approach, crucial for the success of the therapeutic, need to be tailored to the specific animal model utilized. Specifically, patellar maltracking, which can cause mechanical abrasion of the cartilage and intra-articular inflammation, is a major concern when translating surgical techniques from the human to a quadrupedal model. In the human, open surgical exposure of the knee joint is performed by medial arthrotomy, which requires cutting the medial retinaculum, an important stabilizer of the patella. Although this approach rarely causes problems in humans, a medial arthrotomy in animals can lead to patellar maltracking and lateral patellar instability, even after meticulous repair of the medial retinaculum (82). Both medial and lateral patellar subluxation are well-reported problems in large animals (82, 83), which are likely due to two major differences in anatomy between the human and quadruped models (illustrated in Figure 3A). First, compared to animal models, in the human the lateral condyle of the femur and trochlear ridge extend more anteriorly, which helps in preventing lateral patellar instability. Second, in the animal, the patella is located more proximally than in the human, which places it at the shallow portion of the trochlea, thereby predisposing it to patellar instability (84, 85). Due to this risk in large animals, retinaculum-sparing approaches that limit the extent of the proximal arthrotomy to the apex of the patella, as well as transpatellar approaches, have been recommended (82, 86, 87). In short, due to the differences between humans and animal models, one of the major considerations is how the surgery would affect the patella, which, if displaced, can lead to cartilage degeneration and failure of the experiment.

Defect parameters. The depth, size, and location of the defect must reflect the intended indication in the human and, thus, these decisions should be incorporated into the surgical development of preclinical research. Defect depth may be partial-thickness (leaving calcified cartilage layer intact), full-thickness (removing the calcified cartilage but leaving the subchondral bone intact), or osteochondral (penetrating into the subchondral bone), as depicted in Figure 3B. It is traditionally thought that partial-thickness defects do not heal, whereas osteochondral defects that penetrate the subchondral bone more regularly exhibit filling of the defect with reparative tissue due to egress of the underlying marrow elements (such as in microfracture). Based on a study investigating the healing response to isolated microfracture in horses (88), the current clinical paradigm argues for removal of the calcified cartilage layer during cartilage repair treatment. However, if a treatment does not utilize the underlying marrow elements, it may be beneficial to preserve the calcified cartilage and subchondral bone layers. Defect size in animals should mimic either a small or large lesion in humans because lesion size typically dictates the type of clinical treatment. Defect size can be calculated as a proportion of the surface area of the hemicondyle or trochlea in the animal model being utilized, with 2-4 cm2 as the typical threshold differentiating between small versus large defects in humans (89, 90). Although some have described a “critical size” that is needed for lesions to exhibit a limited repair process, in most skeletally mature large animals, even small lesions do not exhibit healing (91). With regard to location, the extensor digitorum longus is an intra-articular structure unique to quadrupeds that originates at the craniolateral aspect of the stifle joint (52). If left intact, this tendon can mechanically abrade any defects or implants placed on the lateral femoral condyle. Overall, the defect parameters selected should mimic the human indication while taking into consideration the anatomy and size of the selected animal model.

Fixation technique. Adequate fixation of the cartilage implants in large animal models is challenging. The four main fixation methods currently employed are depicted in Figure 3C.

Although osteochondral cartilage repair implants can be press-fit into surgically created defects, chondral implants are much more difficult to retain in the defect. The maximum thickness of the articular cartilage in skeletally mature large animals is typically no more than 2 mm (47, 54, 55), making it difficult to adhere constructs within partial-thickness defects. Based on our experience, fibrin sealant, which is the gold standard fixation method for cartilage repair in humans, is typically not strong enough to retain implants in the large animal stifle. Therefore, many investigators have used sutures or suture anchors to fix implants (87, 92). However, these methods are not without their own set of dilemmas. Suture fixation, which secures the implant to the surrounding native articular cartilage rim, is technically challenging, causes iatrogenic perforation injury to both the implant and native cartilage, and can cause abrasive wear from suture knots between the articulating surfaces. Moreover, suture anchor methods, which naturally perforate the subchondral bone, can produce unwanted bleeding, along with carrying the same disadvantages as suture fixation. In addition to robust initial fixation, recession of the implant within the defect seems to be crucial for its retention to avoid any catching of a prominent lip that would lift off the implant. Alternative fixation methods that do not cause damage to the cartilage implant or surrounding native articular cartilage warrant further investigation.

Post-surgery rehabilitation and recovery protocols. Design of an analogous rehabilitation regimen for animals, compared to humans, is challenging. Animals, upon wakening, can exhibit erratic behaviors that jeopardize the success of the surgery (93). These behaviors are practically guaranteed in some species, such as the goat and sheep, where the animal will display a strong run-and-hide response, sometimes jumping energetically regardless of the knee condition. Strategies such as casting, external fixator immobilization, and botulinum toxin paralysis are typically not well tolerated by animals and can introduce other unintended consequences. For example, botulinum toxin-induced muscle paralysis and the resulting underloading of bone structures has been associated with loss of bone density (94). The use of slings and splints may

minimize the load placed on the operated joint immediately after surgery (Figure 3D) (47). The Thomas splint, for example, diverts the load experienced during ambulation from the knee to the hip. This method, however, is prone to failure given the physiognomy of most animal models' knees. Other options could include bodyweight suspension out of surgery to prevent violent loaded motions and thrashing upon awaking from anesthesia, although one must be cognizant of the potential for the development of pressure sores (58). Common clinical rehabilitation programs after knee cartilage procedures include continuous passive motion and progressive weight-bearing to protect the cartilage while healing (95). Many of the current reports for cartilage repair do not include descriptions of post-operative rehabilitation; this is troublesome because it either means rehabilitation is not performed or, if it was, a lack of reporting limits other researchers in replicating and building upon successful methods. Protecting the repair cartilage immediately after surgery in animal studies may contribute to the success of the study and should be a key element in the development and reporting of animal studies.

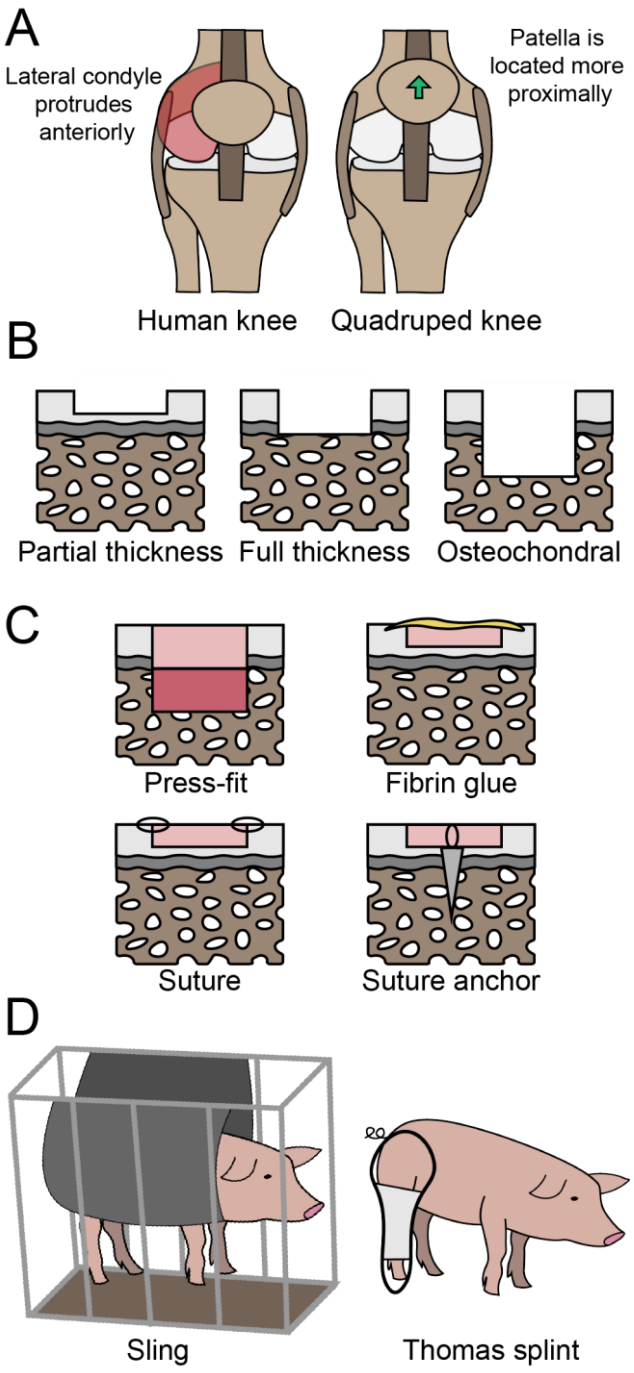

Figure 3. Surgical and rehabilitation protocols for cartilage repair in animal models. **A**. The major anatomical differences between the human and animal knee anatomy that can lead to patellar maltracking. **B**. Depth of defects that may be considered when designing surgical techniques. **C.** Fixation methods that are currently utilized in cartilage repair. **D**. Potential rehabilitation regimens that can be customized for quadruped models.

IND-enabling preclinical animal studies

Once an animal model has been selected and a surgical approach devised, IND-enabling *in vivo* studies are required to "demonstrate an acceptable safety profile" and to obtain "data sufficient to establish scientific support for clinical investigation" (2). While the FDA has released guidance documents to aid in this process, guidance is intentionally flexible to be applicable to a wide range of potential products. Thus, it may be difficult for a sponsor to surmise the appropriate study design for a specific product under development. Guidance documents represent the Agency's current thinking on a subject, but an alternative approach may be deemed acceptable if a sponsor can justify the approach scientifically and it abides by applicable statutes and regulations. Discussion of the preclinical animal studies should occur with the FDA at the stage of the pre-IND meeting. In this section, the design of the preclinical animal studies for cartilage repair will be discussed. The primary guidance documents referred to in this discussion include "Guidance for Industry Preclinical Assessment of Investigational Cellular and Gene Therapy Product" (3) and "Guidance for Industry Preparation of IDEs and INDs for Products Intended to Repair or Replace Knee Cartilage" (2).

Overview of animal study objectives. FDA guidance for cartilage repair products specifically states that animal studies should assess the dose-response, biological response/activity, durability, and toxicology of a product (2). Proof-of-concept (POC) studies should be used to assess feasibility, establish product administration/dosing parameters, and determine a putative mechanism of action (3). Once POC studies have been completed, definitive preclinical studies should be used to assess toxicology and biological activity. In the case of cartilage repair, this will likely consist of a large animal study that assesses both safety and activity within the same study design. For reference, MACI's Pharmacology Toxicology Review lists four studies (two rabbit studies, a pilot horse study, and a definitive horse study). Of these, the safety and activity profile of MACI was entirely based on the definitive horse study (96).

Study duration. Durability of a cartilage repair product is critical "to resist wear, degradation, [and] withstand physiological relevant loads over time" and, thus, has been highlighted as a primary concern within guidance for cartilage repair products (2). The Agency has released guidance stating that long-term (i.e., 12-month) *in vivo* studies are required to demonstrate durability of effect for products intended for cartilage repair (2, 3). Accordingly, a 53-week large animal study was conducted for MACI (96). For perspective, other tissue engineering products such as Gintuit and Stratagraft reported studies up to 6 months and 14 months in duration, respectively (97, 98). Approval of immunotherapy products such as Abecma and Breyanzi only required studies lasting up to 85 days and 100 days, respectively (99, 100). However, considering the mechanical requirements of joint repair, sponsors of cartilage repair products may anticipate a year-long duration for the definitive animal study.

Control selection. Inasmuch as the use of controls in large animal preclinical studies for cartilage treatment is essential, FDA guidance suggests the use of untreated controls (defect generated but no therapeutic treatment applied), sham-surgery controls (surgery performed but no defect or therapeutic agent applied), active-comparator controls (defect generated and another therapeutic treatment applied), or standard of care controls (defect generated and microfracture applied) (2, 3). It should be noted that MACI's definitive *in vivo* study used empty defects and collagen only membranes (ACI-Maix) as controls (96). MACI's lack of active-comparator controls or standard of care controls is consistent with what has been submitted with other cellular and gene therapy products. Furthermore, Stratagraft and Breyanzi received BLAs without controls in some of their animal studies after providing sufficient rationale (98, 100). Although active-comparator controls and standard of care controls may be beneficial for assessing efficacy in clinical studies, as discussed under Perspectives, such controls may be inappropriate for use in animal models.

Thus, based on guidance and the precedent set by previously approved products, empty defects may be the most appropriate controls in the case of cartilage repair studies.

Endpoints. Endpoint selection is crucial to the success of an IND application and should be discussed with the Agency in a pre-IND meeting. Broadly, endpoints are used to assess safety and/or activity of the product. In terms of safety, FDA guidance states that standard endpoints include "mortality (with cause of death determined, if possible), clinical observations, body weights, physical examinations, food consumption/appetite, water consumption (as applicable), clinical pathology (serum chemistry, hematology, coagulation, urinalysis), organ weights, gross pathology, and histopathology" (3). Cell fate post-administration should be considered, and, if appropriate (e.g., in stem cell products), issues such as tumorigenicity should be assessed within the study design (3). Overall, the assays selected should demonstrate that all constituents of the product (e.g., cells, biomaterials) are reasonably safe to administer in future clinical investigations.

The purpose of activity endpoints in animal testing is to obtain "data sufficient to establish scientific support for clinical investigation" (2). In clinical studies for cartilage repair, efficacy is determined by reduced pain and improved physical function using scoring systems such as the Knee Injury and Osteoarthritis Outcome Score (KOOS) or Western Ontario and McMaster Universities Osteoarthritis Index (WOMAC) (2). Because these assessments cannot be used in animals, surrogate measures of efficacy (i.e., biological activity) must be utilized and should "mirror" the endpoints of the clinical study (2). Guidance also suggests the use of arthroscopic and/or magnetic resonance imaging (MRI) evaluations to assess animals in a non-terminal manner (2). Other potential measures that could be utilized in the future include, activity monitors, which have been used in dogs to assess movement after biologic resurfacing of a cartilage defect (101), and clinical evaluation of distress or pain via evaluating facial expressions of animals (102, 103). Although preclinical biologic activity is not equivalent to clinical efficacy, endpoints should be selected to provide scientific support that the treatment would be efficacious in human patients.

Mechanical testing is requested within guidance for cartilage repair products. Specifically, the FDA has categorized mechanical testing into three areas: 1) mechanical characterization of the tissue (as discussed in the *in vitro* evaluation section), 2) evaluation of the fixation method, and 3) degradation behavior (2). Mechanical properties should be tested at discrete time points after implantation into an animal. Degradation behavior is important for degradable scaffolds and synthetic biomaterials, but it may not be directly applicable to cell-based products.

GLP compliance. The Code of Federal Regulations, Title 21, part 58, specifies that GLP work is required for IND-enabling studies, including personnel, facilities, protocols, and all equipment and materials used (37). It is expected that all preclinical safety studies are performed consistent with GLP, and that a statement of compliance is included within the final study report (2, 36). However, the FDA can consider exceptions depending on a case-by-case basis where compliance is not possible (e.g., animal models of disease/injury with unique care requirements). For such cases, a statement of the reasons for the noncompliance should be provided if the study was not conducted according to GLP regulation, which includes the areas of deviation and how these affected the study outcome (3, 37). Similarly, an exemption from GLP provisions can be discussed with the FDA prior to the preclinical studies to ensure that the nonconformance can be justified and that provisions are made to ensure data integrity (36, 37). In the preclinical MACI research, both the small and large animal studies were deemed to be not GLP-compliant (96). As many of the resources needed for conducting preclinical animal research may not be available in GLP facilities, discussing GLP requirements with the Agency at the pre-IND meeting is advised.

Sex as a biologic variable (SABV). Sex is an important source of biological variability and is associated with biologic function, and, therefore, must be factored into the study design where relevant. The ASTM guide for preclinical studies of articular cartilage establishes that sex should be considered in data analysis due to the impact of circulating steroids on cartilage and bone

metabolism and regeneration, and that sex be the same within the cohort, implying that one sex can be used in a study design (104). These recommendations were reconsidered in 2015 by the NIH, with expectations that sex would be factored into the research design, analysis, and reporting in studies of vertebrate animals without calling for doubling of research animals (105, 106). However, the most pertinent directive us from the CGT Guidance which states that adequate numbers from each sex should be included and randomized to each group (3). With a few exceptions, both male and female animals were utilized in most of the approved cellular and gene therapy products, including MACI.

Perspectives

In this review, we have described the main barriers to clinical translation of cartilage repair products. Through these discussions, we have identified six major bottlenecks that hinder translation at the preclinical stage: 1) obtaining FDA guidance early within preclinical development, 2) conducting GLP research to support FDA applications within the infrastructure at research universities, 3) developing an appropriate rehabilitation protocol, 4) selecting appropriate *in vivo* controls, 5) ensuring that the primary outcome measures for activity are relevant to the human condition, and 6) defining standardized endpoints. Here, we provide perspectives on these challenges.

A significant bottleneck in translating cell therapy products for cartilage repair is navigating the regulatory process. Regulatory guidance provided by the FDA is intentionally flexible to accommodate a range of products that may be developed. However, this flexibility can allow for various interpretations of the guidance documents, and there are few relevant, approved cell therapy products to use as a blueprint for this process. Guidance documents “recommend early and ongoing communication with [the Office of Cellular, Tissue and Gene Therapies] Pharmacology/Toxicology staff during product development”(3). However, in practice, this is not possible. The FDA offers, as its first official interaction with the sponsor, the pre-IND meeting, but

for many, this may be too late in the product development process. INTERACT meetings are meant to offer an opportunity for early dialog between sponsors and the Agency, but even these meetings require significant pharmacology and toxicology data for a meeting request to be accepted. Thus, we advocate for a move toward increased and early dialog between translational research groups and regulatory agencies. Such interactions may be facilitated by professional organizations or societies, where common, general issues can be identified through surveys and conferences, and then for these issues to be addressed by the Agency. Moreover, as the regulatory environment of cell therapy matures, more nuanced guidance for specific applications (e.g., meniscus, TMJ disc, facet joint) should also be developed. Increased regulatory dialog would greatly enhance the ability of researchers to translate cartilage repair products and cellular and gene therapy products in general.

A large subset of cellular and gene therapy research is conducted at research universities and academic centers. The infrastructure at such institutions is not conducive to conducting GLP research. For example, we estimate that conducting a year-long study with 24 minipigs would cost approximately $50,000 in procurement, surgery, husbandry, care of animals, and necropsy costs within the University of California research system (which is not GLP) but over $700,000 when outsourced to a GLP facility. Funding mechanisms through the NIH and NSF, which fund research on cellular and gene therapy products, rarely would provide enough support to conduct a GLP-level study of this magnitude. Therefore, there is a disconnect between the funding and resources that researchers have access to and the regulatory requirements of translating cellular and gene therapy products. When we embarked on investigating the documentation of approved cellular and gene therapy products, it was surprising for us to see most of the 22 products that have obtained regulatory approval did not conduct animal research in GLP facilities, even though it appears to be requested by the FDA. Given that there are only 22 translated products with the majority of them not following GLP, GLP requirements may be too stringent to facilitate effective translation of cellular and gene therapy research from universities to clinical use.

Developing appropriate post-operative and rehabilitation protocols for animal models is difficult but necessary, and animal care can have an outsized influence on study results. In the human case, post-surgical immobilization or directed rest after cartilage repair surgeries can be understood by the patient, but in the animal situation rehabilitation strategies cannot be employed in the same manner. No standardized method for post-surgery rehabilitation in large animal models exists due to the wide variety of indications that researchers seek to address. For this reason, investigators would do well in using pilot studies to develop these protocols before commencing animal work at a large scale. For example, for treating defects in knee articular cartilage, we have had success in using a sling to elevate minipigs as they recover from anesthesia to ensure that violent postoperative movements are minimized (58). Toward the end of developing effective post-operative and rehabilitation protocols, researchers should strive to devise protocols that are both relevant to the human situation and tolerable to the animal.

Selecting appropriate controls for definitive preclinical studies is challenging. The FDA suggests the use of active-comparator controls, standard of care controls, or sham-surgery controls within the guidance for the development of cartilage repair products (2). However, the use of active-comparator controls and/or standard of care controls presents a new layer of challenges to a study for cell therapies. If the active comparator is another cell therapy, then it would either have to be xenogeneic or a new, analogous animal product would have to be devised, making such comparisons unusually burdensome for the sponsor. For example, purchasing MACI for xenogeneic use in animals would increase the cost of a study substantially not to mention that such an approach is probably scientifically ill-advised. Similarly, the applicability of microfracture developed in the human knee may not be directly equivalent to such an approach in the animal. Due to the challenges of other controls, empty defects may be the best comparator option for preclinical studies, although active comparators can still be employed in clinical trials.

Selecting endpoints in animal models that mirror the clinical endpoints is difficult, but recent advancements in technology may enable outcome measures that better replicate the human situation. In humans, the primary endpoint of cartilage repair is the reduction in pain, which is in stark contrast to animal studies in which repair is typically evaluated after sacrifice. To simulate the human situation, non-terminal endpoints should be incorporated into animal studies such as non-invasive imaging or arthroscopic protocols. With the emergence of more robust imaging modalities (e.g., near-infrared spectroscopy, arthroscopic optical coherence tomography) we can envision the development of surrogate measures for determining the quality of cartilage repair (107). Moreover, utilizing outcome measures that assess activity and behavior may be beneficial for indicating that a treatment is efficacious. Function can be measured indirectly in animals via an attached activity monitor (101). Additionally, with the advancement of artificial intelligence, in the future, behavioral measures may be able to be quantified in an unbiased manner, similar to poultry monitoring systems currently in development for agricultural purposes (108). Going forward, researchers should take advantage of these technological advancements to enhance the collection of meaningful primary outcome measures in animal studies.

The guidance document on cartilage repair products calls for mechanical testing (2), but it is unclear what data should be collected at the *in vitro* stage and what endpoint data should be collected upon sacrifice during IND-enabling animal studies. For *in vitro* stage research on a product that is a tissue-engineered implant, we suggest that at minimum compressive data (e.g., aggregate modulus, shear modulus, and permeability), tensile data (e.g., Young's modulus, ultimate tensile strength), and tribological data (e.g., coefficient of friction) be collected. Upon sacrifice of an animal, we suggest that the same parameters be measured in the repair tissue along with the integration strength between the native tissue and implant. Standardizing specific mechanical endpoints within FDA guidance would facilitate experimental design development and allow for comparison between studies conducted by different research groups. For a

comprehensive list of recommended *in vitro* and *in vivo* assessments and measurements/assays, see Table 3C based on our thorough review of the literature and regulatory guidance.

Considering the many challenges researchers face, the purpose of this review was to demystify the process and challenges of translating biologic cartilage products from basic research to clinical trials. These challenges may require increased dialog between regulatory agencies and research groups to ensure that therapies that have the potential to treat patients stand a chance of overcoming these barriers to clinical translation.

Acknowledgements: This work was supported by two grants from the NIH (Grant # R01 AR067821 and R01 AR078389). This work was also supported by NIH TL1 TR001415 (RCN). The content is solely the responsibility of the authors and does not necessarily represent the official views of the NIH.

References

1. Approved Cellular and Gene Therapy Products | FDA (available at https://www.fda.gov/vaccines-blood-biologics/cellular-gene-therapy-products/approved-cellular-and-gene-therapy-products).
2. U.S. Food and Drug Administration, Guidance for Industry: Preparation of IDEs and INDs for Products Intented to Repair or Replace Knee Cartilage, www.FDA.gov , 45 (2011).
3. US Food and Drug Administration, FDA/CBER, Guidance for Industry: Preclinical Assessment of Investigational Cellular and Gene Therapy Products (2013; https://www.fda.gov/regulatory-information/search-fda-guidance-documents/preclinical-assessment-investigational-cellular-and-gene-therapy-products).
4. R. Langer, J. P. Vacanti, Tissue Engineering, Science (80-.). 260, 920–926 (1993).
5. D. J. Huey, J. C. Hu, K. A. Athanasiou, Unlike bone, cartilage regeneration remains elusive, Science 338, 917–921 (2012).
6. K. Athanasiou, E. Darling, J. Hu, G. DuRaine, H. Reddi, Articular Cartilage, Second Edition (2017).
7. D. J. Responte, R. M. Natoli, K. A. Athanasiou, Collagens of articular cartilage: Structure, function, and importance in tissue engineeringCrit. Rev. Biomed. Eng. 35, 363–411 (2007).
8. B. J. Bielajew, J. C. Hu, K. A. Athanasiou, Collagen: quantification, biomechanics and role of minor subtypes in cartilage, Nat. Rev. Mater. 2020 510 5, 730–747 (2020).
9. Arthritis-Related Statistics | Data and Statistics | Arthritis | CDC (available at https://www.cdc.gov/arthritis/data_statistics/arthritis-related-stats.htm).

10. D. Wang, B. J. Rebolledo, D. M. Dare, M. D. Pais, M. R. Cohn, K. J. Jones, R. J. Williams, Osteochondral Allograft Transplantation of the Knee in Patients with an Elevated Body Mass Index, Cartilage 10, 214–221 (2019).
11. F. Gaul, L. E. P. Tírico, J. C. McCauley, W. D. Bugbee, Long-term Follow-up of Revision Osteochondral Allograft Transplantation of the Ankle, Foot Ankle Int. 39, 522–529 (2018).
12. A. Pareek, P. J. Reardon, T. G. Maak, B. A. Levy, M. J. Stuart, A. J. Krych, Long-term Outcomes after Osteochondral Autograft Transfer: A Systematic Review at Mean Follow-up of 10.2 YearsArthrosc. - J. Arthrosc. Relat. Surg. 32, 1174–1184 (2016).
13. M. Pellegrino, E. Trinchese, M. Bisaccia, G. Rinonapoli, L. Meccariello, G. Falzarano, A. Medici, L. Piscitelli, P. Ferrara, A. Caraffa, Long-term outcome of grade III and IV chondral injuries of the knee treated with Steadman microfracture technique, Clin. Cases Miner. Bone Metab. 13, 237 (2016).
14. C. Erggelet, P. Vavken, Microfracture for the treatment of cartilage defects in the knee joint – A golden standard?J. Clin. Orthop. Trauma 7, 145–152 (2016).
15. P. Niemeyer, J. M. Pestka, G. M. Salzmann, N. P. Südkamp, H. Schmal, Influence of cell quality on clinical outcome after autologous chondrocyte implantation, Am. J. Sports Med. 40, 556–561 (2012).
16. M. N. Dugard, J. H. Kuiper, J. Parker, S. Roberts, E. Robinson, P. Harrison, J. B. Richardson, Development of a Tool to Predict Outcome of Autologous Chondrocyte Implantation, Cartilage 8, 119–130 (2017).
17. J. R. Ebert, A. Smith, P. K. Edwards, K. Hambly, D. J. Wood, T. R. Ackland, Factors predictive of outcome 5 years after matrix-induced autologous chondrocyte implantation in the tibiofemoral joint, Am. J. Sports Med. 41, 1245–1254 (2013).
18. J. R. Ebert, M. Fallon, D. J. Wood, G. C. Janes, A Prospective Clinical and Radiological Evaluation at 5 Years after Arthroscopic Matrix-Induced Autologous Chondrocyte Implantation, Am. J. Sports Med. 45, 59–69 (2017).
19. K. B. McGowan, G. Stiegman, Regulatory Challenges for Cartilage Repair Technologies, Cartilage 4, 4–11 (2013).
20. B. V Sweet, A. K. Schwemm, D. M. Parsons, Review of the Processes for FDA Oversight of Drugs, Medical Devices, and Combination Products (; www.amcp.org).
21. Fda, Cder, SReese, Guidance for Industry Expedited Programs for Serious Conditions-Drugs and Biologics Guidance for Industry, (2014) (available at http://www.fda.gov/Drugs/GuidanceComplianceRegulatoryInformation/Guidances/default.htmand/orhttp://www.fda.gov/BiologicsBloodVaccines/GuidanceComplianceRegulatoryInformation/Guidances/default.htm).
22. J. Lazar, G. Caressi, A Product and Pipeline Analysis of the Global Knee Cartilage Repair Market. A New Standard of Care May Be on the Horizon. (2014; https://cds.frost.com/p/67239#!/ppt/c?id=NE07-01-00-00-00&hq=cartilage regenerative).
23. H. Kwon, W. E. Brown, C. A. Lee, D. Wang, N. Paschos, J. C. Hu, K. A. Athanasiou, Surgical and tissue engineering strategies for articular cartilage and meniscus repair, Nat. Rev. Rheumatol. 15, 550–570 (2019).
24. REGULATION (EC) No 1394/2007 OF THE EUROPEAN PARLIAMENT AND OF THE COUNCIL of 13 November 2007 on advanced therapy medicinal products and amending Directive 2001/83/EC and Regulation (EC) No 726/2004 (Text with EEA relevance).

25. E. Kleiderman, A. Boily, C. Hasilo, B. M. Knoppers, Overcoming barriers to facilitate the regulation of multi-centre regenerative medicine clinical trialsStem Cell Res. Ther. 9 (2018), doi:10.1186/s13287-018-1055-2.
26. J. M. Link, E. Y. Salinas, J. C. Hu, K. A. Athanasiou, The tribology of cartilage: Mechanisms, experimental techniques, and relevance to translational tissue engineeringClin. Biomech. (2019), doi:10.1016/j.clinbiomech.2019.10.016.
27. B. D. Elder, K. A. Athanasiou, Systematic assessment of growth factor treatment on biochemical and biomechanical properties of engineered articular cartilage constructs, Osteoarthr. Cartil. 17, 114–123 (2009).
28. R. F. MacBarb, A. L. Chen, J. C. Hu, K. A. Athanasiou, Engineering functional anisotropy in fibrocartilage neotissues, Biomaterials 34, 9980–9989 (2013).
29. E. Ito, S. Miyagawa, M. Takeda, A. Kawamura, A. Harada, H. Iseoka, S. Yajima, N. Sougawa, N. Mochizuki-Oda, S. Yasuda, Y. Sato, Y. Sawa, Tumorigenicity assay essential for facilitating safety studies of hiPSC-derived cardiomyocytes for clinical application, Sci. Rep. 9 (2019), doi:10.1038/s41598-018-38325-5.
30. B. G. Stultz, K. McGinnis, E. E. Thompson, J. L. Lo Surdo, S. R. Bauer, D. A. Hursh, Chromosomal stability of mesenchymal stromal cells during *in vitro* culture, Cytotherapy 18, 336–343 (2016).
31. T. Kuroda, S. Yasuda, S. Kusakawa, N. Hirata, Y. Kanda, K. Suzuki, M. Takahashi, S.-I. Nishikawa, S. Kawamata, Y. Sato, E. Chaum, Ed. Highly Sensitive *In vitro* Methods for Detection of Residual Undifferentiated Cells in Retinal Pigment Epithelial Cells Derived from Human iPS Cells, PLoS One 7, e37342 (2012).
32. D. F. Williams, Challenges With the Development of Biomaterials for Sustainable Tissue Engineering, Front. Bioeng. Biotechnol. 7, 127 (2019).
33. A. Lock, J. Cornish, D. S. Musson, The role of *in vitro* immune response assessment for biomaterialsJ. Funct. Biomater. 10 (2019), doi:10.3390/jfb10030031.
34. M. K. Joubert, M. Deshpande, J. Yang, H. Reynolds, C. Bryson, M. Fogg, M. P. Baker, J. Herskovitz, T. J. Goletz, L. Zhou, M. Moxness, G. C. Flynn, L. O. Narhi, V. Jawa, Use of *In vitro* Assays to Assess Immunogenicity Risk of Antibody-Based Biotherapeutics, PLoS One 11 (2016), doi:10.1371/JOURNAL.PONE.0159328.
35. FDA, Guidance for Industry Cell Characterization and Qualification of Cell Substrates and Other Biological Materials Used in the Production of Viral Vaccines for Infectious Disease Indications, , 1–50 (2010).
36. Guidance for Industry, Investigators, and Reviewers Exploratory IND Studies Contains Nonbinding Recommendations Guidance for Industry, Investigators, and Reviewers Exploratory IND Studies (2006; http://www.fda.gov/cder/guidance/index.htm).
37. CFR - Code of Federal Regulations Title 21, (available at https://www.accessdata.fda.gov/scripts/cdrh/cfdocs/cfcfr/CFRSearch.cfm?fr=610.18).
38. FDA, Manual, MDSAP QMS P0001.004: Quality System (2019).
39. M. F. Jarvis, M. Williams, Irreproducibility in Preclinical Biomedical Research: Perceptions, Uncertainties, and Knowledge GapsTrends Pharmacol. Sci. 37, 290–302 (2016).
40. N. A. Karp, Reproducible preclinical research—Is embracing variability the answer?, PLOS Biol. 16, e2005413 (2018).

41. M. Van Putten, A. Aartsma-Rus, M. D. Grounds, J. N. Kornegay, A. Mayhew, T. H. Gillingwater, S. Takeda, M. A. Rüegg, A. De Luca, K. Nagaraju, R. Willmann, in Journal of Neuromuscular Diseases, (IOS Press, 2018), vol. 5, pp. 29–34.
42. J. E. Adamo, G. Bauer, M. Berro, B. K. Burnett, K. A. Hartman, L. M. Masiello, D. Moorman-White, E. P. Rubinstein, K. G. Schuff, A roadmap for academic health centers to establish good laboratory practice-compliant infrastructure, Acad. Med. 87, 279–284 (2012).
43. W. Russell, R. Burch, The principles of humane experimental technique (1959; http://117.239.25.194:7000/jspui/bitstream/123456789/1342/1/PRILIMINERY AND CONTENTS.pdf).
44. M. J. Allen, K. D. Hankenson, L. Goodrich, G. P. Boivin, B. von Rechenberg, Ethical use of animal models in musculoskeletal research, J. Orthop. Res. 35, 740–751 (2017).
45. PHS Policy on Humane Care and Use of Laboratory Animals | OLAW (available at https://olaw.nih.gov/policies-laws/phs-policy.htm).
46. USDA Animal Care: Animal Welfare Act and Animal Welfare Regulations, (available at www.ascr.usda.gov/fling-program-discrimination-).
47. M. B. Hurtig, M. D. Buschmann, L. A. Fortier, C. D. Hoemann, E. B. Hunziker, J. S. Jurvelin, P. Mainil-Varlet, C. W. McIlwraith, R. L. Sah, R. A. Whiteside, Preclinical studies for cartilage repair: Recommendations from the international cartilage repair society, Cartilage 2, 137–152 (2011).
48. S. G. Cone, P. B. Warren, M. B. Fisher, Rise of the Pigs: Utilization of the Porcine Model to Study Musculoskeletal Biomechanics and Tissue Engineering During Skeletal Growth, Tissue Eng. Part C Methods 23, 763–780 (2017).
49. J. L. Cook, C. T. Hung, K. Kuroki, A. M. Stoker, C. R. Cook, F. M. Pfeiffer, S. L. Sherman, J. P. Stannard, Animal models of cartilage repair, Bone Joint Res. 3, 89–94 (2014).
50. B. R. M. A. Committee, Briefing Document Cellular, Tissue, and Gene Therapies Advisory Committee (2005).
51. B. L. Proffen, M. McElfresh, B. C. Fleming, M. Murray, A Comparative Anatomical Study of the Human Knee, Knee 19, 493–499 (2012).
52. M. J. Allen, J. E. F. Houlton, S. B. Adams, N. Rushton, The surgical anatomy of the stifle joint in sheepVet. Surg. 27, 596–605 (1998).
53. J. G. Fowlie, S. P. Arnoczky, J. A. Stick, A. P. Pease, Meniscal translocation and deformation throughout the range of motion of the equine stifle joint: An *in vitro* cadaveric study, Equine Vet. J. 43, 259–264 (2011).
54. D. D. Frisbie, M. W. Cross, C. W. McIlwraith, A comparative study of articular cartilage thickness in the stifle of animal species used in human pre-clinical studies compared to articular cartilage thickness in the human knee, Vet. Comp. Orthop. Traumatol. 19, 142–146 (2006).
55. C. R. Chu, M. Szczodry, S. Bruno, Animal models for cartilage regeneration and repair, Tissue Eng. B, Rev. 16, 105–115 (2010).
56. Y. Pan, Z. Li, T. Xie, C. R. Chu, Hand-held arthroscopic optical coherence tomography for *in vivo* high-resolution imaging of articular cartilage, J. Biomed. Opt. 8, 648 (2003).
57. S. Zelle, T. Zantop, S. Schanz, W. Petersen, Arthroscopic Techniques for the Fixation of a Three-Dimensional Scaffold for Autologous Chondrocyte Transplantation: Structural Properties in an *In vitro* Model, Arthrosc. - J. Arthrosc. Relat. Surg. 23, 1073–1078 (2007).

58. D. Wang, M. Cubberly, W. E. Brown, H. Kwon, J. C. Hu, K. A. Athanasiou, Diagnostic Arthroscopy of the Minipig Stifle (Knee) for Translational Large Animal Research, Arthrosc Tech 10, e297–e301 (2021).
59. K. A. Athanasiou, M. P. Rosenwasser, J. A. Buckwalter, T. I. Malinin, V. C. Mow, Interspecies comparisons of in situ intrinsic mechanical properties of distal femoral cartilage, J. Orthop. Res. 9, 330–340 (1991).
60. N. Vapniarsky, A. Aryaei, B. Arzi, D. C. Hatcher, J. C. Hu, K. A. Athanasiou, The Yucatan Minipig Temporomandibular Joint Disc Structure–Function Relationships Support Its Suitability for Human Comparative Studies, Tissue Eng. Part C Methods 23, 700–709 (2017).
61. S. A. O'Leary, J. M. Link, E. O. Klineberg, J. C. Hu, K. A. Athanasiou, Characterization of facet joint cartilage properties in the human and interspecies comparisons, Acta Biomater. 54, 367–376 (2017).
62. C. J. Moran, A. Ramesh, P. A. J. Brama, J. M. O'byrne, F. J. O'brien, T. J. Levingstone, The benefits and limitations of animal models for translational research in cartilage repair, (2011), doi:10.1186/s40634-015-0037-x.
63. A. G. Bonilla, Equine bone cysts: What do we know about them and their treatment?, (2019), doi:10.1111/eve.13212.
64. H. X. Audrey, H. R. Bin Abd Razak, T. H. C. Andrew, The Truth Behind Subchondral Cysts in Osteoarthritis of the Knee, Open Orthop. J. 8, 7–10 (2014).
65. B. von Rechenberg, M. K. Akens, D. Nadler, P. Bittmann, K. Zlinszky, A. Kutter, A. R. Poole, J. A. Auer, Changes in subchondral bone in cartilage resurfacing - An experimental study in sheep using different types of osteochondral grafts, Osteoarthr. Cartil. 11, 265–277 (2003).
66. P. Orth, L. Goebel, U. Wolfram, M. F. Ong, S. Gräber, D. Kohn, M. Cucchiarini, A. Ignatius, D. Pape, H. Madry, Effect of subchondral drilling on the microarchitecture of subchondral bone: Analysis in a large animal model at 6 months, Am. J. Sports Med. 40, 828–836 (2012).
67. D. W. Jackson, P. A. Lalor, H. M. Aberman, T. M. Simon, Spontaneous repair of full-thickness defects of articular cartilage in a goat model, J Bone Jt. Surg 23-A, 53–64 (2001).
68. A. L. Pallante-Kichura, E. Cory, W. D. Bugbee, R. L. Sah, Bone Cysts After Osteochondral Allograft Repair of Cartilage Defects in Goats Suggest Abnormal Interaction Between Subchondral Bone and Overlying Synovial Joint Tissues, (2013), doi:10.1016/j.bone.2013.08.011.
69. C. W. McIlwraith, D. D. Frisbie, C. E. Kawcak, The horse as a model of naturally occurring osteoarthritis, Bone Joint Res. 1, 297–309 (2012).
70. A. Kol, B. Arzi, K. A. Athanasiou, D. L. Farmer, J. A. Nolta, R. B. Rebhun, X. Chen, L. G. Griffiths, F. J. M. Verstraete, C. J. Murphy, D. L. Borjesson, Companion animals: Translational scientist's new best friends, Sci. Transl. Med. 7, 308ps21-308ps21 (2015).
71. R. C. Murray, C. F. Zhu, A. E. Goodship, K. H. Lakhani, C. M. Agrawal, K. A. Athanasiou, Exercise affects the mechanical properties and histological appearance of equine articular cartilage, J. Orthop. Res. 17, 725–731 (1999).
72. K. Athanasiou, D. Korvick, R. Schenck, Biodegradable Implants for the Treatment of Osteochondral Defects in a Goat Model, https://home.liebertpub.com/ten 3, 363–373 (1997).
73. M. C. H. Van Der Meulen, G. S. Beaupré, R. Lane Smith, V. L. Giddings, W. A. Allen, K. A. Athanasiou, C. Fang Zhu, J. A. Mandell, Y. Song, R. D. Poser, S. B. Goodman, Factors influencing

changes in articular cartilage following hemiarthroplasty in sheep, J. Orthop. Res. 20, 669–675 (2002).
74. N. Vapniarsky, L. W. Huwe, B. Arzi, M. K. Houghton, M. E. Wong, J. W. Wilson, D. C. Hatcher, J. C. Hu, K. A. Athanasiou, Tissue engineering toward temporomandibular joint disc regeneration, Sci. Transl. Med. 10, eaaq1802 (2018).
75. J. K. Lunney, A. Van Goor, K. E. Walker, T. Hailstock, J. Franklin, C. Dai, Importance of the pig as a human biomedical model, Sci. Transl. Med. 13 (2021), doi:10.1126/SCITRANSLMED.ABD5758.
76. M. Sennett, J. Friedman, B. Ashley, B. Stoeckl, J. Patel, M. Alini, M. Cucchiarini, D. Eglin, H. Madry, A. Mata, C. Semino, M. Stoddart3, F. T. Moutos, B. T. Estes, F. Guilak, R. Mauck, G. Dodge, Long Term Outcomes of Biomaterial-Mediated Repair of Focal Cartilage Defects in a Large Animal Model, Ors2019 , 2019 (2019).
77. T. Gotterbarm, S. J. Breusch, U. Schneider, M. Jung, The minipig model for experimental chondral and osteochondral defect repair in tissue engineering: Retrospective analysis of 180 defects, Lab. Anim. 42, 71–82 (2008).
78. M. B. Fisher, N. S. Belkin, A. H. Milby, E. A. Henning, M. Bostrom, M. Kim, C. Pfeifer, G. Meloni, G. R. Dodge, J. A. Burdick, T. P. Schaer, D. R. Steinberg, R. L. Mauck, Cartilage Repair and Subchondral Bone Remodeling in Response to Focal Lesions in a Mini-Pig Model: Implications for Tissue Engineering, Tissue Eng. Part A 21, 850–860 (2015).
79. C. G. Pfeifer, M. B. Fisher, V. Saxena, M. Kim, E. A. Henning, D. A. Steinberg, G. R. Dodge, R. L. Mauck, Age-Dependent Subchondral Bone Remodeling and Cartilage Repair in a Minipig Defect Model, Tissue Eng. Part C Methods 23, 745–753 (2017).
80. T. Gotterbarm, W. Richter, M. Jung, S. Berardi Vilei, P. Mainil-Varlet, T. Yamashita, S. J. Breusch, An *in vivo* study of a growth-factor enhanced, cell free, two-layered collagen-tricalcium phosphate in deep osteochondral defects, Biomaterials 27, 3387–3395 (2006).
81. M. Jung, B. Kaszap, A. Redöhl, E. Steck, S. Breusch, W. Richter, T. Gotterbarm, Enhanced early tissue regeneration after matrix-assisted autologous mesenchymal stem cell transplantation in full thickness chondral defects in a minipig model, Cell Transplant. 18, 923–932 (2009).
82. P. Orth, H. Madry, A low morbidity surgical approach to the sheep femoral trochlea, BMC Musculoskelet. Disord. 14 (2013), doi:10.1186/1471-2474-14-5.
83. F. Di Dona, G. Della Valle, G. Fatone, Patellar luxation in dogs, Vet. Med. Res. Reports Volume 9, 23–32 (2018).
84. A. L. Johnson, K. D. Broaddus, J. G. Hauptman, S. Marsh, J. Monsere, G. Sepulveda, Vertical patellar position in large-breed dogs with clinically normal stifles and large-breed dogs with medial patellar luxation, Vet. Surg. 35, 78–81 (2006).
85. A. A. Mostafa, D. J. Griffon, M. W. Thomas, P. D. Constable, Proximodistal alignment of the canine patella: Radiographic evaluation and association with medial and lateral patellar luxation, Vet. Surg. 37, 201–211 (2008).
86. M. B. Bonadio, J. M. Friedman, M. L. Sennett, R. L. Mauck, G. R. Dodge, H. Madry, A retinaculum-sparing surgical approach preserves porcine stifle joint cartilage in an experimental animal model of cartilage repair, J. Exp. Orthop. 4 (2017), doi:10.1186/s40634-017-0083-7.
87. B. B. Christensen, C. B. Foldager, M. L. Olesen, L. Vingtoft, J. H. D. Rölfing, S. Ringgaard, M. Lind, Experimental articular cartilage repair in the Göttingen minipig: the influence of multiple defects per knee, J. Exp. Orthop. 2, 1–11 (2015).

88. D. D. Frisbie, S. Morisset, C. P. Ho, W. G. Rodkey, J. R. Steadman, C. W. McIlwraith, Effects of calcified cartilage on healing of chondral defects treated with microfracture in horses, Am. J. Sports Med. (2006), doi:10.1177/0363546506289882.
89. B. R. Mandelbaum, † Md, J. E. Browne, F. Fu, L. Micheli, J. B. Mosely, C. Erggelet, T. Minas, L. Peterson, Current Concepts Articular Cartilage Lesions of the Knee, (1998).
90. B. B. Hinckel, D. Thomas, E. E. Vellios, K. J. Hancock, J. G. Calcei, S. L. Sherman, C. D. Eliasberg, T. L. Fernandes, J. Farr, C. Lattermann, A. H. Gomoll, Algorithm for Treatment of Focal Cartilage Defects of the Knee: Classic and New Procedures, Cartilage 13, 473S-495S (2021).
91. E. B. Hunziker, The elusive path to cartilage regeneration, Adv. Mater. 21, 3419–3424 (2009).
92. J. M. Friedman, M. L. Sennett, M. B. Bonadio, K. O. Orji, A. L. Neuwirth, N. Keah, J. L. Carey, F. T. Moutos, B. T. Estes, F. Guilak, H. Madry, R. L. Mauck, G. R. Dodge, Comparison of Fixation Techniques of 3D-Woven Poly(ϵ-Caprolactone) Scaffolds for Cartilage Repair in a Weightbearing Porcine Large Animal Model, Cartilage 9, 428–437 (2018).
93. J. C. Eisenach, D. S. Warner, T. T. Houle, Reporting of preclinical research in anesthesiology transparency and enforcementAnesthesiology 124, 763–765 (2016).
94. K. L. Rafferty, Z. J. Liu, W. Ye, A. L. Navarrete, T. T. Nguyen, A. Salamati, S. W. Herring, Botulinum toxin in masticatory muscles: Short- and long-term effects on muscle, bone, and craniofacial function in adult rabbits, Bone 50, 651–662 (2012).
95. D. S. Sparks, S. Saifzadeh, F. M. Savi, C. E. Dlaska, A. Berner, J. Henkel, J. C. Reichert, M. Wullschleger, J. Ren, A. Cipitria, J. A. McGovern, R. Steck, M. Wagels, M. A. Woodruff, M. A. Schuetz, D. W. Hutmacher, A preclinical large-animal model for the assessment of critical-size load-bearing bone defect reconstruction, Nat. Protoc. 15, 877–924 (2020).
96. MACI ® (autologous cultured chondrocytes on porcine collagen membrane) Cellular sheet for autologous implantation, (available at https://www.fda.gov/downloads/BiologicsBloodVaccines/Vaccines/ApprovedProducts/UCM142569.pdf).
97. US Food and Drug Administration, GINTUIT (Allogeneic Cultured Keratinocytes and Fibroblasts in Bovine Collagen) (2018) (available at https://www.fda.gov/vaccines-blood-biologics/cellular-gene-therapy-products/gintuit-allogeneic-cultured-keratinocytes-and-fibroblasts-bovine-collagen).
98. US Food and Drug Administration, STRATAGRAFT (2021) (available at https://www.fda.gov/vaccines-blood-biologics/stratagraft).
99. US Food and Drug Administration, ABECMA (idecabtagene vicleucel) (2021) (available at https://www.fda.gov/vaccines-blood-biologics/abecma-idecabtagene-vicleucel).
100. US Food and Drug Administration, BREYANZI (lisocabtagene maraleucel) (2021) (available at https://www.fda.gov/vaccines-blood-biologics/cellular-gene-therapy-products/breyanzi-lisocabtagene-maraleucel).
101. F. Guilak, Biological Resurfacing in a Canine Model of Hip Osteoarthritis ORS 2019 Annual Meeting Paper No . 0092, , 55042 (2019).
102. K. M. McLennan, A. L. Miller, E. Dalla Costa, D. Stucke, M. J. Corke, D. M. Broom, M. C. Leach, Conceptual and methodological issues relating to pain assessment in mammals: The development and utilisation of pain facial expression scales, Appl. Anim. Behav. Sci. 217, 1–15 (2019).

103. S. H. Ison, R. Eddie Clutton, P. Di Giminiani, K. M. D. Rutherford, A review of pain assessment in pigs, Front. Vet. Sci. 3, 1–16 (2016).
104. ASTM International, Standard Guide for *in vivo* Assessment of Implantable Devices Intended to Repair or Regenerate Articular Cartilage F2451 − 05 (Withdrawn 2019), ASTM Int. (2010) (available at https://www.astm.org/f2451-05r10.html).
105. J. A. Clayton, Studying both sexes: A guiding principle for biomedicine, FASEB J. 30, 519–524 (2016).
106. NOT-OD-15-102: Consideration of Sex as a Biological Variable in NIH-funded Research (available at https://grants.nih.gov/grants/guide/notice-files/not-od-15-102.html).
107. N. J. Castro, G. Babakhanova, J. Hu, K. A. Athanasiou, Nondestructive testing of native and tissue-engineered medical products: adding numbers to pictures, Trends Biotechnol. 40, 194–209 (2022).
108. C. Okinda, I. Nyalala, T. Korohou, C. Okinda, J. Wang, T. Achieng, P. Wamalwa, T. Mang, M. Shen, A review on computer vision systems in monitoring of poultry: A welfare perspective, Artif. Intell. Agric. 4, 184–208 (2020).
109. US Food and Drug Administration, LAVIV (Azficel-T) (2018) (available at https://www.fda.gov/vaccines-blood-biologics/cellular-gene-therapy-products/laviv-azficel-t).
110. US Food and Drug Administration, RETHYMIC (2021) (available at https://www.fda.gov/vaccines-blood-biologics/rethymic).
111. US Food and Drug Administration, KYMRIAH (tisagenlecleucel) (2021) (available at https://www.fda.gov/vaccines-blood-biologics/cellular-gene-therapy-products/kymriah-tisagenlecleucel).
112. US Food and Drug Administration, PROVENGE (sipuleucel-T) (2019) (available at https://www.fda.gov/vaccines-blood-biologics/cellular-gene-therapy-products/provenge-sipuleucel-t).
113. US Food and Drug Administration, TECARTUS (brexucabtagene autoleucel) (2021) (available at https://www.fda.gov/vaccines-blood-biologics/cellular-gene-therapy-products/tecartus-brexucabtagene-autoleucel).
114. US Food and Drug Administration, YESCARTA (axicabtagene ciloleucel) (2022) (available at https://www.fda.gov/vaccines-blood-biologics/cellular-gene-therapy-products/yescarta-axicabtagene-ciloleucel).
115. US Food and Drug Administration, IMLYGIC (2021) (available at https://www.fda.gov/vaccines-blood-biologics/cellular-gene-therapy-products/imlygic).
116. US Food and Drug Administration, LUXTURNA (2018) (available at https://www.fda.gov/vaccines-blood-biologics/cellular-gene-therapy-products/luxturna).
117. US Food and Drug Administration, ZOLGENSMA (2021) (available at https://www.fda.gov/vaccines-blood-biologics/zolgensma).
118. US Food and Drug Administration, Guidance for FDA Reviewers and Sponsors: Content and Review of Chemistry, Manufacturing, and Control (CMC) Information for Human Somatic Cell Therapy Investigational New Drug Applications (INDs) (2008) (available at https://www.fda.gov/regulatory-information/search-fda-guidance-documents/content-and-review-chemistry-manufacturing-and-control-cmc-information-human-somatic-cell-therapy).

119. US Food and Drug Administration, 21 CFR Part 610 -- General Biological Products Standards, (1973) (available at https://www.ecfr.gov/current/title-21/chapter-I/subchapter-F/part-610).
120. International Conference on Harmonisation, Preclinical Safety Evaluation Of Biotechnology-Derived Pharmaceuticals S6(R1) (2011) (available at https://www.ich.org/page/safety-guidelines).
121. International Conference on Harmonisation, Guidance On Genotoxicity Testing And Data Interpretation For Pharmaceuticals Intended For Human Use S2(R1) (2011) (available at https://www.ich.org/page/safety-guidelines).
122. International Conference on Harmonisation, Testing For Carcinogenicity Of Pharmaceuticals S1B (1997) (available at https://www.ich.org/page/safety-guidelines).
123. International Conference on Harmonisation, Duration Of Chronic Toxicity Testing In Animals (Rodent And Non Rodent Toxicity Testing) S4 (1998) (available at https://www.ich.org/page/safety-guidelines).
124. International Conference on Harmonisation, Note For Guidance On Toxicokinetics: The Assessment Of Systemic Exposure In Toxicity Studies S3A (1994) (available at https://www.ich.org/page/safety-guidelines).
125. International Conference on Harmonisation, Safety Pharmacology Studies For Human Pharmaceuticals S7A (2000) (available at https://www.ich.org/page/safety-guidelines).
126. International Conference on Harmonisation, Detection Of Reproductive And Developmental Toxicity For Human Pharmaceuticals S5(R3), (2020) (available at https://www.ich.org/page/safety-guidelines).
127. International Conference on Harmonisation, Immunotoxicity Studies For Human Pharmaceuticals S8 (2005) (available at https://www.ich.org/page/safety-guidelines).
128. US Food and Drug Administration, Use of International Standard ISO 10993-1, “Biological evaluation of medical devices - Part 1: Evaluation and testing within a risk management process,” (2020) (available at https://www.fda.gov/regulatory-information/search-fda-guidance-documents/use-international-standard-iso-10993-1-biological-evaluation-medical-devices-part-1-evaluation-and).
129. K. A. Athanasiou, G. G. Niederauer, R. C. Schenck Jr., Biomechanical topography of human ankle cartilage, Ann Biomed Eng 23, 697–704 (1995).
130. V. C. Mow, S. C. Kuei, W. M. Lai, C. G. Armstrong, Biphasic creep and stress relaxation of articular cartilage in compression? Theory and experiments, J Biomech Eng 102, 73–84 (1980).
131. M. K. Murphy, B. Arzi, J. C. Hu, K. A. Athanasiou, Tensile characterization of porcine temporomandibular joint disc attachments, J Dent Res 92, 753–758 (2013).
132. G. Espinosa, G. Otarola, J. C. Hu, K. A. Athanasiou, Cartilage assessment requires a surface characterization protocol: roughness, friction, and function, Tissue Eng. Part C Methods , ten.TEC.2020.0367 (2021).
133. R. C. Nordberg, M. G. Espinosa, J. C. Hu, K. A. Athanasiou, A Tribological Comparison of Facet Joint, Sacroiliac Joint, and Knee Cartilage in the Yucatan Minipig., Cartilage , 19476035211021904 (2021).
134. S. Knecht, C. Erggelet, M. Endres, M. Sittinger, C. Kaps, E. Stussi, Mechanical testing of fixation techniques for scaffold-based tissue-engineered grafts, J Biomed Mater Res B Appl Biomater 83, 50–57 (2007).

135. J. M. Link, J. C. Hu, K. A. Athanasiou, Chondroitinase ABC Enhances Integration of Self-Assembled Articular Cartilage, but Its Dosage Needs to Be Moderated Based on Neocartilage Maturity, Cartilage 13, 672S-683S (2021).
136. M. Trimborn, M. Endres, C. Bommer, U. Janke, J. P. Kruger, L. Morawietz, P. C. Kreuz, C. Kaps, Karyotyping of human chondrocytes in scaffold-assisted cartilage tissue engineering, Acta Biomater 8, 1519–1529 (2012).
137. J. W. Calvert, K. Brenner, M. DaCosta-Iyer, G. R. Evans, R. K. Daniel, Histological analysis of human diced cartilage grafts, Plast Reconstr Surg 118, 230–236 (2006).
138. D. D. Cissell, J. M. Link, J. C. Hu, K. A. Athanasiou, A Modified Hydroxyproline Assay Based on Hydrochloric Acid in Ehrlich's Solution Accurately Measures Tissue Collagen Content, Tissue Eng Part C Methods 23, 243–250 (2017).
139. R. W. Farndale, C. A. Sayers, A. J. Barrett, A direct spectrophotometric microassay for sulfated glycosaminoglycans in cartilage cultures, Connect Tissue Res 9, 247–248 (1982).
140. V. L. Singer, L. J. Jones, S. T. Yue, R. P. Haugland, Characterization of PicoGreen reagent and development of a fluorescence-based solution assay for double-stranded DNA quantitation, Anal Biochem 249, 228–238 (1997).
141. B. J. Bielajew, J. C. Hu, K. A. Athanasiou, Methodology to Quantify Collagen Subtypes and Crosslinks: Application in Minipig Cartilages, Cartilage 13, 1742S-1754S (2021).
142. S. Netukova, T. Duspivova, J. Tesar, M. Bejtic, M. Baxa, Z. Ellederova, Z. Szabo, R. Krupicka, Instrumented pig gait analysis: State-of-the-art, J. Vet. Behav. 45, 51–59 (2021).

CHAPTER 2: Cartilage assessment requires a surface characterization protocol: roughness, friction, and function

Abstract

The surface of articular cartilage is integral to smooth, low-friction joint articulation. However, the majority of cartilage literature rarely includes measurements of surface characteristics and function. This may, in part, be due to a shortage of or unfamiliarity with fast, non-destructive, and, preferably, non-contact methods that can be applied to large cartilage surfaces for evaluating cartilage surface characteristics. A comprehensive methodology for characterizing cartilage surfaces is useful in determining changes in tissue function, as for example in cases where the quality of cartilage grafts needs to be assessed. With cartilage storage conditions being an area of ongoing and active research, this study used interferometry and tribology methods as efficient and non-destructive ways of evaluating changes in cartilage surface topography, roughness, and coefficient of friction resulting from various storage temperatures and durations. Standard, destructive testing for bulk mechanical and biochemical properties, as well as immunohistochemistry, were also performed. For the first time, interferometry was used to show cartilage topographical anisotropy through an anterior-posterior striated pattern in the same direction as joint articulation. Another novel observation enabled by tribology was frictional anisotropy, illustrated by a 53% increase in coefficient of friction in the medial-lateral direction compared to the anterior-posterior direction. Of the storage conditions examined, 37°C, 4°C, -20°C, and -80°C for 1 day, 1 week, and 1 month, a 49% decrease in coefficient of friction was observed at 1 week in -80°C. Interestingly, prolonged storage at 37°C resulted in up to an 83% increase in the compressive aggregate modulus by 1 month, with a corresponding increase in the GAG bulk content. This study illustrates the differential effects of storage conditions on cartilage:

Chapter published as: Espinosa, M.G.,* Otarola, G.A.,* Hu, J.C., Athanasiou, K.A. Cartilage assessment requires a surface characterization protocol: roughness, friction, and function. Tissue Engineering Part C; 27(4): 276-286. (*These authors contributed equally.)

freezing tends to target surface properties, while non-freezing storage impacts the tissue bulk. These data show that a bulk-only analysis of cartilage function is not sufficient or representative. The non-destructive surface characterization assays described here enable improvement in cartilage functionality assessment by considering both surface and bulk cartilage properties; this methodology may thus provide a new angle to explore in future cartilage research and tissue engineering endeavors.

Introduction

Cartilage biomechanical function hinges on the tissue's ability to promote both load distribution and low-friction articulation. Preservation of cartilage functionality is of great clinical value, particularly with regards to the use of osteochondral allografts (1). Although allograft functionality is primarily determined by cell viability (2), assessments of biomechanical properties can provide important insights into the success or failure of transplanted tissue. Currently, assessments of articular cartilage mechanical function provide an exceptional amount of information on the bulk tissue properties that confer cartilage's load transferring capability (3). These properties are tested using a wide variety of loading paradigms, including compression, tension, and shear (4). However, few of these protocols include evaluations of the cartilage surface, thus, ignoring the surface's crucial role in smooth joint articulation (5). The lack of surface characterization data is illustrated in a recent review showing that only about 10% of studies on "articular cartilage mechanical testing" from 2009 to 2019 provided surface lubrication data along with bulk mechanical measures (3). Increased investigation in this area will improve the field's current understanding of cartilage function and would be facilitated by the development of a cartilage functionality assessment protocol that includes both bulk and surface characterization.

Articular cartilage's surface function heavily depends on friction, topography, and lubrication. Tribology is often performed to measure the coefficient of friction (CoF) between

cartilage and a testing substrate material, such as polished glass or metals commonly used for implants (6, 7). The CoF broadly describes the interaction between cartilage and other surfaces, but does not provide mechanistic information. To further elucidate a surface-specific structure-function relationship, elements that contribute to the CoF, such as topography and lubrication, must also be considered. White-light interferometry is a non-contact imaging modality that can quickly capture surface topography; however, interferometry has been underused in cartilage research (8). While atomic force microscopy excels at providing nano-scale detail (9), interferometry functions at a larger scale that may be more relevant to assessing overall cartilage function. The impact of topographical imperfections is lessened with increased lubrication. Products of the proteoglycan 4 (PRG4) gene, such as lubricin and surface zone protein (SZP), are well known to enhance boundary lubrication at the cartilage surface and can be localized using immunohistochemistry (IHC) (5), Inclusion of these three surface-related metrics is rarely found in the literature but would greatly enhance evaluations of cartilage function.

Despite decades of study, the preservation of articular cartilage function after long-term storage remains a topic of great interest to both clinicians and basic scientists. The increasing demand for osteochondral allografts (10) and required 14-day donor screening period (1) have resulted in a need for transplant storage. Many preservation studies have focused on cell viability, finding that refrigeration best maintains viability above the 70% threshold generally accepted for allograft use (2, 10). It is also known that cell viability is greatly reduced with freezing (11). Since viability has been extensively studied, the present work is instead focused on the role of surface and bulk tissue properties. The maintenance of these properties is also important in the context of the basic science laboratory. Lengthy experimental protocols commonly used in cartilage research often require tissue storage for long-term functional maintenance. The current understanding amongst most researchers is that cartilage bulk mechanical properties remain intact with freezing (11). but deteriorate with extended refrigeration of three weeks or more (12,

13). Although the cartilage preservation literature is expansive, minimal attention has been given to surface changes due to storage.

Surprisingly, little is known about the effect of storage on cartilage surface properties considering how sliding and lubrication are key to joint function. Prior work has shown that storage-associated cell death is predominantly observed in the superficial zone (14), suggesting that tissue surface properties may be particularly sensitive to storage. Conflicting data from other surface-related assays (15, 16), however, motivate additional research. For example, there was no difference in CoFs between samples stored at 2°C and -80°C (15), but they were not compared to a pre-storage control. In contrast, another study showed that freezing at -70°C had a detrimental effect on PRG4 secretion compared to fresh samples stored at 4°C (16). Clearly, additional work is necessary to understand how storage conditions impact different aspects of cartilage surface function.

The objective of this study was to develop a comprehensive methodology to not only characterize bulk properties but also surface characteristics. Following the establishment of this methodology, we wanted to apply it and determine the effect of storage temperature and duration on surface and bulk cartilage functionality. In addition to a standard array of bulk tissue assays, surface properties using interferometry, tribology, and lubricin IHC were examined. These data will be used to test the hypothesis that surface characteristics significantly change after storage. The results from this work will not only elucidate the impact that frequently used storage protocols have on cartilage surface properties, but also serve as a model for incorporating surface characterization in future cartilage-related studies.

Method

The Method consists of a set of three surface characterization assays: interferometry, tribology, and lubricin IHC. Each of these contributes complementary information regarding the state of the cartilage surface. The Method will then be applied to the Experiment below.

Interferometry

Surface topography was measured using a 20X Mirau objective on an MSA-500 Micro System Analyzer (Polytec, Waldbronn, Germany). Cartilage punches were placed on the stage and lightly blotted to remove excess moisture. When necessary, the stage was tilted to ensure that the sample surface was perpendicular to the objective. The system's focus was adjusted until an interference fringe pattern was clearly observed. Measurement start point was defined as the point where the fringe pattern was first seen, and the endpoint was defined as when the fringe pattern is no longer visible, and topographical data were collected. The topographical data were rendered into images that demonstrate the sample's surface features. Scan times ranged from 45 seconds to 1.5 minutes per sample.

The TMS 3.8 software (Polytec) was used for postprocessing and roughness quantification. A linear regression was applied to the topographical data to correct for any remaining physical tilt. This was followed by a Gaussian low pass filter set to a 1.5μm cutoff wavelength. Average surface roughness (S_a) was then determined for each sample's processed topographical data. Images exported from the Polytec software were further analyzed using the Directionality plugin in ImageJ (National Institutes of Health) and the Circular Statistics toolbox in Matlab (17) to determine anisotropy. The degree of alignment for the observed surface features is defined such that 1 denotes perfect alignment, i.e., all features are aligned in the same direction (18). Greater alignment denotes greater anisotropy.

Tribology

Separate from the samples described in the Experiment, additional, fresh cartilage samples (n=6) were harvested to assess the tribological dependence on measurement direction. Harvested samples were marked for their anatomical directional orientation using India ink. Tribology was performed using a custom-made pin-on-plate tribometer under boundary lubrication conditions (7), with velocity set to 1mm/s and a compressive normal force applied by a 300g weight. The samples were allowed to equilibrate for two minutes and then sheared against the test surface for five minutes. The measured CoF describes the interaction between the articular cartilage sample and the underlying glass plate immersed in phosphate buffered saline (PBS). Each sample was measured along the anterior-posterior and medial-lateral directions.

Immunohistochemistry

Immunohistochemistry (IHC) was used to detect lubricin on the articular surface. Samples were fixed in 10% neutral-buffered formalin, dehydrated, embedded in paraffin, and sectioned at a thickness of 6µm. Sections on silanized slides were baked at 60°C in 2mL of formalin for 1 hour. Sections were quenched of endogenous peroxidase activity using a 3% hydrogen peroxide in methanol solution. Antigen retrieval was performed in citrate buffer at 90-100°C for 30 minutes. After blocking, the slides were incubated overnight with a 1:500 dilution of the mouse anti-lubricin antibody, clone 9G3 (Sigma) at 4°C. Secondary antibody incubation and color development were performed using the mouse IgG Vectastain ABC kit and DAB (Vector Laboratories).

Experiment

The Method described above was applied here to discern surface changes due to the storage of cartilage. Five bovine knee joints from 2-4 week-old calves were obtained 48 hours post-mortem (Research 87). Seventy-two articular cartilage explants from the medial and lateral condyles were harvested using 7mm biopsy punches. The punches were marked to indicate their orientation on the condyle by placing sterile-filtered India ink at the punch's most anterior point. The punches were stored at various storage conditions, detailed below.

Storage conditions

This study employed a full-factorial design of storage temperature (37°C, 4°C, -20°C, and -80°C) and duration (1 day, 1 week, and 1 month) for a total of 12 groups. In this study, 1 month is defined as 4 weeks. Explants were randomly assigned to groups to avoid variation due to the topographic location of the sample. For the 37°C and 4°C conditions, explants were kept in Dulbecco's Modified Eagle Medium containing 4.5g/L glucose and GlutaMAX (DMEM, Gibco), 1% (v/v) penicillin/streptomycin/fungizone (PSF, Lonza), and 25mM HEPES buffer. Samples stored at -20°C and -80°C were placed in individual microcentrifuge tubes. Samples stored at -80°C were snap frozen in liquid nitrogen.

Surface characterization

After storage, explants were trimmed to a 1mm thickness inclusive of the surface zone to ensure a consistent thickness across all samples. Maintaining the orientation, three 3mm punches were obtained from each explant for tribology and interferometry **(Fig. 1)** as described above. Tribological data were only collected in the anterior-posterior direction. IHC was also performed

from sections of the samples as described above. The remaining tissue was used for mechanical testing (creep indentation and uniaxial tensile testing), biochemical assays, and histology.

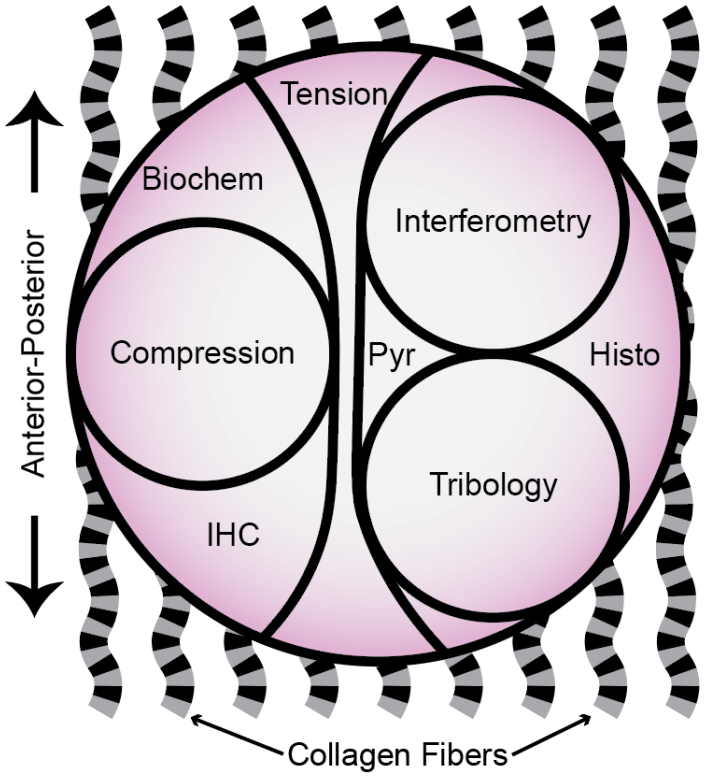

Figure 1. Schematic diagram of the cartilage explants obtained from juvenile bovine femoral condyles and the subdivisions used for mechanical, biochemical, and histological assays. Pyr: pyridinoline crosslinks analysis, Histo: histology, IHC: immunohistochemistry. Wavy, banded lines represent collagen fibers. This schematic illustrates the wide range of assays used to comprehensively examine the effects of storage.

Mechanical testing

Compressive properties of the explants were determined by creep indentation testing. Briefly, 3mm punches obtained from each explant were submerged in PBS and indented with a flat porous 1mm diameter tip perpendicular to the surface of the sample. A tare weight of 0.5g was applied until equilibrium was achieved. Then, a test weight of 7.5-10g was applied, which corresponded

to ~10% strain. The aggregate and shear modulus values were obtained using a biphasic model and finite-element optimization (19). Tensile properties were determined using uniaxial tension in an Instron model 5565 (Instron, Canton, MA). Dogbone-shaped samples were obtained from each explant along the anterior-posterior direction **(Fig. 1)**. The dogbones were photographed to measure thickness and width in ImageJ. The ends of the dogbone were fixed to paper with cyanoacrylate. All samples had a gauge length of 1.55mm. A strain rate of 1% of the gauge length per second was used until failure. The Young's modulus was obtained from the linear region of the stress-strain curve, and the ultimate tensile strength (UTS) was defined as the maximum stress obtained.

Biochemical assays

Cartilage samples were weighed to obtain wet weight (WW), lyophilized, and weighed again to obtain dry weight (DW). Lyophilized samples were digested in 125µg/mL papain (Sigma) +5mM N-acetyl-L-cysteine+5mM EDTA in phosphate buffer pH 6.5 for 18 hours at 60°C. GAG content was quantified using a Blyscan Glycosaminoglycan Assay kit (Biocolor, Newtownabbey, Northern Ireland). Total collagen content was quantified using a modified chloramine-T hydroxyproline assay (20) using Sircol 0.5mg/ml acid-soluble bovine collagen as a standard (Biocolor, Newtownabbey, Northern Ireland). DNA content was quantified with a Picogreen assay (ThermoFisher Scientific). For the quantification of pyridinoline crosslinks, samples were weighed, lyophilized, and acid-digested for 12 hours in 6N HCl at 105°C. After evaporation, each dried hydrolysate was resuspended in a 75%/25% (v/v) solution of 0.1% formic acid and acetonitrile, centrifuged at 15,000g for 5 min, and the supernatant was transferred to a LCMS autosampler vial. Samples were measured via liquid chromatography mass spectrometry using a Cogent diamond hydride HPLC column (2.1mm x 150mm, particle size 2.2µm, pore size 120Å, MicroSolv) and a pyridinoline standard (BOC Sciences) as previously described (21).

Histology

Samples were fixed, dehydrated, embedded, and sectioned as described for IHC above. Sections were subsequently processed and stained with hematoxylin and eosin (H&E), safranin-O and fast green, and picrosirius red using standard protocols (22).

Determination of functionality indices

Previously, a functionality index (FI) was developed to describe, in one value, the bulk characteristics of a sample as compared to a reference sample (23). To differentiate surface and bulk characteristics, the subscripts “s” and “b” are used; i.e., a modified functionality index to represent surface characteristics, or FI_s (**Eq. 1a**), uses values of the CoF and roughness (S_a). The bulk functionality, or FI_b (**Eq. 1b**), includes Young’s modulus (E), UTS, aggregate modulus (H_A), shear modulus (SM), collagen/dry weight (Col), pyridinoline/dry weight (Pyr), and GAG/dry weight (GAG). Differences in cartilage function between each storage condition test group (denoted by superscript “t”) and the 37°C at 1 day control group (denoted by superscript “c”) were quantified using these indices. In addition, a combined FI (**Eq. 1c**) was calculated. In the combined FI, equal weight was apportioned to each assay. Previous iterations of the FI have considered any deviation from the “gold standard” control value a flaw, through the use of absolute values. In the current form of the FI, the possibility for improvement beyond the control is available. For example, an explant may have improved mechanical properties after culturing compared to the unstored control. An FI of 1 indicates that there is no difference with respect to the control group. Improvements will potentially increase the FI to greater than 1. Conversely, degradation of properties will reduce the FI. For the purposes of the present study, decreases in surface properties and increases in bulk properties are deemed as improvements. These assumptions

are based on the need for smooth joint articulation and increased mechanical strength in allografts.

$$FI_s(t|c) = \frac{1}{2}\left[\left(1 - \frac{CoF^t - CoF^c}{CoF^c}\right) + \left(1 - \frac{S_a^t - S_a^c}{S_a^c}\right)\right]$$

(1a)

$$FI_b(t|c) = \frac{1}{7}\left[\begin{array}{c}\left(1 - \frac{E^c - E^t}{E^c}\right) + \left(1 - \frac{UTS^c - UTS^t}{UTS^c}\right) + \left(1 - \frac{H_A^c - H_A^t}{H_A^c}\right) + \left(1 - \frac{SM^c - SM^t}{SM^c}\right) + \\ \left(1 - \frac{Col^c - Col^t}{Col^c}\right) + \left(1 - \frac{Pyr^c - Pyr^t}{Pyr^c}\right) + \left(1 - \frac{GAG^c - GAG^t}{GAG^c}\right)\end{array}\right]$$

(1b)

$$FI(t|c) = \frac{1}{9}\left[\begin{array}{c}\left(1 - \frac{CoF^t - CoF^c}{CoF^c}\right) + \left(1 - \frac{S_a^t - S_a^c}{S_a^c}\right) + \left(1 - \frac{E^c - E^t}{E^c}\right) + \left(1 - \frac{UTS^c - UTS^t}{UTS^c}\right) + \left(1 - \frac{H_A^c - H_A^t}{H_A^c}\right) + \\ \left(1 - \frac{SM^c - SM^t}{SM^c}\right) + \left(1 - \frac{Col^c - Col^t}{Col^c}\right) + \left(1 - \frac{Pyr^c - Pyr^t}{Pyr^c}\right) + \left(1 - \frac{GAG^c - GAG^t}{GAG^c}\right)\end{array}\right]$$

(1c)

Statistical analysis

All quantitative data are presented as mean +/- standard deviation. A paired Student's t-test was used to analyze the directional tribology data. Experimental results were analyzed using two-way ANOVA in Prism 8.1 (GraphPad Software) with a sample size of six per group. A Fisher's LSD *post hoc* test was used to identify significant differences between each storage condition and the control condition, defined as 37°C at 1 day. Lastly, one-way ANOVAs with a Fisher's LSD *post hoc* test were used to compare functionality indices within temperature groups.

Results

Topographical and frictional anisotropy

Prior to examining storage effects, interferometry performed on the condylar surface revealed a well-defined striated pattern in the cartilage surface corresponding to the anterior-posterior direction (**Fig**. **2A**). Although this topographical anisotropy was not always observed, likely due to differences in tissue hydration, this is the first time that interferometry was used to show the striated pattern of the cartilage surface.

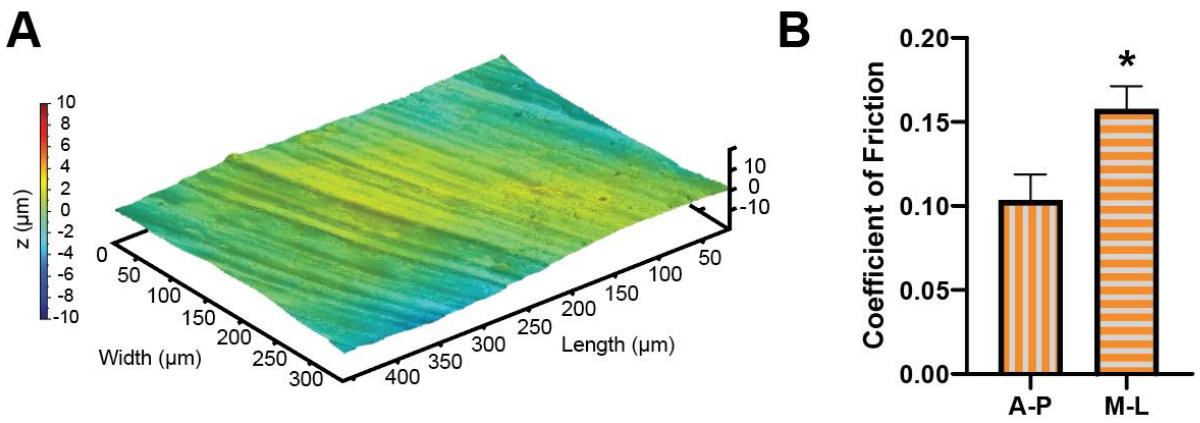

Figure 2. Surface topography impacts tribology measurements. (**A**) A topographical image of a representative sample's surface taken by interferometry reveals a striated pattern in the direction of articulation. (**B**) Tribology measurements performed in the anterior-posterior (A-P) and medial-lateral (M-L) directions indicate that the M-L coefficient of friction is 53% greater than in the A-P direction, providing further support for the anisotropy of articular cartilage surfaces.

Given the observed topographical anisotropy, it was of interest to determine if the functional properties of the articular cartilage surface also vary with the direction of motion. Tribological measurements revealed that a significant difference existed between the CoF obtained along the anterior-posterior and the medial-lateral orientations. When the test was performed in the medial-lateral direction, the CoF was 53% higher (**Fig**. **2B**). The impact of this

novel finding is that it is crucial to control for this topographical and frictional anisotropy for an accurate evaluation of surface-level changes due to storage; the storage data presented below accounted for this anisotropy.

Storage effects on the surface characteristics of cartilage

Storage conditions were found to minimally alter individual surface properties of cartilage. Average surface roughness, determined through interferometry, was significantly reduced at various refrigerated or frozen conditions, starting as early as 1 week (**Fig. 3A**). Despite the changes in roughness, quantification of the surface striation alignment did not reveal changes due to storage time or temperature and averaged at 0.66±0.07 (**Fig**. **3B**). The measurements of CoF were generally lower at frozen temperatures (**Fig**. **3C**). Samples stored at -20°C and -80°C for 1 week showed a 33% and 49% reduction in CoF, respectively, compared to controls ($CoF_{control}$=0.13±0.03), respectively. Our results show that the cartilage surface is unaffected by physiological temperature, but lower temperatures may give rise to surface-level changes.

Localization of lubricin was determined through immunohistochemistry (**Fig**. **4**). As expected and in accordance to its function, coloration against the anti-lubricin antibody revealed the presence of the protein predominantly at the surface after which it rapidly decreases and was only colocalized with lacunae and chondrocytes. No lubricin was found in the deeper zones. Lubricin at the articular surface was not impacted by storage conditions even after a month of storage. However, it is important to note that lubricin cellular localization disappeared at non-physiological temperatures.

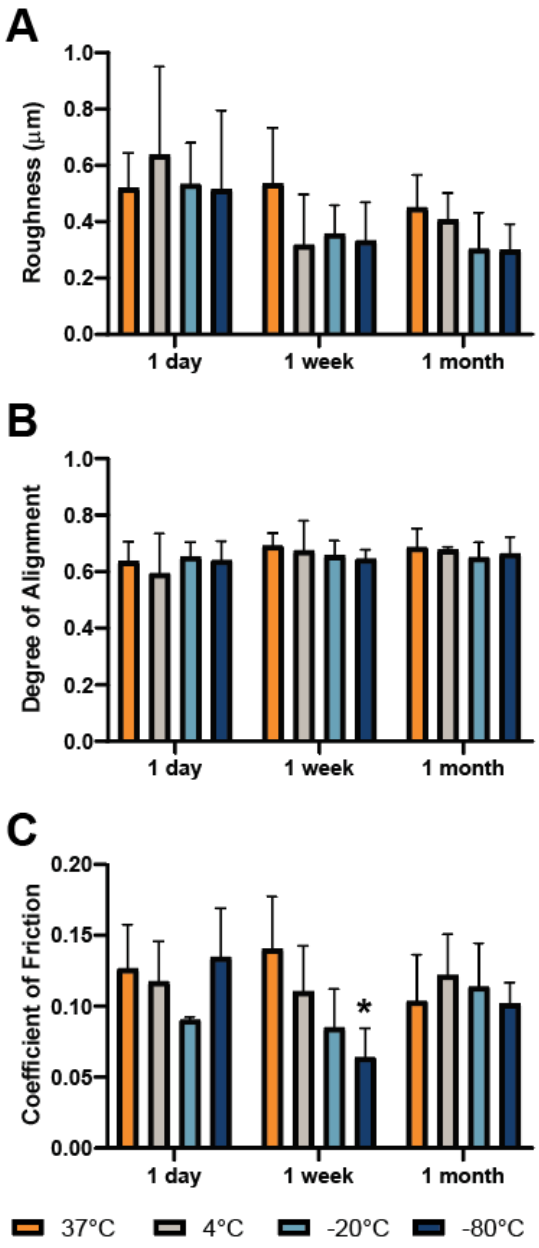

Figure 3. Surface properties are unaffected by storage time or temperature. Using interferometry measurements, no significant differences were detected in (**A**) roughness or (**B**) alignment compared to the control samples (1 day at 37°C). Tribological analysis showed that (**C**) coefficient of friction was also unaffected. These data attest to the stability of the articular cartilage surface.

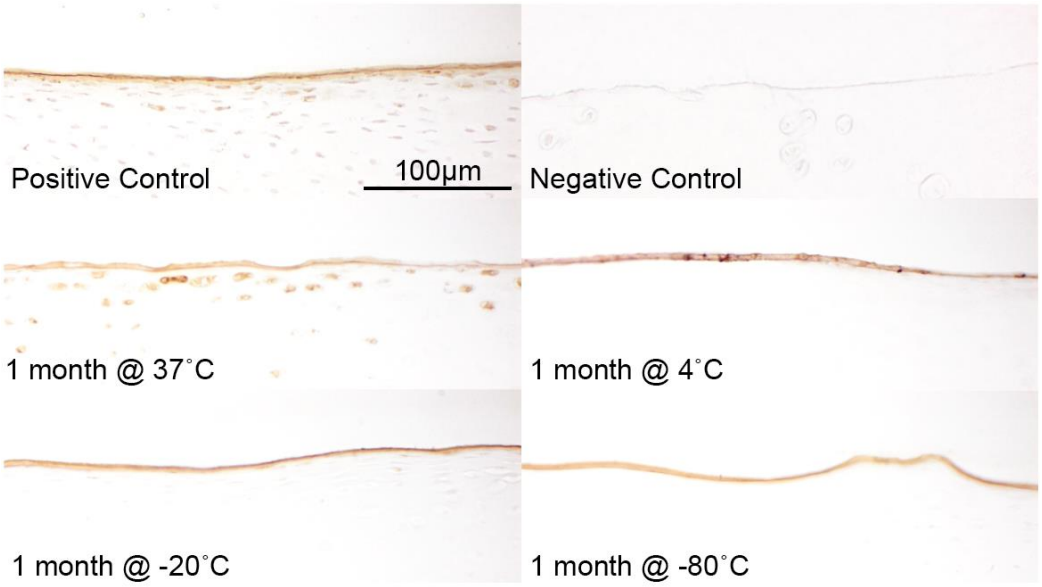

Figure 4. Immunohistochemistry of the femoral condyle. Anti-lubricin shows expression of the protein predominantly in the superficial zone of cartilage in the positive control (1 day at 37°C). No lubricin is detected in non-articulating costal cartilage surfaces (negative control). Even after a month of storage, the surface layer of lubricin is unaffected by temperature, however cellular expression of lubricin is only maintained at 37°C.

Storage effects on the bulk properties of cartilage

Healthy articular cartilage has high biomechanical stability with little to no turnover. However, the tensile mechanical properties of samples stored under different conditions were quite variable. Although the Young's modulus and UTS (**Fig**. **5A-B**) of a few groups significantly differed from the control values (18.2±2.9MPa and 9.9±7.3MPa, respectively) there was no discernable trend in these changes. Biochemical components associated with the tensile properties of cartilage, mainly collagen and pyridinoline crosslinks, were measured at 64.7±7.0% and 0.12±0.01% per dry weight, respectively, for the control group. Their contributions to cartilage content after storage were also variable (**Fig**. **5C-D, Table S1**).

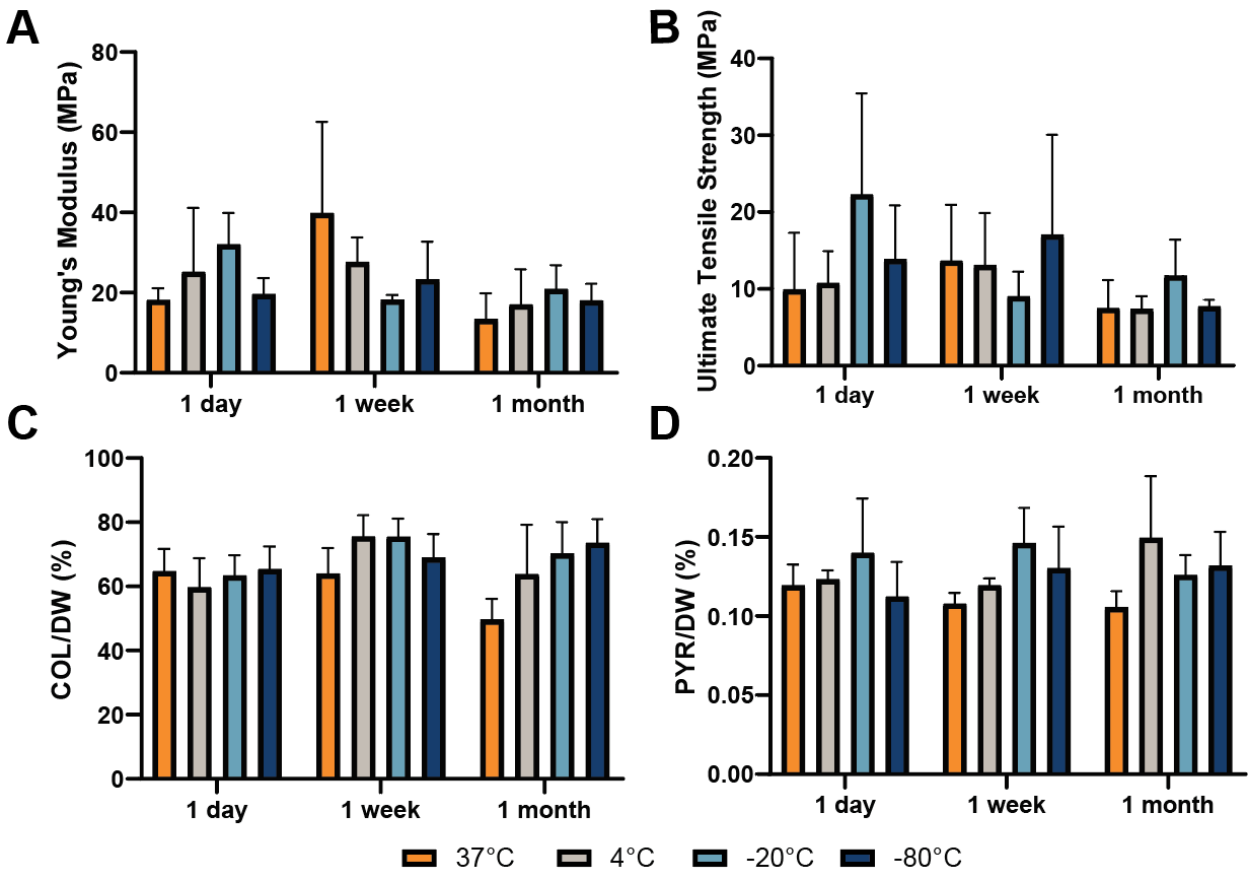

Figure 5. Storage conditions do not affect tensile properties or collagen and pyridinoline content. (**A**) Young's modulus and (**B**) ultimate tensile strength values showed no significant differences at any of the examined temperatures or times compared to the control samples. (**C**) Collagen per dry weight and (**D**) pyridinoline crosslinks per dry weight, both of which are associated with the tensile properties of cartilage, were well maintained for up to a month.

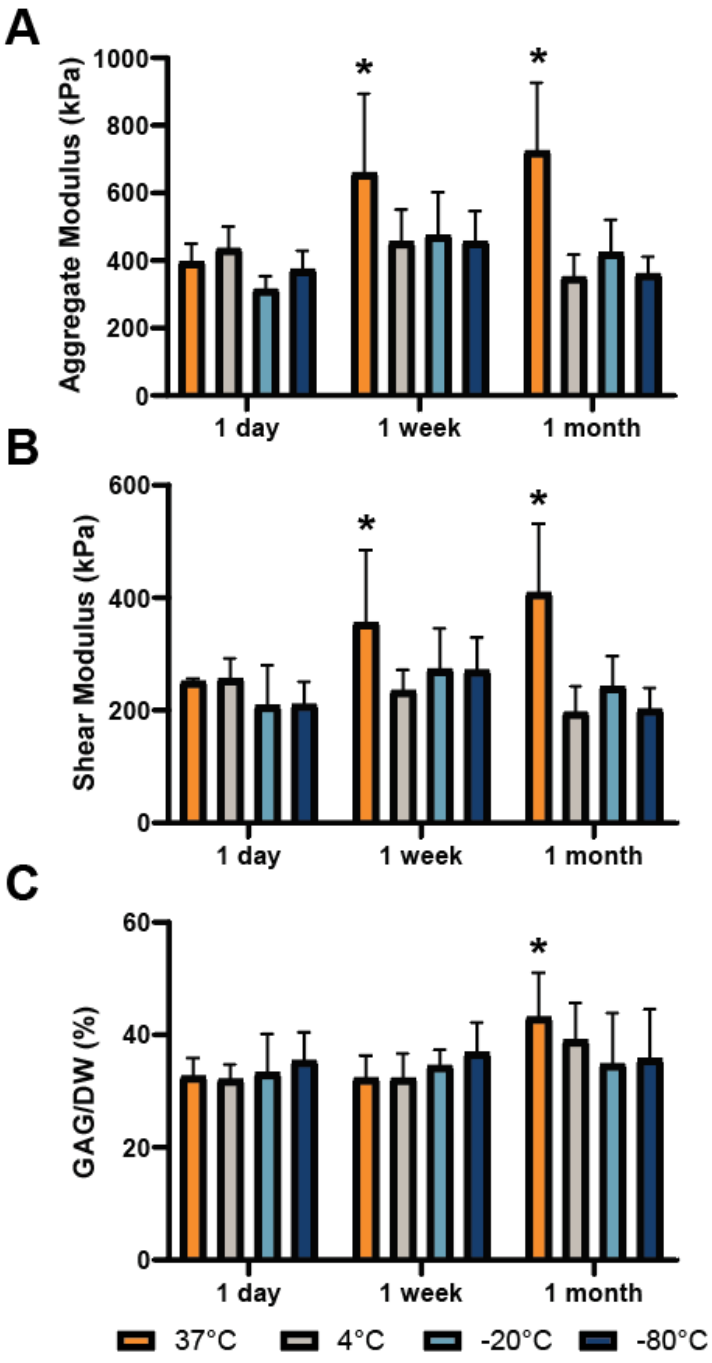

Figure 6. Compressive properties and GAG content increased in samples stored at physiological temperature. A significant increase was found in the (**A**) aggregate modulus and (**B**) shear modulus values of samples stored at 37°C beginning after 1 week. (**C**) GAG normalized by dry weight also increased after a month in samples stored at 37°C. The compressive properties and GAG content were not adversely affected by storage at 4°C or lower.

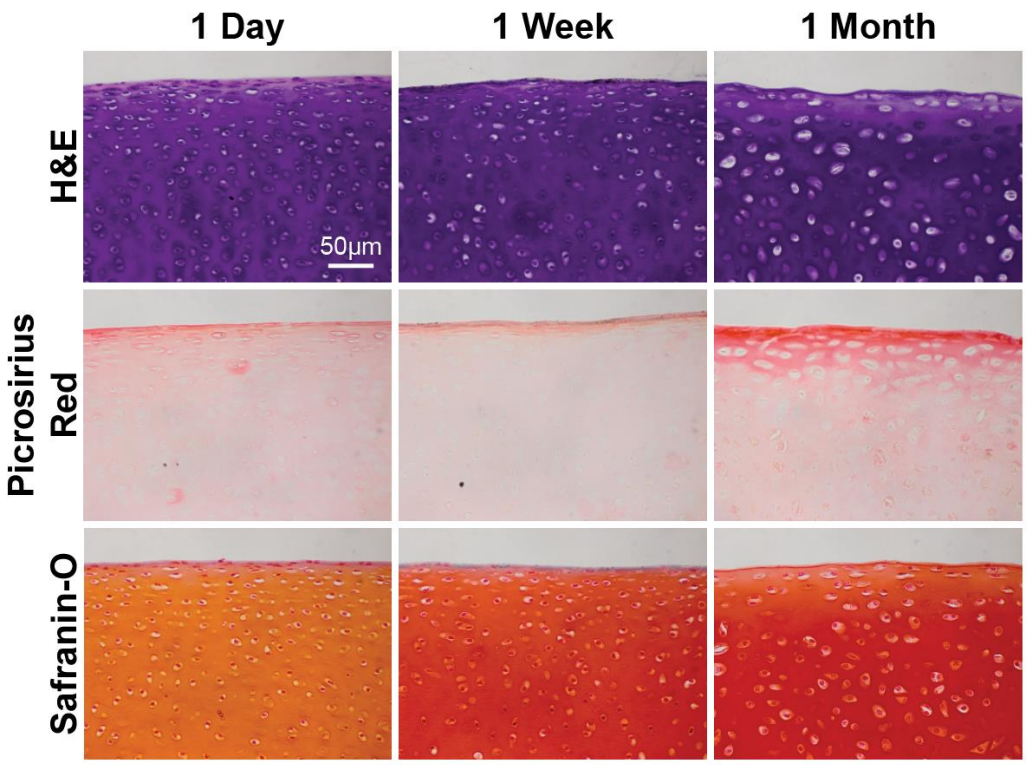

Figure 7. H&E, picrosirius red, and safranin-O stains of samples stored at 37°C. Safranin-O histological stains indicated that the GAG content of cultured cartilage explants increased over time.

While no significant differences in compressive properties were found in explants stored at 4°C, -20°C, and -80°C, prolonged storage at 37°C resulted in 67% and 83% increases in the compressive aggregate modulus value at 1 week and 1 month, respectively, compared to the 395.4±53.9kPa value for the control group (**Fig. 6A**). A significant increase was also observed for the shear modulus value (**Fig. 6B**). Correspondingly, the GAG content, associated with the compressive properties of articular cartilage, was significantly increased by 33% in the same group after 1 month (**Fig. 6C**). Whereas the histological appearance of all other groups besides those stored at 37°C were unremarkable compared to controls, the increase in GAG quantified biochemically was corroborated by histological staining of samples stored at 37°C (**Fig. 7C**).

Table 1. Storage conditions affect surface and bulk functionality (FI) differently. The combined FI incorporates all changes to function. Bolded numbers point to the lowest score per FI category. Colored boxes identify individual surface (green) and bulk (purple) FI values. The colors also denote the source of FI change (surface vs. bulk) in the combined FI. Groups marked with an asterisk (*) are considered significantly different compared to the control.

	Surface FI	**Bulk FI**	**Combined FI**
1 Day			
37°C	Control		
4°C	0.57±0.29	0.79±0.12	0.75±0.10
-20°C	0.71±0.22	0.55±0.26*	0.59±0.22*
-80°C	0.67±0.12	0.78±0.09	0.76±0.09
1 Week			
37°C	0.74±0.12	**0.48±0.22***	**0.54±0.16***
4°C	0.67±0.17	0.76±0.12	0.73±0.10
-20°C	0.69±0.19	0.81±0.07	0.78±0.07
-80°C	**0.56±0.17**	0.67±0.16	0.64±0.14*
1 Month			
37°C	0.81±0.11	0.58±0.12*	0.63±0.10*
4°C	0.81±0.09	0.75±0.08	0.76±0.05
-20°C	0.68±0.12	0.79±0.09	0.77±0.08
-80°C	0.69±0.11	0.80±0.06	0.78±0.05

Functionality indices

Storage-related changes to functionality impacted the cartilage surface and bulk properties differently. On the one hand, FI_s, which accounts for surface roughness and CoF, was significantly different in the -80°C at 1 week and 1 month groups (FI_s=1.43±0.19 and 1.31±0.11, respectively). On the other hand, significant changes in FI_b were observed only after a month at non-physiological temperatures, reaching as low as 0.81. Surface and bulk functionality changes were captured in the combined FI scores (**Table 1**).

Discussion

The role of cartilage surface properties on joint function has been historically understudied in comparison to the tissue's bulk properties. To address this disparity, the first objective of this work was to develop a new methodology that incorporates surface characterization alongside the bulk assessments typically used for cartilage. The second objective was to then apply the methodology to an active area of research: cartilage explant preservation. Both objectives were accomplished, thus providing the field with both a vetted protocol and an example of the impact surface properties may have on cartilage function.

This methodology and subsequent experiment employed primarily non-destructive surface characterization techniques that relate to roughness, friction, and lubrication. While compressive and tensile properties (12, 24) are routinely measured to assess the state of cartilage tissue, the surface properties listed above are infrequently evaluated. This is true as well of most studies on cartilage storage and preservation for clinical use, although a functional therapeutic would require a smooth cartilage surface exhibiting low friction. To-date, little attention has been given to the effect of storage conditions on surface characteristics. Except for brief reports comparing two temperatures (15, 16, 25), no studies have been conducted with the main objective of examining how storage conditions affect the cartilage surface. Thus, the field currently operates

under the assumption that cartilage surface characteristics are either insensitive to storage or respond similar to the often-examined bulk characteristics. By applying the tribology and interferometry methods described here, this assumption was tested based on the null hypothesis that no differences would be found among surface characteristics for cartilages stored under various temperatures and durations. The null hypothesis was rejected due to observing significant surface and bulk changes. In general, changes to cartilage surface function were greatest at freezing temperatures after at least a week of storage. Interestingly, bulk properties were well maintained in storage at 37°C (14, 26, 27), which is akin to culturing. In contrast, there was a significant reduction in bulk function after a month of refrigeration, often considered the gold standard for cartilage storage. The use of surface characterization methods offers new information to the field and is an important complement to the bulk data in this study. These assays also paved the way to novel observations, such as determining topographical anisotropy using interferometry and finding frictional anisotropy through tribology. Further use of roughness and coefficient of friction values to assess the quality of cartilage, may hold significant relevance to many, ranging from the tissue engineer creating biomimetic neocartilage to the surgeon implanting an allograft at a given orientation. Together, these findings not only elucidate important cartilage surface characteristics, but also make a compelling case for their inclusion in any comprehensive study of cartilage function.

Interferometry and tribology were used to quantify storage-related surface-level changes. Interferometry proved to be a fast, non-contact imaging modality well-suited for assessing cartilage surface roughness and topography. Although interferometry has been previously used to image individual chondrocytes (28) and articular cartilage (8), this technology has not become a standard tool in cartilage research. Our work with interferometry revealed topographical anisotropy in the form of striations along the anterior-posterior direction. Tribological testing was exceptionally consistent: each individual sample displayed frictional anisotropy. These data

conclusively demonstrated that the friction-related function of articular cartilage was anisotropic. With regards to storage, significant changes in both roughness and CoF were included in the calculations of surface function, FI_s. When roughness and CoF are considered together, surface functionality appears to be most affected by storage at -80°C and as early as 1 week. While not quantitively measured here, lubricin also plays an important role in joint articulation. Previous work has shown topographical differences in both SZP and CoF across the cartilages of the knee joint (7). In this study, we only used explants from the femoral condyle to mitigate these regional differences. Lubricin localization at the surface was generally unaffected by storage, even up to a month. Our results showed that cartilage roughness and CoF are most impacted by freezing temperatures, which is accurately reflected in our quantification of surface functionality. Although a reduction in roughness or CoF may be interpreted as an improvement in function, it is also possible that surface-level changes are due to tissue damage caused by ice crystal formation and warrants further investigation (29). Thus, the reduction in these two parameters can potentially be detrimental to surface function. For example, reduced roughness and CoF could indicate a loss of surface anisotropy and impact joint articulation. Although there is no significant difference in surface alignment along the direction of articulation from this study's interferometry data, the observed surface striations may be diminished in magnitude and therefore, have a reduced influence on articulation. As further improvements to cartilage storage protocols are developed, it is in the best interest of the field to include surface characterization in functional assessments of potential osteochondral grafts.

Changes to the bulk ECM and mechanical properties of articular cartilage due to prolonged storage at various temperatures are still not well understood. At freezing temperatures, decreases in collagen fibril diameter and increases in interfibrillar space have been observed in highly collagenous tissue, but statistical significance is not always achieved (30-32). Similarly, there are several conflicting reports on changes in GAG content due to freezing or refrigeration

(12, 33). Although many of these papers note changes to the ECM ultrastructure, few provide corresponding mechanical data. When mechanical function is assessed, freezing does not typically result in significant changes, while long-term refrigeration seems to result in degradation of mechanical properties (12, 13, 24). The data in this study provide a broader picture of both the biochemical and biomechanical state of stored articular cartilage. These data were then used to determine bulk functionality, FI_b. Given the importance of collagen to cartilage mechanics, pyridinoline crosslinks across each of the examined groups were assayed and were also included in FI_b calculations. Tensile properties, which are often overlooked but inherently related to collagen structure and content, were also measured. These data support previous work showing that collagen-related content and tensile mechanics minimally change with freezing (12, 13), but additionally show that tensile properties may have a variable response to long-term refrigeration.

Many previous studies on cartilage preservation exclude storage at physiological temperature. At 37°C, the data show a marked increase in GAG content and a concomitant increase in aggregate and shear modulus values. This is contrary to the response seen in explants from adult bovine elbows that were cultured for 4 weeks (34). A key difference between this prior study and the present work is the use of fetal bovine serum (FBS) in the prior study. In cartilage explants cultured at 37°C, increased FBS concentration reduced chondrocyte viability (14). The present study stands in agreement with the work of others that have shown the benefits of cartilage tissue culture with serum-free media (14, 26, 27). These enhancements to compressive mechanics and GAG content countered the tensile and collagen-related data, thus maintaining the FI_b stable with culturing. Our safranin-O staining further supported the positive effects of storage at physiological temperature on GAG content. Additionally, the 37°C, 1 month group also appears to display an increase in lacuna size and in the frequency of cell division, reminiscent of cartilage developmental processes (35). Taking into account the immature state of the chondrocytes used in this study and that aging chondrocytes show a decrease in biosynthesis of

protein and GAG, it is likely that this effect will be less noticeable if more mature tissues are used (e.g., osteochondral allografts from middle-aged donors) (36). For the purposes of this investigation, where differences in function were used to interrogate the proposed methodology, the use of immature chondrocytes was appropriate. While this study is specific to immature cartilage, our quantitative measures of composition and mechanics suggest that storage at physiological temperature not only preserves cartilage, but may also promote further growth and compressive function in immature tissue.

This study not only shows a comprehensive picture of the effect of storage on cartilage bulk properties, but it is also the first to significantly include effects on surface function using interferometry, tribology, and lubricin staining. While this study focused on storage temperature and duration, there are many other factors that should also be considered. One such factor is medium composition, which can dramatically influence explant biochemical content and mechanics (27). Distributors of fresh allografts in the United States all use different formulations, with some even including FBS (1). Our results with a serum-free medium suggest that these differences may be impactful and warrant standardization of storage media. Similarly, thawing protocols should also be examined as these may be as critical to cartilage preservation as storage conditions. In addition to studying storage effects on native tissue, similar studies should be conducted on tissue engineered cartilage. These studies would all benefit from the use of surface- and bulk-specific FIs to allow for a more focused interpretation of functional changes. The combined FI then ensures that cartilage function is evaluated holistically, without ignoring the important role of surface function.

Recommendations on cartilage function preservation depend on cell viability, bulk mechanics, and surface articulation, all of which may be included in the calculation of an FI. This study did not revisit the effects of storage on chondrocyte viability because this is already well established for the storage conditions examined here (11). However, viability can be easily added

to an FI should this be of interest, such as in clinical applications. If maintaining cell viability is of interest, storage at freezing temperatures should be avoided. In this study, assumptions were made on whether an observed change in bulk or surface function was beneficial or detrimental to a tissue's use as an implant; however, other studies may value parameters differently. While this allows researchers flexibility to optimize the FI score for specific studies, we recommend that value judgements on parameter changes be made based on each study's particular hypothesis, design, or desired outcomes. Given the assumptions used here, freezing specifically impacts surface function, but it is currently unclear if this is beneficial. Additionally, bulk properties appear to be negatively affected after a month of storage at sub-physiological temperature. Therefore, for the purpose of graft transplantation, we encourage that culturing at physiological temperature be further investigated and strongly considered, particularly in light of the reduced FI observed with long-term refrigeration.

Conclusion

Although the cartilage surface plays a critical role in proper joint articulation, it is often ignored in assessments of cartilage tissue and function. Tribology, interferometry, and lubricin staining each provide unique and important information about the cartilage surface. In addition to obtaining baseline surface characteristics, these measurements also revealed topographical and frictional anisotropy. Quantitative surface metrics, such as roughness and coefficient of friction, were used to identify groups with significant changes in surface functionality due to storage. Interestingly, these did not necessarily coincide with the groups displaying significant changes in bulk functionality, suggesting that bulk tissue behavior alone is not representative of cartilage function. These findings most immediately convey the importance of surface characterization in determining cartilage storage conditions for laboratory and clinical use but may also have far-reaching applications. Surface functionality measures of cartilage tissue are not only sorely

needed in native tissue studies but are also instrumental for developing design criteria for functional tissue engineered cartilage.

Funding

The authors acknowledge support from the National Institutes of Health (R01 DE015038 and R01 AR067821), National Institutes of Health Diversity Supplement (for MGE), Fulbright Chile scholarship (for GO), and Becas Chile scholarship (for GO).

References

1. Goodfriend B, Essilfie AA, Jones IA, Thomas Vangsness C. Fresh osteochondral grafting in the United States: the current status of tissue banking processing. Cell and Tissue Banking. 2019;20(3):331-7. doi: 10.1007/s10561-019-09768-5.
2. Cook JL, Stannard JP, Stoker AM, Bozynski CC, Kuroki K, Cook CR, Pfeiffer FM. Importance of donor chondrocyte viability for osteochondral allografts. The American Journal of Sports Medicine. 2016;44(5):1260-8.
3. Patel JM, Wise BC, Bonnevie ED, Mauck RL. A Systematic Review and Guide to Mechanical Testing for Articular Cartilage Tissue Engineering. Tissue Engineering Part C: Methods. 2019;25(10):593-608.
4. Salinas EY, Hu JC, Athanasiou K. A guide for using mechanical stimulation to enhance tissue-engineered articular cartilage properties. Tissue Engineering Part B: Reviews. 2018;24(5):345-58.
5. Link JM, Salinas EY, Hu JC, Athanasiou KA. The tribology of cartilage: Mechanisms, experimental techniques, and relevance to translational tissue engineering. Clinical Biomechanics. 2019.
6. Oungoulian SR, Durney KM, Jones BK, Ahmad CS, Hung CT, Ateshian GA. Wear and damage of articular cartilage with friction against orthopedic implant materials. Journal of biomechanics. 2015;48(10):1957-64.
7. Peng G, McNary SM, Athanasiou KA, Reddi AH. The distribution of superficial zone protein (SZP)/lubricin/PRG4 and boundary mode frictional properties of the bovine diarthrodial joint. Journal of biomechanics. 2015;48(12):3406-12.
8. Shekhawat V, Laurent M, Muehleman C, Wimmer M. Surface topography of viable articular cartilage measured with scanning white light interferometry. Osteoarthritis and cartilage. 2009;17(9):1197-203.

9. Achanta S, Celis J-P. On the scale dependence of coefficient of friction in unlubricated sliding contacts. Wear. 2010;269(5-6):435-42.
10. Torrie AM, Kesler WW, Elkin J, Gallo RA. Osteochondral allograft. Current reviews in musculoskeletal medicine. 2015;8(4):413-22.
11. Pisanu G, Cottino U, Rosso F, Blonna D, Marmotti AG, Bertolo C, Rossi R, Bonasia DE. Large osteochondral allografts of the knee: surgical technique and indications. Joints. 2018;6(01):042-53.
12. Szarko M, Muldrew K, Bertram JE. Freeze-thaw treatment effects on the dynamic mechanical properties of articular cartilage. BMC musculoskeletal disorders. 2010;11(1):231.
13. Williams SK, Amiel D, Ball ST, Allen RT, Wong VW, Chen AC, Sah RL, Bugbee WD. Prolonged storage effects on the articular cartilage of fresh human osteochondral allografts. JBJS. 2003;85(11):2111-20.
14. Pallante AL, Bae WC, Chen AC, Görtz S, Bugbee WD, Sah RL. Chondrocyte viability is higher after prolonged storage at 37 C than at 4 C for osteochondral grafts. The American journal of sports medicine. 2009;37(1_suppl):24-32.
15. Moore AC, Burris DL. Tribological and material properties for cartilage of and throughout the bovine stifle: support for the altered joint kinematics hypothesis of osteoarthritis. Osteoarthritis and cartilage. 2015;23(1):161-9.
16. Pallante-Kichura AL, Chen AC, Temple-Wong MM, Bugbee WD, Sah RL. *In vivo* efficacy of fresh versus frozen osteochondral allografts in the goat at 6 months is associated with PRG4 secretion. J Orthop Res. 2013;31(6):880-6. Epub 2013/01/29. doi: 10.1002/jor.22319. PubMed PMID: 23362152.
17. Berens P. CircStat: A MATLAB Toolbox for Circular Statistics. 2009. 2009;31(10):21. Epub 2009-08-04. doi: 10.18637/jss.v031.i10.
18. Espinosa MG, Taber LA, Wagenseil JE. Reduced embryonic blood flow impacts extracellular matrix deposition in the maturing aorta. Developmental Dynamics. 2018;247(7):914-23.
19. Athanasiou K, Niederauer G, Schenck R. Biomechanical topography of human ankle cartilage. Annals of biomedical engineering. 1995;23(5):697-704.
20. Cissell DD, Link JM, Hu JC, Athanasiou KA. A modified hydroxyproline assay based on hydrochloric acid in Ehrlich's solution accurately measures tissue collagen content. Tissue Engineering Part C: Methods. 2017;23(4):243-50.
21. Gonzalez-Leon EA, Bielajew BJ, Hu JC, Athanasiou KA. Engineering self-assembled neomenisci through combination of matrix augmentation and directional remodeling. Acta biomaterialia. 2020;109:73-81. doi: 10.1016/j.actbio.2020.04.019. PubMed PMID: 32344175; PubMed Central PMCID: PMC7987216.
22. Carson FL, Hladik C. Histotechnology: a self-instructional text: ASCP press Chicago:; 1997.
23. Huwe LW, Brown WE, Hu JC, Athanasiou KA. Characterization of costal cartilage and its suitability as a cell source for articular cartilage tissue engineering. J Tissue Eng Regen Med. 2018;12(5):1163-76. doi: 10.1002/term.2630.
24. Changoor A, Fereydoonzad L, Yaroshinsky A, Buschmann MD. Effects of refrigeration and freezing on the electromechanical and biomechanical properties of articular cartilage. Journal of biomechanical engineering. 2010;132(6):064502.
25. Gleghorn JP, Bonassar LJ. Lubrication mode analysis of articular cartilage using Stribeck surfaces. Journal of biomechanics. 2008;41(9):1910-8.

26. Bian L, Lima EG, Angione SL, Ng KW, Williams DY, Xu D, Stoker AM, Cook JL, Ateshian GA, Hung CT. Mechanical and biochemical characterization of cartilage explants in serum-free culture. Journal of Biomechanics. 2008;41(6):1153-9. doi: https://doi.org/10.1016/j.jbiomech.2008.01.026.
27. Garrity JT, Stoker AM, Sims HJ, Cook JL. Improved osteochondral allograft preservation using serum-free media at body temperature. The American journal of sports medicine. 2012;40(11):2542-8.
28. Scott CC, Luttge A, Athanasiou KA. Development and validation of vertical scanning interferometry as a novel method for acquiring chondrocyte geometry. Journal of Biomedical Materials Research Part A: An Official Journal of The Society for Biomaterials, The Japanese Society for Biomaterials, and The Australian Society for Biomaterials and the Korean Society for Biomaterials. 2005;72(1):83-90.
29. Pegg DE. The relevance of ice crystal formation for the cryopreservation of tissues and organs. Cryobiology. 2010;60(3, Supplement):S36-S44. doi: https://doi.org/10.1016/j.cryobiol.2010.02.003.
30. Gelber PE, Gonzalez G, Torres R, Garcia Giralt N, Caceres E, Monllau JC. Cryopreservation does not alter the ultrastructure of the meniscus. Knee Surgery, Sports Traumatology, Arthroscopy. 2009;17(6):639-44. doi: 10.1007/s00167-009-0736-x.
31. Jacquet C, Erivan R, Argenson J-N, Parratte S, Ollivier M. Effect of 3 Preservation Methods (Freezing, Cryopreservation, and Freezing + Irradiation) on Human Menisci Ultrastructure: An Ex Vivo Comparative Study With Fresh Tissue as a Gold Standard. The American Journal of Sports Medicine. 2018;46(12):2899-904. doi: 10.1177/0363546518790504. PubMed PMID: 30141963.
32. Ozcelikkale A, Han B. Thermal Destabilization of Collagen Matrix Hierarchical Structure by Freeze/Thaw. PLoS One. 2016;11(1):e0146660-e. doi: 10.1371/journal.pone.0146660. PubMed PMID: 26765741.
33. Zheng S, Xia Y, Bidthanapally A, Badar F, Ilsar I, Duvoisin N. Damages to the extracellular matrix in articular cartilage due to cryopreservation by microscopic magnetic resonance imaging and biochemistry. Magn Reson Imaging. 2009;27(5):648-55. Epub 2008/12/23. doi: 10.1016/j.mri.2008.10.003. PubMed PMID: 19106023.
34. Natoli RM, Scott CC, Athanasiou KA. Temporal effects of impact on articular cartilage cell death, gene expression, matrix biochemistry, and biomechanics. Annals of biomedical engineering. 2008;36(5):780-92.
35. Pavasant P, Shizari T, Underhill CB. Hyaluronan contributes to the enlargement of hypertrophic lacunae in the growth plate. Journal of cell science. 1996;109(2):327-34.
36. Sandy J, Barrach H, Flannery C, Plaas A. The biosynthetic response of the mature chondrocyte in early osteoarthritis. The Journal of rheumatology. 1987;14:16-9.

Supplementary material

Supplementary table. Gross morphology and biochemical data. Data is presented as mean ± standard deviation (unbiased). Groups marked with asterisk (*) are considered significantly different compared to its respective control group at day 1 at 37°C ($p<0.05$) based of Dunnett´s *post hoc* test.

	Wet weight (mg)	Dry weight (mg)	Hydration (%)	COL/WW (%)	GAG/WW (%)	DNA/WW (%)	PYR/WW (ng/µg)
1 Day							
37°C	3.04±0.43	0.67±0.17	78.06±2.93	13.59±1.56	7.15±1.12	0.05±0.02	0.26±0.04
4°C	3.46±0.28	0.75±0.14	78.55±2.78	12.95±3.49	6.90±1.15	0.05±0.01	0.27±0.04
-20°C	3.43±0.66	0.71±0.16	79.27±2.74	13.12±1.90	6.89±1.70	0.04±0.01	0.29±0.08
-80°C	3.15±0.33	0.64±0.09	79.60±1.92	13.32±1.84	7.16±0.84	0.04±0.01	0.23±0.05
1 Week							
37°C	2.71±0.49	0.69±0.10	74.57±1.27	16.20±1.51	8.19±0.88	0.04±0.01	0.29±0.03
4°C	3.10±0.48	0.77±0.14	75.02±2.31	18.90±2.81*	7.97±0.89	0.03±0.01*	0.29±0.02
-20°C	2.76±0.75	0.64±0.23	77.17±3.28	17.16±2.26	7.89±1.43	0.05±0.01	0.33±0.06
-80°C	3.48±0.46	0.80±0.14	77.08±2.03	15.73±1.37	8.43±1.35	0.04±0.004	0.35±0.14
1 Month							
37°C	3.04±0.17	0.57±0.12	81.25±4.10	9.48±3.07	8.05±1.92	0.03±0.01*	0.25±0.08
4°C	3.09±0.65	0.60±0.20	81.08±3.05	12.08±3.38	7.51±2.28	0.04±0.01	0.28±0.06
-20°C	3.26±0.49	0.68±0.07	79.07±1.16	14.69±2.13	7.28±2.00	0.04±0.004	0.24±0.08
-80°C	3.46±0.34	0.70±0.08	79.91±1.05	14.77±1.70	7.21±1.99	0.03±0.01	0.26±0.04

CHAPTER 3: Vibrometry as a noncontact alternative to dynamic and viscoelastic mechanical testing in cartilage

Abstract

Physiological loading of knee cartilage is highly dynamic and may contribute to the progression of osteoarthritis. Thus, an understanding of cartilage's dynamic mechanical properties is crucial in cartilage research. In this study, vibrometry was used as a fast (2 hours), non-contact, and novel alternative to the slower (30 hours), traditional mechanical and biochemical assays for characterization of cartilage from the condyle, patella, trochlear groove, and meniscus. Finite-element models predicted tissue resonant frequencies and bending modes, which strongly correlated with experiments (R^2=0.93). Vibrometry-based viscoelastic properties significantly correlated with moduli from stress relaxation and creep tests, with correlation strengths reaching up to 0.78. Loss modulus also strongly correlated with GAG content. Dynamic properties measured by vibrometry significantly differed among various knee cartilages, ranging between 6.1-56.4MPa. Interestingly, meniscus viscoelastic properties suggest that contrary to common belief, it may lack shock absorption abilities; instead, condylar hyaline cartilage may be a better shock absorber. These data demonstrate for the first time that vibrometry is a non-contact approach to dynamic mechanical characterization of hyaline and fibrocartilage cartilage with concrete relationships to standard quasistatic mechanical testing and biochemical composition. Thus, with a single tool, vibrometry greatly facilitates meeting multiple regulatory recommendations for mechanical characterization of cartilage replacements.

Chapter published as: Espinosa, M.G., Otarola, G.A., Hu, J.C., Athanasiou, K.A. Vibrometry as a noncontact alternative to dynamic and viscoelastic mechanical testing in cartilage. Journal of the Royal Society Interface 2021; 18: 20210765

Introduction

Cartilage is a dynamically loaded tissue. Typical activities, such as walking, can generate large stresses between 1 and 6MPa, but may even peak up to 12MPa (1). These stresses are applied cyclically at frequencies ranging from 0.01 to 2Hz, typically resulting in up to 4 million loading cycles per year (1, 2). Several factors, such as cyclical mechanical fatigue, excessive strains, and rapid strain rates, are often implicated with the onset of osteoarthritis, a condition afflicting approximately 14% of adults (3). Under cyclical compression, cartilage's biphasic and dynamic mechanical properties protect against these potentially damaging factors via interstitial fluid pressurization (1). Despite this arguably hostile mechanical environment, cartilage actually relies on cyclic loading for processes such as solute transport and matrix protein synthesis (4). Given its relevance to daily activities and role in maintaining tissue homeostasis, cartilage dynamic mechanical properties are a crucial component to the field's ongoing research endeavours and to those seeking to replace or regenerate cartilage's function in a dynamic environment.

The importance of cartilage dynamics has not gone unnoticed. Cyclic loading has been used to enhance the functional properties of both native and tissue-engineered cartilages (5-7). Also, for translational purposes, the Food and Drug Administration (FDA) specifically recommends that both static and dynamic mechanical properties of any knee cartilage repair or replacement product be ascertained (8). Quasistatic mechanical measurements using viscoelastic testing conditions, such as stress relaxation and creep indentation, are routinely employed to evaluate cartilage and its replacements (9). Dynamic mechanical testing is often performed under confined compression, unconfined compression, or indentation to obtain a dynamic modulus and, occasionally, viscoelastic properties (10, 11). However, most of these mechanical testing modalities are destructive, which either limit the pursuit of certain investigations or require a large amount of testable tissue. It is certain that a non-contact form of dynamic mechanical testing would garner much attention among cartilage researchers.

Laser Doppler vibrometry has been extensively used in various engineering applications, such as for the assessment of structural stability and rotor vibrations, and for the fabrication of micro-electro-mechanical systems devices (12). One of the first biological applications of vibrometry was in auditory research, specifically measuring vibrations of the tympanic membrane and cochlea (13, 14). Vibrometry has slowly been adopted by others studying biological specimens, such as single cells (15), arteries (16), skin (17), and hydrogels (18). A major advantage of vibrometry showcased in these works is the ability to perform non-contact and noninvasive measurements. Given this key characteristic, vibrometry is well poised to become a valuable measurement modality in the biological sciences.

The objective of this work was to investigate the use of vibrometry as a non-contact dynamic mechanical testing modality in comparison to quasistatic mechanical and biochemical assays for articular cartilage characterization. Other forms of dynamic testing have shown that dynamic mechanical properties correlate well with quasistatic properties in many biological materials and are typically greater than their quasistatic counterparts (19-22). This study focuses on the cartilages of the knee, which are known to have differing mechanical properties (23). We hypothesized that vibrometer-based measurements would recapitulate the relationship between dynamic and quasistatic mechanical properties found through other testing modalities. We further hypothesized that a dynamic structure-function relationship could be ascertained by studying dynamic mechanical properties along with biochemical composition. Lastly, we hypothesized that non-contact laser vibrometry can measure differences in the dynamic modulus and viscoelastic properties of cartilage explants from the condyle, patella, trochlear groove, and meniscus. Inclusion of the meniscus, a fibrocartilage, is important for validating vibrometry-based measurements on cartilage tissues with differing mechanical, structural, and biochemical properties than hyaline cartilage. The results from this work will enable cartilage researchers to examine native and engineered tissue dynamics without damage, which could facilitate time-

course studies surrounding development, disease, and repair. These studies may further propel the characterization of cartilage restoration therapies and determine their ability to withstand the dynamic mechanical demands of the native cartilage environment.

Methods

Tissue Harvest

Six bovine knee joints from 2-4 week-old calves were obtained 48 hours post-mortem (Research 87). Using a biopsy punch, 5mm plugs of cartilaginous tissue were obtained from four different locations: femoral condyle (medial and lateral load-bearing regions), trochlear groove, patella, and meniscus (Figure 1A). All punches were trimmed down to a height of 1.5-2mm for consistency, maintaining the superficial zone intact and removing the calcified zone. Meniscus punches remained thicker in order to avoid compressive deformation and uneven cutting. The punches were then washed in phosphate buffered saline (PBS), and stored at -20°C. Before testing, all samples were thawed at room temperature in fresh PBS for 1 hr. These tissue punches were used for all of the mechanical testing modalities: vibrometry, stress relaxation, and creep. The cartilage explants were allowed to recover and equilibrate between tests. It is noteworthy that the geometrical requirements for the samples are imposed by the stress relaxation and creep tests and are not necessary for vibrometry.

Vibrometry

Tissue deformation due to axial vibrations were measured using a PSV-500-B Xtra Laser Scanning Vibrometer (Polytec). As shown in Figure 2A, the tissue punch was placed on top of a piezoelectric actuator (P-885.3 PICMA). The punch's bottom surface was secured with wax. The piezo's motion was controlled by the vibrometer's internal function generator. The vibrometer lens was focused on the entire sample surface. Using the high-contrast display option in the PSV 9.4 software (Polytec), a grid with approximately 20 points covering both the sample and piezo was

used to align the laser with the live video display. A second higher density grid (100-150 points) over the same area was then defined to establish the measurement points. It is important to note that measurements were taken of both the sample and the piezo. The function generator was used to generate a chirp signal ranging from 10Hz to 100,000Hz to identify resonant frequencies. This was followed by a 500Hz sinusoidal excitation. Further details on the acquisition settings can be found in the Supplementary Material (Table S1). The samples were not damaged and then used to perform destructive mechanical testing.

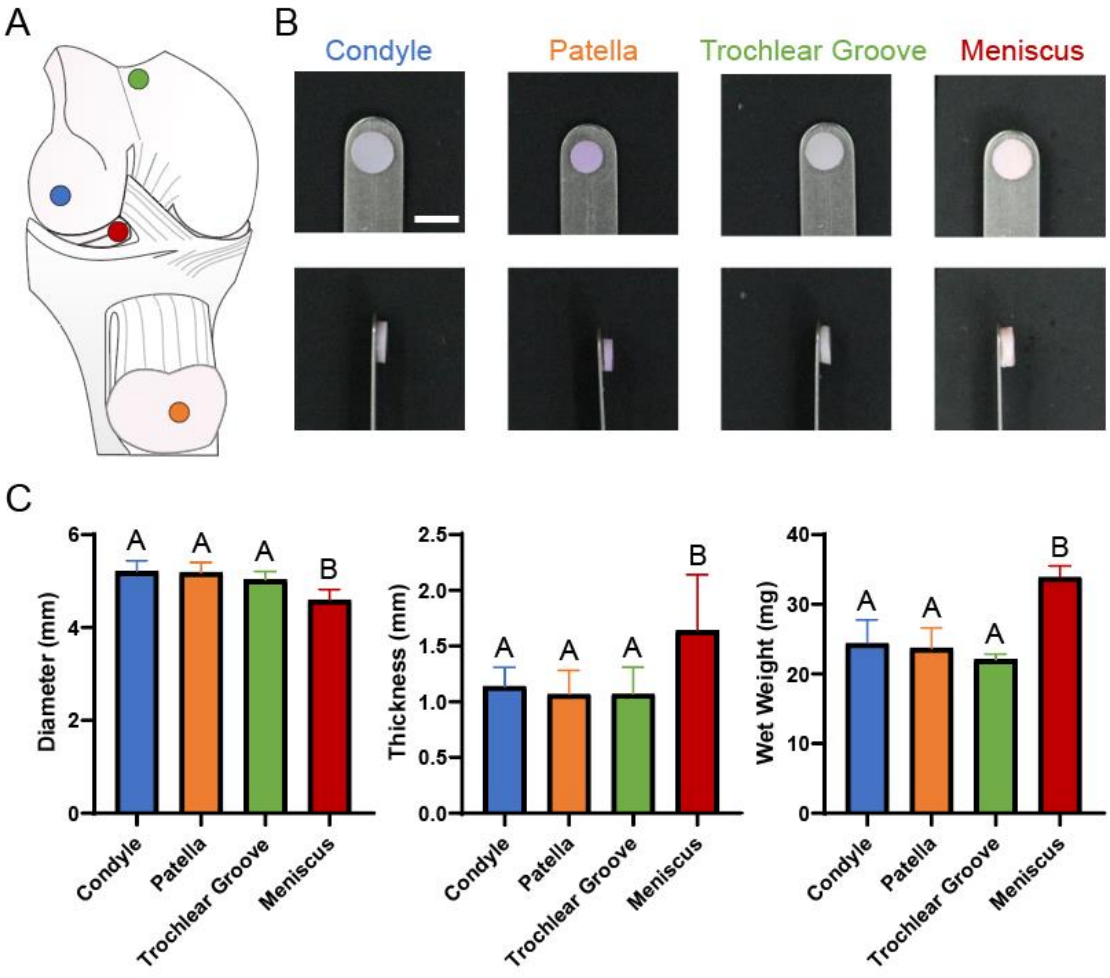

Figure 1: (**A**) Cartilage punches were taken from the condyle (blue), patella (orange), trochlear groove (green), and meniscus (red). (**B**) Punches were photographed to measure diameter and thickness. Scale bar = 5mm. (**C**) Average diameter, thickness, and wet weight for each of the

groups. Error bars represent standard deviation. Groups that do not share the same letter are statistically different.

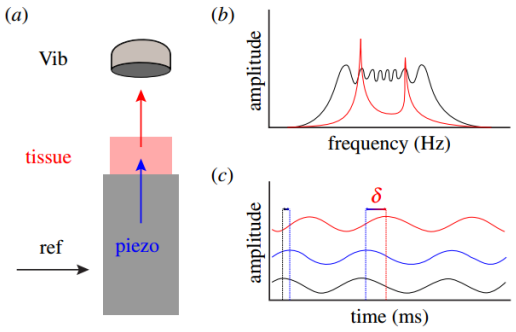

Figure 2: Experimental setup for vibrometry of cartilage tissue. (**A**) A reference signal (Ref) is sent to the piezoelectric actuator which results in tissue sample deformation. The axial displacement of the tissue's top surface is measured by the vibrometer (Vib). (**B**) A frequency sweep reference signal (black) is used to identify the tissue's resonance peaks (red). (**C**) A sinusoidal reference signal (black) drives the slightly shifted piezo's response (blue). The shift is shown as the difference between the black and blue dashed lines. The tissue's periodic deformation is shown in red with the phase shift with respect to the piezo signal given by δ.

Vibrometry Analysis

First and second resonant frequencies were found by identifying peaks in the sample velocity data across the frequency sweep (Figure 2B) using the PSV 9.4 software. To differentiate from peaks due to rigid body motion, velocity and deformation were plotted as two-dimensional surfaces to verify the presence of a bending mode at resonance (Figure 5). For this analysis, data from the piezo were only used to confirm that the piezo's resonant frequencies do not interfere with those of the sample (Figure 4B). The dynamic modulus, G*, of each sample was determined based on ASTM guidelines for calculating dynamic mechanical properties for disk-shaped

specimens via vibration (24, 25). Briefly, for each resonant frequency, a dynamic modulus was calculated,

$$G_i^* = \frac{[37.6991 f_i^2 d^2 m(1-\nu^2)]}{(K_i^2 t^3)}, \quad \text{Eq. 1}$$

where i is an index referencing either the first or second resonant frequency, f_i are the resonant frequencies, d is diameter, m is mass, and t is thickness. Poisson's ratio, v, is a function of the ratio of the second to first resonant frequencies (f_2/f_1) and the ratio of sample thickness to radius (t/r). In turn, the geometric factors, K_i, are functions of v and t/r. Functions for v and K_i were fit to previous empirical data (24, 25) using MATLAB (Figure S1) and used to determine values for the present study. The dynamic moduli for both frequencies were averaged to give a single G* value per sample.

The viscoelastic properties were determined using the data from sinusoidal excitation (Figure 2C). Using the PSV 9.4 software, an inverse Fourier transform was used to convert data from the frequency domain to the time domain. In this analysis, data from both the piezo and sample were necessary to measure the phase shift, δ, between the piezo's and tissue's response to the reference signal. The tangent of the phase shift is known to be the ratio of viscous to elastic contributions (26), also known as the loss and storage moduli, respectively. Using G* and δ, storage and loss moduli were calculated as follows:

$$G' = G^* \cos\delta \quad \text{Eq. 2a}$$

$$G'' = G^* \sin\delta \quad \text{Eq. 2b}$$

where G' is the storage modulus and G'' is the loss modulus.

It is important to note that since none of the expressions used to calculate G*, G', or G'' depend on the displacement or velocity signal amplitudes, there is no need to normalize the tissue response by the piezo data.

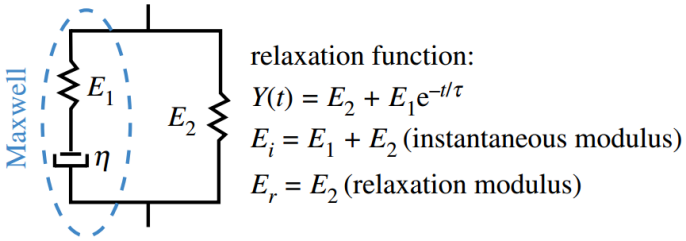

Figure 3. The standard linear solid model consists of a Maxwell component (blue dashed circle) in parallel with a spring. Its relaxation function and definitions for the instantaneous and relaxation moduli are given, where t is time and τ is the relaxation time constant

Stress Relaxation

Unconfined stress relaxation compressive testing was performed on the 5mm diameter tissue punches using an Instron model 5565 (Instron, Canton, MA). The samples, which were previously used for non-destructive vibrometry, were placed in a PBS bath at room temperature. Sample heights were determined by lowering a platen that contacts the entire surface until a load change of 0.2N was detected, and samples were preconditioned at 5% compressive strain for 15 cycles. Stress relaxation tests were performed as follows: samples were compressed to 10% strain at a rate of 1% sample height/s, held for 200s, and then compressed to 20% strain, held for 450s. The instantaneous modulus (E_i), relaxation modulus (E_r), and coefficient of viscosity of the 10% and 20% strain curves were determined by using the Standard Linear Solid viscoelastic model to fit the data in MATLAB (MathWorks) (27). The relationships between the instantaneous and relaxation moduli and the component spring elements (E_1 and E_2) are shown in Figure 3. The viscoelastic model's springs and dashpot can also be directly related to G' and G'' as shown here:

$$G' = E_2 + \frac{E_1\omega^2}{\frac{E_1^2}{\eta^2}+\omega^2} \qquad \text{Eq. 3a}$$

$$G'' = \frac{\left(\frac{E_1^2}{\eta^2}\right)\omega^2}{\frac{E_1^2}{\eta^2}+\omega^2}$$ Eq. 3b

where ω is the frequency and η is the coefficient of viscosity.

Creep Indentation

A compression indentation apparatus was used to assess creep and recovery deformation of the cartilaginous tissues (28). Briefly, the 5mm punches were photographed and glued to a cylindrical sample holder. Indentation was performed using a 1mm flat-ended, porous indenter tip, perpendicular to the surface at the centre of the sample. The sample surface is assumed to be a semi-infinite half space, which allows the single measurement point to be representative of the whole sample. A 0.5g tare weight was applied at samples' indentation site, and a variable weight (7.5-10g for patella and condyle, 4-7.5g for trochlear, 2-4g for meniscus) was used to achieve a ~10% strain. Sample height was digitally measured using ImageJ (National Institutes of Health).

The aggregate modulus (H_A), shear modulus (μ_s), and permeability were obtained using a semi-analytical, semi-numerical, biphasic model followed by finite-element optimization (29). The solution process begins with the calculation of μ_s at equilibrium (t=∞) for a specified set of v values ranging from 0 to 0.499 using

$$\frac{u(\infty)}{h} = \frac{a}{h}\left[\frac{P_0}{2a^2\mu_s}\right]\left[\frac{(1-\nu)}{2\kappa(a/h,\nu)}\right],$$ Eq. 4

where u is displacement, h is sample height, a is radius, P_0 is load, and κ is a function of a/h and v known as the geometric scaling function (30). With the exception of v and κ, all parameters are obtained experimentally. This is followed by the use of a set of specified time (t) values in the expression below:

$$u[\log_{10}(t), S]/h = G[\log_{10}(t); S, P_0/(2\mu_s a^2), a/h, \nu_s] \quad \text{Eq. 5a}$$

$$S = \log_{10}(a^2/kH_A) \quad \text{Eq. 5b}$$

$$H_A = 2\mu_s(1-\nu)/(1-2\nu), \quad \text{Eq. 5c}$$

where G is the inverse Laplace transform of the creep function. This produces a family of solutions in the (v,t) plane which can be represented by a bicubic function whose parameters are numerically obtained via curve fitting. This algorithm is described in detail elsewhere (31). Lastly, these parameters were used as initial guesses for a biphasic model finite element optimization algorithm that fits the entirety of the creep curve, including the initial rise toward equilibrium (32).

Validation through Finite Element Modelling

Abaqus/CAE 2018 (Dassault Systèmes) was used to validate our approach for determining the dynamic modulus of cartilage based on resonance. One representative sample from each group was used to define geometry, mass, G*, and permeability for the models. These values were all directly measured from the methods described above. An encastre boundary condition was imposed on the bottom surface. The models were meshed with 10,344 C3D8R elements. Given the small deformations of the experiment, linear elasticity was assumed. In addition to G* and permeability, the solid phase of the porous elastic model was also defined by a void ratio, set to 0.5, based on the literature (33, 34). The fluid phase was characterized by the specific weight of the wetting liquid and also based on previous cartilage studies (20, 35). All parameters are listed in Table S2. A linear perturbation frequency analysis was performed to find all the resonant frequencies found within 0-20kHz and their corresponding bending modes. The frequency range was based on the experimental frequency sweeps showing that all first and second resonant frequencies occurred below 20kHz.

Biochemical Assays

Cartilage tissue samples (~2-3mg) were weighed before and after lyophilization. The lyophilized samples were digested in 125μg/mL papain (Sigma) + 5mM N-acetyl-L-cysteine + (Sigma) 5mM EDTA in phosphate buffer pH 6.5 for 18 hours at 60°C. DNA content was measured with a Picogreen assay (ThermoFisher Scientific). GAG content was measured using a Blyscan glycosaminoglycan assay kit (Biocolor, Newtownabbey, Northern Ireland). Total collagen content was measured using a modified chloramine-T hydroxyproline assay using a bovine Sircol™ collagen standard (Biocolor, Newtownabbey, Northern Ireland) (36). DNA, GAG, and collagen content were measured on a GENios microplate reader (Tecan). For the quantification of pyridinoline (PYR) crosslinks, separate tissue samples (~1mg wet weight) were weighed, lyophilized, and acid digested for 12 hours in 6N HCl. After evaporation, the dried hydrolysate was resuspended in a 75%/25% (v/v) solution of 0.1% formic acid and acetonitrile. Samples were measured through mass spectrometry using a PYR standard (BOC Sciences) and a Cogent diamond hydride 2.0 HPLC column (Avantor, VWR) with a flow rate of 400μL/min on an ACQUITY UPLC I-Class core system with an ACQUITY Qda quadrupole mass spectrometer (Waters) (37).

Statistics and Accessibility

All data are reported as average ± standard deviation. Two-way and one-way ANOVAs with Tukey's *post hoc* test (GraphPad Prism 8.1.1) were used to determine statistical significance. Measured and modelled resonant frequencies were found to be normally distributed and were correlated using the Pearson correlation test. Correlations between dynamic vibrometer measures and quasistatic and biochemical measures were performed using the Spearman's ρ test. Correlation strengths, ρ, are generally considered strong if greater than or equal to 0.7, moderate if between 0.4 and 0.69, and weak if less than 0.4 (38). This study's datasets can be found on the Dryad Digital Repository (39).

Results

Tissue Sample Physical Properties

Tissue punches were obtained from the condyle, patella, trochlear groove, and meniscus. Although the punches from the other groups were consistent in size, meniscus punches had a significantly smaller diameter (Figure 1C). Compared to the condyle, patella, and trochlear groove, meniscus explant diameters were 11.9%, 11.5%, and 8.7% smaller, respectively. The meniscus punches also had a significantly greater thickness and wet weight (WW) compared to all other groups. The meniscus samples showed a 44.2%, 53.8%, and 53.4% increased thickness and 39.0%, 43.0%, and 53.4% increased WW when compared to the condyle, patella, and trochlear groove, respectively. Dimensional and weight data were used to normalize data and obtain mechanical properties.

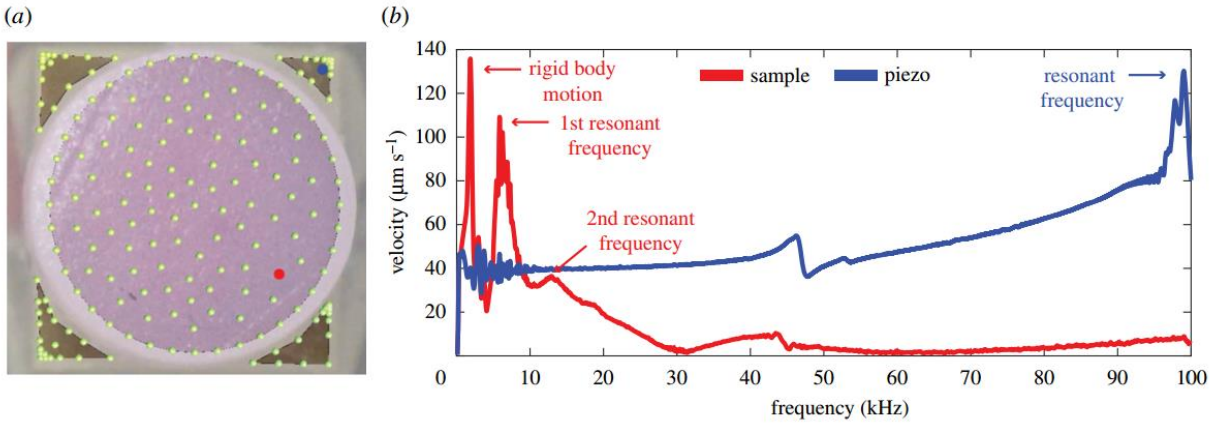

Figure 4. Green points show measurement locations throughout both the sample and the piezo (**a**). Frequency spectra from the red and blue dots are shown in (**b**), with rigid body motion and resonant peaks labelled

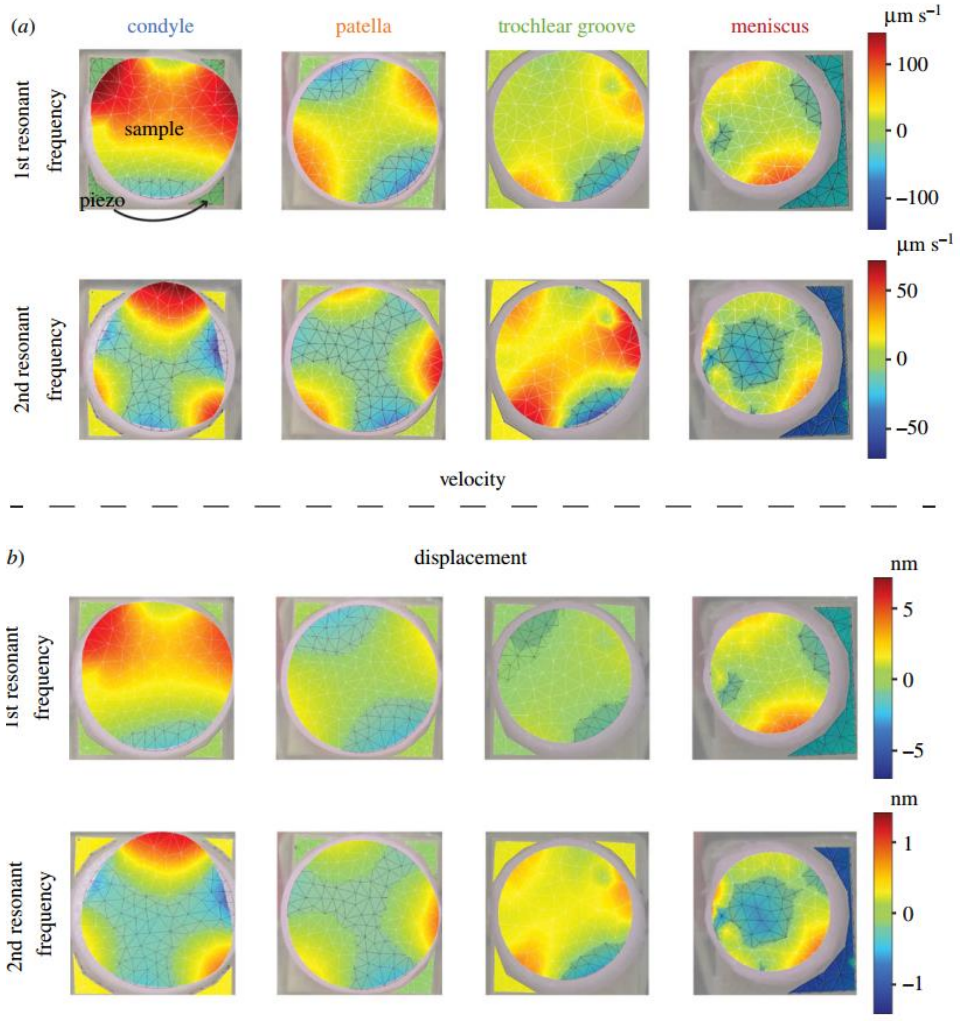

Figure 5. (**a**) Representative images of velocity plotted over the tissue and underlying piezo platform (arrow). (**b**) Tissue displacements demonstrate the bending modes for samples from each group at their respective first and second resonant frequencies

Vibrometry

Vibrational spectra were obtained for measurement points on the sample and piezo, as depicted in Figure 4A. Representative data are shown in Figure 4B. In order to distinguish between rigid body motion and resonance, bending mode shapes were identified for each group's first and second resonant frequencies (Figure 5 and Videos S1 and S2 in the Supplementary Material). Mode shapes are often described by nodal lines or circles (Figure S2) (40). For example, a mode with one nodal line, but no circles is denoted by (0, 1). Points along nodal lines and circles are relatively stable at resonance compared to other areas. The first resonant frequency's bending mode, (0, 2), was characterized by displacements that were symmetrical around two orthogonal nodal diameters in-plane with the sample and is known as a saddle mode (24). This shape was consistent across all groups. The second resonant frequency for the condyle, patella, and trochlear groove was characterized by symmetry around three nodal diameters, (0, 3). The second resonant frequency for the meniscus differed from the rest, consisting of a single nodal circle, (1, 0). This mode is often referred to as a breathing mode. Videos of the bending modes at resonance can be found in the Supplementary Material.

i. Resonant Frequencies and Dynamic Moduli

First resonant frequencies for the condyle, patella, and trochlear groove were 5,352 ± 2,011Hz, 7,823 ± 2,682Hz, and 8,768 ± 1,957Hz, respectively (Figure 6A). An increasing trend was observed, with the trochlear groove being significantly greater than the condyle. The first resonant frequency for the meniscus was 2,708 ± 65Hz, significantly lower than all the other groups. The trends observed with the first resonant frequencies were repeated with the second resonant frequencies. Figure 6B shows the dynamic moduli, calculated based on resonant frequencies. The relationship among the groups was maintained. Dynamic moduli were 27.4 ± 14.3MPa, 46.7 ±11.0MPa, 56.4 ± 29.9, and 6.1 ± 0.5MPa for the condyle, patella, trochlear groove, and meniscus, respectively.

ii. Viscoelastic Properties

In addition to the significant differences in dynamic modulus, there were also considerable differences among the groups' phase shifts, δ. The measured phase shifts were 7.0 ± 1.4°, 3.8 ± 2.0°, 2.1 ± 1.0°, and 8.2 ± 0.2° for the condyle, patella, trochlear groove, and meniscus, respectively. The tangent of the phase shifts for the patella and trochlear groove were 46% and 70% lower compared to the condyle, respectively. Although this did not result in significant differences in G' among these three groups, the differences in their G'' did reach statistical significance. The loss moduli for the condyle, patella, and trochlear groove were 4.0 ± 0.3MPa, 3.1 ± 1.6MPa, and 1.6 ± 0.2MPa, respectively. The meniscus followed a different pattern from the hyaline cartilage groups (G''=0.9 ± 0.1MPa). Although the tangent of the phase was comparable to the condyle's, the meniscus had a substantially lower G' and G'' compared to the condyle, reaching statistical significance in the case of the loss modulus.

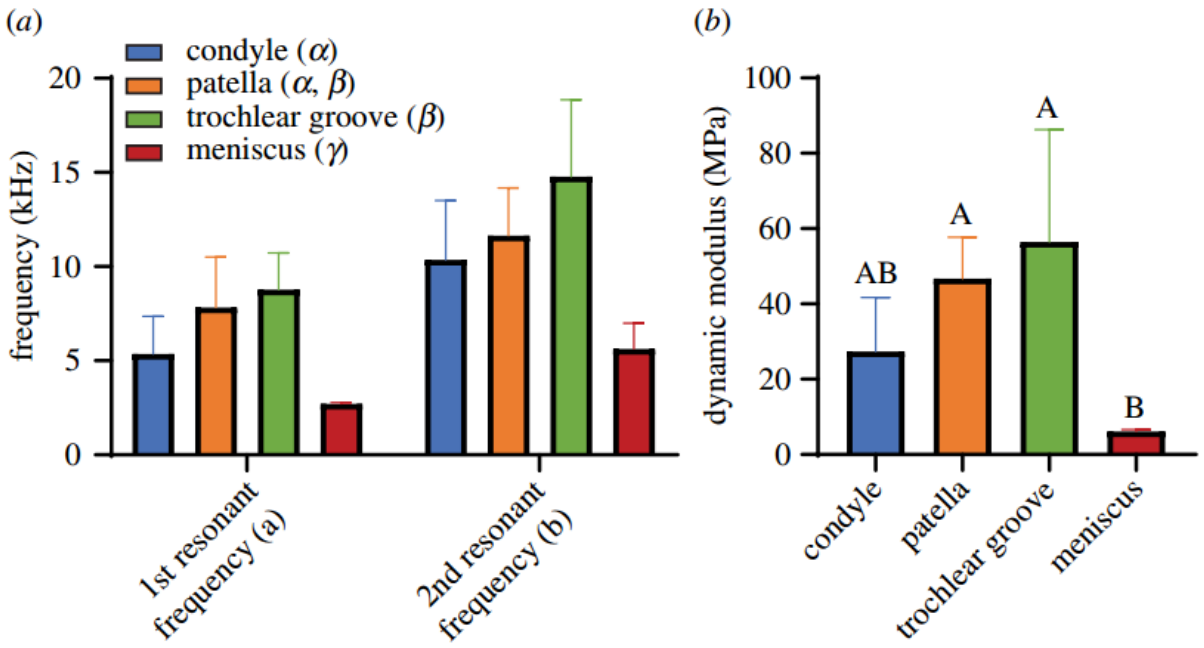

Figure 6. (**a**) Average first and second resonant frequencies significantly differ among the cartilages of the knee. A two-way ANOVA is presented with the factors of frequency (lower case Latin characters) and cartilage group (Greek characters). Both factors were significant. Letters not shared between groups within a factor denote significant differences. (**b**) The dynamic moduli are determined from the resonant frequencies and follow a similar trend. Capitalized letters not shared between groups denote significant differences by a one-way ANOVA. For all data, error bars show the positive standard deviation and n = 6

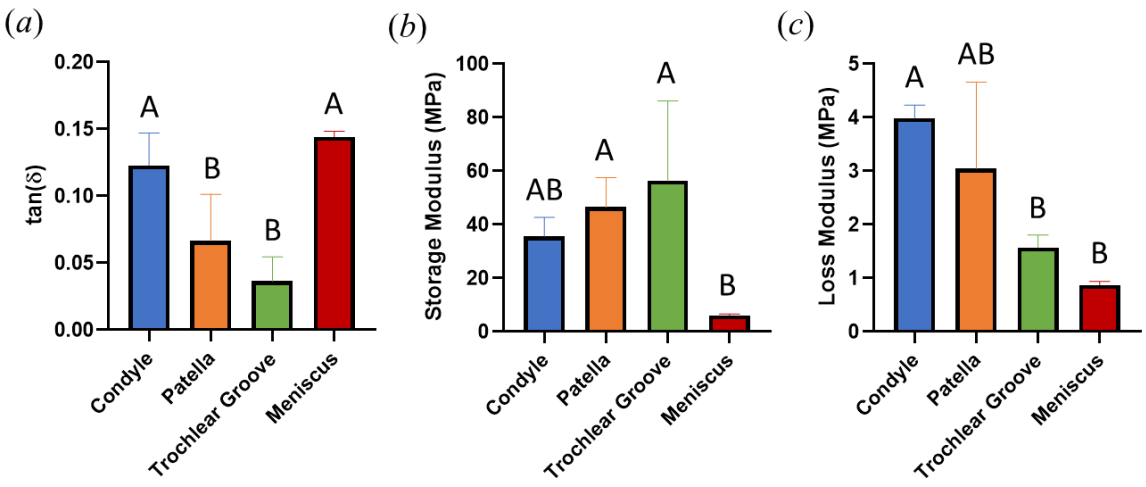

Figure 7. Phase shifts (δ) were measured to determine viscoelastic properties. (**a**) The tangent of δ represents the ratio of viscous to elastic contributions to the tissue's mechanics. This is significantly greater for the condyle and meniscus than the patella and trochlear groove. The storage (**b**) and loss (**c**) moduli trend differently, but in both cases, the meniscus has the lowest values. Error bars represent standard deviation and n = 6

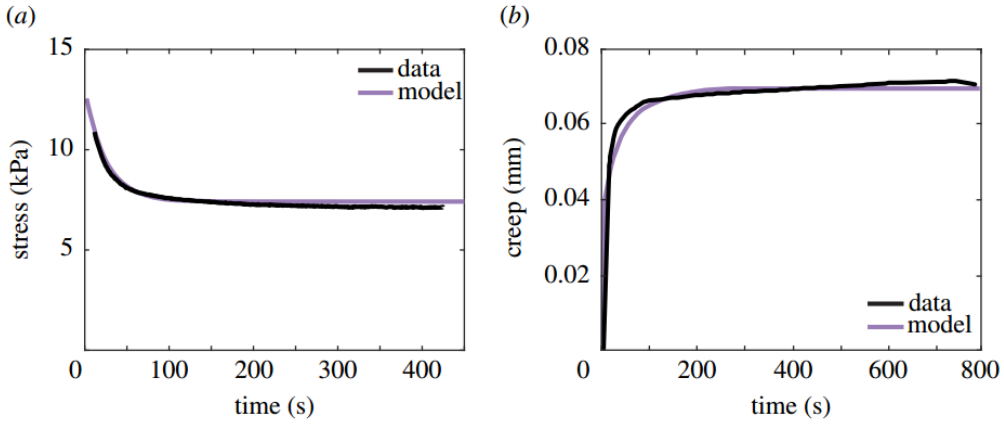

Figure 8. Representative data (black) and model fits (purple) for stress relaxation (**a**) and creep (**b**) experiments.

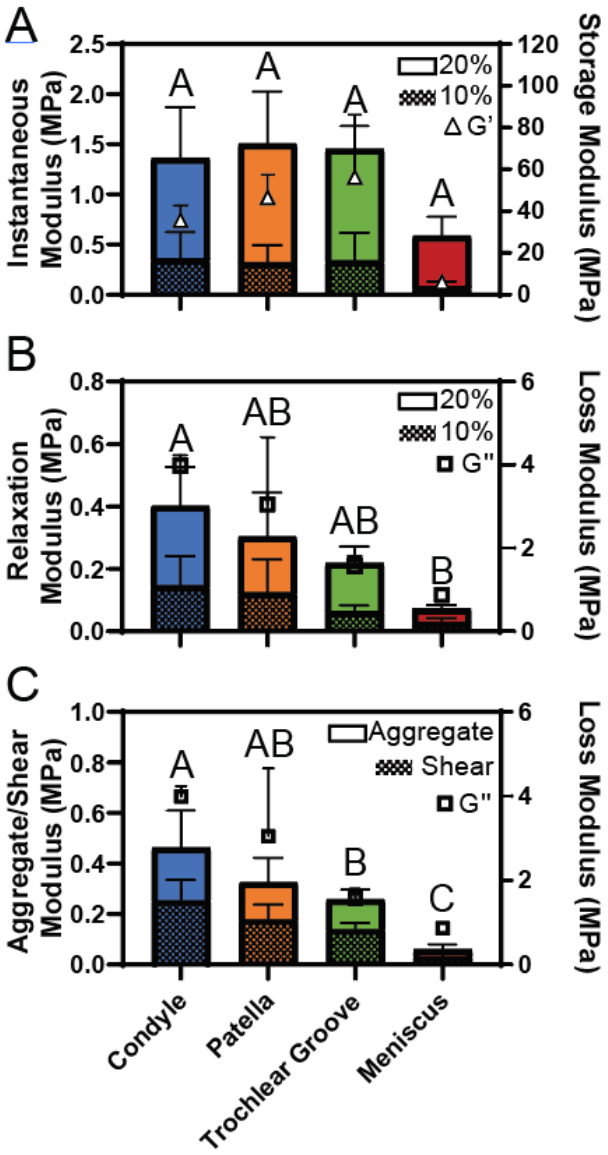

Figure 9. Quasi-static viscoelastic measurements with statistically significant correlations to dynamic measurements. Instantaneous (**a**) and relaxation (**b**) moduli from stress relaxation tests correlate to the storage (triangles) and loss (squares) moduli obtained from vibrometry, respectively. (**c**) Creep indentation tests show that both the aggregate and shear moduli also strongly correlate with the loss modulus. For simplicity, statistical differences shown here only pertain to the quasi-static measures (20% moduli for stress relaxation and aggregate modulus for creep indentation). Vibrometry values are only shown here as a reference. Error bars represent standard deviation and n = 6

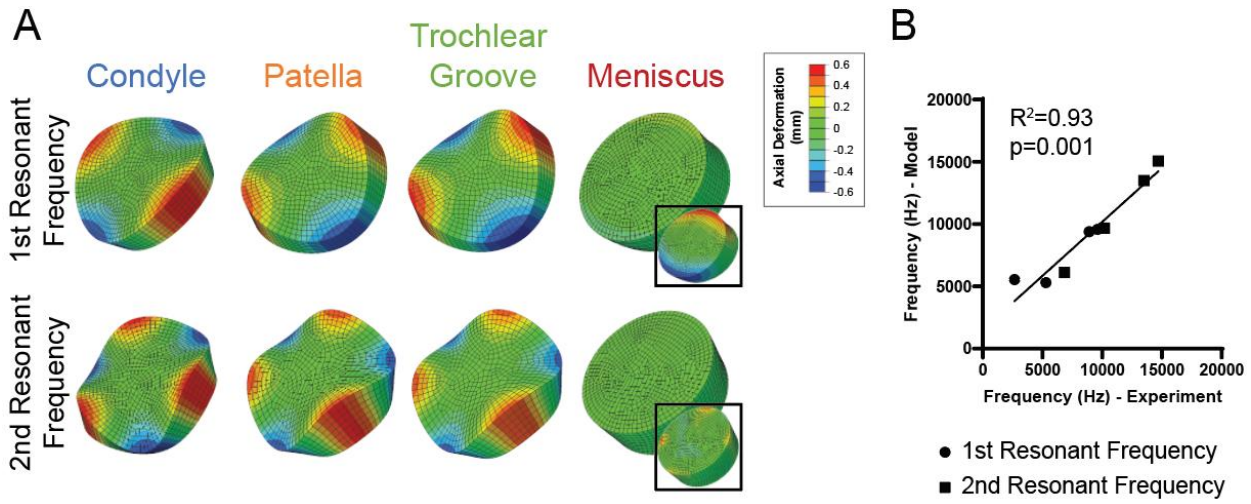

Figure 10. (**a**) Finite-element models predict resonant frequencies for each group based on input material properties. Predicted bending mode shapes resemble those observed experimentally. Meniscus deformations are small and autoscaled to observe the mode shapes (insets). (**b**) There is a strong correlation between experimental and modelled first (circles) and second (triangles) resonant frequencies (R^2 = 0.93)

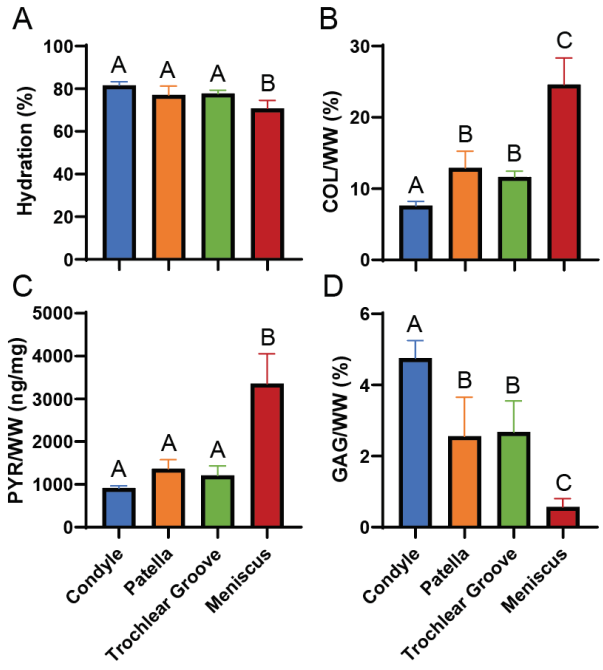

Figure 11 (previous page). Biochemical composition differs across the cartilages of the knee. (**a**) Tissue hydration is relatively constant, with a slight, but significant decrease in meniscus samples. Collagen (**b**) and pyridinoline (**c**) content per wet weight (WW) are significantly higher in the meniscus compared to all other groups. (**d**) GAG content shows an inverse trend as compared to collagen and pyridinoline, with the condyle showing the highest percentages. Error bars represent standard deviation and n = 6

Quasistatic Mechanics

Representative curves and model fits for stress relaxation and creep tests are shown in Figure 8. Stress relaxation was performed at 10% and 20% strain. There were no statistically significant differences among the groups for either instantaneous modulus (Figure 9A) or viscosity (not shown) at either strain. The relaxation modulus (Figure 9B) for the meniscus at 20% strain was significantly lower than the condyle's by 83%. Both aggregate and shear moduli (Figure 9C) from creep indentation tests were significantly different among the groups. For example, the trochlear groove and meniscus aggregate moduli were reduced by 44% and 87% compared to the condyle, respectively. Several quasistatic measures followed similar trends to those obtained through vibrometry. Instantaneous modulus correlated with G', while relaxation, aggregate, and shear moduli correlated with G''.

Finite Element Validation

The experimental (Figure 5) and computationally predicted (Figure 10A) bending modes were strikingly similar for the condyle, patella, and trochlear groove. The predicted displacements for the meniscus were small and thus, scaled differently (Figure 10A-insets). For the meniscus, the predicted first and second resonant frequency modes were characterized by one and four nodal

diameters, respectively. Taken together, the measured and modelled resonant frequencies significantly and strongly correlated across all tissues (R^2=0.93, Figure 10B) with a slope of approximately 1, providing strong validation of the experimental approach.

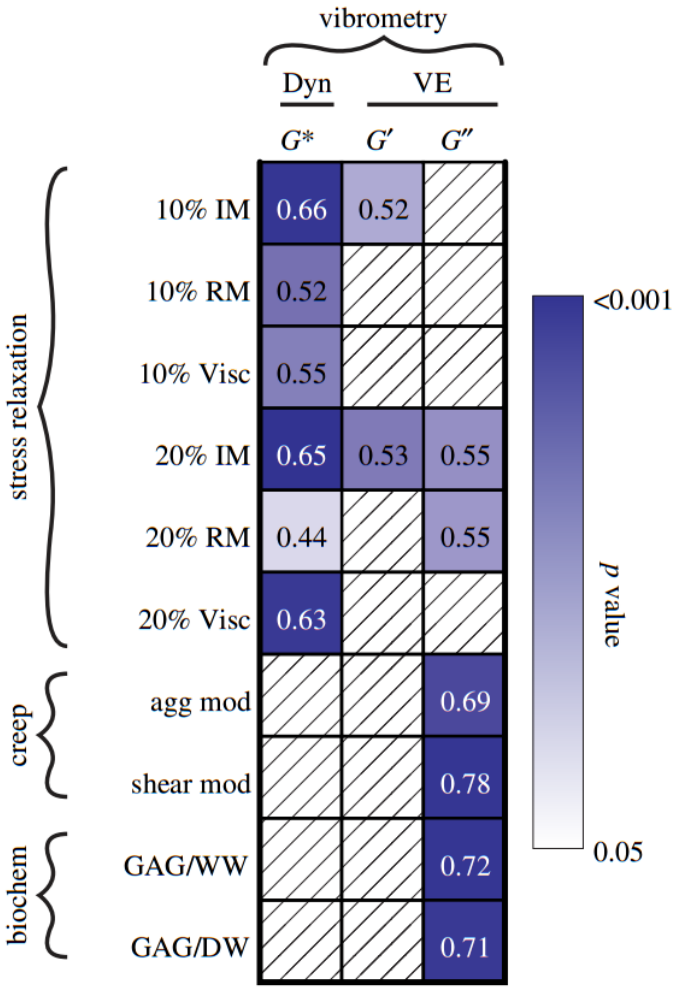

Figure 12. Strength and significance of Spearman ρ correlations between dynamic mechanical properties determined by vibrometry and quasi-static viscoelastic properties and biochemical content. Measurements are grouped together by curly brackets. With vibrometry, dynamic (Dyn) and viscoelastic (VE) properties can be obtained. IM, instantaneous modulus; RM, relaxation modulus; Visc, coefficient of viscosity; agg mod, aggregate modulus; and shear mod, shear modulus. Numbers indicate the strength of the correlation (ρ), and colour indicates the degree of significance. White boxes with diagonal lines denote that statistical significance was not achieved.

Biochemical Composition

Hydration of the tissue samples was relatively similar among the condyle, patella, and trochlear groove, averaging around 79% (Figure 11A). The meniscus was significantly less hydrated at 71±4%. With regards to collagen/WW (Figure 11B), the condyle's collagen content was significantly lower than all other groups at only 7.6 ± 0.6%. The patella (12.9 ± 2.3%) and trochlear groove (11.6 ± 0.8%) were not statistically different from each other, but both had significantly less collagen than the meniscus (24.6 ± 3.7%). The meniscus had over three times the collagen content that was present in the condyle. Pyridinoline/WW (Figure 11C) followed the same trend as collagen: 916.1 ± 48.2ng/mg, 1,363 ± 217.3ng/mg, 1,208 ± 233.0ng/mg, and 3,355 ± 697.0ng/mg for the condyle, patella, trochlear groove, and meniscus, respectively. The inverse trend was observed with GAG content (Figure 11D). The condyle's GAG content (4.8 ± 0.5%) was more than eight times that found in the meniscus (0.6 ± 0.2%). The GAG content found in the patella and trochlear groove were 2.6 ± 1.1% and 2.7 ± 0.9%, respectively.

Comparison Between Measurement Techniques

Several correlations between dynamic mechanical properties and quasistatic properties and between dynamic mechanical properties and biochemical composition were found (Figure 12). The dynamic modulus, G*, was most strongly and significantly correlated with the 10% and 20% instantaneous moduli from stress relaxation ($\rho \geq 0.65$, $p=0.001$). No associations were found between G* and creep indentation parameters or between G* and biochemical components. The storage modulus, G', which was proportional to G*, was solely correlated to the instantaneous moduli. The loss modulus, G'', trended with the relaxation moduli, reaching statistical significance with the values from the 20% strain stress relaxation tests. G'' was more strongly related to the properties obtained from creep indentation. For example, the correlation between G'' and shear

modulus had a strength of 0.78 (p=0.002). Similarly, G'' was also strongly correlated with GAG content (ρ=0.72, p=0.002).

Discussion

Physiological loading of knee articular cartilage is highly dynamic. This loading environment is necessary for nutrient transport and mechanical signalling (4), but may also result in tissue fatigue and the eventual onset of osteoarthritis (3). Therefore, as recommended by the FDA (8), mechanical characterization of cartilage replacements should include both static and dynamic testing. Most dynamic tests used in cartilage research are destructive, often limiting the scope of a study due to tissue scarcity. Given the success of vibrometry in engineering and even a few biological applications, this study's objective was to investigate the use of vibrometry as a non-contact method for dynamic mechanical testing of cartilage. Our first hypothesis was that dynamic measurements from vibrometry would correlate with those obtained from quasistatic mechanical testing, as shown in previous studies using other dynamic mechanical testing modalities (20). The second hypothesis was that vibrometry and biochemical assays would elucidate cartilage's dynamic structure-function relationship. Lastly, the third hypothesis was that vibrometry would detect the differences in the dynamic mechanical properties among four regions of the knee, consisting of both hyaline and fibrocartilage. All three hypotheses were upheld. Vibrometry allowed for the measurement of phase shifts and calculation of storage and loss moduli, which correlated well with several standard quasistatic mechanical properties. Additionally, the loss moduli correlated strongly with GAG content, the tissue constituent that is typically related to compressive properties (41). Moreover, dynamic properties not only differed among cartilage groups, but also agreed with previously published work using non-vibrometry methods. These data show that the sole use of vibrometry can yield data obtained from three distinct assays. We found that vibrometry is an efficient and non-contact testing modality for native cartilage dynamic

and viscoelastic testing, and is well suited for providing necessary data in the regulatory process for knee cartilage replacement products.

This study showed that vibrometry is an important advancement toward non-contact dynamic mechanical testing of cartilage. Several strong correlations between traditional destructive assays used in cartilage research and dynamic mechanical properties obtained from non-contact vibrometry were found (Figure 12). In this work, cartilage's viscoelasticity was described by the Standard Linear Solid model, consisting of two elastic springs and a viscous dashpot (Figure 3). Although the storage modulus (G') is associated with the relaxation modulus (Eq. 3a and Figure 3), it is also dependent on the spring-related 10% and 20% instantaneous moduli obtained from stress relaxation. Given the multiple relationships between G' and all of the Standard Linear Solid's viscoelastic parameters, it was not surprising to find significant, albeit muted, correlations. With regards to biochemical components, there were no correlations with G'. The loss moduli (G''), associated with viscous behaviour, was correlated with measures from all the assays performed in this work. Previously described mathematical relationships between G'' and the mechanical components of the Standard Linear Solid model imply that G'' should correlate with the Maxwell portion of the Standard Linear Solid (Figure 3) (26). The present data's correlations between G'' and the 10% and 20% relaxation moduli were unexpected (statistical significance determined by p=0.052 for 10% and p=0.031 for 20%), given that the Maxwell spring depends on both the instantaneous and relaxation moduli ($E_1=E_i-E_r$) but the single spring, E_2, is equivalent to the relaxation modulus. Since G'' only depends on E_1, its relationship may be related to other factors not contained within the Standard Linear Solid's model. In this and other studies performed by our group, we have frequently found a similar relationship between the relaxation moduli from stress relaxation and aggregate moduli from creep experiments (data not shown). This is further reinforced by the correlations between G'' and the aggregate and shear moduli from creep indentation, as these are also measures of the long-term elastic response. It is

possible that these surprising associations with G'' may be due to the high frequency excitation used in our vibrometry experiments. It is well known that G' and G'' are frequency-dependent and may even reach a "crossover point" at which the relative relationship between these two moduli plateaus and is inverted (42, 43). This phenomenon has been observed in several biomaterials and tissues, such as collagen/hyaluronan gels (44), vocal fold tissue (45), and airway smooth muscle (46). Therefore, although these particular relationships were not anticipated and merit further investigation, independent verification through both stress relaxation and creep indentation makes a very strong case for their validity. Notably, the correlations found in this study, especially between G'' and the creep-related parameters, suggest that quasistatic mechanical properties may predict dynamic properties. Inasmuch as the FDA and ASTM recommends that both dynamic and viscoelastic properties be reported (8, 47), these correlations demonstrate that vibrometry may obtain both dynamic and viscoelastic properties, an important observation in light of the regulatory requirements for cartilage tissue replacements.

Although biochemical composition is frequently used to describe cartilage's structure-function relationships, it is often only related to quasistatic mechanical measures. A few studies have investigated the association between cartilage composition and dynamic properties, but typically only measure G* without examining its elastic and viscous components (48, 49). In this study, the strongest correlations were found between the loss modulus (G'') and GAG content. This was not unexpected given the relationships between G'' and the relaxation, aggregate, and shear moduli, described above. There were no correlations with collagen content. In the present work, the tissue was only axially perturbed. However, perturbations in different directions (for example, parallel to the direction of articulation), may provide additional insights. A three-dimensional vibrometry setup would detect radial and circumferential deformations, which would likely be correlated to collagen content. Further work to understand how dynamic mechanical

properties relate to biochemical composition is needed, especially given the strong correlations reported in this study.

Vibrometer-based dynamic testing revealed differences in viscoelastic characteristics among the cartilage groups. G' (Figure 7B) was similar to the dynamic modulus, G* (Figure 6B), for all groups. It has been previously reported that at high frequencies (>40Hz), cartilage behaves more like an elastic solid with reduced viscous contributions (1). The small phase shifts (Figure 7A) in the present study in which dynamic loading at 500Hz (Figure 2C) were employed support this, thus resulting in a relatively low G'' compared to the corresponding G' value (Figure 7C). Phase shifts previously reported at 10Hz (1) were comparable (approximately 5°) to our measured values, which averaged at 5.2°. However, despite these low phase shift values, there are significant differences in G'' among the groups. Interestingly, the meniscus, which is often described as a shock absorber, had the lowest G''. This is in contrast to condylar cartilage, which has the greatest G''. Values reported here are comparable to previously published data for both the condyle (50) and the meniscus (19). Though the role of the meniscus as a shock absorber has been questioned (51, 52), this is the first time that it is quantitatively established that, using G'' as the outcome measure, condylar hyaline cartilage has a superior energy dissipation capacity when compared to the meniscus. Shock absorption has been quantified in numerous ways (53, 54), however, in this work, G'', was selected because it describes viscous energy dissipation independently from elastic energy storage. The vibrometer's ability to reproduce the viscoelastic properties of different knee cartilages is strongly demonstrated in this work and may continue to shed light into the function of other types of cartilage in future studies.

The dynamic modulus of cartilage is the most basic measure of tissue function under the cyclic loading conditions found in daily locomotive activities. It should be noted that the dynamic moduli measured here (Figure 6B) and reported elsewhere (1, 20) are significantly greater (>10X) than the moduli measured using quasistatic approaches (Figure 9). This is due to internal fluid

pressurization. Similar to quasistatic properties, there are topographical variations in dynamic properties across the different knee cartilages (Figure 6). Here, an increasing trend was found from the condyle, patella, to trochlear groove groups; this has also been found by others in bovine tissues (20). However, it is important to note that studies using human tissue report significantly greater compressive moduli for the condyle compared to the trochlear groove (55, 56). With regards to the meniscus, a separate study using human tissue (57) agreed with the meniscus data presented here. Both the data contained within the present study and independent studies (19, 20, 57) focusing on individual cartilages show that the meniscus has a lower dynamic compressive modulus when compared to values for the condyle, patella, and trochlear groove. The compressive properties of the meniscus are known to be relatively small in comparison to its tensile properties, likely due to compressive load transfer into hoop stresses (19). The hoop stresses are largely borne by the circumferential fibres found in the meniscus. This structural difference, as compared to the structure of hyaline cartilage, is likely responsible for the meniscus second mode shape and expected given the literature on the effect of structure on the bending modes of composites (58-60). Regardless of structure, the agreement in knee cartilage dynamic moduli obtained through non-contact vibrometry with previous reports using destructive methods is impressive and lends credence to vibrometry's efficacy.

Vibrometry's use for mechanical characterization of biological tissue is in its nascent stage, thus, requiring further study and improvements to reach this tool's potential. A limitation of this study is the use of high frequencies, beyond what is typically observed physiologically. This was required in our setup in order to excite the entire specimen without damage. At low frequencies, vibrations merely resulted in translation, not the deformation or bending necessary to identify resonant frequencies. Although vibrometers can measure displacements at low frequencies, the mode of excitation would require increased contact, such as what is used in destructive mechanical testing, such as DMA. Therefore, it is expected that cartilage's viscoelastic

properties would differ at lower frequencies typically utilized by other testing systems (61). Despite this constraint, others have shown that cartilage's dynamic properties are relatively frequency-stable when viscous properties are minimized at approximately 40Hz and beyond (1, 62-64). This is supported by the similarity in G* values reported here by resonant frequencies up to 15kHz and those measured at 40Hz (1). Furthermore, our vibrometry-based storage and loss moduli measurements obtained for bovine hyaline articular cartilage at 15kHz are within the same order of magnitude as those reported for human and bovine specimens using dynamic mechanical analysis at 88Hz (62-64). A related limitation to the translation of this work is the use of a piezoelectric drive to induce vibrations. The piezo did not damage the sample, thus allowing it to be used for other mechanical testing. However, *in situ* applications will require other means of vibrational excitation, such as ultrasound transducers (65). A third limitation in this study may be that tissues remained in ambient conditions for the duration of the measurement. Although measurements were relatively short (<5 minutes), drying may be a concern. Given this concern, we have fabricated a fluid-filled sample chamber that nonetheless permits the piezo-mediated vibrations to excite the tissue and does not obstruct measurement. Preliminary data using this chamber (data not shown) are encouraging, yielding comparable results to those shown here and assuaging concerns regarding drying. It is important to note that vibrometry-based measurements for the entire study were completed in approximately 2 hours and provided information obtained from quasistatic mechanical tests and biochemical assays that collectively required 30 hours. This represents a 93% reduction in time. Lastly, we do not expect changes in tissue properties arising from enzymatic degradation or the freeze-thaw cycle in this work given that the joint remained closed prior to testing, cartilage cells are known to very metabolically inactive (66), and that refrigeration is standard way of storing cartilage tissue (67). However, this might not be the case when working with large samples, where properties can be affected by testing times, thus, groups working with large tissues and/or requiring a fast turnover will find this decrease in time of utmost

importance. Given the benefits and advantages of vibrometry, optimization of this tool for cartilage research is well justified.

This study successfully shows the use of vibrometry in a non-contact manner to measure cartilage's dynamic mechanical properties. These properties were particularly distinctive to higher frequency dynamics, which may be representative of the high strain rates observed in traumatic injury. The dynamic properties reported here showed several correlations with quasistatic and biochemical properties, thus providing important insights into cartilage function under cyclic loading. Vibrometer-based measurements were also precise enough to detect differences in viscoelastic properties among the cartilages of the knee. This work not only solidifies the relationship among quasistatic, viscoelastic, and dynamic properties over a short testing time, but also presents a practical option for high-throughput non-destructive testing, ideal for applications in cartilage developmental biology, tissue engineering, and translational medicine.

Acknowledgements

We thank Eric Lawrence, Jerome Eichenberger, Vicky Lu, and Kilian Shambaugh from Polytec, Inc for their technical support.

Funding Statement

The authors acknowledge support from the National Institutes of Health (R01 AR067821 and R01 AR071457), the National Institutes of Health Diversity Supplement (MGE), Fulbright Chile scholarship (GO), and Becas Chile scholarship (GO).

References

1. Park S, Hung CT, Ateshian GA. Mechanical response of bovine articular cartilage under dynamic unconfined compression loading at physiological stress levels. Osteoarthritis and Cartilage. 2004;12(1):65-73. doi: https://doi.org/10.1016/j.joca.2003.08.005.
2. Barker MK, Seedhom BB. Articular cartilage deformation under physiological cyclic loading—apparatus and measurement technique. Journal of biomechanics. 1997;30(4):377-81.
3. Kaplan JT, Neu CP, Drissi H, Emery NC, Pierce DM. Cyclic loading of human articular cartilage: The transition from compaction to fatigue. J Mech Behav Biomed Mater. 2017;65:734-42. doi: https://doi.org/10.1016/j.jmbbm.2016.09.040.
4. Zhang L, Miramini S, Smith DW, Gardiner BS, Grodzinsky AJ. Time evolution of deformation in a human cartilage under cyclic loading. Annals of biomedical engineering. 2015;43(5):1166-77.
5. Bian L, Fong JV, Lima EG, Stoker AM, Ateshian GA, Cook JL, Hung CT. Dynamic mechanical loading enhances functional properties of tissue-engineered cartilage using mature canine chondrocytes. Tissue Engineering Part A. 2010;16(5):1781-90.
6. Krishnan R, Mariner EN, Ateshian GA. Effect of dynamic loading on the frictional response of bovine articular cartilage. Journal of Biomechanics. 2005;38(8):1665-73. doi: https://doi.org/10.1016/j.jbiomech.2004.07.025.
7. Mauck RL, Nicoll SB, Seyhan SL, Ateshian GA, Hung CT. Synergistic action of growth factors and dynamic loading for articular cartilage tissue engineering. Tissue engineering. 2003;9(4):597-611.
8. Administration FaD. Preparation of IDEs and INDs for Products Intended to Repair or Replace Knee Cartilage. 2011. p. 1-18.
9. Patel JM, Wise BC, Bonnevie ED, Mauck RL. A Systematic Review and Guide to Mechanical Testing for Articular Cartilage Tissue Engineering. Tissue Engineering Part C: Methods. 2019;25(10):593-608.
10. Olvera D, Daly A, Kelly DJ. Mechanical Testing of Cartilage Constructs. In: Doran PM, editor. Cartilage Tissue Engineering: Methods and Protocols. New York, NY: Springer New York; 2015. p. 279-87.
11. Ronken S, Arnold M, Garcia HA, Jeger A, Daniels A, Wirz D. A comparison of healthy human and swine articular cartilage dynamic indentation mechanics. Biomechanics and modeling in mechanobiology. 2012;11(5):631-9.
12. Rothberg SJ, Allen MS, Castellini P, Di Maio D, Dirckx JJJ, Ewins DJ, Halkon BJ, Muyshondt P, Paone N, Ryan T, Steger H, Tomasini EP, Vanlanduit S, Vignola JF. An international review of laser Doppler vibrometry: Making light work of vibration measurement. Optics and Lasers in Engineering. 2017;99:11-22. doi: https://doi.org/10.1016/j.optlaseng.2016.10.023.
13. Dong W, Xia A, Raphael PD, Puria S, Applegate B, Oghalai JS. Organ of Corti vibration within the intact gerbil cochlea measured by volumetric optical coherence tomography and vibrometry. J Neurophysiol. 2018;120(6):2847-57. doi: 10.1152/jn.00702.2017. PubMed PMID: 30281386.
14. Wang X, Guan X, Pineda M, Gan RZ. Motion of tympanic membrane in guinea pig otitis media model measured by scanning laser Doppler vibrometry. Hear Res. 2016;339:184-94. doi: https://doi.org/10.1016/j.heares.2016.07.015.
15. Corbin EA, Adeniba OO, Ewoldt RH, Bashir R. Dynamic mechanical measurement of the viscoelasticity of single adherent cells. Applied Physics Letters. 2016;108(9):093701.

16. Desjardins CL, Antonelli LT, Soares E, editors. A remote and non-contact method for obtaining the blood-pulse waveform with a laser Doppler vibrometer. Advanced Biomedical and Clinical Diagnostic Systems V; 2007: International Society for Optics and Photonics.
17. Zhang X, Kinnick R, Pittelkow M, Greenleaf JF, editors. Skin viscoelasticity with surface wave method. 2008 IEEE Ultrasonics Symposium; 2008: IEEE.
18. Schwarz S, Hartmann B, Sauer J, Burgkart R, Sudhop S, Rixen D, Clausen-Schaumann H. Contactless Vibrational Analysis of Transparent Hydrogel Structures Using Laser-Doppler Vibrometry. Experimental Mechanics. 2020;60(8):1067-78.
19. Danso E, Mäkelä J, Tanska P, Mononen M, Honkanen J, Jurvelin J, Töyräs J, Julkunen P, Korhonen R. Characterization of site-specific biomechanical properties of human meniscus—Importance of collagen and fluid on mechanical nonlinearities. Journal of biomechanics. 2015;48(8):1499-507.
20. Laasanen M, Töyräs J, Korhonen R, Rieppo J, Saarakkala S, Nieminen M, Hirvonen J, Jurvelin J. Biomechanical properties of knee articular cartilage. Biorheology. 2003;40(1, 2, 3):133-40.
21. Richler D, Rittel D. On the testing of the dynamic mechanical properties of soft gelatins. Experimental Mechanics. 2014;54(5):805-15.
22. Rotbaum Y, Puiu C, Rittel D, Domingos M. Quasi-static and dynamic *in vitro* mechanical response of 3D printed scaffolds with tailored pore size and architectures. Materials Science and Engineering: C. 2019;96:176-82.
23. Jurvelin JS, Arokoski JPA, Hunziker EB, Helminen HJ. Topographical variation of the elastic properties of articular cartilage in the canine knee. Journal of Biomechanics. 2000;33(6):669-75. doi: https://doi.org/10.1016/S0021-9290(00)00007-5.
24. International A. Standard Test Method for Dynamic Young's Modulus, Shear Modulus, and Poisson's Ratio by Impulse Excitation of Vibration.
25. Martinček G. The determination of poisson's ratio and the dynamic modulus of elasticity from the frequencies of natural vibration in thick circular plates. Journal of Sound and Vibration. 1965;2(2):116-27. doi: https://doi.org/10.1016/0022-460X(65)90089-1.
26. Athanasiou KA, Natoli RM. Introduction to Continuum Biomechanics. Synthesis Lectures on Biomedical Engineering. 2008;3(1):1-206. doi: 10.2200/S00121ED1V01Y200805BME019.
27. Allen KD, Athanasiou KA. Viscoelastic characterization of the porcine temporomandibular joint disc under unconfined compression. Journal of biomechanics. 2006;39(2):312-22.
28. Athanasiou K, Agarwal A, Dzida F. Comparative study of the intrinsic mechanical properties of the human acetabular and femoral head cartilage. J Orthop Res. 1994;12(3):340-9.
29. Athanasiou K, Niederauer G, Schenck R. Biomechanical topography of human ankle cartilage. Annals of biomedical engineering. 1995;23(5):697-704.
30. Mow VC, Kuei S, Lai WM, Armstrong CG. Biphasic creep and stress relaxation of articular cartilage in compression: theory and experiments. Journal of biomechanical engineering. 1980;102(1):73-84.
31. Mow VC, Gibbs MC, Lai WM, Zhu WB, Athanasiou KA. Biphasic indentation of articular cartilage—II. A numerical algorithm and an experimental study. Journal of Biomechanics. 1989;22(8):853-61. doi: https://doi.org/10.1016/0021-9290(89)90069-9.

32. Athanasiou K, Agarwal A, Muffoletto A, Dzida F, Constantinides G, Clem M. Biomechanical properties of hip cartilage in experimental animal models. Clin Orthop Relat Res. 1995(316):254-66.
33. Ateshian G, Lai W, Zhu W, Mow V. An asymptotic solution for the contact of two biphasic cartilage layers. Journal of biomechanics. 1994;27(11):1347-60.
34. Lilledahl MB, Pierce DM, Ricken T, Holzapfel GA, de Lange Davies C. Structural analysis of articular cartilage using multiphoton microscopy: input for biomechanical modeling. IEEE Trans Med Imaging. 2011;30(9):1635-48.
35. Ferguson S, Bryant J, Ganz R, Ito K. The influence of the acetabular labrum on hip joint cartilage consolidation: a poroelastic finite element model. Journal of biomechanics. 2000;33(8):953-60.
36. Cissell DD, Link JM, Hu JC, Athanasiou KA. A modified hydroxyproline assay based on hydrochloric acid in Ehrlich's solution accurately measures tissue collagen content. Tissue Engineering Part C: Methods. 2017;23(4):243-50.
37. Gonzalez-Leon EA, Bielajew BJ, Hu JC, Athanasiou KA. Engineering self-assembled neomenisci through combination of matrix augmentation and directional remodeling. Acta Biomater. 2020.
38. Schober P, Boer C, Schwarte LA. Correlation coefficients: appropriate use and interpretation. Anesth Analg. 2018;126(5):1763-8.
39. Espinosa MG, Otarola GA, Hu JC, Athanasiou K. Dataset for Vibrometry as a Noncontact Alternative to Dynamic and Viscoelastic Mechanical Testing in Cartilage. Dryad Digital Repository2021.
40. Thompson D. Railway noise and vibration: mechanisms, modelling and means of control: Elsevier; 2008.
41. Kim Y-J, Grodzinsky AJ, Plaas AH. Compression of cartilage results in differential effects on biosynthetic pathways for aggrecan, link protein, and hyaluronan. Arch Biochem Biophys. 1996;328(2):331-40.
42. Mason TG, Weitz DA. Optical measurements of frequency-dependent linear viscoelastic moduli of complex fluids. Phys Rev Lett. 1995;74(7):1250.
43. Winter HH. Can the gel point of a cross-linking polymer be detected by the G′–G ″crossover? Polymer Engineering & Science. 1987;27(22):1698-702.
44. Yang Y-l, Kaufman LJ. Rheology and confocal reflectance microscopy as probes of mechanical properties and structure during collagen and collagen/hyaluronan self-assembly. Biophys J. 2009;96(4):1566-85.
45. Chan RW, Rodriguez ML. A simple-shear rheometer for linear viscoelastic characterization of vocal fold tissues at phonatory frequencies. The Journal of the Acoustical Society of America. 2008;124(2):1207-19.
46. Ito S, Majumdar A, Kume H, Shimokata K, Naruse K, Lutchen KR, Stamenovic D, Suki B. Viscoelastic and dynamic nonlinear properties of airway smooth muscle tissue: roles of mechanical force and the cytoskeleton. American Journal of Physiology-Lung Cellular and Molecular Physiology. 2006;290(6):L1227-L37.
47. International A. Standard Guide for *in vivo* Assessment of Implantable Devices Intended to Repair or Regenerate Articular Cartilage.

48. Burgin LV, Edelsten L, Aspden RM. The mechanical and material properties of elderly human articular cartilage subject to impact and slow loading. Med Eng Phys. 2014;36(2):226-32. doi: https://doi.org/10.1016/j.medengphy.2013.11.002.
49. Gannon AR, Nagel T, Kelly DJ. The role of the superficial region in determining the dynamic properties of articular cartilage. Osteoarthritis and Cartilage. 2012;20(11):1417-25. doi: https://doi.org/10.1016/j.joca.2012.08.005.
50. Fulcher GR, Hukins DWL, Shepherd DET. Viscoelastic properties of bovine articular cartilage attached to subchondral bone at high frequencies. BMC Musculoskeletal Disorders. 2009;10(1):61. doi: 10.1186/1471-2474-10-61.
51. Andrews S, Shrive N, Ronsky J. The shocking truth about meniscus. Journal of biomechanics. 2011;44(16):2737-40.
52. Gaugler M, Wirz D, Ronken S, Hafner M, Göpfert B, Friederich NF, Elke R. Fibrous cartilage of human menisci is less shock-absorbing and energy-dissipating than hyaline cartilage. Knee surgery, sports traumatology, arthroscopy. 2015;23(4):1141-6.
53. Dahl MC, Jacobsen S, Metcalf N, Jr., Sasso R, Ching RP. A comparison of the shock-absorbing properties of cervical disc prosthesis bearing materials. SAS J. 2011;5(2):48-54. doi: 10.1016/j.esas.2011.01.002. PubMed PMID: 25802668.
54. Durá Gil J, García Belenguer AC, Solaz J. Testing shock absorbing materials: The application of viscoelastic linear model. Sports Engineering. 2002;5:9-14. doi: 10.1046/j.1460-2687.2002.00085.x.
55. Lyyra T, Kiviranta I, Väätäinen U, Helminen HJ, Jurvelin JS. *In vivo* characterization of indentation stiffness of articular cartilage in the normal human knee. J Biomed Mater Res. 1999;48(4):482-7.
56. Shepherd D, Seedhom B. The'instantaneous' compressive modulus of human articular cartilage in joints of the lower limb. Rheumatology (Oxford). 1999;38(2):124-32.
57. Chia HN, Hull M. Compressive moduli of the human medial meniscus in the axial and radial directions at equilibrium and at a physiological strain rate. J Orthop Res. 2008;26(7):951-6.
58. Hou JP, Jeronimidis G. Bending stiffness of composite plates with delamination. Composites Part A: Applied Science and Manufacturing. 2000;31(2):121-32. doi: https://doi.org/10.1016/S1359-835X(99)00064-0.
59. Lv N, Zhong C, Wang L. Bending vibration characteristics of the piezoelectric composite double laminated vibrator. Ceramics International. 2021. doi: https://doi.org/10.1016/j.ceramint.2021.07.302.
60. Oh K, Nayfeh AH. Nonlinear combination resonances in cantilever composite plates. Nonlinear Dynamics. 1996;11(2):143-69.
61. Cacopardo L, Mattei G, Ahluwalia A. A new load-controlled testing method for viscoelastic characterisation through stress-rate measurements. Materialia. 2020;9:100552. doi: https://doi.org/10.1016/j.mtla.2019.100552.
62. Cooke ME, Lawless BM, Jones SW, Grover LM. Matrix degradation in osteoarthritis primes the superficial region of cartilage for mechanical damage. Acta Biomater. 2018;78:320-8.
63. Lawless BM, Sadeghi H, Temple DK, Dhaliwal H, Espino DM, Hukins DW. Viscoelasticity of articular cartilage: Analysing the effect of induced stress and the restraint of bone in a dynamic environment. J Mech Behav Biomed Mater. 2017;75:293-301.

64. Temple DK, Cederlund AA, Lawless BM, Aspden RM, Espino DM. Viscoelastic properties of human and bovine articular cartilage: a comparison of frequency-dependent trends. BMC musculoskeletal disorders. 2016;17(1):1-8.
65. Castro NJ, Babakhanova G, Hu J, Athanasiou KA. Nondestructive testing of native and tissue-engineered medical products: adding numbers to pictures. Trends Biotechnol. 2021. doi: https://doi.org/10.1016/j.tibtech.2021.06.009.
66. Das R, Van Osch G, Kreukniet M, Oostra J, Weinans H, Jahr H. Effects of individual control of pH and hypoxia in chondrocyte culture. J Orthop Res. 2010;28(4):537-45.
67. Espinosa MG, Otarola GA, Hu JC, Athanasiou KA. Cartilage assessment requires a surface characterization protocol: roughness, friction, and function. Tissue Engineering Part C: Methods. 2021;27(4):276-86.

Supplementary material

Vibrometer Acquisition Settings	
Acquisition Mode	FFT
Averaging	5
FFT Lines	6400
Sample Frequency	250 kHz
Sample Time	64 ms
Resolution	15.625 Hz

Table S1: Vibrometer settings used to obtain dynamic mechanical properties of cartilage punches.

CHAPTER 4: Topographical characterization of the young, healthy human femoral medial condyle

Abstract

The medial femoral condyle of the knee exhibits some of the highest incidences of chondral degeneration, particularly within the posterior region. However, a dearth of healthy human tissues has rendered it difficult to ascertain whether cartilage in this compartment possesses properties that predispose it to injuries. Assessment of young, healthy tissue would be most representative of the tissue's intrinsic properties. This work examined the topographical differences in tribological, tensile, and compressive properties of young (26.2±5.6 years old), healthy, human medial femoral condyles, obtained from viable allograft specimens. Corresponding to clinical incidences of pathology, it was hypothesized that the lowest mechanical properties would be found in the posterior region of the medial condyle, and that tissue composition would correspond to the established structure-function relationships of cartilage. The Young's modulus, ultimate tensile strength, aggregate modulus, and shear modulus in the posterior region were 1.0-, 2.8-, 1.1-, and 1.0- fold less than the values in the anterior region, respectively. Surprisingly, although glycosaminoglycan content is thought to correlate with compressive properties, in this study, the aggregate and shear moduli correlated more robustly to the amount of pyridinoline crosslinks per collagen. Also, the coefficient of friction ranged 0.22-0.26 throughout the condyle, and did not differ with regard to direction of articulation. This work showed that the lower tensile and compressive properties of the posterior medial condyle have the potential of predisposing this region to injuries. Furthermore, new structure-function relationships may need to be developed to account for the role of collagen crosslinks in compressive properties.

Chapter submitted as: Salinas, E.Y.,* Otarola, G.A.,* Kwon, H., Wang, D., Hu, J.C., Athanasiou, K.A. Topographical characterization of the young, healthy human femoral medial condyle. Submitted to Osteoarthritis and Cartilage. (*These authors contributed equally.)

Introduction

Articular cartilage degeneration, affecting over 30 million US adults, usually occurs at specific regions of the distal femur (1). The patellofemoral groove and the lateral and medial condyles are exposed to different strains that contribute to characteristic lesion patterns (2-6). Grade IV chondral defects, the highest grade in which >50% of the cartilage thickness is affected and shows irregularities in the subchondral bone plate, are found predominantly in the medial femoral condyle (2, 3). These results are in agreement with radiological studies, which identified 60% of osteoarthritic lesions to be in the medial condyle, followed by the lateral condyle and the patellofemoral groove (7). Chondral defects, moreover, show topographical patterns; an examination of 127 distal femora not only confirmed higher incidence of lesions in the medial condyle compartment, but specifically identified a majority to localize in the posteromedial region (8). The higher incidences of degeneration in the posterior medial condyle may be due to topographical differences in biochemical and biomechanical properties, although this has yet to be verified due to the paucity of young, healthy specimens for characterization studies.

The mechanical properties of articular cartilage, which allow it to decrease the contact stresses in the joint and minimize friction and wear among opposing surfaces, differ throughout the knee, and evidence in multiple animals suggest that the posterior region of the medial condyle possesses inferior properties. For example, in terms of compressive properties, adult equine posterior medial condyles showed significantly lower aggregate and shear modulus values than the anterior region (9). Tensile Young's modulus and ultimate tensile strength (UTS) values were also found to be lower in the posterior medial condyle when compared to the anterior region in the sheep (10). Interestingly, in terms of the coefficient of friction, some of the highest values were observed in the posterior part of the medial condyle, while the anterior medial condyle showed the lowest coefficient of friction when examined in 1-3 month old calves (11). Thus, if humans share similar topographical trends as what has been observed in animals, one would expect to

find that the posterior medial condyle, a site of frequent degeneration, may also exhibit inferior compressive and tensile properties.

In contrast to the animal data presented above, only scant data exist on the human femoral condyle, especially of young, healthy tissue. The existing literature provides comparisons between the patellar groove and the medial and lateral condyles; a study that compared the femoral condyle cartilage across multiple species determined that, in the human knee, the aggregate modulus of the posterior region of the medial condyle was 16% lower than the modulus of the anterior region of the lateral condyle (12). However, no comparisons within the femoral condyles were included (12). Likewise, the same problem exists for the tensile properties in the femoral condyle. For example, studies have compared the tensile properties of medial and lateral condyles, associating them to biochemical changes that follow aging and chondral degeneration, but have not included different regions within the medial condyle (13, 14). Lastly, tribological data on the human medial condyle do not appear to be available. One study compared the coefficient of friction of tissue-engineered constructs to a human native tissue value (~0.25) (15). In short, the determination of mechanical properties and their correlation to biochemical properties for the human medial condyle, especially with respect to its regions, would represent information that has been long absent from the field despite the posterior medial condyle's predisposition for pathologies.

The lack of studies on human samples may be due to the scarcity of healthy, undamaged, young joint samples. This is relevant, because age affects the properties of cartilage, even if considered healthy. For example, in a study that examined the tensile properties of healthy and diseased human cartilage, the authors noted that even their control (i.e., non-degenerative) samples, with a mean age of 68±2 years, showed age-related damages such as surface roughness and fibrillation (13). Most human tissues found in other characterization studies were derived from middle aged (44-60) and elderly (60-75) donors, stages of life where sign of wear and susceptibility to osteoarthritis are expected (13, 16, 17). Moreover, as evidenced by prior

reports of “clinically silent” injuries, where the cartilage morphology appears undisturbed but the cells within the tissue are dead or dying, the chances of cartilage that appears morphologically normal but exhibits diminished functional properties also increases with age (18). Thus, for determining how the biomechanical properties of healthy cartilage are related to injuries and pathology, it would be desirable to assay healthy tissues derived from young donors. An updated characterization of the tribological, tensile, and compressive properties of a young adult cohort with healthy human femoral cartilage tissue, such as those used for allograft transplantation, is needed but not currently available in the literature.

In lieu of the limited characterization of the human condyle thus far, and the significance of the material properties of the medial condyle, the goal of this study was to provide a thorough, topographical characterization of healthy articular cartilage of the human medial condyle. This work includes the characterization of three locations of the articular cartilage of the medial femoral condyle: anterior, central, and posterior regions. Histological analysis was performed by staining for collagen, glycosaminoglycan, and cellular content. Extracellular matrix components were also quantified for glycosaminoglycan, collagen, and pyridinoline (PYR) crosslink contents. For tribological properties and tensile properties, the coefficient of friction, the Young’s modulus, and the ultimate tensile strength (UTS) were measured in both the direction of articulation and the direction perpendicular to articulation. Finally, for compressive assessment, the aggregate modulus, shear modulus, the 10% and 20% instantaneous moduli, the 10% and 20% relaxation moduli, and coefficient of viscosity were quantified. Corresponding to clinical incidences of pathology, it was hypothesized that the lowest mechanical properties would be found in the posterior region of the medial condyle, and that the biochemical composition and biomechanical properties would follow the well-established structure-function relationships for articular cartilage.

Methods

a

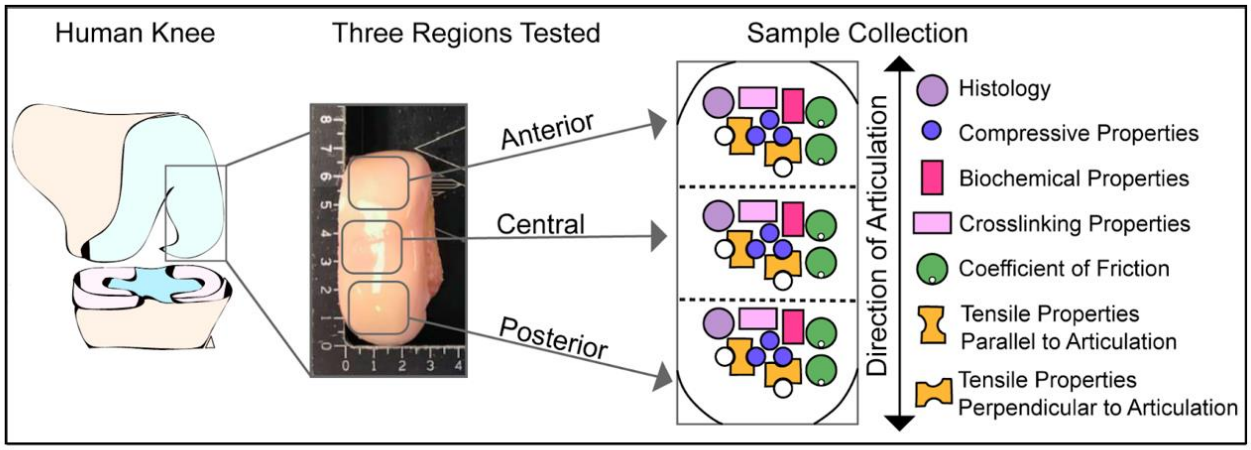

b

Sample	Donor Gender	Donor Age	Regions harvested	Condyle	Leg	Condyle Length (cm)	Condyle Width (cm)	Harvest Date	Company
1	F	19	**A, C, P**	**Medial**	Left	6	3	01.24.19	MTF
2	M	27	**A,C**	**Medial**	Left	7.6	3	03.28.19	JRF
3	M	31	**A,C,P**	**Medial**	Left	8.2	2.6	02.11.20	JRF
4	M	22	**A,P**	**Medial**	Right	6.3	2.9	06.16.20	JRF
5	M	32	**A,C,P**	**Medial**	Right	7.3	3.1	06.24.20	JRF

Figure 1. Experimental design for the characterization of the human medial femoral condyle. **(a)** Representative diagram of donor grafts used for specimen collection. All grafts were divided into three regions: anterior, central, and posterior. Samples were taken from each of these three regions to perform the assessments listed. **(b)** Detailed information regarding donors sampled. The mean age of the donors was 26.2±5.6 years.

Sample Collection

Human femoral condyle cartilage samples were collected from allograft transplantation surgeries at the University of California Irvine Medical Center. The femoral condyle allografts were initially collected from donors by JRF Ortho or MTF Biologics. The allografts were kept in a proprietary preservation solution for 2-6 weeks at 4°C until donor matching and transplantation surgery. During the allograft transplantation surgery, the patient would receive an 15-22.5mm diameter

core allograft taken from the donor condyle. The remaining tissue was immediately processed for testing and characterization for this study.

Five medial condyle allografts were collected for this study over a period of 18 months. The specimens were separated into three regions: anterior, central, and posterior (**Fig. 1a**). Samples from each region were obtained for histology, biochemical properties, tribology, tensile testing, and compressive testing. Sample collection was performed as follows: 1) histology: a 5mm diameter sample from each region of each condyle was taken and fixed in formalin. 2) Biochemical properties: 2x1mm samples were taken and frozen until testing. 3) Tribology: two 5mm diameter pieces were taken per region, and a 1mm diameter hole was marked in the bottom to indicate orientation. 4) Tensile properties: two dog bone-shaped pieces of tissue were taken, one in the anteroposterior direction and one in the mediolateral direction. 5) Compressive properties: 3mm biopsy punches were used to obtain separate samples for each region of each femoral condyle. Samples that were obtained for evaluation of the tribological, tensile, or compressive properties were preserved in protease inhibitor solution and frozen for a maximum of 18 months (19). The samples were then fully thawed before testing. The specimens used in this study came from four male and one female donors, with an age of 26.2±5.6 years (**Fig. 1b**).

Histology

Samples were fixed in 10% neutral-buffered formalin, embedded, and sectioned at a thickness of 6μm for histological evaluation. The sections were subsequently processed and stained with hematoxylin and eosin (H&E), safranin-O and fast green, and picrosirius red using standard protocols.

Biochemical Properties

Cartilage samples were trimmed to a similar size, excluding any calcified tissue. The samples were then weighed to obtain wet weight (WW), lyophilized for 3 days, and weighed again to obtain dry weight (DW). Lyophilized samples were digested in 125μg/mL papain (Sigma), 5mM N-acetyl-L-cysteine, and 5mM EDTA in phosphate buffer pH 6.5 for 18 hours at 60°C. DNA content was quantified with a Picogreen assay (ThermoFisher Scientific). Sulfated GAG content was quantified using a Blyscan Glycosaminoglycan Assay kit (Biocolor, Newtownabbey, Northern Ireland). Total collagen content was quantified using a modified chloramine-T hydroxyproline assay using Sircol 0.5 mg/ml acid-soluble bovine collagen as a standard (Biocolor) (20).

For the quantification of collagen PYR crosslinks, separate samples (~0.2-0.6 mg) were weighed, lyophilized, and acid-digested for 12 hours in 6N HCl at 105°C. After evaporation, dried hydrolysates were resuspended in a 75%/25% (v/v) solution of 0.1% formic acid and acetonitrile, filtered-centrifuged at 15,000g for 5 min, and the supernatant was transferred to a LCMS autosampler vial. Samples were measured via liquid chromatography mass spectrometry using a Cogent diamond hydride HPLC column (2.1mm x 150mm, particle size 2.2μm, pore size 120Å, MicroSolv) and a pyridinoline standard (BOC Sciences), as previously described (21).

Tribological Properties

Tribology was assessed using a custom pin-on-disk tribometer, as described previously under boundary lubrication conditions (11). For every donor tissue, two India ink-labelled 3mm punches were obtained and glued to the pin of the tribometer either parallel to the direction of articulation, or perpendicular, to obtain measurements in both orientations. All samples were immersed in phosphate buffered saline (PBS), allowed to reach equilibrium for 2 minutes, and then sheared against the test surface for 5 minutes with velocity set to 0.5mm/s and a compressive normal force applied by a 200g mass. The measured coefficient of friction describes the interaction between

the articular cartilage sample and the underlying glass plate immersed in PBS. Data were collected at a rate of 50Hz.

Tensile Properties

Uniaxial tension was performed in an Instron model 5565 (Instron, Canton, MA). Multiple dog bone-shaped samples were obtained from every donor sample, both parallel and perpendicular to the direction of articulation, with a gauge length of 1.55mm. For each direction, the top 1mm layer and full-thickness samples were prepared and photographed to measure thickness and width in ImageJ. The ends of the dog bone were fixed to paper tabs with cyanoacrylate outside the gauge length to increase the gripping area for testing, and pulled at a strain rate of 1% of the gauge length/second until failure. Using the cross-sectional area, the Young's modulus was obtained from the linear region of the stress-strain curve and the ultimate tensile strength (UTS) was defined as the maximum stress obtained.

Compressive Properties

The aggregate modulus and shear modulus were obtained using a semi-analytical, semi-numerical, biphasic model and finite-element optimization (22). Briefly, 3mm punches were obtained from each donor tissue sample and trimmed to a height of 1mm approx. Each sample was photographed, then submerged in PBS until equilibrium, and indented with a flat porous 1mm diameter tip perpendicular to the surface of the sample. A tare mass of 0.5g was applied until equilibrium was achieved, and a test mass of 7.5-12g was applied during testing, which corresponded to ~10% strain.

Relaxation modulus, instantaneous modulus, and coefficient of viscosity were calculated using a standard linear solid viscoelasticity model and an Instron model 5565 (Instron, Canton, MA) (23). For height detection, samples were submerged in PBS and compressed until reaching

a 0.2N force at a rate of 0.025mm/second, and compared to a reference value set prior to testing. For testing, samples were preconditioned with 10 cycles at 5% strain and a 10% strain rate of the sample height/second, and incremental stress-relaxation was performed at 10% and 20% strain.

Statistical Analysis

All quantitative biochemical and biomechanical tests were performed using a samples size of n=4-5. All data were presented as mean±standard deviation. A single factor one-way analysis of variance was used to assess differences among experimental groups. Multiple comparisons were performed using Tukey's *post hoc* test. All statistical analyses were performed using GraphPad Prism version 8.4.1 for Windows (GraphPad Software, San Diego, California USA). Groups marked with * indicate that there are statistically significant differences compared to the control group ($p<0.05$). The correlation analyses were also performed in GraphPad Prism using a two-tailed parametric Pearson correlation.

Results

Histological Evaluation

Histologic staining was used to visualize tissue morphology and distribution of collagen and glycosaminoglycan (**Fig. 2**). Per the companies providing the tissues for allograft transplantation, all donors' medical and social history were screened for medical conditions or diseases that could contraindicate the donation of tissues, in compliance with the FDA regulations published in 21 CFR Part 1271 Human Cells, Tissues, and Cellular and Tissue Based Products (24). Moreover, a physical assessment was performed by the companies in order to provide tissues that consist in mature, viable hyaline cartilage matrix, and proprietary processing methods for prolonged storage were used (e.g., JRF uses proprietary processing methods shown to maintain 80% absolute cartilage viability). Thus, considering the source of the samples and their intended use,

all chondral tissues were considered to be healthy (e.g., with no signs of chondral degeneration, morphological abnormalities, or physical/chemical damage) after a gross morphological examination.

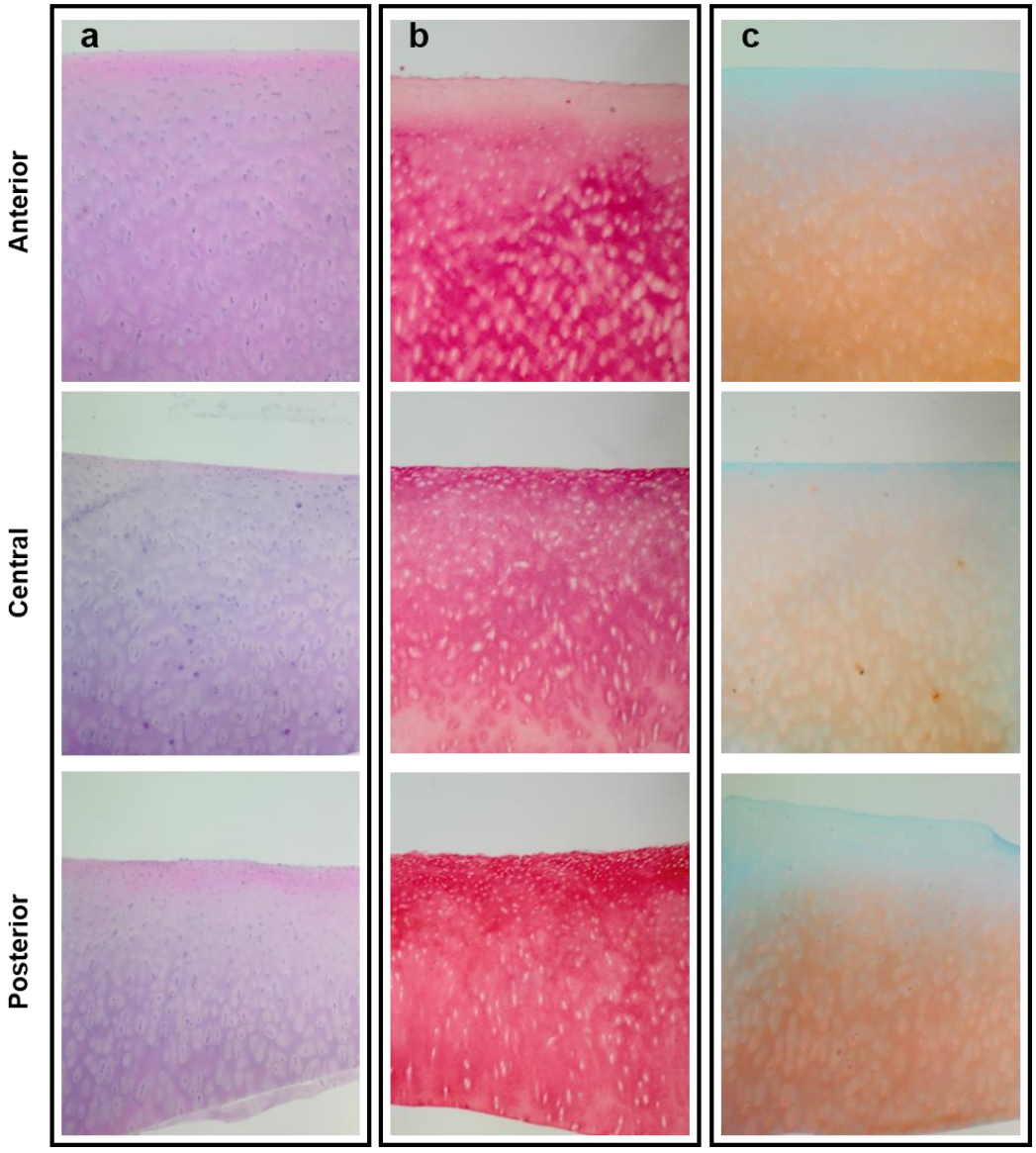

Figure 2. Histological analysis of the medial condyle. **(a)** Hematoxylin and eosin, **(b)** Picrosirius Red, and **(c)** Safranin-O staining obtained from a single representative donor. Isogenous groups were observed in all regions. Collagen staining was more intense toward the posterior regions, whereas GAG tended to accumulate in the deeper zone on all regions.

The adult cartilage H&E staining revealed a predominant basophilic stain, and an eosinophilic surface layer toward the anterior and posterior regions. Cell lacunae were observed in all regions of the medial condyle (**Fig. 2a**). Multiple isogenous groups and vertically arranged cells were also found toward the deep zone in all regions. The picrosirius red stain, to visualize total collagen distribution, showed a high intensity throughout the tissue and an increased intensity on the superficial zone toward the posterior region (**Fig. 2b**). The safranin-O stain, with a fast green counterstain, showed that GAG is primarily concentrated in the deep zone of cartilage, as reflected by the intensity of the stain (**Fig. 2c**).

Biochemical Properties

Glycosaminoglycan content, collagen content, and pyridinoline content of the native articular cartilage in the three topographical locations of the condyle are shown in Figure 3. Glycosaminoglycan content was normalized to both wet weight and dry weight (**Fig. 3a**). There were no significant differences among the regions in terms of glycosaminoglycan normalized to wet weight, with an averaged content ranging between 5% and 6.8%. Likewise, there were no significant differences in terms of glycosaminoglycan content normalized to dry weight. The anterior region contained 20.9±3.7% glycosaminoglycan per dry weight, whereas the central and posterior regions contained 18.8±7.4% and 18.2±2.6% glycosaminoglycan per dry weight respectively. Similarly, no significant differences the collagen content per wet weight showed, albeit with an increase in the posterior region (**Fig. 3b**). This difference is significant when normalizing the collagen content per dry weight; the posterior region showed significantly higher amount of collagen (78.4±11.8%) compared to the anterior (52.3±11.2%) and central (47.1±22.2%) regions. Finally, no significant differences among the regions were found when comparing the quantification of pyridinoline crosslinks content per wet weight (**Fig. 3c**). However,

the pyridinoline content per collagen content revealed a significant increase of the collagen crosslinking toward the central and the anterior region.

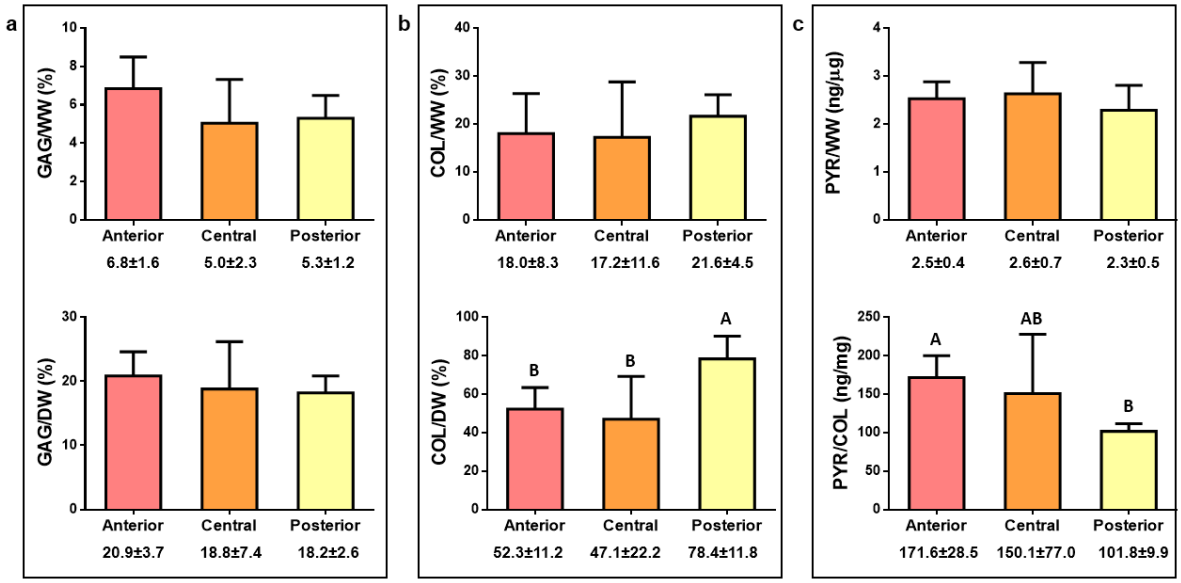

Figure 3. Biochemical properties of the human medial femoral cartilage. **(a)** GAG/WW and GAG/DW, **(b)** COL/WW and COL/DW, and **(c)** PYR/WW and PYR/COL. The posterior region of the medial condyle showed higher collagen content, albeit less crosslinked compared to the collagen in anterior and central regions. Different uppercase letters over bars indicate statistical difference between groups. Absence of letters indicate no significant differences.

Tribological Properties

The coefficient of friction of the anterior, central, and posterior regions of the human femoral condyle were characterized using a tribometer as described previously (11). The coefficients of friction for each region were obtained in two directions: 1) in the direction of articulation, and 2) perpendicular to articulation (**Fig. 4**). Interestingly, there were no significant differences in the coefficient of friction when comparing directionality. Additionally, there were also no significant

differences among the coefficient of friction of the three regions. For all regions, regardless of the location and direction tested, the coefficient of friction varied between 0.22 and 0.26 (**Fig. 4**).

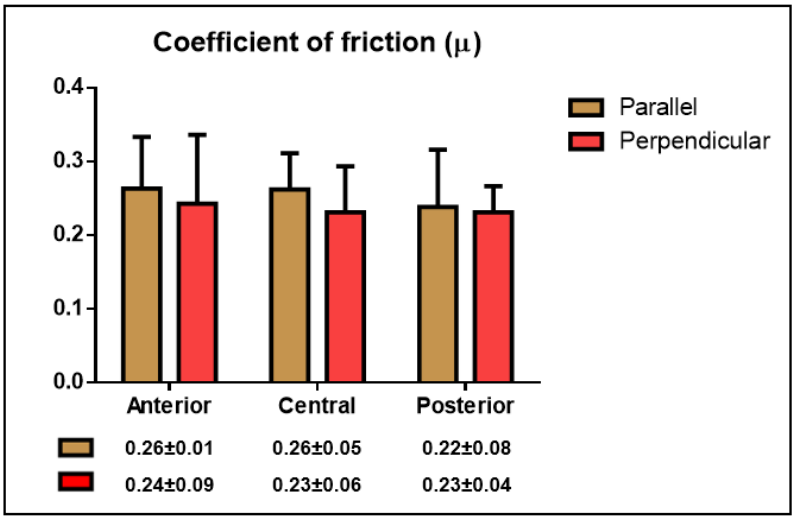

Figure 4. Coefficient of friction of the articular cartilage surface. Three distinct regions of human femoral cartilage were tested in two directions: parallel to the direction of articulation and perpendicular to the direction of articulation. The Coefficient of friction was isotropic and homogeneous throughout the medial condyle in young, healthy tissues.

Tensile Properties

For the characterization of the tensile properties, all three regions (anterior, central, and posterior) were tested in the direction of articulation and perpendicular to the direction of articulation (**Fig. 5a and 5b**). Furthermore, both the top 1mm layer and full-thickness (~2.5mm) tissue were tested and compared (25).

The Young's modulus and UTS of the human femoral condyle were characterized in the direction parallel to articulation (**Fig. 5a**). The anterior region possessed significantly higher Young's modulus values for both top 1mm layer and full-thickness tissues (32.5±11.7MPa and 22.9±7MPa, respectively) compared to top 1mm layer and full-thickness tissues of the central

region (12.4±4.5MPa and 7.0±0.5MPa, respectively). The posterior region was also less stiff compared to the anterior region, albeit only significant for the full-thickness tissue (11.6±3.3MPa). In terms of the UTS, the anterior region of the condyle had a significantly higher strength compared to the central and posterior regions, regardless of the layer measured. Lastly, and although the stiffness of the top 1mm layer trended higher than the stiffness of the full-thickness tissue, the comparison between both measurements showed no significant differences in this study.

The tensile properties of the human femoral condyle were also characterized in the direction perpendicular to articulation, as indicated in the schematic shown in Figure 1a. No regional differences of the Young's modulus or the UTS were observed when testing the tissue in this direction (**Fig. 5b**).

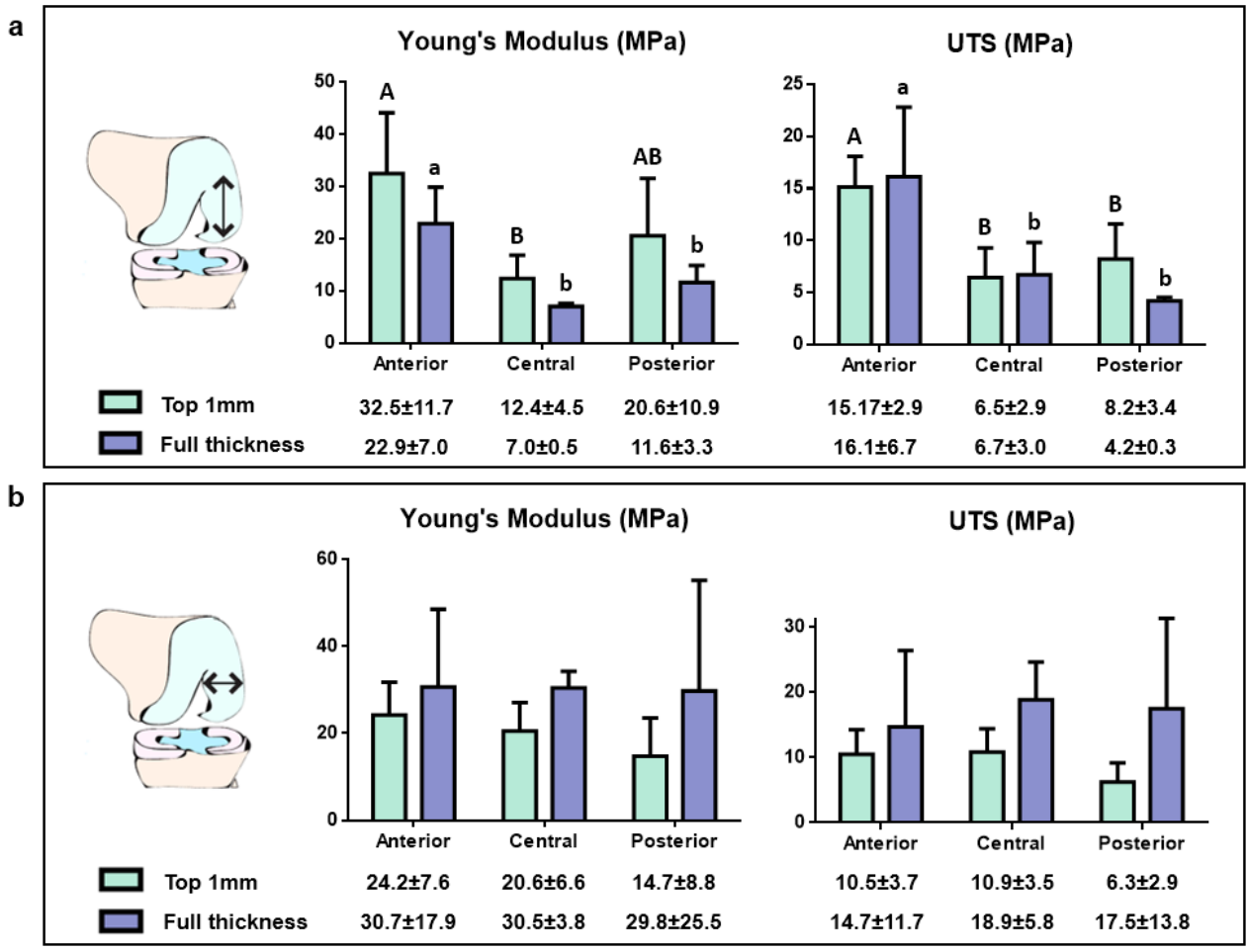

Figure 5. Tensile properties of the human medial femoral condyle. **(a)** Young's modulus and ultimate tensile strength (UTS) of articular cartilage in the anteroposterior direction. **(b)** Young's modulus and ultimate tensile strength (UTS) of articular cartilage in the mediolateral direction. Letters depict the connecting letters report. Different uppercase or lowercase letters over bars indicate statistical difference between groups for the top 1mm layer and the full-thickness tissue (~2.5mm) measurements, correspondingly. Absence of letters indicate no significant differences.

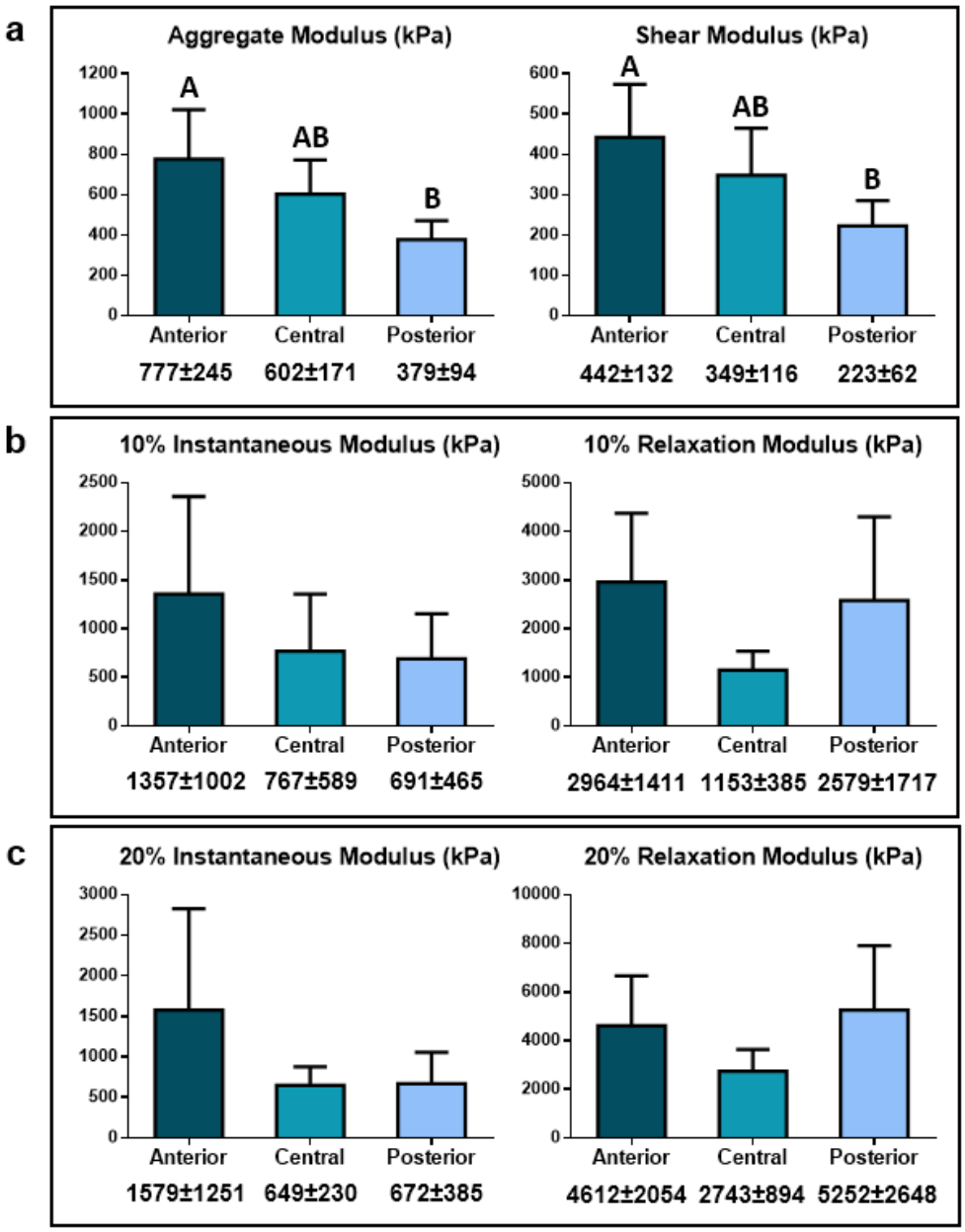

Figure 6. Compressive properties of three distinct regions of human femoral cartilage. **(a)** Aggregate modulus and shear modulus. **(b)** Instantaneous modulus and relaxation modulus at 10% strain. **(c)** Instantaneous modulus and relaxation modulus at 20% strain. Different uppercase letters over bars indicate statistical difference between groups. Absence of letters indicate no significant differences.

Compressive properties

The compressive properties of articular cartilage were characterized using two different modalities: compressive creep indentation was performed to obtain the aggregate and shear modulus values, and unconfined compression was performed to determine the compressive instantaneous modulus and relaxation modulus at 10% and 20% strains.

Aggregate modulus obtained from creep indentation varied significantly between the anterior and posterior regions of the medial condyle. The aggregate modulus of the anterior region was 777±245kPa, whereas for the posterior region 379±94kPa. The central region, with an aggregate modulus of 602±171kPa, represents a transition region between the regions with highest and lowest compressive values (**Fig. 6a**). Shear modulus values also varied significantly following the same pattern observed for the aggregate modulus. The shear modulus values for the anterior, central, and posterior regions of the human femoral condyle were 442±132kPa, 349±116kPa, and 223±62kPa, respectively, with the anterior and posterior regions being significantly different (**Fig. 6a**).

Compressive stress-relaxation testing showed no significant differences among the condylar regions (**Fig. 6b**). The average instantaneous modulus at 10% strain was 1357±1002kPa for the anterior region, 767±589kPa for the central region, and 691±465kPa for the posterior region of the human femoral condyle. The average relaxation modulus at 10% strain was 2964±1411kPa for the anterior region, 1153±385kPa for the central region, and 2579±1717kPa for the posterior region of the human femoral condyle. No significant differences between the measured regions were observed at 20% strain (**Fig. 6c**). The average instantaneous modulus at 20% strain was 1579±1251kPa for the anterior region, 649±230kPa for the central region, and 672±385kPa for the posterior region of the human femoral condyle. The average relaxation modulus at 20% strain was 4612±2054kPa for the anterior region, 2743±894kPa for the central region, and 5252±2648kPa for the posterior region of the human

femoral condyle. No significant differences were observed in the coefficient of viscosity (**Supplementary Table 1**).

A high correlation was found between the compressive properties and the PYR/COL content, for both the aggregate modulus (R^2=0.98) and the shear modulus (R^2=0.98) (**Supplementary Table 2**). The correlation between the compressive properties and the PYR crosslinks was higher than the correlation of compressive properties and GAG/DW content (R^2=0.86 and R^2=0.85 for aggregate modulus and shear modulus, respectively), and higher than the correlation between tensile properties and PYR crosslinks (R^2=0.26 and R^2=0.73 for Young's modulus and UTS, respectively).

Discussion

Toward elucidating whether topographical differences in cartilage properties exist in the medial femoral condyle and whether such differences inform the incidences of pathology, this study applied histological, biochemical, and mechanical assays to the anterior, central, and posterior regions of young (mean age of 26.2±5.6 years), healthy human medial condyles. It was hypothesized that the posterior region of the medial condyle would exhibit the lowest mechanical properties, and that tissue composition would follow the established structure-function paradigm for articular cartilage. The rationale for this hypothesis comes from the limited data currently available on human tissues, together with animal characterization studies (9, 12). Although the tribological characteristics of bovine, equine, porcine, and ovine cartilage have been previously investigated (26), to the best of our knowledge, this study is the first to provide a detailed description of the tribological properties of human femoral condyle articular cartilage, including topographical and directional data. It was found that, for the young, healthy tissues examined, tribological properties did not significantly differ when testing in the direction of articulation or perpendicular to articulation, indicating frictional isotropy. In contrast to the coefficient of friction, the Young's modulus and UTS showed topographical variation when measured in the direction of

articulation. For the full-thickness samples, the anterior region showed the highest values, which were 3.3 and 2.0 times greater than the central and posterior regions for the Young's modulus, and 2.4 and 3.8 times greater than in the central and posterior regions for UTS. The compressive properties also varied within the medial condyle. The aggregate modulus of the anterior region was 1.4 and 2.1 times greater than the central and posterior regions, and the shear modulus was 1.3 and 2.0 times greater than in the central and posterior regions. Collagen content and PYR crosslink per collagen content also showed topographical variations. Importantly, the collagen crosslink content was correlated with UTS (R^2=0.73), but this correlation was much stronger with the compressive properties (R^2=0.98). This work's findings are significant for providing 1) tribological properties of young, healthy human cartilage in multiple directions, 2) evidence of new structure-function relationships between collagen crosslinks and compressive properties in healthy, young samples, and 3) an assessment of healthy human articular cartilage of the medial condyle toward understanding degenerative processes.

While the compressive and tensile properties have been extensively covered in literature, the tribological properties of articular cartilage have, thus far, been overlooked, and limited data have been collected from human tissues. Thus, the assessment of the tribological properties of articular cartilage is relevant toward the development of new functional cartilage therapies (15, 26). In this study, characterization of young, healthy human medial condyle cartilage showed that the coefficient of friction under boundary lubrication appeared isotropic and ranged between 0.22 and 0.26, with no significant differences among topographical regions. This finding is significant because it provides a target value for the coefficient of friction of engineered implants intended to repair or replace human cartilage. For comparison, a wide range of coefficient of friction (from 0.002 to 0.5) has been reported for animal cartilages in the past depending on the tissue and loading configuration used (11, 27-30), and, of these, only one reported topographical differences, showing that the posterior medial condyle had the highest value (11). It should be noted that the coefficient of friction varies from study to study due to differences in tissue age, testing

configuration (boundary vs. dynamic lubrication), and the presence of PBS or synovial fluid (31, 32). In a recent review (33), the only human tribological data provided was a coefficient of friction of 0.013 for the human hip, highlighting the dearth of information on this topic. The lack of additional evidence of human articular cartilage coefficient of friction values highlights the significance of the tribological results obtained in this work.

The friction coefficient of bovine articular cartilage has been shown to depend on testing direction (19), leading one to anticipate anisotropy for human cartilage tribology as well. However, no significant differences in the coefficient of friction were observed when testing parallel or perpendicular to the direction of articulation. A possible cause for the lack of anisotropy may be the age of the donors used in this study. With an average age of 26.2±5.6 years and all tissues in healthy condition (approved for their use as allogeneic implants), the articular cartilage examined in this study might have been exposed to considerably less age-related wear, a factor known to affect tissue properties (14, 33). The observation that young, healthy tissue does not display anisotropy in its frictional properties may indicate that implants, including tissue-engineered neocartilage, would not have to be designed to have directional coefficients of friction.

This study found that tensile properties of the medial condyle vary according to location. The posterior region showed significantly lower Young's modulus and UTS values compared to the central and anterior regions, when the testing was performed anteroposteriorly in the direction of articulation. In contrast, the collagen content was significantly larger in the posterior region compare to the central and anterior regions. From established structure-function relationships for articular cartilage, e.g., collagen content correlates with tensile properties, one would infer that the collagen content in the posterior region would be lower as well. In this study, the collagen/DW content found for the anterior, central, and posterior regions were 52.3±11.2%, 47.1±22.2%, and 78.4±11.8%, respectively. These values were on par with literature; previous reports have found collagen content to be ~60% of the dry weight of cartilage (34). However, collagen did not correlate with tensile properties. This may be due to several reasons, such as variable collagen

organization from region to region due to the different stresses to which different regions are exposed (35). Our results showed that the PYR crosslink per collagen correlates with the tensile properties, especially the UTS (R^2=0.73). Differences in crosslinks may better explain the increase in the tensile properties, as the formation of covalent PYR crosslinks between individual collagen fibers stabilizes the formation of heterotypic fibrils and the tissue ECM (36). It is, thus, suggested that the PYR crosslink content is an important contributor to tensile properties.

The tensile properties in the top layer as well as the full-thickness of articular cartilage were also quantified. The Young's modulus values consistently trended higher in the top 1mm layer samples compared to the full-thickness samples, when testing in the direction of articulation. This is in agreement with prior work in the bovine model, which showed that the superficial zone, corresponding to 250-500μm of the top surface, has a higher tensile stiffness than the full-thickness tissue (37). Also, although tissues were tested in two directions, the tensile properties did not differ significantly between the anteroposterior and mediolateral directions. This could be because in this study we tested the top 1mm layer, which includes not only the superficial zone (top 250-500μm), but also portions of the middle zone. More work needs to be done on characterizing the tensile properties of young, healthy knee cartilage, especially to establish zonal effects.

The compressive properties of the medial condyle also decrease in the anterior-posterior direction. As shown in Figure 6, the aggregate modulus and the shear modulus of the posterior region were 2.1 and 2.0 times lower than those of the anterior region. Similar results were observed for the 10% instantaneous modulus, however, the high variability observed in the stress-relaxation data calls for a larger number of samples. In terms of the known relationship between GAGs and compressive properties (38), our results showed correlations between GAG/DW and aggregate modulus (R^2=0.93) and shear modulus (R^2=0.86) (**Supplementary Table 2**). Surprisingly, higher correlation values were found between the degree of collagen crosslinking and aggregate modulus (R^2=0.98) as well as shear modulus (R^2=0.98). As shown in Figure 3, the

PYR per collagen of the posterior region was 1.7 and 1.5 times lower than that of the anterior and central region. While GAG content did not differ among the regions tested, the crosslink content was significantly lower in the posterior region, just like the compressive properties. Thus, it is suggested that the structure-function paradigm in articular cartilage should include consideration of collagen crosslinks. Compared to the correlation of GAG content to compressive properties, the correlation of crosslink content to compressive properties not only showed higher R^2 values but similar differences across regions.

While the coefficient of friction was isotropic and homogeneous throughout the medial condyle, the lower tensile and compressive properties identified in the posterior medial condyle of young, healthy donors may be associated with the higher prevalence of tissue degeneration in the posterior region (8). Our results show that UTS, aggregate modulus, and shear modulus have a strong and positive correlation to the degree of collagen crosslinking (PYR/Col). Thus, articular cartilage's predisposition to pathologies may be better predicted by the degree of PYR crosslinks. This new emerging relationship between PYR crosslinks and strength and stiffness of the articular cartilage matrix may also be linked to degenerative diseases in the knee joint.

The biochemical and mechanical properties of the human condyle, especially from young and healthy donors, are yet to be fully determined. In this study, a topographical analysis of the medial condyle was performed, including biochemical, tribological, tensile, and compressive properties. The results showed isotropy and homogeneity of the coefficient of friction, whereas the tensile and compressive properties varied according to location. Also, new structure-function relationships emerged. Specifically, UTS, aggregate modulus, and shear modulus were shown to have a strong correlation with the PYR crosslink per collagen content. Lastly, the posterior region of the condyle, which has been shown to be the region with the highest incidence of chondral degeneration, was identified as the region with the lowest tensile properties, compressive properties, and PYR/collagen, indicating that these tissue properties may predispose the cartilage to injuries and degeneration.

Acknowledgements

The authors acknowledge support from the National Institutes of Health (NIH) R01 AR067821 and Fulbright Chile scholarship.

References

1. Chen D, Shen J, Zhao W, Wang T, Han L, Hamilton JL, Im HJ. Osteoarthritis: toward a comprehensive understanding of pathological mechanism. Bone research. 2017;5:16044. doi: 10.1038/boneres.2016.44. PubMed PMID: 28149655; PubMed Central PMCID: PMC5240031.
2. Widuchowski W, Lukasik P, Kwiatkowski G, Faltus R, Szyluk K, Widuchowski J, Koczy B. Isolated full thickness chondral injuries. Prevalance and outcome of treatment. A retrospective study of 5233 knee arthroscopies. Acta chirurgiae orthopaedicae et traumatologiae Cechoslovaca. 2008;75(5):382-6. PubMed PMID: 19026193.
3. Curl WW, Krome J, Gordon ES, Rushing J, Smith BP, Poehling GG. Cartilage injuries: a review of 31,516 knee arthroscopies. Arthroscopy : the journal of arthroscopic & related surgery : official publication of the Arthroscopy Association of North America and the International Arthroscopy Association. 1997;13(4):456-60. doi: 10.1016/s0749-8063(97)90124-9. PubMed PMID: 9276052.
4. Aroen A, Loken S, Heir S, Alvik E, Ekeland A, Granlund OG, Engebretsen L. Articular cartilage lesions in 993 consecutive knee arthroscopies. The American journal of sports medicine. 2004;32(1):211-5. doi: 10.1177/0363546503259345. PubMed PMID: 14754746.
5. Figueroa D, Calvo R, Vaisman A, Carrasco MA, Moraga C, Delgado I. Knee chondral lesions: incidence and correlation between arthroscopic and magnetic resonance findings. Arthroscopy : the journal of arthroscopic & related surgery : official publication of the Arthroscopy Association of North America and the International Arthroscopy Association. 2007;23(3):312-5. doi: 10.1016/j.arthro.2006.11.015. PubMed PMID: 17349476.
6. Widuchowski W, Widuchowski J, Trzaska T. Articular cartilage defects: study of 25,124 knee arthroscopies. The Knee. 2007;14(3):177-82. doi: 10.1016/j.knee.2007.02.001. PubMed PMID: 17428666.
7. Davies AP, Vince AS, Shepstone L, Donell ST, Glasgow MM. The radiologic prevalence of patellofemoral osteoarthritis. Clinical orthopaedics and related research. 2002(402):206-12. doi: 10.1097/00003086-200209000-00020. PubMed PMID: 12218486.
8. Bae WC, Payanal MM, Chen AC, Hsieh-Bonassera ND, Ballard BL, Lotz MK, Coutts RD, Bugbee WD, Sah RL. Topographic Patterns of Cartilage Lesions in Knee Osteoarthritis. Cartilage. 2010;1(1):10-9. doi: 10.1177/1947603509354991. PubMed PMID: 20664706; PubMed Central PMCID: PMC2909594.
9. White JL, Salinas EY, Link JM, Hu JC, Athanasiou KA. Characterization of Adult and Neonatal Articular Cartilage From the Equine Stifle. Journal of equine veterinary science. 2021;96:103294. doi: 10.1016/j.jevs.2020.103294. PubMed PMID: 33349403.

10. Huwe LW, Brown WE, Hu JC, Athanasiou KA. Characterization of costal cartilage and its suitability as a cell source for articular cartilage tissue engineering. Journal of tissue engineering and regenerative medicine. 2018;12(5):1163-76. doi: 10.1002/term.2630. PubMed PMID: 29286211; PubMed Central PMCID: PMC5948132.
11. Peng G, McNary SM, Athanasiou KA, Reddi AH. The distribution of superficial zone protein (SZP)/lubricin/PRG4 and boundary mode frictional properties of the bovine diarthrodial joint. Journal of biomechanics. 2015;48(12):3406-12. doi: 10.1016/j.jbiomech.2015.05.032. PubMed PMID: 26117076; PubMed Central PMCID: PMC4615312.
12. Athanasiou KA, Rosenwasser MP, Buckwalter JA, Malinin TI, Mow VC. Interspecies comparisons of in situ intrinsic mechanical properties of distal femoral cartilage. Journal of orthopaedic research : official publication of the Orthopaedic Research Society. 1991;9(3):330-40. doi: 10.1002/jor.1100090304. PubMed PMID: 2010837.
13. Temple-Wong MM, Bae WC, Chen MQ, Bugbee WD, Amiel D, Coutts RD, Lotz M, Sah RL. Biomechanical, structural, and biochemical indices of degenerative and osteoarthritic deterioration of adult human articular cartilage of the femoral condyle. Osteoarthritis and cartilage. 2009;17(11):1469-76. doi: 10.1016/j.joca.2009.04.017. PubMed PMID: 19464244; PubMed Central PMCID: PMC2763930.
14. Temple MM, Bae WC, Chen MQ, Lotz M, Amiel D, Coutts RD, Sah RL. Age- and site-associated biomechanical weakening of human articular cartilage of the femoral condyle. Osteoarthritis and cartilage. 2007;15(9):1042-52. doi: 10.1016/j.joca.2007.03.005. PubMed PMID: 17468016.
15. Middendorf JM, Griffin DJ, Shortkroff S, Dugopolski C, Kennedy S, Siemiatkoski J, Cohen I, Bonassar LJ. Mechanical properties and structure-function relationships of human chondrocyte-seeded cartilage constructs after *in vitro* culture. Journal of orthopaedic research : official publication of the Orthopaedic Research Society. 2017;35(10):2298-306. doi: 10.1002/jor.23535. PubMed PMID: 28169453.
16. Shane Anderson A, Loeser RF. Why is osteoarthritis an age-related disease? Best practice & research Clinical rheumatology. 2010;24(1):15-26. doi: 10.1016/j.berh.2009.08.006. PubMed PMID: 20129196; PubMed Central PMCID: PMC2818253.
17. Castell MV, van der Pas S, Otero A, Siviero P, Dennison E, Denkinger M, Pedersen N, Sanchez-Martinez M, Queipo R, van Schoor N, Zambon S, Edwards M, Peter R, Schaap L, Deeg D. Osteoarthritis and frailty in elderly individuals across six European countries: results from the European Project on OSteoArthritis (EPOSA). BMC musculoskeletal disorders. 2015;16:359. doi: 10.1186/s12891-015-0807-8. PubMed PMID: 26578262; PubMed Central PMCID: PMC4650343.
18. Natoli RM, Scott CC, Athanasiou KA. Temporal effects of impact on articular cartilage cell death, gene expression, matrix biochemistry, and biomechanics. Annals of biomedical engineering. 2008;36(5):780-92. doi: 10.1007/s10439-008-9472-5. PubMed PMID: 18299988.
19. Espinosa MG, Otarola GA, Hu JC, Athanasiou KA. Cartilage Assessment Requires a Surface Characterization Protocol: Roughness, Friction, and Function. Tissue engineering Part C, Methods. 2021;27(4):276-86. doi: 10.1089/ten.TEC.2020.0367. PubMed PMID: 33678002; PubMed Central PMCID: PMC8064968.
20. Cissell DD, Link JM, Hu JC, Athanasiou KA. A Modified Hydroxyproline Assay Based on Hydrochloric Acid in Ehrlich's Solution Accurately Measures Tissue Collagen Content. Tissue

engineering Part C, Methods. 2017;23(4):243-50. doi: 10.1089/ten.tec.2017.0018. PubMed PMID: 28406755; PubMed Central PMCID: PMC5397204.
21. Bielajew BJ, Hu JC, Athanasiou KA. Methodology to Quantify Collagen Subtypes and Crosslinks: Application in Minipig Cartilages. Cartilage. 2021;13(2_suppl):1742S-54S. doi: 10.1177/19476035211060508. PubMed PMID: 34823380; PubMed Central PMCID: PMC8804780.
22. Athanasiou KA, Niederauer GG, Schenck RC, Jr. Biomechanical topography of human ankle cartilage. Annals of biomedical engineering. 1995;23(5):697-704. doi: 10.1007/bf02584467. PubMed PMID: 7503470.
23. Mow VC, Kuei SC, Lai WM, Armstrong CG. Biphasic creep and stress relaxation of articular cartilage in compression? Theory and experiments. Journal of biomechanical engineering. 1980;102(1):73-84. doi: 10.1115/1.3138202. PubMed PMID: 7382457.
24. US Food and Drug Administration. Guidance for Industry: Regulation of Human Cells, Tissues, and Cellular and Tissue-Based Products (HCT/Ps)2007.
25. Akizuki S, Mow VC, Muller F, Pita JC, Howell DS. Tensile properties of human knee joint cartilage. II. Correlations between weight bearing and tissue pathology and the kinetics of swelling. Journal of orthopaedic research : official publication of the Orthopaedic Research Society. 1987;5(2):173-86. doi: 10.1002/jor.1100050204. PubMed PMID: 3572588.
26. Link JM, Salinas EY, Hu JC, Athanasiou KA. The tribology of cartilage: Mechanisms, experimental techniques, and relevance to translational tissue engineering. Clinical biomechanics. 2020;79:104880. doi: 10.1016/j.clinbiomech.2019.10.016. PubMed PMID: 31676140; PubMed Central PMCID: PMC7176516.
27. Forster H, Fisher J. The influence of continuous sliding and subsequent surface wear on the friction of articular cartilage. Proceedings of the Institution of Mechanical Engineers Part H, Journal of engineering in medicine. 1999;213(4):329-45. doi: 10.1243/0954411991535167. PubMed PMID: 10466364.
28. Schmidt TA, Sah RL. Effect of synovial fluid on boundary lubrication of articular cartilage. Osteoarthritis and cartilage. 2007;15(1):35-47. doi: 10.1016/j.joca.2006.06.005. PubMed PMID: 16859933.
29. Oungoulian SR, Durney KM, Jones BK, Ahmad CS, Hung CT, Ateshian GA. Wear and damage of articular cartilage with friction against orthopedic implant materials. Journal of biomechanics. 2015;48(10):1957-64. doi: 10.1016/j.jbiomech.2015.04.008. PubMed PMID: 25912663; PubMed Central PMCID: PMC4492870.
30. Warnecke D, Messemer M, de Roy L, Stein S, Gentilini C, Walker R, Skaer N, Ignatius A, Durselen L. Articular cartilage and meniscus reveal higher friction in swing phase than in stance phase under dynamic gait conditions. Scientific reports. 2019;9(1):5785. doi: 10.1038/s41598-019-42254-2. PubMed PMID: 30962482; PubMed Central PMCID: PMC6453962.
31. Caligaris M, Canal CE, Ahmad CS, Gardner TR, Ateshian GA. Investigation of the frictional response of osteoarthritic human tibiofemoral joints and the potential beneficial tribological effect of healthy synovial fluid. Osteoarthritis and cartilage. 2009;17(10):1327-32. doi: 10.1016/j.joca.2009.03.020. PubMed PMID: 19410031; PubMed Central PMCID: PMC2753744.
32. Caligaris M, Ateshian GA. Effects of sustained interstitial fluid pressurization under migrating contact area, and boundary lubrication by synovial fluid, on cartilage friction. Osteoarthritis and

cartilage. 2008;16(10):1220-7. doi: 10.1016/j.joca.2008.02.020. PubMed PMID: 18395475; PubMed Central PMCID: PMC2622427.
33. Lin W, Klein J. Recent Progress in Cartilage Lubrication. Advanced materials. 2021;33(18):e2005513. doi: 10.1002/adma.202005513. PubMed PMID: 33759245.
34. Sophia Fox AJ, Bedi A, Rodeo SA. The basic science of articular cartilage: structure, composition, and function. Sports health. 2009;1(6):461-8. doi: 10.1177/1941738109350438. PubMed PMID: 23015907; PubMed Central PMCID: PMC3445147.
35. Shriram D, Praveen Kumar G, Cui F, Lee YHD, Subburaj K. Evaluating the effects of material properties of artificial meniscal implant in the human knee joint using finite element analysis. Scientific reports. 2017;7(1):6011. doi: 10.1038/s41598-017-06271-3. PubMed PMID: 28729605; PubMed Central PMCID: PMC5519683.
36. Eleswarapu SV, Responte DJ, Athanasiou KA. Tensile properties, collagen content, and crosslinks in connective tissues of the immature knee joint. PloS one. 2011;6(10):e26178. doi: 10.1371/journal.pone.0026178. PubMed PMID: 22022553; PubMed Central PMCID: PMC3192771.
37. Oinas J, Ronkainen AP, Rieppo L, Finnila MAJ, Iivarinen JT, van Weeren PR, Helminen HJ, Brama PAJ, Korhonen RK, Saarakkala S. Composition, structure and tensile biomechanical properties of equine articular cartilage during growth and maturation. Scientific reports. 2018;8(1):11357. doi: 10.1038/s41598-018-29655-5. PubMed PMID: 30054498; PubMed Central PMCID: PMC6063957.
38. Willard VP, Kalpakci KN, Reimer AJ, Athanasiou KA. The regional contribution of glycosaminoglycans to temporomandibular joint disc compressive properties. Journal of biomechanical engineering. 2012;134(1):011011. doi: 10.1115/1.4005763. PubMed PMID: 22482666; PubMed Central PMCID: PMC3616643.

Supplementary material

Supplementary table 1. Coefficients of viscosity at 10% and 20% strain. Data are presented as means ± standard deviation.

Region	10% Viscosity (MPa*s)	20% Viscosity (MPa*s)
Anterior	43.05±32.98	240.26±168.86
Central	67.29±55.06	321.88±213.83
Posterior	89.56±73.11	411.92±296.88

Supplementary table 2. Correlation analyses performed using a two-tailed parametric Pearson correlation. r, Pearson correlation coefficient, R^2, Coefficient of determination. Ey, Young's modulus. UTS, ultimate tensile strength. H_A, aggregate modulus. S.M., shear modulus.

Correlation	Pearson r	R^2
Ey and PYR/Col	0.5100	0.2601
UTS and PYR/Col	0.8523	0.7264
H_A and GAG/DW	0.9281	0.9223
S.M. and GAG/DW	0.8614	0.8506
H_A and PYR/Col	0.9875	0.9752
S.M. and PYR/Col	0.9898	0.9798

CHAPTER 5: Intracellular calcium and sodium modulation of self-assembled neocartilage using costal chondrocytes

Abstract

Ion signaling via Ca^{2+} and Na^{+} plays a key role in mechanotransduction and encourages a chondrogenic phenotype and tissue maturation. Here, we propose that the pleiotropic effects of Ca^{2+} and Na^{+} modulation can be used to induce maturation and improvement of neocartilage derived from re-differentiated expanded chondrocytes from minipig rib cartilage. Three ion modulators were employed: 1) 4α-phorbol-12,13-didecanoate (4-αPDD), an agonist of the Ca^{2+}-permeable transient receptor potential vanilloid 4 (TRPV4), 2) ouabain, an inhibitor of the Na^{+}/K^{+} pump, and 3) ionomycin, a Ca^{2+} ionophore. These ion modulators were used individually or in combination. While no beneficial effects were observed when using combinations of the ion modulators, single treatment of constructs with the three ion modulators resulted in multiple effects in structure-function relationships. The most significant findings were related to ionomycin. Treatment of neocartilage with ionomycin produced 61% and 115% increases in glycosaminoglycan and pyridinoline crosslink content, respectively, compared to the control. Moreover, treatment with this Ca^{2+} ionophore resulted in a 45% increase of the aggregate modulus, and a 63% increase in the tensile Young's modulus, resulting in aggregate and Young's moduli of 567 kPa and 8.43 MPa, respectively. These results support the use of ion modulation to develop biomimetic neocartilage using expanded re-differentiated costal chondrocytes.

Chapter published as: Otarola, G.A., Hu, J.C., Athanasiou, K.A. Intracellular calcium and sodium modulation of self-assembled neocartilage using costal chondrocytes. Tissue Engineering Part A; 27(4): 276-286.

Introduction

Stimulation of tissue maturation via mechanotransduction stands as a promising strategy to engineer neocartilage with appropriate biomechanical properties. Maturation of neotissues grown *in vitro* is a key step toward improving the mimicry of neocartilage to its native counterpart. For example, treatment of neocartilage constructs with Lysyl oxidase-like 2 (LoxL2), which catalyzes the pyridinoline (PYR) crosslink typically found in mature articular cartilage (AC), is highly efficient but has a narrow target effect (1). Conversely, the use of bioreactors to simulate mechanical cues found in the joint enable the activation of signaling cascades with pleiotropic effects in the neotissue (2). Stimuli such as compression, tension, fluid shear, and hydrostatic pressure have been employed to improve the biomechanical properties of engineered neocartilage (3-6). The activation of chondrogenic signaling pathways via mechanotransduction has been shown to favor a more cartilaginous extracellular matrix (ECM) in terms of composition (*e.g.*, collagen types and content), macromolecule bonding (*e.g.*, PYR crosslinks), and collagen alignment (anisotropy) (7, 8). Taking into consideration the multiple targets of mechanical stimulation, it is essential that a more critical breakdown of its various effects is carried out to inform cogent tissue engineering approaches.

Ion signaling plays a key role in mechanotransduction. The well characterized mechanoelectrical transduction (MET) channels found in the stereocilia of hair cells are directly modulated by sound waves, which open the channels by bending of the stereocilia (9). Opening of the MET channels allows the influx of Ca^{2+}, depolarizing the cell and converting the mechanical stimuli into an electrical signal. Piezo1, a depolarizing non-selective cationic channel permeable to Na^{+}, K^{+}, and Ca^{2+} that regulates vascular development, is activated by deformations in the plasma membrane induced by blood flow-derived shear stress (10). Similarly, the mechanosensitive K^{+} TREK-1 channel responsible for pain perception in neurons is opened by cell swelling and membrane stretching, and has further shown sensitivity to changes in

temperature and voltage (11, 12). In chondrocytes, compressive loading on AC causes fluid loss and osmotic changes that induce an increase in intracellular Ca^{2+}, which in turn drives gene expression toward ECM synthesis (13, 14). Likewise, Na^{+} concentration is involved in the regulation of chondrocyte hydration and osmosis through interaction with positively charged molecules, such as glycosaminoglycan (GAG), thus attracting water (15). Modulation of intracellular ion concentrations, particularly Ca^{2+}, is a common downstream effect of various responses to mechanical stimuli.

Ion modulation regulates the chondrogenic phenotype and encourages tissue development through multiple ion-specific and loading-specific mechanisms. For example, TRPV4 mediates the response to osmotic changes and mechanical stimuli through its interactions with integrins and other elements of the cytoskeleton, using Ca^{2+} as a secondary messenger (16). The current understanding points that the pro-chondrogenic gene expression is activated via the Ca^{2+}/calmodulin pathway (17). Ca^{2+} modulation is also necessary for mechanotransduction of hydrostatic pressure, as evidenced by a lack of response in the presence of Ca^{2+} chelators (18). In this case, mechanosensitive Ca^{2+} channels induce an increase in the intracellular concentration of the cation. The increase in Ca^{2+} concentration activates secondary messengers such as calmodulin, calmodulin kinase type II, and calcineurin, which in turn initiate signaling cascades toward changes in gene expression, likely via Indian hedgehog (Ihh) and Parathyroid hormone-related peptide (PTHrP) pathways (19, 20).

Modulation of intracellular Na^{+} has also been implicated as an effector of mechanical cues in chondrocytes. Previous work has shown that hydrostatic pressure inhibits Na^{+}/K^{+} pumps, producing an accumulation of intracellular Na^{+} (21). Moreover, epithelial sodium channels (ENaC), which are expressed in articular chondrocytes, are also believed to enable mechanotransduction in chondrocytes (22). Co-localization of ENaC with integrins, voltage-activated Ca^{2+} channels, and Na^{+}/K^{+} pumps has provided further support to ENaC playing a part

in the molecular machinery of mechanotransduction. Other sodium channels that belong to the degenerin/epithelial sodium channel (DEG/ENaC) superfamily are acid-sensing ion channels (ASICs). A study published this year linked ASICs to transduction of mechanical cues (23). While the exact role of ASICs has yet to be determined, their functionality during mechanotransduction has been shown in gastrointestinal responses, bladder compliance, and vascular remodeling, among others (24-26). ASIC1 is expressed in chondrocytes, and a recent study has shown that deregulation of ASIC1 function is associated with the degradation of articular cartilage (27). In short, regardless of upstream activation or downstream effects, ion modulation has often associated with a pro-chondrogenic response.

Ion modulation, hence, could serve to improve tissue-engineered neocartilage. Using neocartilage constructs derived from primary bovine articular chondrocytes, the effects of Ca^{2+} modulation were determined using the TRPV4 agonist 4α-phorbol-12,13-didecanoate (4-αPDD) to promote TRPV4 activation and Ca^{2+} influx (28, 29). The increase in intracellular Ca^{2+} resulted in an increase in the collagen content and tensile properties. The involvement of the TRPV4 ion channel in remodeling and strengthening the matrix of neocartilage constructs was further proven using tensile bioreactors (4). Similar work was performed involving Na^{+} and Ca^{2+} modulation using ouabain, an inhibitor of the Na^{+}/K^{+} pump, and ionomycin, a Ca^{2+} ionophore (30-32). This work reported an increase in the tensile modulus compared to the untreated control by both ion modulators, and an increase in the ultimate tensile stress (UTS) by ouabain. A more recent study aiming to induce maturation of cardiomyocytes with electrical stimulation found that Ca^{2+} influx mediated by ionomycin also triggers a comparable intracellular cation increase, possibly mediating a similar response (33). Ion modulation, as an effector of mechanotransduction, could bypass the need of mechanical stimulation bioreactors and be used as a downstream prompt to enhance engineered tissues.

In this work, we applied, for the first time, the Ca^{2+} modulators 4-αPDD and ionomycin and the Na^{+} modulator ouabain on neocartilage derived from minipig expanded and re-differentiated costal chondrocytes to improve the properties of the tissue-engineered cartilage. It was hypothesized that the modulation of Ca^{2+} and Na^{+} ions would modify the biochemical content of the neotissues, resulting in an improvement of the mechanical properties. This hypothesis was tested by determining the effects of 4-αPDD, ouabain, and ionomycin on their own (Phase 1) and in combination (Phase 2).

Methods

Isolation and expansion of costal chondrocytes

Juvenile porcine costal chondrocytes were isolated from the unmineralized portion of floating ribs of three juvenile minipigs obtained from Premier BioSource (California, USA) no later than 48 hours after slaughter. Cartilage from ribs cleaned of all non-cartilaginous tissue was cut into 1 mm^3 pieces and washed three times with GlutaMAX Dulbecco's Modified Eagle Medium containing 4.5 g/L glucose (DMEM; Gibco) and 1% (v/v) penicillin/streptomycin/fungizone (PSF; Lonza, Basel, Switzerland). The cartilage was then digested with 0.4% pronase (Sigma) in DMEM for 1 hour at 37°C, and then in 0.2% collagenase type II (Worthington Biochemical, Lakewood, NJ) in DMEM supplemented with 3% (v/v) fetal bovine serum (FBS; Atlanta Biologicals, Lawrenceville, GA) for 18 hours at 37°C. Cells were then strained through a 70 µm strainer, washed with red blood cell lysis buffer (34) for 4 min, counted, and frozen in freezing medium containing 90% (v/v) FBS + 10% (v/v) DMSO (Sigma). Primary (P0) costal chondrocytes were thawed and seeded in T225 flasks at a density of ~2.5 million cells per flask in chondrogenic medium (CHG) consisting of GlutaMAX DMEM, 1% (v/v) PSF, 1% (v/v) insulin-transferrin-selenium (BD Biosciences, San Jose, CA), 1% (v/v) non-essential amino acids (Thermo Fisher Scientific), 100 mg/mL sodium pyruvate (Thermo Fischer Scientific), 50 mg/mL ascorbate-2-

phosphate (Sigma, St. Louis, MO), 40 mg/mL L-proline (Sigma), and 100 nM dexamethasone (Sigma). Throughout expansion, medium was supplemented with 2% (v/v) FBS, 1 ng/mL TGF-β1, 5 ng/mL bFGF, and 10 ng/mL PDGF (PeproTech). Cells were cultured at 37°C in 10% CO_2, and passaged to P3 at confluence using 0.05% trypsin-EDTA (Invitrogen) and 0.2% collagenase type II solutions.

Aggregate culture re-differentiation and neocartilage construct seeding

Passaged costal chondrocytes from each donor were seeded in equal parts on 1% (w/v) agarose-coated plates at a density of 750,000 cells/mL (30 mL total) per plate with CHG supplemented with 10 ng/ml TGF-β1, 100 ng/ml GDF-5, and 100 ng/ml BMP-2 (PeproTech). Plates were placed on an orbital shaker at 50 rpm for 24 hours at 37°C in 10% CO_2, and then kept static, changing medium every 4 days. At 14 days of aggregate re-differentiation, the aggregates were digested using 0.05% trypsin-EDTA and 0.2% collagenase type II solutions. Cells were strained through a 70 µm cell strainer, washed twice, and resuspended in CHG. For the self-assembling of neocartilage constructs, 2 million cells were seeded in 5 mm diameter non-adherent 2% (w/v) agarose wells at a density of 20 million cells/mL. At 4 hours post self-assembling, additional 400 µL of CHG (control) or CHG supplemented with 10 ng/ml TGF-β1 were added. This medium was replaced daily until unconfinement (at day 3 post self-assembly), after which, constructs were kept in 2 mL of medium, replaced every 2 days. The CHG control group was maintained in CHG medium. For all other groups, TGF-β1, chondroitinase ABC (c-ABC), and LoxL2 treatment (termed TCL) was used as follows: TGF-β1 was applied at 10 ng/ml after seeding and until day 28, c-ABC (Sigma) was applied at 2 Units per mL for 4 hours in day 7, and LoxL2 (Signal Chem) was applied at 0.15 ug/mL between days 7 and 21 post self-assembly, together with 0.146 µg/mL hydroxylysine (Sigma) and 1.6 µg/mL copper sulfate (Sigma).

Chemical treatments

For all experiments, the constructs were randomly assigned across treatment groups. Modulation of ions in the constructs was performed between days 12 and 16 (*i.e.*, for 5 days) post self-assembly. For every group in Phase 1, medium was replaced with 400 µL of CHG containing 10 µM 4-αPDD (4α; Enzo life sciences), 20 µM ouabain (Ou; Sigma), 0.3 µM ionomycin (Io; Sigma), or blank CHG (control), incubated for 1 hour, and then washed twice using DMEM 1% (v/v) PSF before resuming culture in CHG media. A full-factorial design was used in Phase 2 to determine any additive or synergistic effects across treatments. Ion modulation was performed at the same time using 400 µL of CHG containing the four possible combinations of 4-αPDD, ouabain, and ionomycin, and compared to an additional TCL-treated control group ($control^{+}$), the current gold standard in tissue-engineered constructs, to examine further changes.

Mechanical testing

Tensile properties were determined using uniaxial tension in an Instron model 5565 (Instron, Canton, MA). Dog bone-shaped samples were obtained from every engineered cartilage construct with a gauge length of 1.55 mm and photographed to measure thickness and width in ImageJ. The ends of the dog-bone were fixed to paper with cyanoacrylate to increase the gripping area for testing. A strain rate of 1% of the gauge length per second was used until failure. The Young's modulus was obtained from the linear region of the stress-strain curve and the ultimate tensile strength (UTS) was defined as the maximum stress obtained.

Compressive properties of the engineered cartilage constructs were determined by creep indentation testing. Briefly, 2.5 mm punches obtained from every construct were submerged in phosphate buffered saline (PBS) until equilibrium and indented with a flat porous 0.5 mm diameter tip perpendicular to the surface of the sample to ~10% strain. The aggregate modulus (H_A) and shear modulus (μ_s) were obtained using a semi-analytical, semi-numerical, biphasic model and finite-element optimization (35, 36).

Biochemical testing

Cartilage constructs (~2-3 mg) were weighed to obtain wet weight, lyophilized for 3 days, and weighed again to obtain dry weight. Lyophilized samples were digested in 125 µg/mL papain (Sigma) +5 mM N-acetyl-L-cysteine +5 mM EDTA in phosphate buffer pH 6.5 for 18 hours at 60°C. GAG content was quantified using a Blyscan glycosaminoglycan assay kit (Biocolor, Newtownabbey, Northern Ireland). Total collagen content was quantified using a chloramine-T hydroxyproline assay (Accurate Chemical and Scientific Corp., Westbury, NY). DNA content was quantified with a picogreen assay (ThermoFisher Scientific). For the quantification of PYR crosslinks, separate tissue samples (~0.2-1 mg) were weighed, lyophilized, and acid digested for 12 hours in 6N HCl. After evaporation, the dried hydrolysate was resuspended in a 75%/25% (v/v) solution of 0.1% formic acid and acetonitrile. Samples were measured through mass spectrometry using a cogent diamond hydride column and a PYR standard.

Histology

Samples were fixed in 10% neutral-buffered formalin, embedded in paraffin, and sectioned at a thickness of 6 µm for histological evaluation. Sections were later processed and stained with hematoxylin and eosin (H&E), safranin-O, and picrosirius red using standard protocols.

Statistical analysis

All quantitative biochemical and biomechanical tests were performed using n= 6-8. All data are presented as means ± standard deviations. A single factor one-way ANOVA was employed in each phase of the study to assess differences among experimental groups. Multiple comparison was performed using a Dunnett's *post hoc* test. The Dunnett's test compares the means from every experimental group against a control group mean to determine significant differences. All statistical analyses were performed using GraphPad Prism version 8.4.1 for Windows (GraphPad Software, San Diego, California USA). Groups marked with * indicate that there are statistically significant differences compared to the control group ($p < 0.05$).

Experiment

Gross morphology and histology of stimulated neocartilage constructs

Neocartilage constructs engineered using expanded costal chondrocytes were exposed to exogenous stimuli corresponding to 4-αPDD, ouabain, or ionomycin to investigate their effects on improving functional properties. Gross morphology images of the self-assembled constructs of each group and overall values are shown in **Figure 1A** and **Table 1**. Treated groups showed on average a 3.33% reduction in the diameter compared to the untreated control group. However, treated groups were 18.5% thicker compared to the control group, with a significant increase in the 4-αPDD and ionomycin-treated constructs. A similar trend was observed in the mean wet weights amongst groups, with all constructs having on average a 70.5% water content.

For histological evaluation, the neocartilage constructs were assessed using H&E, safranin-O, and picrosirius red staining (**Fig. 1B**). Picrosirius red staining showed a localized increase in collagen deposition in the outermost region of untreated controls and, more markedly, in ouabain treated constructs. Collagen deposition in 4-αPDD and in ionomycin treated constructs appeared more homogeneous and evenly distributed throughout the construct. GAG deposition, as seen in safranin-O staining, appeared more intense in ionomycin treated constructs, followed by 4-αPDD treated constructs. In contrast to picrosirius red staining, the untreated constructs and ouabain treated constructs showed a decrease in safranin-O intensity, especially in the outermost region.

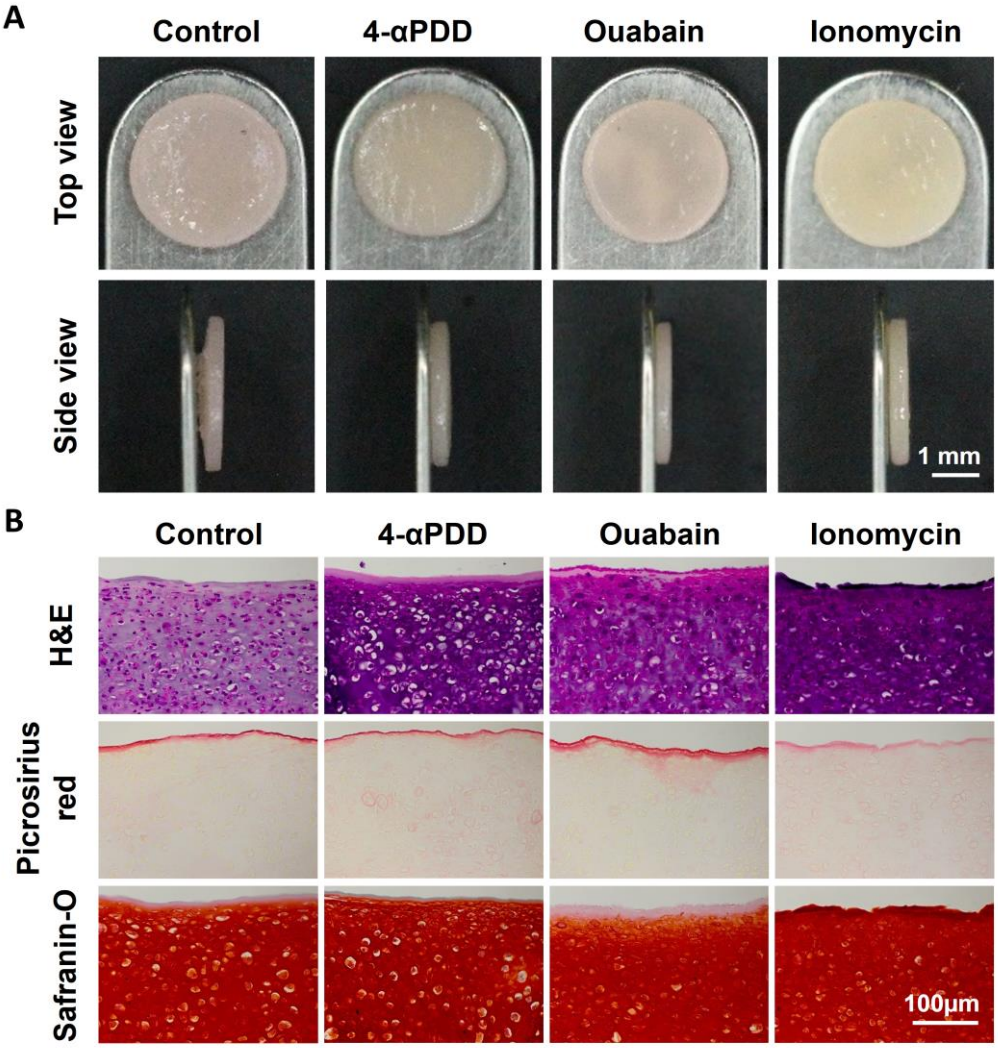

Figure 1. (**A**) Gross morphology of neocartilage constructs: All constructs appear homogeneous, flat, and with no visible abnormalities. The ionomycin treated constructs appear to be the thickest. (**B**) Histological analysis of neocartilage constructs: Overall cellularity and neotissue composition appears comparable among all groups as observed in hematoxylin and eosin staining. Picrosirius red staining shows a localized distribution in untreated constructs and ouabain treated constructs display. Safranin-O intensity is higher in 4-αPDD and ionomycin treated constructs.

Table 1. Gross morphology values. Data are presented as means ± standard deviation. The asterisks denote significant differences compared to the control group based of Dunnett´s *post hoc* test (* denotes p<0.05; ** denotes p<0.01, *** denotes p<0.005).

	Diameter (mm)	Thickness (mm)	Wet weight (mg)	Hydration (%)
Control	5.51 ± 0.08	0.45 ± 0.02	13.52 ± 0.35	73.33 ± 6.85
4-αPDD	5.38 ± 0.05	**0.51 ± 0.03***	**14.65 ± 0.57***	72.33 ± 2.42
Ouabain	**5.25 ± 0.06****	0.50 ± 0.04	12.89 ± 0.48	67.66 ± 9.03
Ionomycin	5.35 ± 0.06	**0.54 ± 0.03*****	14.36 ± 0.67	68.67 ± 3.25

Effect of ion modulation in the biochemical and mechanical properties of neocartilage constructs

The amounts of DNA, total collagen, GAG, and PYR crosslink content of the different groups at 4 weeks were evaluated per wet weight (**Fig. 2**). All treated constructs showed an increase in the DNA content, with an averaged 34% increase in all groups compared to the control group. The amount of collagen was also increased with all treatments, but only significantly higher in constructs treated with ouabain, which showed a 63% increase over the untreated group. In accordance to the histological the observations, all treatment groups showed an increase in the GAG content, with a 61% significant increase in ionomycin-treated constructs. Ionomycin also had an effect in the concentration of PYR crosslinks, which bond collagen triple helices through the oxidation of lysine residues by lysyl oxidases. The amount of PYR crosslinks was significantly higher in the presence of ionomycin, with a 115% increase compared to the control group.

The H_A increased an 18% with 4-αPDD or ouabain treatments, but only ionomycin induced a significant increase, with an H_A of 567 kPa, resulting in a 45% increase over the control group (**Fig. 3A**). The same trend was observed in the μ_s, but with no significant differences (**Fig. 3B**). Likewise, 4-αPDD and ouabain resulted in higher Young's modulus values compared to the

control group (7.37 and 6.67 MPa, respectively), albeit not significant. Ionomycin, however, produced a significant increase in the Young's modulus (8.43 MPa), corresponding to a 63% increase over the control group (5.16 MPa) (**Fig. 3C**). The UTS values of 4-αPDD, ouabain, and ionomycin corresponded to 1.87, 2.02, and 2.24 MPa, respectively, compared to the 1.79 MPa observed in the control group (**Fig. 3D**).

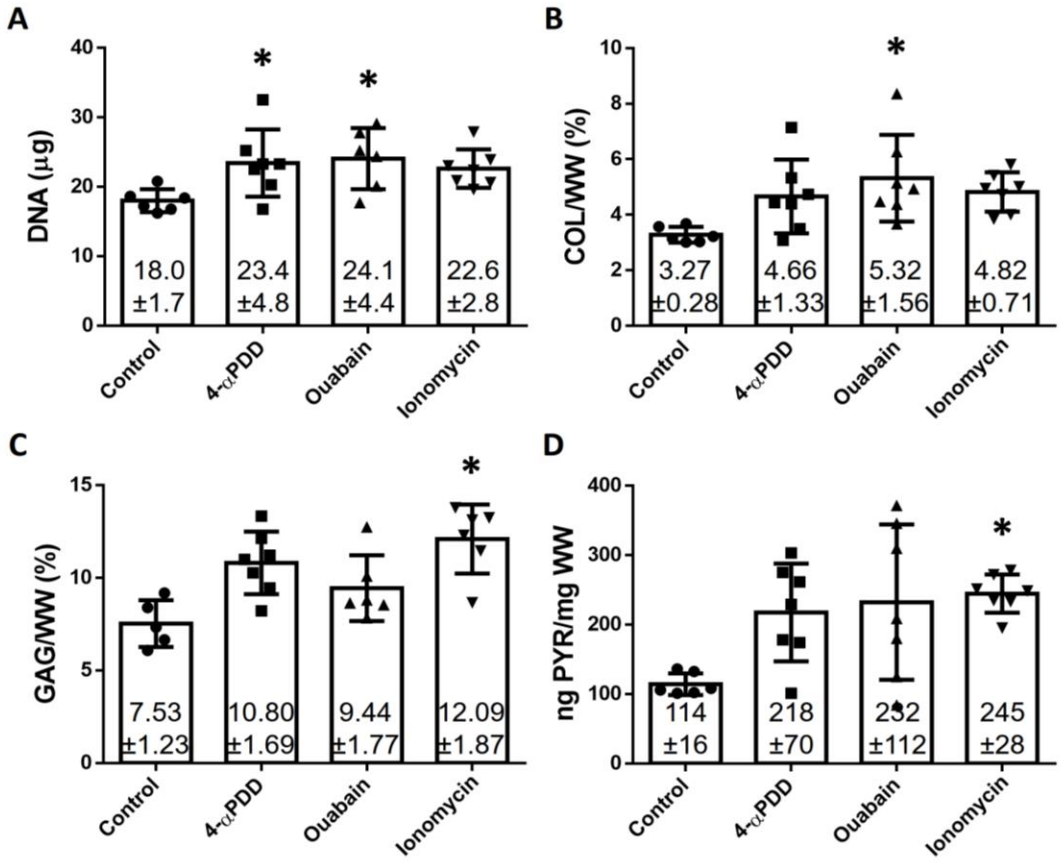

Figure 2. Biochemical properties of neocartilage constructs treated with 4-αPDD, ouabain, or ionomycin. (**A**) DNA per construct, (**B**) collagen/WW, (**C**) GAG/WW, and (**D**) Pyridinoline/WW. Ouabain-treated constructs showed a 63% increase in the collagen content. Conversely, ionomycin-treated constructs showed a 61%, and a 115% increase in the amount of GAG and PYR crosslinks, respectively.

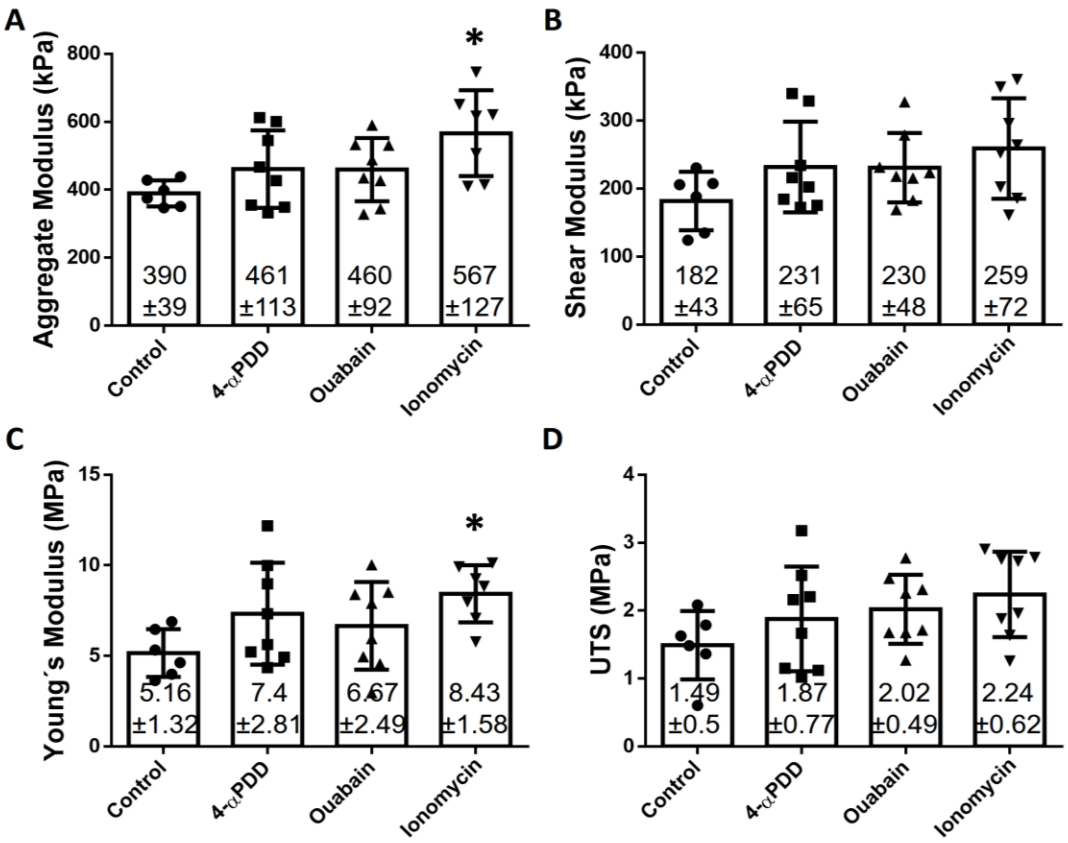

Figure 3. Biomechanical properties of neocartilage constructs treated with 4-αPDD, ouabain, or ionomycin. (**A**) Aggregate modulus, (**B**) shear modulus, (**C**) tensile Young's modulus, and (**D**) UTS. Ionomycin-treated constructs showed a 45% increase in the aggregate modulus and a 63% increase in the Young's modulus.

Effect of treatment combinations in neocartilage constructs

To study possible synergistic effects among 4-αPDD, ouabain, and ionomycin, the four different combinations ("4α+Ou", "4α+Io", "Ou+Io", and "4α+Ou+Io") were tested. In consideration of the potential effects the TCL treatment, data for TCL-treated constructs were additionally collected in Phase 2 as control (Control^{+}). The values for the phase 2 untreated constructs (Control) for gross morphology (diameter: 5.96±0.17 mm; thickness: 0.47±0.04 mm; wet weight: 14.7±2.03 mg;

hydration: 80.85±2.3%), biochemical content (DNA: 17.02±2.19 µg; collagen: 2.4±0.12%; GAG: 8.74±1.03%; PYR: 113.6±46.3 ng/mg) and mechanical properties (H_A: 431.8±37 kPa; Shear modulus: 208.7±40.63 kPa; Young's modulus: 5.24±1.25 MPa; UTS: 1.07±0.49 MPa) were comparable to values obtained for the control group in Phase 1. Uniformly, the biochemical and mechanical properties of the TCL-treated constructs ($Control^+$) were higher than the values of the untreated control; the biochemical values for the TCL-treated constructs were DNA: 25.7±4.3 µg; collagen: 5.01±0.13%; GAG: 12.19±0.97%; PYR: 150.09±76.51 ng/mg, and the mechanical values were H_A: 499±111 kPa; Shear modulus: 242±61 kPa; Young's modulus: 7.8±0.6 MPa; UTS: 2.2±0.3 MPa. The properties of untreated and the TCL-treated constructs differ in accordance to the literature (37). For the test groups, diameter and thickness were unaffected by the treatment combinations (**Table 2**). Wet weight was significantly lower in the groups were "4α+Ou" and "4α+Ou+Io" was supplied, resulting in a 7% and 8% decrease, respectively (**Table 2**). Hydration values and cell/DNA content were unaffected by the different treatments, however. The amount of GAG was significantly lower in "Ou+Io" treated constructs, showing a 34% decrease compared to the TCL control group (**Table 2**). The amount of total collagens remained stable, with no differences found with any treatments, however, the concentration of PYR crosslinks was significantly higher in the group treated with "4α+Ou", with a 58% increase (**Table 2**).

The compressive and tensile properties of constructs in the presence of two or more ion modulators were also tested (**Fig. 4**). The H_A and μ_s showed no significant differences, and while only one group, "4α+Ou", displayed an increase in the H_A, all other combinations resulted in equal or lower compressive properties (**Fig. 4A and 4B**); the constructs treated with all three modulators showed a ~25% decrease compared to the TCL control group in both H_A and μ_s. On the contrary, and compared to the control group, all groups except the "Ou+Io" group showed increases in the tensile Young's modulus and UTS, with 1%-25% and 18-31% increases, respectively (**Fig. 4C**

and 4D). Still, the combination of treatments did not show additive or synergistic effects toward improving the compressive or tensile properties.

Table 2. Gross morphology and biochemical data of neocartilage constructs treated with two or more ion modulators. Data are presented as means ± standard deviation. The asterisks denotes significant differences compared to the control^{+} group based of Dunnett´s *post hoc* test (* denotes $p<0.05$).

	Diameter (mm)	**Thickness (mm)**	**Wet weight (mg)**	**Hydration (%)**	**DNA/ const. (µg)**	**Collagen (%WW)**	**GAG (%WW)**	**PYR (ng PYR/ mg WW)**
Control^{+}	5.28 ±0.02	0.51 ±0.02	14.5 ±0.4	66.5 ±7.1	25.7 ±4.3	5.01 ±0.13	12.19 ±0.97	150.09 ±76.51
4α+Ou	5.32 ±0.07	0.46 ±0.05	**13.3 ±0.6***	71.5 ±2.5	21.1 ±1.5	4.75 ±0.57	10.27 ±0.95	**237.17 ±24.54***
4α+ Io	5.36 ±0.07	0.51 ±0.03	14.4 ±1.2	70.5 ±4.0	19.2 ±5.9	4.49 ±0.68	11.76 ±1.74	157.73 ±60.74
Ou+ Io	5.29 ±0.10	0.51 ±0.03	13.7 ±0.4	74.9 ±8.2	22.2 ±7.5	4.33 ±1.39	**8.00 ±3.28***	174.63 ±64.84
4α+Ou+ Io	5.35 ±0.08	0.49 ±0.04	13.5 ±0.6*	71.9 ±8.4	27.3 ±4.5	5.17 ±1.31	9.92 ±2.16	141.24 ±33.71

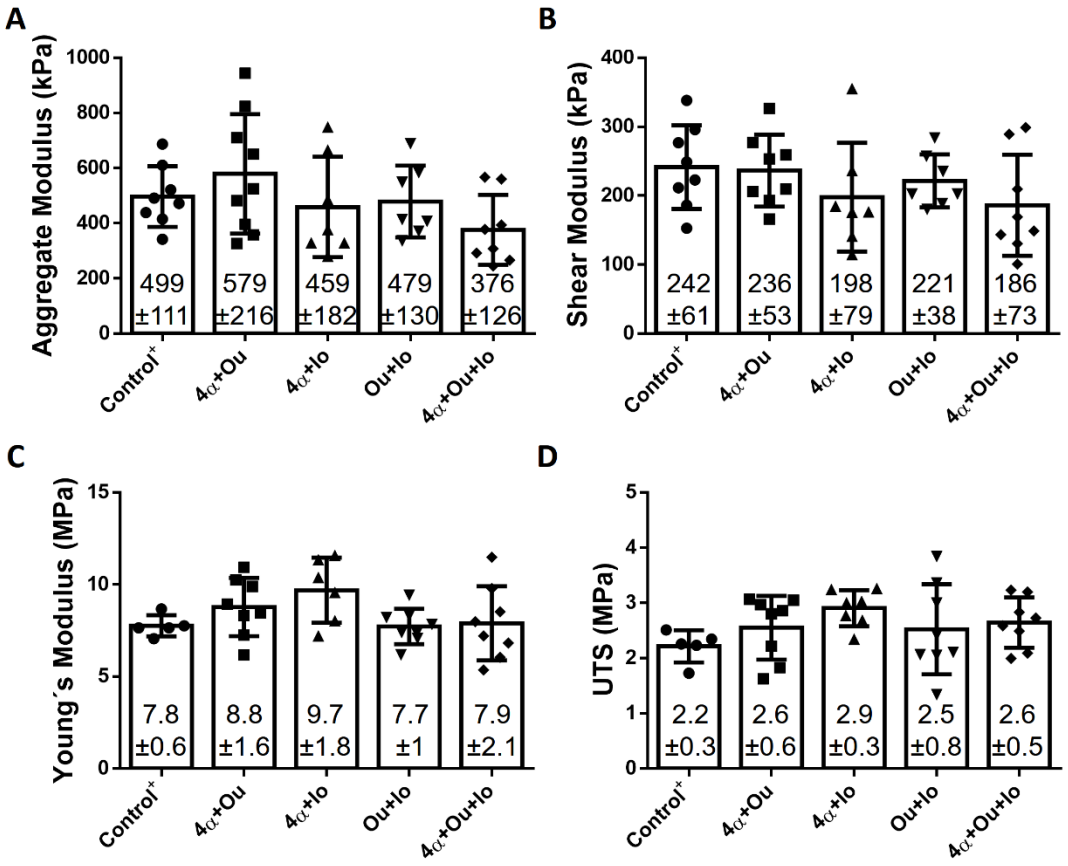

Figure 4. Biomechanical properties of neocartilage constructs treated with combinations of 4-αPDD, ouabain, and ionomycin. (A) Aggregate modulus, (B) shear modulus, (C) tensile Young's modulus, and (D) tensile UTS. Abbreviations as follows: 4-αPDD (4α), ouabain (Ou), and ionomycin (Io). No statistical significance was found in any of the mechanical properties.

Discussion

The overall objective of this work was to employ ion modulation to develop biomimetic neocartilage using expanded re-differentiated costal chondrocytes. Expansion and re-differentiation of chondrocytes obtained from the rib tackles three long-standing issues in cartilage tissue engineering: 1) it eliminates donor site morbidity in the joint, 2) it avoids cell-number limitations, and 3) it provides cells with a suitable chondrogenic phenotype toward building a

hyaline cartilage (38). The ion modulators 4-αPDD, ouabain, and ionomycin change the intracellular ion concentration through different mechanisms **(Fig. 5)**. This work is the first to quantify the effects of single and combined ion modulation in neocartilage constructs and to report the measurement of PYR crosslink, a key component of the mature cartilage ECM (39).

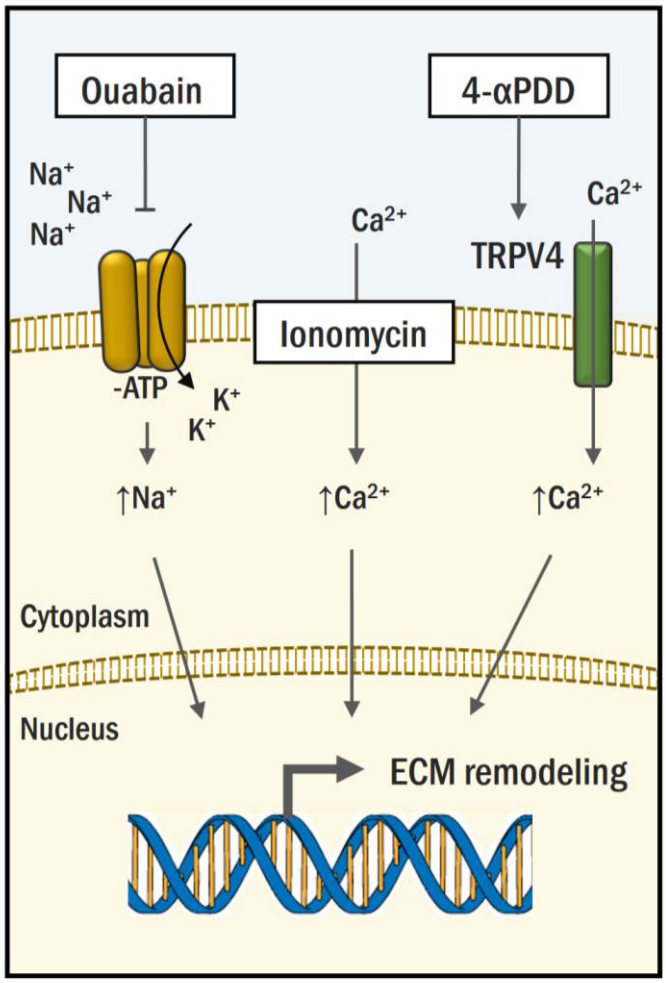

Figure 5. 4-αPDD, ouabain, and ionomycin modulate intracellular ion concentrations. 4-αPDD activates the TRPV4 transmembrane receptor, promoting intake of Ca^{2+}. Ouabain inhibits the Na^{+}/K^{+} pump, enabling passive diffusion and accumulation of Na^{+} into the cell. Ionomycin allows influx of Ca^{2+} from the extracellular compartment and internal Ca^{2+} stores into the cytoplasm.

The experimental results supported the hypothesis that the modulation of Ca^{2+} and Na^{+} ions result in biochemical content changes, which translate to an improvement of neotissue mechanical properties. Particularly, neocartilage constructs treated with ionomycin showed the highest improvement in mechanical properties. Ionomycin-treated constructs showed the largest turnover of ECM components, with a 61% increase in GAG and a 115% increase in PYR crosslink content. These changes in the biochemical content were accompanied by an improvement in mechanical properties. Constructs treated with the Ca^{2+} ionophore showed a 45% improvement in the compressive properties, increasing the H_A from 389.5 kPa (control) to 566.6 kPa. Furthermore, treatment with ionomycin also showed a 63% improvement in its tensile properties, increasing the Young's modulus from 5.16 MPa (control) to 8.43 MPa. The relationship between an increase in the GAG content and the H_A has been reported in the past, as the negatively charged GAG attract water and provide compressive resistance to AC and high osmotic pressure (40, 41). The connection between PYR crosslinks and compressive properties, however, has been less discussed; it is inferred here that a more mature collagen network with a higher presence of crosslinks provides a restraining structure that decreases GAG leaking and impedes interstitial fluid movement from the engineered constructs (42). Strategies that result in crosslink increases, such as hypoxia or *in vivo* maturation (39, 43), support our observations that a higher crosslink content improves the compressive properties, and the opposite is observed in diseased intervertebral disk where crosslinks are lost (44). The increase in the Young's modulus, conversely, may be induced by a strengthening of the collagen network, also derived from the increase in PYR crosslink (45). These results demonstrate that Ca^{2+} modulation can be directed to enhance the mechanical properties in engineered cartilage.

Ionomycin treatment of engineered neocartilage also resulted in a 20% increase of construct thickness compared to the control group. In a similar fashion, 4-αPDD also produced a significant 13% increase in thickness. Therefore, it may be inferred that an intracellular increase

in Ca^{2+} supports construct thickening. While diameter and shape can be successfully manipulated, control over the resulting thickness of self-assembled neotissues has proven more challenging (46, 47). Measurements of human samples have reported the AC thickness to range between 0.35 to 6.25 mm in the tibial plateau and from 0.89 to 5.94 mm in the patella (48). Constructs that aim translation should span the thickness of human AC, and at this moment, any strategy that enables or supports the growth of neocartilage to treat larger and deeper chondral injuries (i.e., over the range from partial to full thickness defects) is highly desirable. Consequently, the improvement of gross morphology features also motivates the use of ion modulators toward clinical translation. Ca^{2+} signaling regulates many processes in chondrocytes including division, migration, death, and differentiation, and more studies are required to determine the cause of this increase in thickness (49).

Treatment with ouabain and 4-αPDD resulted in significant differences on the gross morphology and biochemical content of neocartilage constructs. Ouabain treatment was the only regime to affect construct size, reducing construct diameter by 5%, while 4-αPDD increased wet weight. Ouabain treatment was also the only regime to induce a significant variation in collagen content, with a 62% increase compared to control. Similar effects have been reported in cartilage constructs cultured in hypertonic medium, resulting in an increase of collagen content and Young's modulus (15). In relation to collagens, the self-assembling process was chosen as a model to examine these ionophores due not only to prior work demonstrating their efficacy in this system but also because the self-assembling process has been demonstrated in ample prior work as yielding neocartilage with abundant collagen type II and no discernable collagen type I using immunohistochemistry and proteomic analysis (50, 51). In our study, ouabain also increased neocartilage tensile and compressive properties, albeit not significantly. Due to the multiple signaling pathways in which both ouabain and the Na^+/K^+ ATP-dependent ion pump are involved, the mechanisms behind these effects require further study (52, 53). Still, these results

demonstrate that TRPV4 activation or Na^+ modulation influence morphological and biochemical properties of neocartilage constructs.

The existence of different independent mechanisms of signaling via ion modulation that take place during mechanotransduction imply the potential of synergistic or additive effects between two or more modulators. From the Phase 2 study it was observed that gross morphological characteristics, diameter, thickness, and hydration, were unaffected by combinatorial treatments. Incubation with “4α+Ou” and “4α+Ou+Io” caused decreases of the wet weight compared to the control$^+$ group. Contrary to exposure to one ion modulator, incubation with two or more modulators did not further increase the amount of GAG. DNA and collagen content were also unaffected. Only constructs treated with “4α+Ou” showed an increase in PYR crosslinks, but with no synergistic or additive effects in compressive or tensile properties. Although the PYR crosslink per wet weight was significantly different between 4α+Ou and the control group, the PYR crosslink per collagen only trended higher for the 4α+Ou group and not significantly different than the control, which may, in part, explain the observation that the compressive aggregate modulus for the 4α+Ou group only trended higher than the control as well but was not significant (Supplementary Figure 1). The observations reported in this second experiment may be due to cell saturation with ions and the desensitization of signaling pathways, inhibiting a further response regardless of the increase in cation influx. Furthermore, high magnitudes of mechanical stimulation can elicit damaging effects in cartilage constructs (54), and a similar effect may be replicated when two or more ion modulators are used simultaneously. Overstimulation with ion modulators did not elicit additive or synergistic effects on construct mechanical properties.

The effects of ion modulators on neocartilage derived from expanded and re-differentiated costal chondrocytes were partially comparable to those seen when employing primary articular chondrocytes. Treatment of constructs derived from primary bovine articular chondrocytes with 4-αPDD produced an 88% increase in collagen content and a 153% increase in tensile stiffness

(29). It was also found that Na^+ and Ca^{2+} modulation with ouabain and ionomycin, or their combination, increased the Young's modulus by 40–95% compared with untreated control (31). These observations differ from the results of the present study, and these variations may be due to differences in cell phenotype between bovine primary articular chondrocytes and minipig costal chondrocytes, which were expanded and re-differentiated. The present work suggests that the effect of ion modulators depends on the construct used, including cell type (articular vs. costal), passage (P0 vs. P3), chondrogenic state (primary vs. re-differentiated), and species (bovine vs. minipig).

The effects reported in this study are comparable to those observed when implementing mechanical stimuli on similar scaffoldless tissue-engineered constructs. For example, tension stimulation induced an increase in tensile properties of bovine neocartilage constructs. Constant tension resulted in a Young's modulus of 5.1±2 MPa, which constitutes a 4.6-fold and a 1.6-fold increase in the modulus compared to untreated (1.1±0.3 MPa) and TCL-treated controls (3.1±1.1 MPa), respectively (4). Microarray analysis revealed that the TRPV4 ion channel was involved in the matrix remodeling initiated by the tensile stimulus, and inhibition of the channel with GSK205 abolished the tissue-level response to tension. In this study, 4-αPDD, known to activate TRPV4, was used. Likewise, fluid-induced shear prompted a 2.7-fold increase in the Young's modulus (2.18±0.74 MPa), a 1.9-fold increase in the aggregate modulus (64±20 kPa), and a 1.4-fold increase in the collagen content (15±3 %/DW) compared to controls in human neocartilage (55). Analogous changes were found in this study; specifically, with ionomycin, we show a 1.6-fold increase in the tensile properties, a 1.5-fold increase in the aggregate modulus, and 1.6-fold increase in GAG content (12.09 %/WW). In agreement with our hypothesis on using ionomycin in lieu of mechanotransduction, the RNA-seq data suggest that these changes may be induced by the perturbation of primary cilia and the opening of the PC1/2 complex, which allows the influx of Ca^{2+}. The specific mechanisms that follow ion modulation remain ill-defined, as multiple signaling

pathways can interplay in accordance to the initial mechanical stimulus (56). While Wnt, TGF-β1, and YAP/TAZ pathways have been reported become active following mechanical stresses, the activation of the Ihh pathway and the MAPK-ERK pathway may play a predominant role after ion modulation. With Ca^{2+} mediating the initial response, Ihh transduces the stimuli from the primary cilia (57, 58). The MAPK-ERK pathway, on the other hand, is highly dependent on ion concentration, particularly Ca^{2+}, to induce a transcriptional response (59). Future studies should aim at determining which specific pathways are involved in transducing the effects of both mechanically and chemically induced ion modulation and how these pathways compare.

Intracellular Ca^{2+} modulation presents an attractive and novel strategy to engineer robust neocartilage using expanded and re-differentiated chondrocytes from the rib, a non-articular cartilage cell source. The manipulation in ion concentration through the use of chemical modulators is an innovative method to enhance the mechanical properties of engineered cartilage compared to the use of targeted enzymatic treatments and bioreactors. Ionomycin may be used to replace mechanical stimulation bioreactors, often used *ex vivo* to induce neotissue maturation (60, 61). In spite of exhibiting beneficial effects, bioreactors are prone to contamination and user-error, whereas chemical ion modulation has multiple advantages: it is cost-effective, replicable, and highly controllable.

In summary, this study investigated whether ion modulation would improve the mechanical properties of engineered neocartilage constructs derived from expanded and re-differentiated costal chondrocytes. It was shown that ionomycin treatment resulted in an increase of neocartilage compressive and tensile properties. This increase may be a result of the higher GAG content coupled with an increase in the PYR crosslinking. The use of two or more ion modulators in combination did not produce additive nor synergistic effects. The results of this study demonstrate that ion modulation with ionomycin is a powerful tool in tissue engineering.

Acknowledgements

The authors acknowledge support from the National Institutes of Health (NIH) R01 AR067821 and Fulbright Chile scholarship.

References

1. Makris EA, MacBarb RF, Paschos NK, Hu JC, Athanasiou KA. Combined use of chondroitinase-ABC, TGF-beta1, and collagen crosslinking agent lysyl oxidase to engineer functional neotissues for fibrocartilage repair. Biomaterials. 2014;35(25):6787-96. doi: 10.1016/j.biomaterials.2014.04.083. PubMed PMID: 24840619; PubMed Central PMCID: PMC4105108.
2. Leipzig ND, Athanasiou KA. Static compression of single chondrocytes catabolically modifies single-cell gene expression. Biophysical journal. 2008;94(6):2412-22. doi: 10.1529/biophysj.107.114207. PubMed PMID: 18065463; PubMed Central PMCID: PMC2257883.
3. Huey DJ, Athanasiou KA. Tension-compression loading with chemical stimulation results in additive increases to functional properties of anatomic meniscal constructs. PloS one. 2011;6(11):e27857. doi: 10.1371/journal.pone.0027857. PubMed PMID: 22114714; PubMed Central PMCID: PMC3218070.
4. Lee JK, Huwe LW, Paschos N, Aryaei A, Gegg CA, Hu JC, Athanasiou KA. Tension stimulation drives tissue formation in scaffold-free systems. Nature materials. 2017;16(8):864-73. doi: 10.1038/nmat4917. PubMed PMID: 28604717; PubMed Central PMCID: PMC5532069.
5. Ofek G, Dowling EP, Raphael RM, McGarry JP, Athanasiou KA. Biomechanics of single chondrocytes under direct shear. Biomechanics and modeling in mechanobiology. 2010;9(2):153-62. doi: 10.1007/s10237-009-0166-1. PubMed PMID: 19644718.
6. Elder BD, Athanasiou KA. Synergistic and additive effects of hydrostatic pressure and growth factors on tissue formation. PloS one. 2008;3(6):e2341. doi: 10.1371/journal.pone.0002341. PubMed PMID: 18523560; PubMed Central PMCID: PMC2394656.
7. Oinas J, Ronkainen AP, Rieppo L, Finnila MAJ, Iivarinen JT, van Weeren PR, Helminen HJ, Brama PAJ, Korhonen RK, Saarakkala S. Composition, structure and tensile biomechanical properties of equine articular cartilage during growth and maturation. Scientific reports. 2018;8(1):11357. doi: 10.1038/s41598-018-29655-5. PubMed PMID: 30054498; PubMed Central PMCID: PMC6063957.
8. Huey DJ, Athanasiou KA. Maturational growth of self-assembled, functional menisci as a result of TGF-beta1 and enzymatic chondroitinase-ABC stimulation. Biomaterials. 2011;32(8):2052-8. doi: 10.1016/j.biomaterials.2010.11.041. PubMed PMID: 21145584; PubMed Central PMCID: PMC3038547.
9. Qiu X, Muller U. Mechanically Gated Ion Channels in Mammalian Hair Cells. Frontiers in cellular neuroscience. 2018;12:100. doi: 10.3389/fncel.2018.00100. PubMed PMID: 29755320; PubMed Central PMCID: PMC5932396.

10. Douguet D, Honore E. Mammalian Mechanoelectrical Transduction: Structure and Function of Force-Gated Ion Channels. Cell. 2019;179(2):340-54. doi: 10.1016/j.cell.2019.08.049. PubMed PMID: 31585078.
11. Djillani A, Mazella J, Heurteaux C, Borsotto M. Role of TREK-1 in Health and Disease, Focus on the Central Nervous System. Frontiers in pharmacology. 2019;10:379. doi: 10.3389/fphar.2019.00379. PubMed PMID: 31031627; PubMed Central PMCID: PMC6470294.
12. Alloui A, Zimmermann K, Mamet J, Duprat F, Noel J, Chemin J, Guy N, Blondeau N, Voilley N, Rubat-Coudert C, Borsotto M, Romey G, Heurteaux C, Reeh P, Eschalier A, Lazdunski M. TREK-1, a K+ channel involved in polymodal pain perception. The EMBO journal. 2006;25(11):2368-76. doi: 10.1038/sj.emboj.7601116. PubMed PMID: 16675954; PubMed Central PMCID: PMC1478167.
13. Madden RM, Han SK, Herzog W. The effect of compressive loading magnitude on in situ chondrocyte calcium signaling. Biomechanics and modeling in mechanobiology. 2015;14(1):135-42. doi: 10.1007/s10237-014-0594-4. PubMed PMID: 24853775; PubMed Central PMCID: PMC4282695.
14. Fitzgerald JB, Jin M, Dean D, Wood DJ, Zheng MH, Grodzinsky AJ. Mechanical compression of cartilage explants induces multiple time-dependent gene expression patterns and involves intracellular calcium and cyclic AMP. The Journal of biological chemistry. 2004;279(19):19502-11. doi: 10.1074/jbc.M400437200. PubMed PMID: 14960571.
15. Sampat SR, Dermksian MV, Oungoulian SR, Winchester RJ, Bulinski JC, Ateshian GA, Hung CT. Applied osmotic loading for promoting development of engineered cartilage. Journal of biomechanics. 2013;46(15):2674-81. doi: 10.1016/j.jbiomech.2013.07.043. PubMed PMID: 24035014; PubMed Central PMCID: PMC3902123.
16. O'Conor CJ, Leddy HA, Benefield HC, Liedtke WB, Guilak F. TRPV4-mediated mechanotransduction regulates the metabolic response of chondrocytes to dynamic loading. Proceedings of the National Academy of Sciences of the United States of America. 2014;111(4):1316-21. doi: 10.1073/pnas.1319569111. PubMed PMID: 24474754; PubMed Central PMCID: PMC3910592.
17. Muramatsu S, Wakabayashi M, Ohno T, Amano K, Ooishi R, Sugahara T, Shiojiri S, Tashiro K, Suzuki Y, Nishimura R, Kuhara S, Sugano S, Yoneda T, Matsuda A. Functional gene screening system identified TRPV4 as a regulator of chondrogenic differentiation. The Journal of biological chemistry. 2007;282(44):32158-67. doi: 10.1074/jbc.M706158200. PubMed PMID: 17804410.
18. Steward AJ, Kelly DJ, Wagner DR. The role of calcium signalling in the chondrogenic response of mesenchymal stem cells to hydrostatic pressure. European cells & materials. 2014;28:358-71. doi: 10.22203/ecm.v028a25. PubMed PMID: 25350251.
19. Riddle RC, Taylor AF, Genetos DC, Donahue HJ. MAP kinase and calcium signaling mediate fluid flow-induced human mesenchymal stem cell proliferation. American journal of physiology Cell physiology. 2006;290(3):C776-84. doi: 10.1152/ajpcell.00082.2005. PubMed PMID: 16267109.
20. Liu Q, Yang HX, Wan XH, Zhang M, Zhang J, Lu L, Xie M, Ren HT, Yu SB, Liu XD, Wang M. Calcium-/calmodulin-dependent protein kinase II in occlusion-induced degenerative cartilage of rat mandibular condyle. Journal of oral rehabilitation. 2018;45(6):442-51. doi: 10.1111/joor.12629. PubMed PMID: 29603329.

21. Elder BD, Athanasiou KA. Hydrostatic pressure in articular cartilage tissue engineering: from chondrocytes to tissue regeneration. Tissue engineering Part B, Reviews. 2009;15(1):43-53. doi: 10.1089/ten.teb.2008.0435. PubMed PMID: 19196119; PubMed Central PMCID: PMC2817666.
22. Shakibaei M, Mobasheri A. Beta1-integrins co-localize with Na, K-ATPase, epithelial sodium channels (ENaC) and voltage activated calcium channels (VACC) in mechanoreceptor complexes of mouse limb-bud chondrocytes. Histology and histopathology. 2003;18(2):343-51. doi: 10.14670/HH-18.343. PubMed PMID: 12647783.
23. Ruan N, Tribble J, Peterson AM, Jiang Q, Wang JQ, Chu XP. Acid-Sensing Ion Channels and Mechanosensation. International journal of molecular sciences. 2021;22(9). doi: 10.3390/ijms22094810. PubMed PMID: 34062742; PubMed Central PMCID: PMC8125064.
24. Yoshiyama M, Kobayashi H, Takeda M, Araki I. Blockade of Acid-Sensing Ion Channels Increases Urinary Bladder Capacity With or Without Intravesical Irritation in Mice. Frontiers in physiology. 2020;11:592867. doi: 10.3389/fphys.2020.592867. PubMed PMID: 33192609; PubMed Central PMCID: PMC7649782.
25. Jernigan NL, Herbert LM, Walker BR, Resta TC. Chronic hypoxia upregulates pulmonary arterial ASIC1: a novel mechanism of enhanced store-operated Ca2+ entry and receptor-dependent vasoconstriction. American journal of physiology Cell physiology. 2012;302(6):C931-40. doi: 10.1152/ajpcell.00332.2011. PubMed PMID: 22205392; PubMed Central PMCID: PMC3311238.
26. Alcaino C, Farrugia G, Beyder A. Mechanosensitive Piezo Channels in the Gastrointestinal Tract. Current topics in membranes. 2017;79:219-44. doi: 10.1016/bs.ctm.2016.11.003. PubMed PMID: 28728818; PubMed Central PMCID: PMC5606247.
27. Xu Y, Chen F. Acid-Sensing Ion Channel-1a in Articular Chondrocytes and Synovial Fibroblasts: A Novel Therapeutic Target for Rheumatoid Arthritis. Frontiers in immunology. 2020;11:580936. doi: 10.3389/fimmu.2020.580936. PubMed PMID: 33584647; PubMed Central PMCID: PMC7876322.
28. Strotmann R, Harteneck C, Nunnenmacher K, Schultz G, Plant TD. OTRPC4, a nonselective cation channel that confers sensitivity to extracellular osmolarity. Nature cell biology. 2000;2(10):695-702. doi: 10.1038/35036318. PubMed PMID: 11025659.
29. Eleswarapu SV, Athanasiou KA. TRPV4 channel activation improves the tensile properties of self-assembled articular cartilage constructs. Acta biomaterialia. 2013;9(3):5554-61. doi: 10.1016/j.actbio.2012.10.031. PubMed PMID: 23128162; PubMed Central PMCID: PMC3562419.
30. Sandtner W, Egwolf B, Khalili-Araghi F, Sanchez-Rodriguez JE, Roux B, Bezanilla F, Holmgren M. Ouabain binding site in a functioning Na+/K+ ATPase. The Journal of biological chemistry. 2011;286(44):38177-83. doi: 10.1074/jbc.M111.267682. PubMed PMID: 21911500; PubMed Central PMCID: PMC3207469.
31. Natoli RM, Skaalure S, Bijlani S, Chen KX, Hu J, Athanasiou KA. Intracellular Na(+) and Ca(2+) modulation increases the tensile properties of developing engineered articular cartilage. Arthritis and rheumatism. 2010;62(4):1097-107. doi: 10.1002/art.27313. PubMed PMID: 20131245; PubMed Central PMCID: PMC2909188.
32. Morgan AJ, Jacob R. Ionomycin enhances Ca2+ influx by stimulating store-regulated cation entry and not by a direct action at the plasma membrane. The Biochemical journal. 1994;300 (Pt

3):665-72. doi: 10.1042/bj3000665. PubMed PMID: 8010948; PubMed Central PMCID: PMC1138219.
33. Ma R, Liang J, Huang W, Guo L, Cai W, Wang L, Paul C, Yang HT, Kim HW, Wang Y. Electrical Stimulation Enhances Cardiac Differentiation of Human Induced Pluripotent Stem Cells for Myocardial Infarction Therapy. Antioxidants & redox signaling. 2018;28(5):371-84. doi: 10.1089/ars.2016.6766. PubMed PMID: 27903111; PubMed Central PMCID: PMC5770128.
34. Brown WE, Hu JC, Athanasiou KA. Ammonium-Chloride-Potassium Lysing Buffer Treatment of Fully Differentiated Cells Increases Cell Purity and Resulting Neotissue Functional Properties. Tissue engineering Part C, Methods. 2016;22(9):895-903. doi: 10.1089/ten.TEC.2016.0184. PubMed PMID: 27553086; PubMed Central PMCID: PMC5035916.
35. Athanasiou KA, Niederauer GG, Schenck RC, Jr. Biomechanical topography of human ankle cartilage. Annals of biomedical engineering. 1995;23(5):697-704. doi: 10.1007/bf02584467. PubMed PMID: 7503470.
36. Mow VC, Kuei SC, Lai WM, Armstrong CG. Biphasic creep and stress relaxation of articular cartilage in compression? Theory and experiments. Journal of biomechanical engineering. 1980;102(1):73-84. doi: 10.1115/1.3138202. PubMed PMID: 7382457.
37. Kwon H, O'Leary SA, Hu JC, Athanasiou KA. Translating the application of transforming growth factor-beta1, chondroitinase-ABC, and lysyl oxidase-like 2 for mechanically robust tissue-engineered human neocartilage. Journal of tissue engineering and regenerative medicine. 2019;13(2):283-94. doi: 10.1002/term.2791. PubMed PMID: 30557915.
38. Kwon H, Brown WE, Lee CA, Wang D, Paschos N, Hu JC, Athanasiou KA. Surgical and tissue engineering strategies for articular cartilage and meniscus repair. Nature reviews Rheumatology. 2019;15(9):550-70. doi: 10.1038/s41584-019-0255-1. PubMed PMID: 31296933.
39. Makris EA, Hu JC, Athanasiou KA. Hypoxia-induced collagen crosslinking as a mechanism for enhancing mechanical properties of engineered articular cartilage. Osteoarthritis and cartilage. 2013;21(4):634-41. doi: 10.1016/j.joca.2013.01.007. PubMed PMID: 23353112; PubMed Central PMCID: PMC3670708.
40. Chahine NO, Chen FH, Hung CT, Ateshian GA. Direct measurement of osmotic pressure of glycosaminoglycan solutions by membrane osmometry at room temperature. Biophysical journal. 2005;89(3):1543-50. doi: 10.1529/biophysj.104.057315. PubMed PMID: 15980166; PubMed Central PMCID: PMC1366659.
41. Gu WY, Yao H. Effects of hydration and fixed charge density on fluid transport in charged hydrated soft tissues. Annals of biomedical engineering. 2003;31(10):1162-70. doi: 10.1114/1.1615576. PubMed PMID: 14649490.
42. Han EH, Chen SS, Klisch SM, Sah RL. Contribution of proteoglycan osmotic swelling pressure to the compressive properties of articular cartilage. Biophysical journal. 2011;101(4):916-24. doi: 10.1016/j.bpj.2011.07.006. PubMed PMID: 21843483; PubMed Central PMCID: PMC3175069.
43. Vapniarsky N, Huwe LW, Arzi B, Houghton MK, Wong ME, Wilson JW, Hatcher DC, Hu JC, Athanasiou KA. Tissue engineering toward temporomandibular joint disc regeneration. Science translational medicine. 2018;10(446). doi: 10.1126/scitranslmed.aaq1802. PubMed PMID: 29925634.
44. Bezci SE, Nandy A, O'Connell GD. Effect of Hydration on Healthy Intervertebral Disk Mechanical Stiffness. Journal of biomechanical engineering. 2015;137(10):101007. doi: 10.1115/1.4031416. PubMed PMID: 26300418.

45. Eleswarapu SV, Responte DJ, Athanasiou KA. Tensile properties, collagen content, and crosslinks in connective tissues of the immature knee joint. PloS one. 2011;6(10):e26178. doi: 10.1371/journal.pone.0026178. PubMed PMID: 22022553; PubMed Central PMCID: PMC3192771.
46. Huang BJ, Brown WE, Keown T, Hu JC, Athanasiou KA. Overcoming Challenges in Engineering Large, Scaffold-Free Neocartilage with Functional Properties. Tissue engineering Part A. 2018;24(21-22):1652-62. doi: 10.1089/ten.TEA.2017.0495. PubMed PMID: 29766751; PubMed Central PMCID: PMC6238610.
47. Bryant SJ, Anseth KS. The effects of scaffold thickness on tissue engineered cartilage in photocrosslinked poly(ethylene oxide) hydrogels. Biomaterials. 2001;22(6):619-26. doi: 10.1016/s0142-9612(00)00225-8. PubMed PMID: 11219727.
48. Ateshian GA, Soslowsky LJ, Mow VC. Quantitation of articular surface topography and cartilage thickness in knee joints using stereophotogrammetry. Journal of biomechanics. 1991;24(8):761-76. doi: 10.1016/0021-9290(91)90340-s. PubMed PMID: 1918099.
49. Lv M, Zhou Y, Chen X, Han L, Wang L, Lu XL. Calcium signaling of in situ chondrocytes in articular cartilage under compressive loading: Roles of calcium sources and cell membrane ion channels. Journal of orthopaedic research : official publication of the Orthopaedic Research Society. 2018;36(2):730-8. doi: 10.1002/jor.23768. PubMed PMID: 28980722; PubMed Central PMCID: PMC5839963.
50. Natoli RM, Responte DJ, Lu BY, Athanasiou KA. Effects of multiple chondroitinase ABC applications on tissue engineered articular cartilage. Journal of orthopaedic research : official publication of the Orthopaedic Research Society. 2009;27(7):949-56. doi: 10.1002/jor.20821. PubMed PMID: 19123232; PubMed Central PMCID: PMC2819396.
51. Donahue RP, Nordberg RC, Bielajew BJ, Hu JC, Athanasiou KA. The effect of neonatal, juvenile, and adult donors on rejuvenated neocartilage functional properties. Tissue engineering Part A. 2021. doi: 10.1089/ten.TEA.2021.0167. PubMed PMID: 34605665.
52. Contreras RG, Flores-Beni Tez D, Flores-Maldonado C, Larre I, Shoshani L, Cereijido M. Na+,K+-ATPase and hormone ouabain:new roles for an old enzyme and an old inhibitor. Cellular and molecular biology. 2006;52(8):31-40. PubMed PMID: 17535734.
53. Ou Y, Pan CX, Zuo J, van der Hoorn FA. Ouabain affects cell migration via Na,K-ATPase-p130cas and via nucleus-centrosome association. PloS one. 2017;12(8):e0183343. doi: 10.1371/journal.pone.0183343. PubMed PMID: 28817661; PubMed Central PMCID: PMC5560699.
54. Salinas EY, Hu JC, Athanasiou K. A Guide for Using Mechanical Stimulation to Enhance Tissue-Engineered Articular Cartilage Properties. Tissue engineering Part B, Reviews. 2018;24(5):345-58. doi: 10.1089/ten.TEB.2018.0006. PubMed PMID: 29562835; PubMed Central PMCID: PMC6199627.
55. Salinas EY, Aryaei A, Paschos N, Berson E, Kwon H, Hu JC, Athanasiou KA. Shear stress induced by fluid flow produces improvements in tissue-engineered cartilage. Biofabrication. 2020;12(4):045010. doi: 10.1088/1758-5090/aba412. PubMed PMID: 32640430.
56. Zhao Z, Li Y, Wang M, Zhao S, Zhao Z, Fang J. Mechanotransduction pathways in the regulation of cartilage chondrocyte homoeostasis. Journal of cellular and molecular medicine. 2020;24(10):5408-19. doi: 10.1111/jcmm.15204. PubMed PMID: 32237113; PubMed Central PMCID: PMC7214151.

57. Thompson CL, Chapple JP, Knight MM. Primary cilia disassembly down-regulates mechanosensitive hedgehog signalling: a feedback mechanism controlling ADAMTS-5 expression in chondrocytes. Osteoarthritis and cartilage. 2014;22(3):490-8. doi: 10.1016/j.joca.2013.12.016. PubMed PMID: 24457103; PubMed Central PMCID: PMC3988976.
58. Shao YY, Wang L, Welter JF, Ballock RT. Primary cilia modulate Ihh signal transduction in response to hydrostatic loading of growth plate chondrocytes. Bone. 2012;50(1):79-84. doi: 10.1016/j.bone.2011.08.033. PubMed PMID: 21930256; PubMed Central PMCID: PMC3246537.
59. He Z, Leong DJ, Zhuo Z, Majeska RJ, Cardoso L, Spray DC, Goldring MB, Cobelli NJ, Sun HB. Strain-induced mechanotransduction through primary cilia, extracellular ATP, purinergic calcium signaling, and ERK1/2 transactivates CITED2 and downregulates MMP-1 and MMP-13 gene expression in chondrocytes. Osteoarthritis and cartilage. 2016;24(5):892-901. doi: 10.1016/j.joca.2015.11.015. PubMed PMID: 26687824.
60. Darling EM, Athanasiou KA. Articular cartilage bioreactors and bioprocesses. Tissue engineering. 2003;9(1):9-26. doi: 10.1089/107632703762687492. PubMed PMID: 12625950.
61. Mabvuure N, Hindocha S, Khan WS. The role of bioreactors in cartilage tissue engineering. Current stem cell research & therapy. 2012;7(4):287-92. doi: 10.2174/157488812800793018. PubMed PMID: 22563665.

Supplementary Material

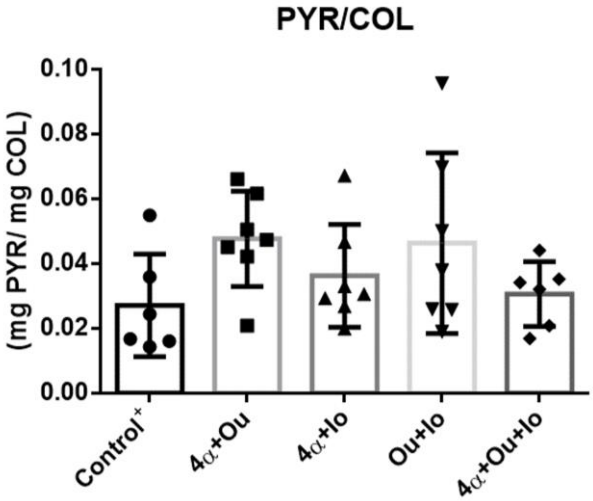

CHAPTER 6: Ion modulatory treatments toward functional self-assembled neocartilage

Abstract

The development of strategies to produce engineered tissues with adequate biomechanical properties is still needed. In cartilage tissue engineering, signals that recapitulate *in vitro* the conditions found *in vivo*, such as hypoxia or mechanical forces, contribute to the generation of hyaline-like tissues. The cell regulatory processes behind hypoxic and mechanical stimuli rely on ion concentration; iron is required to degrade the hypoxia inducible factor 1a (HIF1α) under normoxia, whereas the initiation of mechanotransduction requires the cytoplasmic increase of calcium concentration. In this work, we propose that ion modulation can be used to improve the biomechanical properties of self-assembled neocartilage constructs derived from rejuvenated expanded minipig rib chondrocytes. The objectives of this work were 1) to determine the effects of iron sequestration on self-assembled neocartilage constructs using two doses of the iron chelator deferoxamine (DFO), and 2) to evaluate the performance of the combined treatment of DFO and ionomycin, a calcium ionophore that triggers cytoplasmic calcium accumulation. This study employed a two-phase approach. In Phase I, constructs treated with a high dose of DFO (100 μM) exhibited an 87% increase in pyridinoline crosslinks, a 57% increase in the Young's modulus, and a 112% increase in the ultimate tensile strength (UTS) of the neotissue. In Phase II, the combined use of both ion modulators resulted in 150% and 176% significant increases in the Young's modulus and UTS of neocartilage constructs, respectively; for the first time, neocartilage constructs achieved a Young's modulus of 11.76±3.29 MPa and UTS of 4.20±1.24 MPa. The results of this work provide evidence that ion modulation can be employed to improve the biomechanical properties in engineered neotissues.

Chapter submitted as: Otarola, G.A., Hu, J.C., Athanasiou, K.A. Ion modulatory treatments toward functional self-assembled neocartilage. Submitted to Acta Biomaterialia.

Introduction

Articular cartilage is a highly acellular and avascular tissue with little to no turnover that lacks the capacity to heal in response to degeneration or injury (1). Current surgical therapies such as microfracture, osteochondral grafts, and autologous chondrocyte implantation fail to provide long-term restoration, and tissue engineering strategies provide a promising strategy to produce biomimetic neotissues (2-5). The self-assembling process, for example, allows for the development of hyaline-like neotissues by inducing chondrocytes into generating a cartilaginous extracellular matrix (ECM) without the need of a scaffold. Because clinical treatment of chondral diseases would require neotissues capable of resisting the harsh joint environment, methods to modulate neocartilage stiffness have included investigations into the exogenous application of growth factors, proteins, hypoxia and mechanical stimuli, as well as the modulation of ions involved in translating such stimuli to ECM production and neocartilage maturation (6-10). The development of clinically appropriate neocartilage constructs relies on efficient strategies to generate tissues with proper biomechanical properties.

As an avascular tissue, cartilage is recognized to exist under hypoxia, which is a well-characterized chondrogenic stimulus (11). Under hypoxia, the presence of reactive oxygen species and lack of oxygen inhibits prolyl hydroxylase (PHD)-mediated hydroxylation of hypoxia inducible factor 1α (HIF1α), which allows HIF1α to accumulate and interact with HIF1β. In the nucleus, the active HIF1α/HIF1β complex binds to hypoxia response elements (HREs) and triggers the transcriptional activation of genes that control ECM remodeling, angiogenesis, glycolysis, mitophagy, and cell survival, among others (12). Given the hypoxic nature of cartilage, HIF1α activity plays a pivotal role in maintaining chondrocyte homeostasis; in cartilage, HIF1α inhibits MMP13-mediated breakdown of the ECM, plays a role in controlling catabolism by inhibiting Wnt signaling, and promotes protective mitophagy (13, 14). *In vitro* hypoxic conditions

are imparted by bioreactors to achieve low oxygen tension, typically ~2-4% (vol/vol) O_2 and improve neocartilage tissue properties. For example, neocartilage constructs cultured at 4% O_2 showed significant increases in their collagen content, Young's modulus, and pyridinoline (PYR) crosslink content, the collagen crosslink typically found in mature articular cartilage (8). Interestingly, the catalytic center of PHD requires α-ketoglutarate and ferrous iron to hydroxylate and downregulate HIF1α activity.

Mechanical stimuli have also been shown to be beneficial for the development of cartilage neotissues. The simulation of mechanical signals found in the joint enables the activation of signaling cascades with pleiotropic effects in the neotissue (15). Example stimuli that have been used to improve the biomechanical properties of engineered neocartilage include compression, tension, fluid shear, and hydrostatic pressure (16-19). The activation of mechanotransduction via mechanical stimulus has been shown to favor a chondrogenic ECM in terms of composition (e.g., collagen types and content), collagen alignment (anisotropy), and macromolecular bonds (e.g., PYR crosslinks) (20, 21). In self-assembled neocartilage constructs, particularly, mechanical stimuli result in multiple improvements. Tension stimulation induced a 1.6 fold increase in tensile properties of bovine neocartilage constructs, compared to untreated controls (17). Microarray analysis revealed that the TRPV4 ion channel was involved in the matrix remodeling initiated by the tensile stimulus. Likewise, fluid-induced shear resulted in a 2.7-fold increase in the Young's modulus, a 1.9-fold increase in the aggregate modulus, and a 1.4-fold increase in the collagen content, compared to controls in human neocartilage (9). The putative mechanisms for mechanical stimuli rely on Ca^{2+} functioning as a second messenger toward gene transcriptional regulation (9, 22).

Inasmuch ions such as Fe^{2+} and Ca^{2+} play key roles within signaling cascades of both hypoxia and mechanotransduction, it is instructive to consider their modulation for tissue engineering purposes. For hypoxia, the transcriptional activation of chondrogenic genes is

mediated by HIF1α (23). Under normoxia, PHD hydroxylates HIF1α in a reaction that requires Fe^{2+}, marking it for ubiquitination via Von Hippel Lindau (VHL) and proteosomal degradation. At physiological pH, ferrous iron (Fe^{2+}) is oxidized to ferric iron (Fe^{3+}). Chemical sequestration of Fe^{3+} by the iron chelator deferoxamine (DFO) inhibits hydroxylation of HIF1α and promotes a hypoxic response via accumulation of the transcription factor (24, 25). For mechanical stimuli, mechanosensing proteins such as the mechanoelectrical transduction (MET) channels, found in the stereocilia of hair cells or the depolarizing non-selective cationic channel Piezo1, trigger an influx of Ca^{2+} following membrane deformations resulting from mechanical displacement and flow-induced shear stress, respectively (26, 27). Likewise, in chondrocytes, the Ca^{2+}-permeable transient receptor potential vanilloid 4 (TRPV4) mediates the response to osmotic changes and mechanical stimuli through its interactions with integrins and other elements of the cytoskeleton, using Ca^{2+} as a secondary messenger (28). Modulation of intracellular Ca^{2+} concentration using ionomycin, a Ca^{2+} ionophore, has the potential of replicating the effects elicited by mechanical stimuli, such as an increase in PYR content and improvement of the compressive and tensile properties (29). Thus, it is expected that the discrete modulation of ions responsible for hypoxia and mechanotransduction may be associated with an increase in the biomechanical properties of tissue-engineered neocartilage.

In this work, we aimed to improve the mechanical properties of neocartilage constructs, derived from expanded and rejuvenated minipig costal chondrocytes, using two distinct strategies based on ion modulation: 1) sequestration of Fe^{3+} using DFO to induce a hypoxic response, and 2) the combined treatment of Fe^{3+} and Ca^{2+} modulation using DFO and ionomycin. This work employed a two-phase approach. In Phase I, two concentration of DFO (10 µM and 100 µM) were tested and compared to an untreated group (control) and a group treated with glucose oxidase-catalase (GOX/CAT), an established system for depleting solubilized O_2 and inducing hypoxia (30). It was hypothesized that the induction of a hypoxic response using DFO, prompted by the

sequestration of Fe^{3+}, would outperform the untreated controls and mirror the hypoxic response induced by GOX/CAT treatment, in terms of neocartilage biochemical and mechanical properties. In Phase II, the DFO concentration yielding neocartilage properties most similar to those of native tissue was used in combination with ionomycin, a Ca^{2+} modulator that mimics mechanotransduction, and compared to either treatment alone and to the untreated controls. It was hypothesized that modulating both Fe^{3+} and Ca^{2+} would result in neocartilage constructs with improved mechanical properties and an overall superior tensile properties compared to prior literature.

Methods

Isolation and expansion of costal chondrocytes

Juvenile porcine costal chondrocytes (CC) were isolated from the unmineralized portion of floating ribs of three juvenile Yucatan minipigs obtained from Premier BioSource (California, USA) no later than 48 hours after slaughter. Cartilage from ribs cleaned of all non-cartilaginous tissue was cut into 1 mm^3 pieces and washed three times with GlutaMAX Dulbecco's Modified Eagle Medium containing 4.5 g/L glucose (DMEM; Gibco) and 1% (v/v) penicillin/streptomycin/fungizone (PSF; Lonza, Basel, Switzerland). The cartilage was then digested with 0.4% pronase (Sigma) in DMEM for 1 hour at 37°C, and then in 0.2% collagenase type II (Worthington Biochemical, Lakewood, NJ) in DMEM supplemented with 3% (v/v) fetal bovine serum (FBS; Atlanta Biologicals, Lawrenceville, GA) for 18 hours at 37°C. Cells were then strained through a 70 µm strainer, washed with red blood cell lysis buffer (31) for 4 min, counted, and frozen in freezing medium containing 90% (v/v) FBS + 10% (v/v) DMSO (Sigma). Primary (P0) CC were thawed and seeded in T225 flasks at a density of ~2.5 million cells per flask in chondrogenic medium (CHG) consisting of GlutaMAX DMEM, 1% (v/v) PSF, 1% (v/v) insulin-transferrin-selenium (BD Biosciences, San Jose, CA), 1% (v/v) non-essential amino acids (Thermo Fisher Scientific), 100 mg/mL sodium

pyruvate (Thermo Fischer Scientific), 50 mg/mL ascorbate-2-phosphate (Sigma, St. Louis, MO), 40 mg/mL L-proline (Sigma), and 100 nM dexamethasone (Sigma). Throughout expansion, medium was supplemented with 2% (v/v) FBS, 1 ng/mL TGF-β1, 5 ng/mL bFGF, and 10 ng/mL PDGF (PeproTech). Cells were cultured at 37°C in 10% CO_2, and passaged to P3 at confluence using 0.05% trypsin-EDTA (Invitrogen) and 0.2% collagenase type II solutions.

Chondrogenic differentiation in aggregate rejuvenation and neocartilage construct seeding

Passaged CC were seeded on 1% (w/v) agarose-coated plates at a density of 750,000 cells/mL (30 mL total) per plate with CHG supplemented with 10 ng/ml TGF-β1, 100 ng/ml GDF-5, and 100 ng/ml BMP-2 (PeproTech) (32). Plates were placed on an orbital shaker at 50 rpm for 24 hours at 37°C in 10% CO_2, and then kept static, changing medium every 4 days. At 14 days of aggregate rejuvenation, the aggregates were digested using 0.05% trypsin-EDTA and 0.2% collagenase type II solutions. Cells were strained through a 70 µm cell strainer, washed twice, resuspended in CHG, and seeded. For the self-assembling process of neocartilage constructs, 2 million cells were seeded in 5 mm diameter non-adherent 2% (w/v) agarose wells at a density of 20 million cells/mL. At 4 hours post self-assembly, additional 400 µL of CHG or CHG supplemented with 10 ng/ml TGF-β1 were added. This medium was replaced daily until unconfinement (at day 3 post self-assembly), after which, constructs were kept in 2 mL of medium, replaced every 2 days. The CHG control group was maintained in CHG medium. For all other groups, TGF-β1, chondroitinase ABC (c-ABC), and LOXL2 treatment (termed TCL) was used as follows: TGF-β1 was applied at 10 ng/ml after seeding and until day 28, c-ABC (Sigma) was applied at 2 Units per mL for 4 hours in day 7, and LOXL2 (Signal Chem) was applied at 0.15 µg/mL between days 7 and 21 post self-assembly, together with 0.146 µg/mL hydroxylysine (Sigma) and 1.6 µg/mL copper sulfate (Sigma).

Ion modulation

For all experiments, the constructs were randomly assigned across treatment groups. Modulation of ions in the constructs was performed between days 12 and 16 post self-assembly. For every group in Phase I, medium was replaced with 400 µL of CHG containing 10 µM DFO (Sigma), or 100 µM DFO, or blank CHG for the untreated control group. For the enzymatic system GOX/CAT, 3 Un/mL glucose oxidase (GOX; Sigma) and 30 Un/mL catalase (CAT; Sigma) were used. Incubation was performed for 1 hour, after which constructs were washed twice using DMEM 1% (v/v) PSF before resuming culture in CHG medium. The same incubation procedure was followed for Phase II, using 400 µL of 100 µM DFO, 0.3 µM ionomycin (Io; Sigma), and 100 µM DFO + 0.3 µM Io.

Mechanical testing

Tensile properties were determined using uniaxial tension in an Instron model 5565 (Instron, Canton, MA). Dog bone-shaped samples were obtained from every engineered cartilage construct with a gauge length of 1.55 mm. The dog bones were photographed to measure thickness and width in ImageJ. The ends of the dog-bone were fixed to paper with cyanoacrylate to increase the gripping area for testing. A strain rate of 1% of the gauge length per second was used until failure. The Young's modulus was obtained from the linear region of the stress-strain curve, and the ultimate tensile strength (UTS) was defined as the maximum stress obtained.

Compressive properties of the neocartilage constructs were determined by creep indentation testing. Briefly, 2.5 mm punches obtained from every construct were submerged in PBS until equilibrium and indented with a flat porous 0.5 mm diameter tip perpendicular to the surface of the sample to ~10% strain. The aggregate modulus (H_A) and shear modulus (μ_s) were obtained using a semi-analytical, semi-numerical, biphasic model and finite-element optimization (33, 34).

Biochemical testing

Cartilage constructs (~2-3 mg) were weighed to obtain wet weight, lyophilized for 3 days, and weighed again to obtain dry weight. Lyophilized samples were digested in 125 µg/mL papain (Sigma) +5 mM N-acetyl-L-cysteine +5 mM EDTA in phosphate buffer pH 6.5. for 18 hours at 60°C. GAG content was quantified using a Blyscan glycosaminoglycan assay kit (Biocolor, Newtownabbey, Northern Ireland). Total collagen content was quantified using a modified chloramine-T hydroxyproline assay (35). DNA content was quantified with a picogreen assay (ThermoFisher Scientific). For the quantification of PYR crosslinks, separate tissue samples (~0.2-1 mg) were weighed, lyophilized, and acid-digested for 12 hours in 6N HCl. After evaporation, the dried hydrolysate was resuspended in a 75%/25% (v/v) solution of 0.1% formic acid and acetonitrile. Samples were measured through mass spectrometry using a cogent diamond hydride column and a PYR standard (36).

Histology

Samples were fixed in 10% neutral-buffered formalin, embedded in paraffin, and sectioned at a thickness of 6 µm for histological evaluation. Sections were subsequently processed and stained with hematoxylin and eosin (H&E), safranin-O, and picrosirius red using standard protocols.

Statistical analysis

All quantitative biochemical and biomechanical tests were performed using n= 6-8. All data are presented as means ± standard deviations. A single factor one-way ANOVA was employed in each phase of the study to assess differences among experimental groups. Multiple comparisons were performed using a Dunnett's *post hoc* test. The Dunnett's test compares the means from every experimental group against a control group mean to determine significant differences. All statistical analyses were performed using GraphPad Prism version 8.4.1 for Windows (GraphPad Software, San Diego, California USA). Groups marked with * indicate that there are statistically significant differences compared to the control group ($p < 0.05$).

Results

Effect of iron chelation on the mechanical properties of neocartilage constructs

Self-assembled neocartilage constructs, formed using expanded and rejuvenated costal chondrocytes, were treated with a low dose of deferoxamine (DFO 10 μM), or a high dose of deferoxamine (DFO 100 μM). A treatment with a combination of glucose oxidase and catalase (GOX/CAT), an established method for inducing a hypoxic condition by depleting O_2 in the medium, was also examined, and all treated groups were compared to untreated construct. As depicted in the gross morphology images of representative samples (**Fig. 1A**), none of the treatments affected the morphological features of the constructs. No statistical differences were observed in the diameter, thickness, wet weight, and water content among untreated and various treatment groups (**Table 1**).

Histological evaluation was performed to assess any variations in the ECM structure of the neocartilage constructs (H&E staining) or in the GAG and collagen distribution within the constructs (safranin-O and picrosirius red, respectively). With H&E, all groups showed a homogeneous cell distribution (**Fig. 1B**). Similarly, safranin-O stain was found to be evenly distributed throughout constructs in all groups, albeit absent in the outermost acellular layer of all constructs. Likewise, no differences were observed for collagen staining among groups. For all constructs, the GAG-free layer showed increased staining for picrosirius red, indicating a collagenous composition in this layer. Biochemical quantification of GAGs and total collagens further supported these findings, showing no variation among groups (**Table 1**). Likewise, DNA content was unaffected.

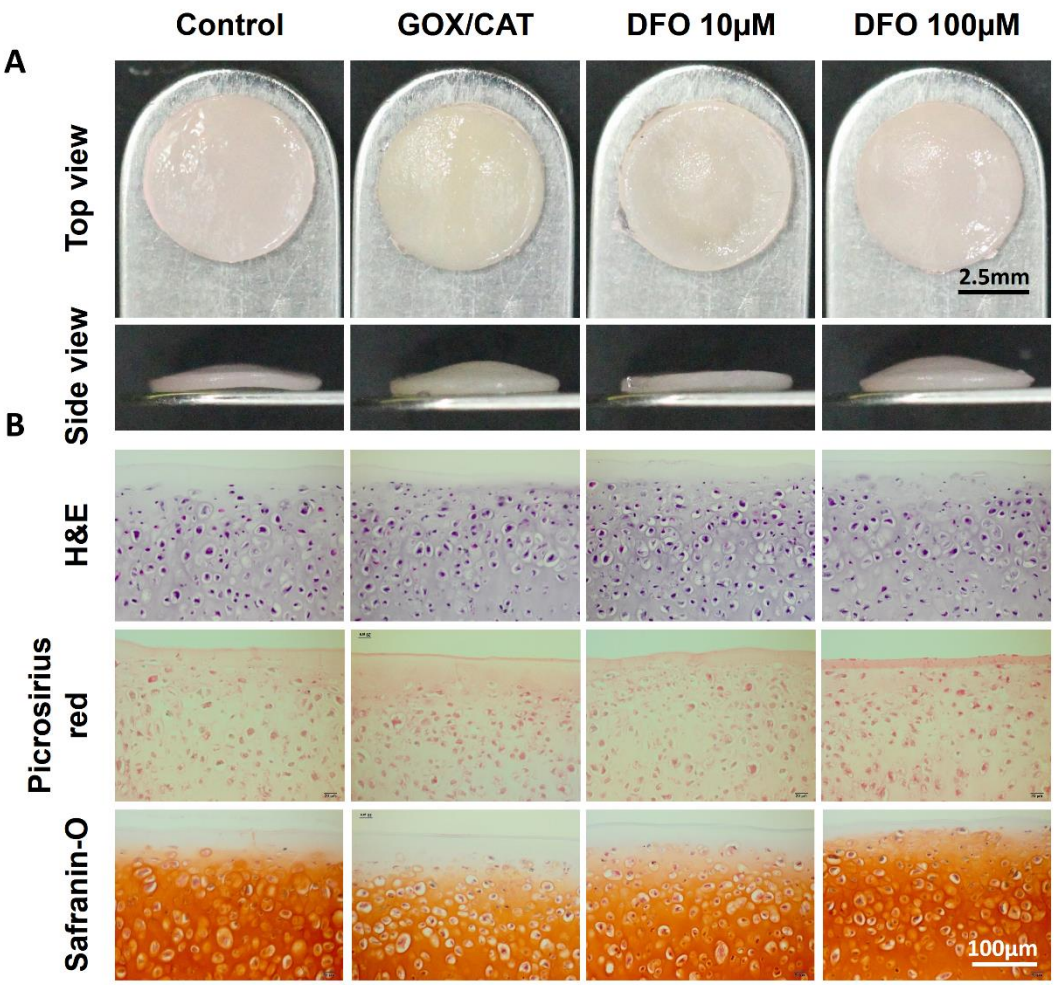

Figure 1. Gross morphology and histological staining of self-assembled constructs treated with GOX/CAT or DFO. (**A**) All constructs appear homogeneous, flat, and with no visible abnormalities. (**B**) The histological analysis of neocartilage constructs showed that overall cellularity and neotissue composition appears comparable among all groups as observed in hematoxylin and eosin staining. Similarly, none of the treatments elicit any noticeable variation in the Picrosirius red staining or the Safranin-O staining.

Table 1. Gross morphology and biochemical data. Data are presented as means ± standard deviation.

	Diameter (mm)	Thickness (mm)	Wet weight (mg)	Hydration (%)	DNA (µg/ construct)	GAG/DW (%DW)	COL/DW (%DW)
Control	5.54±0.12	0.45±0.02	13.17±0.87	77.79±1.98	19.54±1.9	44.58±1.48	15.66±0.78
GOX/CAT	5.45±0.06	0.44±0.06	13.29±1.36	78.91±0.77	18.94±1.87	41.43±3.54	15.77±1.00
DFO 10uM	5.57±0.06	0.44±0.06	13.73±1.77	77.53±4.97	19.24±4.41	46.23±2.50	15.75±1.98
DFO 100uM	5.57±0.07	0.47±0.05	14.83±1.24	77.47±2.24	19.29±2.06	45.01±2.94	15.30±0.84

The compressive and tensile biomechanical properties, along with the quantification of the PYR crosslinks, were assessed to determine the effects of the treatments. The compressive properties appeared unaffected by either treatment, and although a ~15% increase was observed in the aggregate modulus of DFO-treated constructs, but there was no significance. On the other hand, the Young's modulus and the UTS values were higher in constructs exposed to the iron chelator compared to the untreated group (**Fig. 2A-D**). Constructs treated with 100 µM DFO showed a 57% significant increase in the Young's modulus over the untreated constructs. Treatment with GOX/CAT and 10 µM DFO also reported higher Young's modulus, with a 7% and a 40% increase, respectively, albeit not significant. Constructs treated with 10 µM or 100 µM DFO showed 72% and 112% significant increases in the UTS, respectively, compared to the untreated constructs. Similar effects were observed in the quantification of the crosslink content (**Fig. 2E**). All treated groups showed a significant increase of PYR crosslinks, with 58%, 64%, and 87% increases induced by GOX/CAT, 10 µM DFO, and 100 µM DFO, respectively, over the untreated group.

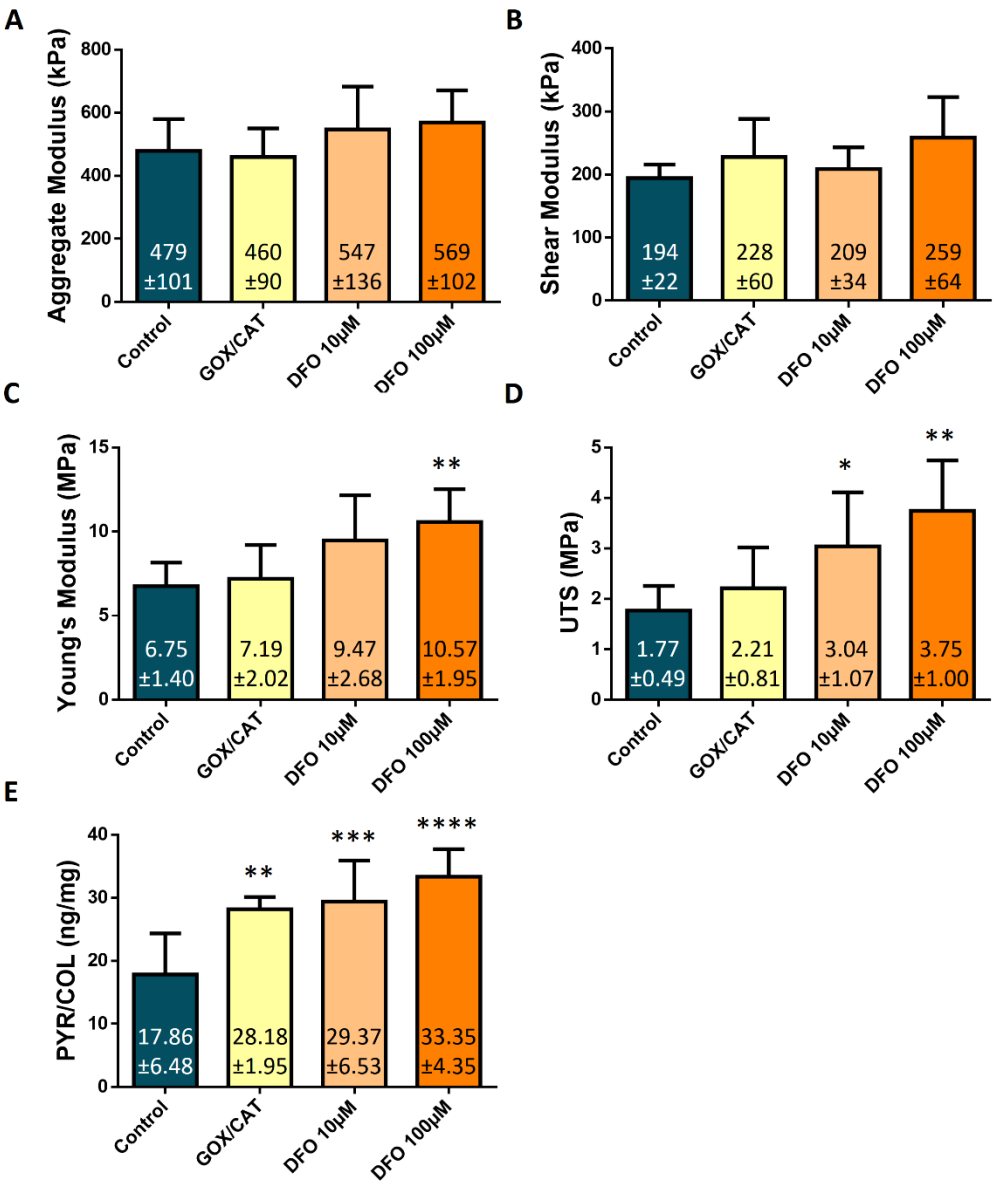

Figure 2. Biomechanical and crosslink properties of neocartilage constructs treated with GOX/CAT and DFO. (**A**) Aggregate modulus, (**B**) shear modulus, (**C**) tensile Young's modulus, (**D**) UTS, and (**E**) PYR crosslinks. A high dose of DFO showed a 57% increase in the Young's modulus and a 112% increase in the UTS, so as an 87% increase in the PYR crosslink content. The asterisks denote significant differences compared to the control group based of Dunnett´s *post hoc* test (* denotes $p<0.05$; ** denotes $p<0.01$, *** denotes $p<0.005$).

Table 2. Gross morphology and biochemical data of neocartilage constructs treated ionomycin and DFO. Data are presented as means ± standard deviation. The asterisks denotes significant differences compared to the control group based of Dunnett´s *post hoc* test (* denotes $p<0.05$).

	Diameter (mm)	Thickness (mm)	Wet weight (mg)	Hydration (%)	DNA (µg/ construct)	GAG/DW (%DW)	COL/DW (%DW)
Control	5.70±0.07	0.49±0.05	14.14±0.91	79.69±1.86	16.61±2.93	40.21±0.46	15.14±1.12
Io	5.65±0.06	0.49±0.05	14.22±0.49	79.76±1.56	15.80±1.82	40.06±1.57	15.16±0.92
DFO	5.71±0.05	0.49±0.05	14.84±0.84	80.19±0.90	14.77±1.3	41.78±1.91	14.16±0.67
Io+DFO	5.70±0.03	0.50±0.03	14.72±0.79	79.40±0.93	15.38±1.14	37.99±1.52	14.09±1.12

Effect of combined ion treatment in neocartilage constructs

To study possible interactions between the two ion modulators, DFO and ionomycin were applied in combination to sequester Fe^{2+} and increase intracellular Ca^{2+} concentration, respectively. The effects of the combined treatment were interrogated in Phase II and compared to constructs treated with either ion modulator alone and untreated constructs. In agreement with Phase I data, neither ionomycin nor DFO induced changes in the gross morphology of the constructs. The same results were reported for the combined treatment (**Fig. 3A**). As in Phase I, morphological features were quantified, showing no differences among groups in terms of diameter, thickness, wet weight, and water content (**Table 2**). Likewise, and with the exception of the groups treated with DFO which showed a decrease in the total collagen content, the overall histological properties and biochemical content were unaffected by the treatments compared to the untreated group (**Table 2** and **Fig. 3B**). The use of ion modulators did not affect gross tissue formation.

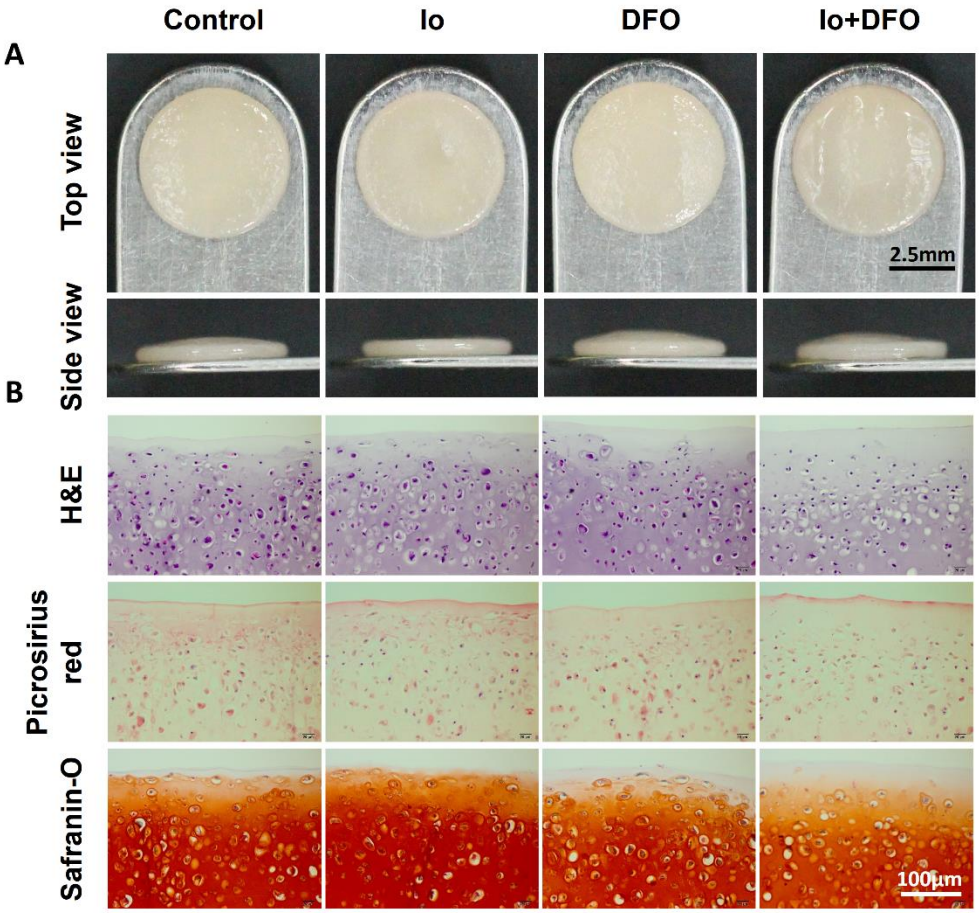

Figure 3. Gross morphology and histological staining of self-assembled constructs treated with ionomycin and/or DFO. (A) All constructs appear homogeneous, flat, with no visible abnormalities, and similar coloration and opacity. (B) The histological analysis of neocartilage constructs showed that Fe^{2+} and Ca^{2+} modulation did not affect the neotissue histological appearance, alone or in combination. Overall cellularity and neotissue composition appears comparable among all groups. Similarly, none of the treatments elicit any noticeable variation in the Picrosirius red staining or the Safranin-O staining.

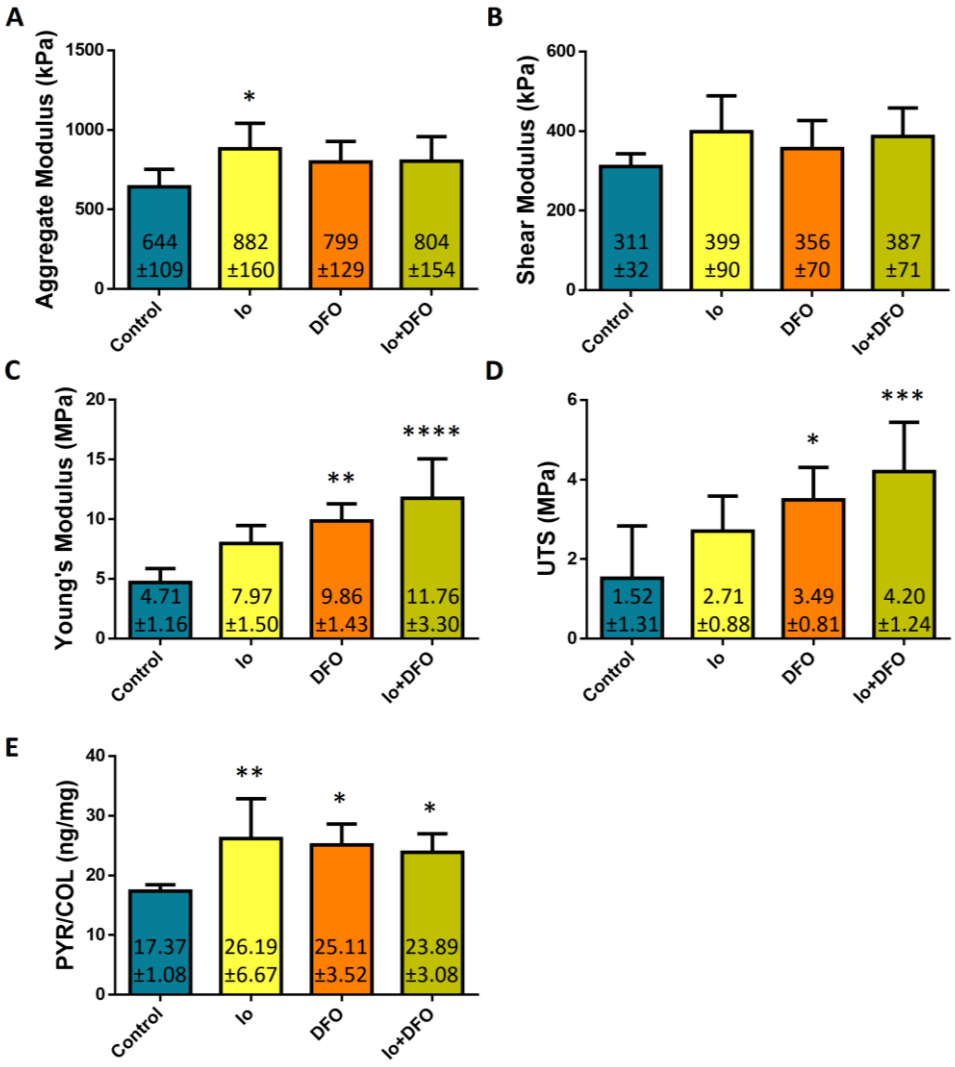

Figure 4. Biomechanical properties and crosslink of neocartilage constructs treated with ionomycin (Io) and DFO. (A) Aggregate modulus, (B) shear modulus, (C) tensile Young's modulus, (D) UTS, and (E) PYR crosslinks. Constructs treated with a combination of ionomycin and DFO showed a 150% and a 176% increase in the Young's modulus and UTS, respectively, over the untreated control, and with better performance compared to both treatments alone. This effect cannot be attributed to an increase in of PYR crosslinks, where the combination treatment also increased the PYR content a 38% compared to the control, on par or below to the individual treatments. The asterisks denote significant differences compared to the control group based of Dunnett´s *post hoc* test (* denotes $p<0.05$; ** denotes $p<0.01$, *** denotes $p<0.005$).

Ionomycin and DFO affect the mechanical properties of self-assembled neocartilage constructs alone and in combination. All treatment groups showed an increase in the compressive or tensile properties (**Fig. 4A-D**). While ionomycin-treated constructs showed a 37% significant increase in the aggregate modulus, the groups including DFO displayed the same non-significant ~20% increase compared to the untreated group observed in Phase I (**Fig. 4A**). A similar trend was observed for the shear modulus (**Fig. 4B**). The tensile properties, shown to increase after treatment with DFO, were further improved after combining the two ion modulators. Treatment with DFO alone produced a 109% significant increase in the Young's modulus over the untreated control. The simultaneous application of both ion modulators, however, resulted in a 150% significant increase in the measurement, resulting in constructs with a Young's modulus of 11.76±3.29 MPa (**Fig. 4C**). The same result was observed for the UTS of treated constructs, in which DFO induced 130% significant increase when administered alone, compared to a 176% increase when administered together with ionomycin. Thus, the combined treatment resulted in constructs with a UTS of 4.20±1.24 MPa (**Fig. 4D**). Lastly, all treatments increased the PYR crosslink content. Ionomycin, DFO, and the combination of both produced 51%, 45%, and 38% increases over the untreated group, respectively (**Fig. 4E**).

Discussion

The development of biomimetic tissue-engineered neocartilage implants is emerging as a new solution for the treatment of articular cartilage lesions. Using ion modulation, this work's objective was to improve the biomechanical properties of self-assembled neocartilage constructs. Overall, it was hypothesized that the sequestration of Fe^{3+} (by DFO, Phase I), and the combination of Fe^{3+} sequestration with an induced cytoplasmic accumulation of Ca^{2+} (by DFO and ionomycin, Phase II), would result in neocartilage constructs with improved mechanical properties. The rationale for these hypotheses comes from the capability of the iron chelator DFO to avoid HIF1α degradation

and induce a putative hypoxic response, and the capability of the Ca^{2+} ionophore ionomycin to increase the cytoplasmic concentration of Ca^{2+} and induce mechanotransduction-like conditions. Indeed, the functional properties were improved in both phases: in Phase I, of the dosages examined, treatment of constructs with 100 µM DFO improved the PYR crosslink content by 87%, Young's modulus by 57%, and UTS by 112% in self-assembled neocartilage constructs, engineered from minipig expanded and rejuvenated costal chondrocytes. In Phase II, the combined treatment of DFO and ionomycin improved the PYR crosslink content by 38%, Young's modulus by 150%, and UTS by 176% in the same neotissue model. This work's findings are significant, as this is the first study to show improved mechanical properties of neocartilage constructs via the use of soluble small molecules, 1) Fe^{2+} chelator and 2) Fe^{2+} + Ca^{2+} modulators, to achieve neocartilage with the best tensile properties thus far.

Toward achieving native tissue-level mechanical properties, the proper DFO concentration was identified. Because homeostasis of ions is required to maintain proper cell function, an appropriate concentration of DFO needed to be identified so as to improve the construct mechanical properties while avoiding any damaging effects on the chondrocytes and neocartilage constructs. In Phase I of this work, two concentrations of DFO were examined, 10 µM and 100 µM. These concentrations were determined based on the use of DFO in studies using osteoarthritic chondrocytes and cancer cell lines (37-39). Treatment with 10 µM DFO increased the Young's modulus and UTS by 40% and 72% over untreated controls, respectively, whereas the 100 µM treatment increased the same tensile properties by 57% and 112%, respectively. These results demonstrate the existence of a dose-dependent response to DFO and are comparable to previous studies that use hypoxic stimulation. For example, neocartilage constructs derived from primary bovine articular chondrocytes exposed to 4% O_2 had a 2-fold increase in tensile modulus, resulting in a Young's modulus of 0.82±0.53 MPa (8); to place this in context, in the present study, under 10 µM and 100 µM DFO treatments, the construct Young's

moduli were 9.47±2.69 and 10.57±1.95 MPa, respectively. Another study using tissue constructs formed using cell encapsulation exposed to 5% O_2 during 7 days not only showed an increase in equilibrium Young's modulus by 22% (510.01±28.15 kPa) compared to the group exposed to normoxic conditions (417.60±68.46 kPa), but also increased expression of various chondrogenic genes such as COL2A1, SOX9, and ACAN (40). The increase in tensile properties of DFO-treated constructs, presumably due to HIF1α-induced gene expression, demonstrates the feasibility of using the iron chelator as a tool in tissue engineering development efforts.

The modulation of ion concentration results in changes on the collagen crosslinks of the neotissue, which translate to an improvement of construct stiffness. Enzymatic collagen crosslinks, such as the mature trivalent PYR crosslink, play important roles in the mechanical properties of collagenous tissues. Strategies that increase crosslink content, such as hypoxia or *in vivo* maturation, improve the mechanical properties of engineered neotissues, particularly the tensile properties (29, 41, 42). In this work, self-assembled constructs exposed to DFO showed 64% and 87% significant increases in the PYR crosslink content in a dose-dependent manner, following treatment with 10 μM and 100 μM DFO, respectively. This finding is significant as it validates the hypothesized function of iron chelation as a medium of inducing HIF1α activation, which prompts the expression of lysyl oxidase-like 2 (LOXL2), the protein that catalyzes the PYR crosslinks (8, 24). Neocartilage constructs derived from primary bovine articular chondrocytes exposed to 4% O_2 for 2 weeks not only showed a 2-fold increase in the Young's modulus, but also a 20-fold increase in the gene expression of LOXL2 (8). While the changes in PYR crosslink content are not sufficient to explain the mechanical data and future experiments should aim at identifying the mechanisms behind the effects shown here, the literature is consistent in demonstrating that an increase in the crosslink content is associated with an increase in the tensile properties. This finding is also significant because it provides an explanation for the

increase in the tensile properties, as the increase of PYR crosslinks is directly associated with an increase in Young's modulus (42).

Separate cellular components are affected by Fe^{2+} depletion and cytoplasmic Ca^{2+} uptake, suggesting that the activation of distinct signaling cascades by different ion modulators may be used in combination. Ionomycin increases cytoplasmic Ca^{2+} concentration, an early signal that follows a mechanical stimulus, presumably via calmoduline (CaM)-dependent factors (43-46). The results shown here were expected based on prior work showing ionomycin's use for the improvement of tensile stiffness of constructs derived from primary bovine articular chondrocytes as well as constructs derived from expanded and rejuvenated minipig costal chondrocytes (10, 29). As hypothesized, the combination of DFO with the Ca^{2+} ionophore resulted in a larger increase of the tensile properties compared to the untreated constructs or constructs treated with one ion modulator, with an average Young's modulus of 11.76±3.29 MPa. This value corresponds to a 150% significant increase over the control group, and a 48% or 19% increase compared to the ionomycin or DFO treatments alone. Similarly, the UTS of the constructs exposed to the combined treatment was 176% higher compared to the control group, and 55% or 20% higher compared to the UTS of constructs treated with ionomycin or DFO alone, respectively. The findings shown in this work are significant, as they are, to the best of our knowledge, the first evidence that two different ion modulation strategies, one aiming at inducing a hypoxic effect and one aiming at inducing mechanotransduction, can be used together to attain a larger effect. Inasmuch as previous studies on self-assembled cartilage have examined the use of Na^{+} and Ca^{2+} modulation as a stimulation factor, this study showed that Fe^{2+} and Ca^{+2} modulation yield better results compared to Fe^{2+} alone, Ca^{2+} alone, and Na^{+} and Ca^{2+} combined, in terms of producing a mechanically robust neocartilage suitable for translation (**Fig. 5**).

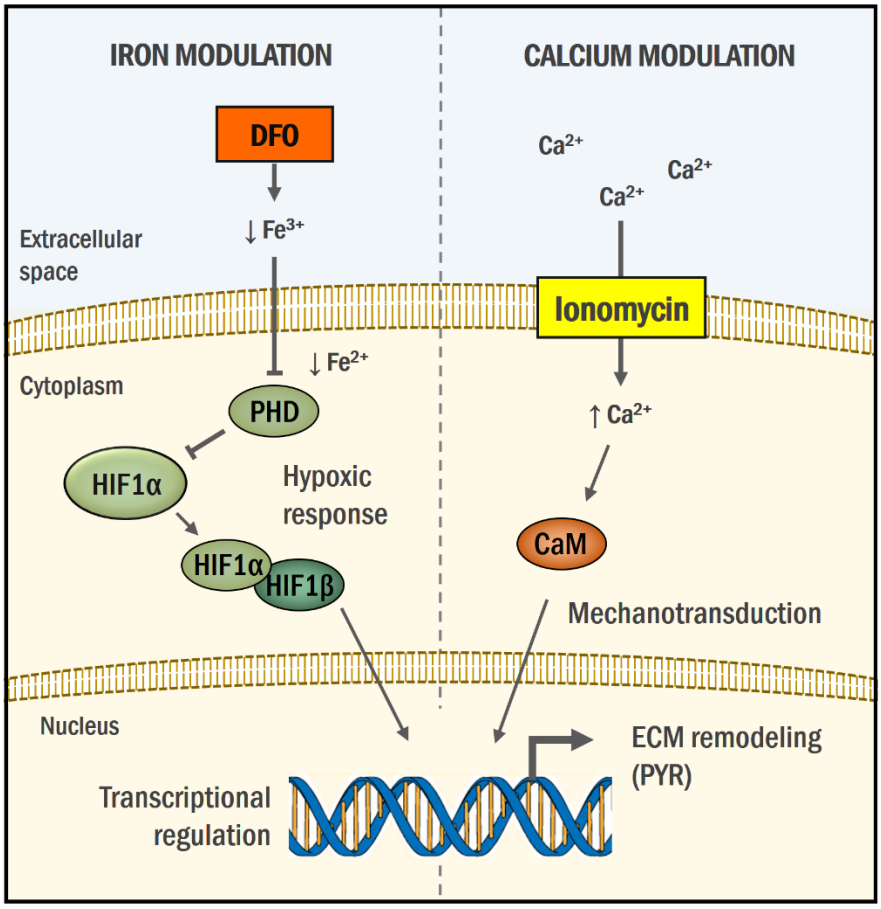

Figure 5. Deferoxamine and ionomycin mediated modulation of ions trigger signaling cascades, which result in improved structure-function relationships of neocartilage constructs.

Considering that Fe^{2+} and Ca^{2+} ions are involved in multiple processes within the cell, this work examined the potential toxic effects of ion modulation. Aside from its role in PHD function, iron is involved in various cell processes, including erythropoiesis, mitochondrial function, immune response, and DNA synthesis and repair (47). In view of the possible adverse effects of iron depletion, a short-duration 1-hour daily treatment over 5 days was used. The rationale behind the dosage selection comes from the following findings: transcription factors of the same highly conserved family as HIF1α elicit a 24-hour long sustained transcriptional activation in response

to a 2-hour long stimulation (48). A similar effect was found in fibrochondrocytes. Engineered meniscus exposed to 3% O_2 for 24 hours followed by 5 minutes of dynamic compression displayed over 40 genes supporting a chondrogenic phenotype, as revealed by RNA sequencing performed 30 min after the end of stimuli (49). These data suggest that short Fe^{2+} and Ca^{2+} modulation stimuli are enough to elicit changes in the biomechanical properties, but not long enough to induce adverse effects. Our results found no alterations in the appearance and structure of the neocartilage tissues, as evidence by their gross morphology and histology. Moreover, no differences were found in the DNA content, a measure of construct cellularity. These results are significant, as they demonstrate no toxicity induced by the ion modulation treatments.

The use of ion modulation via DFO and ionomycin allows for treatment modalities that cannot be replicated with the use of bioreactors. Hypoxia and mechanical stimuli have been used in the past to induce neotissue maturation. These strategies, however, need dedicated equipment, require significant manipulation of the tissues, and may be difficult to control temporally. As a result, neotissues may display higher variability and become prone to contamination and user errors, compared to non-bioreactor cultures (50). For example, short-duration treatments are not feasible using hypoxic chambers, which rely on passive mixture of gases and their solubilization into the culture medium, and therefore, show a slow onset of hypoxia as opposed to the treatments used in this study (51). Moreover, combination of stimuli results in added complexity that makes these strategies less feasible for translational purposes. A recent work combined hypoxia and dynamic compression by culturing tissue-engineered meniscus at 3% O_2 and exposing it to 5 min of dynamic compression, 4 times a day, at a 30-45% strain. The combined use of hypoxic and mechanical stimuli, termed mechano-hypoxia conditioning, resulted in upregulation of chondrogenic genes (e.g., SOX5/6) and down regulation of hypertrophic genes (e.g., COL10A1) on meniscus fibrochondrocytes (52). The authors, however, reported several limitations in the study, including a high variability within the results and possible confounding

effects due to the media not being changed during the whole 3-weeks culture to maintain hypoxia (52). DFO and ionomycin are safe, long-lasting, low-cost exogenous agents with high reproducibility and efficacy without added complexity and costs of bioreactors.

Previously identified analog methods to induce hypoxia, for example via the use of GOX/CAT, do not necessarily result in functional improvements of neocartilage constructs. In Phase I, in addition to DFO, the enzymatic system GOX/CAT was also examined as a means of eliciting HIF1α accumulation due to hypoxia (30). This method uses two enzymes to induce hypoxia within the culture medium: glucose oxidase is used to consume oxygen by generating H_2O_2, and catalase to degrade H_2O_2. This treatment induced a 58% significant increase of the PYR content, suggesting that a hypoxic response may have been induced. However, the increase in crosslinks did not translate into improvements on the compressive or tensile properties. It is possible that the system, while depleting oxygen from the medium by consuming glucose and inducing a hypoxic response on the cells, also confers other effects that may not be conducive toward the improvement of functional properties. Such effects can include producing oxidative stress through the accumulation of H_2O_2 in spite of the catalase reaction, or the consumption of glucose, also required by the cells (53, 54). Chondrocytes are particularly sensitive to H_2O_2 accumulation, and the availability of glucose in the medium has been directly associated with ECM deposition (54, 55). The GOX/CAT system requires further characterization toward its application in cartilage tissue engineering platforms.

This work represents significant progress toward generating a tissue-engineered neocartilage solution for addressing articular cartilage lesions. Molecular assays were not employed in this work since the mechanisms of action of DFO and ionomycin have been examined by others (24, 29, 37, 56). However, future studies with Fe^{2+} and Ca^{2+} modulators should aim to identify the mechanisms that take place in self-assembled neocartilage to explain the mechanical data obtained in this work. The findings shown provide a valuable new approach

for the tissue-engineering field. The use of hypoxic and mechanical stimuli, often used to improve the biomechanical properties of engineered tissues, such as neocartilage, carry added limitations, technical complications, and costs. The use of ion modulation poses an analog method to elicit biomechanical improvements, while avoiding the potential complications of using bioreactors. As shown in this work, ion modulation is highly controllable, replicable, cost-effective, and allows the combination of treatments without added methodological difficulty. Particularly, this work used 1) costal chondrocytes, a novel cell source that eliminates donor site morbidity; 2) cell expansion to eliminate cell scarcity limitations; and 3) rejuvenation of passaged chondrocytes to recapitulate a proper chondrogenic phenotype and ensure assembly of chondrocytes into hyaline cartilage. After a combined treatment of DFO and ionomycin, the neocartilage constructs achieved a Young's modulus of 11.76±3.29 MPa and UTS of 4.20±1.24 MPa, the highest recorded tensile properties for self-assembled neocartilage constructs.

Conclusion

This study examined the use of two ion modulation strategies to improve the mechanical properties of engineered neocartilage constructs derived from expanded and rejuvenated minipig costal chondrocytes: 1) sequestration of Fe^{3+} using DFO, and 2) the combined treatment of Fe^{3+} and Ca^{2+} modulation using DFO and ionomycin. The results shown in this work demonstrate that DFO, an iron chelator, induces tissue maturation, as reflected in the PYR crosslink content, and an improvement in the tensile properties. In addition, this work shows the feasibility of combining different ion modulation strategies by using ionomycin, a calcium ionophore, together with DFO. The combined treatment of these ion modulators resulted in the highest tensile values ever obtained for self-assembled neocartilage constructs and provides evidence of the utility of ion modulation within tissue engineering efforts.

Acknowledgements

The authors acknowledge support from the National Institutes of Health (NIH) R01 AR067821 and Fulbright Chile scholarship.

References

1. Heinemeier KM, Schjerling P, Heinemeier J, Moller MB, Krogsgaard MR, Grum-Schwensen T, Petersen MM, Kjaer M. Radiocarbon dating reveals minimal collagen turnover in both healthy and osteoarthritic human cartilage. Science translational medicine. 2016;8(346):346ra90. doi: 10.1126/scitranslmed.aad8335. PubMed PMID: 27384346.
2. Steadman JR, Rodkey WG, Rodrigo JJ. Microfracture: surgical technique and rehabilitation to treat chondral defects. Clinical orthopaedics and related research. 2001(391 Suppl):S362-9. doi: 10.1097/00003086-200110001-00033. PubMed PMID: 11603719.
3. Hangody L, Rathonyi GK, Duska Z, Vasarhelyi G, Fules P, Modis L. Autologous osteochondral mosaicplasty. Surgical technique. The Journal of bone and joint surgery American volume. 2004;86-A Suppl 1:65-72. PubMed PMID: 14996923.
4. Huang BJ, Hu JC, Athanasiou KA. Cell-based tissue engineering strategies used in the clinical repair of articular cartilage. Biomaterials. 2016;98:1-22. doi: 10.1016/j.biomaterials.2016.04.018. PubMed PMID: 27177218; PubMed Central PMCID: PMC4899115.
5. Kwon H, Brown WE, Lee CA, Wang D, Paschos N, Hu JC, Athanasiou KA. Surgical and tissue engineering strategies for articular cartilage and meniscus repair. Nature reviews Rheumatology. 2019;15(9):550-70. doi: 10.1038/s41584-019-0255-1. PubMed PMID: 31296933.
6. Makris EA, MacBarb RF, Paschos NK, Hu JC, Athanasiou KA. Combined use of chondroitinase-ABC, TGF-beta1, and collagen crosslinking agent lysyl oxidase to engineer functional neotissues for fibrocartilage repair. Biomaterials. 2014;35(25):6787-96. doi: 10.1016/j.biomaterials.2014.04.083. PubMed PMID: 24840619; PubMed Central PMCID: PMC4105108.
7. Gonzalez-Leon EA, Bielajew BJ, Hu JC, Athanasiou KA. Engineering self-assembled neomenisci through combination of matrix augmentation and directional remodeling. Acta biomaterialia. 2020;109:73-81. doi: 10.1016/j.actbio.2020.04.019. PubMed PMID: 32344175; PubMed Central PMCID: PMC7987216.
8. Makris EA, Hu JC, Athanasiou KA. Hypoxia-induced collagen crosslinking as a mechanism for enhancing mechanical properties of engineered articular cartilage. Osteoarthritis and cartilage. 2013;21(4):634-41. doi: 10.1016/j.joca.2013.01.007. PubMed PMID: 23353112; PubMed Central PMCID: PMC3670708.
9. Salinas EY, Aryaei A, Paschos N, Berson E, Kwon H, Hu JC, Athanasiou KA. Shear stress induced by fluid flow produces improvements in tissue-engineered cartilage. Biofabrication. 2020;12(4):045010. doi: 10.1088/1758-5090/aba412. PubMed PMID: 32640430; PubMed Central PMCID: PMC8020626.

10. Natoli RM, Skaalure S, Bijlani S, Chen KX, Hu J, Athanasiou KA. Intracellular Na(+) and Ca(2+) modulation increases the tensile properties of developing engineered articular cartilage. Arthritis and rheumatism. 2010;62(4):1097-107. doi: 10.1002/art.27313. PubMed PMID: 20131245; PubMed Central PMCID: PMC2909188.
11. Lafont JE. Lack of oxygen in articular cartilage: consequences for chondrocyte biology. International journal of experimental pathology. 2010;91(2):99-106. doi: 10.1111/j.1365-2613.2010.00707.x. PubMed PMID: 20384821; PubMed Central PMCID: PMC2965894.
12. Guo X, Chen G. Hypoxia-Inducible Factor Is Critical for Pathogenesis and Regulation of Immune Cell Functions in Rheumatoid Arthritis. Frontiers in immunology. 2020;11:1668. doi: 10.3389/fimmu.2020.01668. PubMed PMID: 32849577; PubMed Central PMCID: PMC7399093.
13. Ummarino D. Osteoarthritis: Hypoxia protects against cartilage loss by regulating Wnt signalling. Nature reviews Rheumatology. 2016;12(6):315. doi: 10.1038/nrrheum.2016.66. PubMed PMID: 27170507.
14. Hu S, Zhang C, Ni L, Huang C, Chen D, Shi K, Jin H, Zhang K, Li Y, Xie L, Fang M, Xiang G, Wang X, Xiao J. Stabilization of HIF-1alpha alleviates osteoarthritis via enhancing mitophagy. Cell death & disease. 2020;11(6):481. doi: 10.1038/s41419-020-2680-0. PubMed PMID: 32587244; PubMed Central PMCID: PMC7316774.
15. Leipzig ND, Athanasiou KA. Static compression of single chondrocytes catabolically modifies single-cell gene expression. Biophysical journal. 2008;94(6):2412-22. doi: 10.1529/biophysj.107.114207. PubMed PMID: 18065463; PubMed Central PMCID: PMC2257883.
16. Huey DJ, Athanasiou KA. Tension-compression loading with chemical stimulation results in additive increases to functional properties of anatomic meniscal constructs. PloS one. 2011;6(11):e27857. doi: 10.1371/journal.pone.0027857. PubMed PMID: 22114714; PubMed Central PMCID: PMC3218070.
17. Lee JK, Huwe LW, Paschos N, Aryaei A, Gegg CA, Hu JC, Athanasiou KA. Tension stimulation drives tissue formation in scaffold-free systems. Nature materials. 2017;16(8):864-73. doi: 10.1038/nmat4917. PubMed PMID: 28604717; PubMed Central PMCID: PMC5532069.
18. Ofek G, Dowling EP, Raphael RM, McGarry JP, Athanasiou KA. Biomechanics of single chondrocytes under direct shear. Biomechanics and modeling in mechanobiology. 2010;9(2):153-62. doi: 10.1007/s10237-009-0166-1. PubMed PMID: 19644718.
19. Elder BD, Athanasiou KA. Synergistic and additive effects of hydrostatic pressure and growth factors on tissue formation. PloS one. 2008;3(6):e2341. doi: 10.1371/journal.pone.0002341. PubMed PMID: 18523560; PubMed Central PMCID: PMC2394656.
20. Oinas J, Ronkainen AP, Rieppo L, Finnila MAJ, Iivarinen JT, van Weeren PR, Helminen HJ, Brama PAJ, Korhonen RK, Saarakkala S. Composition, structure and tensile biomechanical properties of equine articular cartilage during growth and maturation. Scientific reports. 2018;8(1):11357. doi: 10.1038/s41598-018-29655-5. PubMed PMID: 30054498; PubMed Central PMCID: PMC6063957.
21. Huey DJ, Athanasiou KA. Maturational growth of self-assembled, functional menisci as a result of TGF-beta1 and enzymatic chondroitinase-ABC stimulation. Biomaterials. 2011;32(8):2052-8. doi: 10.1016/j.biomaterials.2010.11.041. PubMed PMID: 21145584; PubMed Central PMCID: PMC3038547.

22. Madden RM, Han SK, Herzog W. The effect of compressive loading magnitude on in situ chondrocyte calcium signaling. Biomechanics and modeling in mechanobiology. 2015;14(1):135-42. doi: 10.1007/s10237-014-0594-4. PubMed PMID: 24853775; PubMed Central PMCID: PMC4282695.
23. Iommarini L, Porcelli AM, Gasparre G, Kurelac I. Non-Canonical Mechanisms Regulating Hypoxia-Inducible Factor 1 Alpha in Cancer. Frontiers in oncology. 2017;7:286. doi: 10.3389/fonc.2017.00286. PubMed PMID: 29230384; PubMed Central PMCID: PMC5711814.
24. Woo KJ, Lee TJ, Park JW, Kwon TK. Desferrioxamine, an iron chelator, enhances HIF-1alpha accumulation via cyclooxygenase-2 signaling pathway. Biochemical and biophysical research communications. 2006;343(1):8-14. doi: 10.1016/j.bbrc.2006.02.116. PubMed PMID: 16527254.
25. Wu LY, He YL, Zhu LL. Possible Role of PHD Inhibitors as Hypoxia-Mimicking Agents in the Maintenance of Neural Stem Cells' Self-Renewal Properties. Frontiers in cell and developmental biology. 2018;6:169. doi: 10.3389/fcell.2018.00169. PubMed PMID: 30619851; PubMed Central PMCID: PMC6297135.
26. Qiu X, Muller U. Mechanically Gated Ion Channels in Mammalian Hair Cells. Frontiers in cellular neuroscience. 2018;12:100. doi: 10.3389/fncel.2018.00100. PubMed PMID: 29755320; PubMed Central PMCID: PMC5932396.
27. Douguet D, Honore E. Mammalian Mechanoelectrical Transduction: Structure and Function of Force-Gated Ion Channels. Cell. 2019;179(2):340-54. doi: 10.1016/j.cell.2019.08.049. PubMed PMID: 31585078.
28. O'Conor CJ, Leddy HA, Benefield HC, Liedtke WB, Guilak F. TRPV4-mediated mechanotransduction regulates the metabolic response of chondrocytes to dynamic loading. Proceedings of the National Academy of Sciences of the United States of America. 2014;111(4):1316-21. doi: 10.1073/pnas.1319569111. PubMed PMID: 24474754; PubMed Central PMCID: PMC3910592.
29. Otarola G, Hu JC, Athanasiou KA. Intracellular Calcium and Sodium Modulation of Self-Assembled Neocartilage Using Costal Chondrocytes. Tissue engineering Part A. 2021. doi: 10.1089/ten.TEA.2021.0169. PubMed PMID: 34877888.
30. Mueller S, Millonig G, Waite GN. The GOX/CAT system: a novel enzymatic method to independently control hydrogen peroxide and hypoxia in cell culture. Advances in medical sciences. 2009;54(2):121-35. doi: 10.2478/v10039-009-0042-3. PubMed PMID: 20022860.
31. Brown WE, Hu JC, Athanasiou KA. Ammonium-Chloride-Potassium Lysing Buffer Treatment of Fully Differentiated Cells Increases Cell Purity and Resulting Neotissue Functional Properties. Tissue engineering Part C, Methods. 2016;22(9):895-903. doi: 10.1089/ten.TEC.2016.0184. PubMed PMID: 27553086; PubMed Central PMCID: PMC5035916.
32. Kwon H, Brown WE, O'Leary SA, Hu JC, Athanasiou KA. Rejuvenation of extensively passaged human chondrocytes to engineer functional articular cartilage. Biofabrication. 2021;13(3). doi: 10.1088/1758-5090/abd9d9. PubMed PMID: 33418542; PubMed Central PMCID: PMC8263804.
33. Athanasiou KA, Niederauer GG, Schenck RC, Jr. Biomechanical topography of human ankle cartilage. Annals of biomedical engineering. 1995;23(5):697-704. doi: 10.1007/bf02584467. PubMed PMID: 7503470.

34. Mow VC, Kuei SC, Lai WM, Armstrong CG. Biphasic creep and stress relaxation of articular cartilage in compression? Theory and experiments. Journal of biomechanical engineering. 1980;102(1):73-84. doi: 10.1115/1.3138202. PubMed PMID: 7382457.
35. Cissell DD, Link JM, Hu JC, Athanasiou KA. A Modified Hydroxyproline Assay Based on Hydrochloric Acid in Ehrlich's Solution Accurately Measures Tissue Collagen Content. Tissue engineering Part C, Methods. 2017;23(4):243-50. doi: 10.1089/ten.tec.2017.0018. PubMed PMID: 28406755; PubMed Central PMCID: PMC5397204.
36. Bielajew BJ, Hu JC, Athanasiou KA. Methodology to Quantify Collagen Subtypes and Crosslinks: Application in Minipig Cartilages. Cartilage. 2021;13(2_suppl):1742S-54S. doi: 10.1177/19476035211060508. PubMed PMID: 34823380; PubMed Central PMCID: PMC8804780.
37. Tchetina EV, Markova GA, Poole AR, Zukor DJ, Antoniou J, Makarov SA, Kuzin AN. Deferoxamine Suppresses Collagen Cleavage and Protease, Cytokine, and COL10A1 Expression and Upregulates AMPK and Krebs Cycle Genes in Human Osteoarthritic Cartilage. International journal of rheumatology. 2016;2016:6432867. doi: 10.1155/2016/6432867. PubMed PMID: 28042296; PubMed Central PMCID: PMC5155111 Poole who is a consultant to IBEX, Montreal, Canada, who manufacture and market the C1,2C ELISA assay.
38. Jiang Y, Xue ZH, Shen WZ, Du KM, Yan H, Yu Y, Peng ZG, Song MG, Tong JH, Chen Z, Huang Y, Lubbert M, Chen GQ. Desferrioxamine induces leukemic cell differentiation potentially by hypoxia-inducible factor-1 alpha that augments transcriptional activity of CCAAT/enhancer-binding protein-alpha. Leukemia. 2005;19(7):1239-47. doi: 10.1038/sj.leu.2403734. PubMed PMID: 15902299.
39. Yeung HY, Lai KP, Chan HY, Mak NK, Wagner GF, Wong CK. Hypoxia-inducible factor-1-mediated activation of stanniocalcin-1 in human cancer cells. Endocrinology. 2005;146(11):4951-60. doi: 10.1210/en.2005-0365. PubMed PMID: 16109785.
40. Yodmuang S, Gadjanski I, Chao PH, Vunjak-Novakovic G. Transient hypoxia improves matrix properties in tissue engineered cartilage. Journal of orthopaedic research : official publication of the Orthopaedic Research Society. 2013;31(4):544-53. doi: 10.1002/jor.22275. PubMed PMID: 23203946; PubMed Central PMCID: PMC4136653.
41. Makris EA, MacBarb RF, Responte DJ, Hu JC, Athanasiou KA. A copper sulfate and hydroxylysine treatment regimen for enhancing collagen cross-linking and biomechanical properties in engineered neocartilage. FASEB journal : official publication of the Federation of American Societies for Experimental Biology. 2013;27(6):2421-30. doi: 10.1096/fj.12-224030. PubMed PMID: 23457219; PubMed Central PMCID: PMC3659348.
42. Makris EA, Responte DJ, Paschos NK, Hu JC, Athanasiou KA. Developing functional musculoskeletal tissues through hypoxia and lysyl oxidase-induced collagen cross-linking. Proceedings of the National Academy of Sciences of the United States of America. 2014;111(45):E4832-41. doi: 10.1073/pnas.1414271111. PubMed PMID: 25349395; PubMed Central PMCID: PMC4234579.
43. Han SK, Wouters W, Clark A, Herzog W. Mechanically induced calcium signaling in chondrocytes in situ. Journal of orthopaedic research : official publication of the Orthopaedic Research Society. 2012;30(3):475-81. doi: 10.1002/jor.21536. PubMed PMID: 21882238.
44. Benavides Damm T, Egli M. Calcium's role in mechanotransduction during muscle development. Cellular physiology and biochemistry : international journal of experimental cellular

physiology, biochemistry, and pharmacology. 2014;33(2):249-72. doi: 10.1159/000356667. PubMed PMID: 24525559.
45. Matta C, Fodor J, Szijgyarto Z, Juhasz T, Gergely P, Csernoch L, Zakany R. Cytosolic free Ca2+ concentration exhibits a characteristic temporal pattern during *in vitro* cartilage differentiation: a possible regulatory role of calcineurin in Ca-signalling of chondrogenic cells. Cell calcium. 2008;44(3):310-23. doi: 10.1016/j.ceca.2007.12.010. PubMed PMID: 18291522.
46. Valhmu WB, Raia FJ. myo-Inositol 1,4,5-trisphosphate and Ca(2+)/calmodulin-dependent factors mediate transduction of compression-induced signals in bovine articular chondrocytes. The Biochemical journal. 2002;361(Pt 3):689-96. doi: 10.1042/0264-6021:3610689. PubMed PMID: 11802800; PubMed Central PMCID: PMC1222353.
47. Bogdan AR, Miyazawa M, Hashimoto K, Tsuji Y. Regulators of Iron Homeostasis: New Players in Metabolism, Cell Death, and Disease. Trends in biochemical sciences. 2016;41(3):274-86. doi: 10.1016/j.tibs.2015.11.012. PubMed PMID: 26725301; PubMed Central PMCID: PMC4783254.
48. Dere E, Lo R, Celius T, Matthews J, Zacharewski TR. Integration of genome-wide computation DRE search, AhR ChIP-chip and gene expression analyses of TCDD-elicited responses in the mouse liver. BMC genomics. 2011;12:365. doi: 10.1186/1471-2164-12-365. PubMed PMID: 21762485; PubMed Central PMCID: PMC3160422.
49. Szojka AR, Marqueti RC, Li DX, Molter CW, Liang Y, Kunze M, Mulet-Sierra A, Jomha NM, Adesida AB. Human engineered meniscus transcriptome after short-term combined hypoxia and dynamic compression. Journal of tissue engineering. 2021;12:2041731421990842. doi: 10.1177/2041731421990842. PubMed PMID: 33613959; PubMed Central PMCID: PMC7874349.
50. Martin I, Smith T, Wendt D. Bioreactor-based roadmap for the translation of tissue engineering strategies into clinical products. Trends in biotechnology. 2009;27(9):495-502. doi: 10.1016/j.tibtech.2009.06.002. PubMed PMID: 19651453.
51. Allen CB, Schneider BK, White CW. Limitations to oxygen diffusion and equilibration in *in vitro* cell exposure systems in hyperoxia and hypoxia. American journal of physiology Lung cellular and molecular physiology. 2001;281(4):L1021-7. doi: 10.1152/ajplung.2001.281.4.L1021. PubMed PMID: 11557606.
52. Szojka ARA, Li DX, Sopcak MEJ, Ma Z, Kunze M, Mulet-Sierra A, Adeeb SM, Westover L, Jomha NM, Adesida AB. Mechano-Hypoxia Conditioning of Engineered Human Meniscus. Frontiers in bioengineering and biotechnology. 2021;9:739438. doi: 10.3389/fbioe.2021.739438. PubMed PMID: 34540817; PubMed Central PMCID: PMC8446439.
53. Ransy C, Vaz C, Lombes A, Bouillaud F. Use of H2O2 to Cause Oxidative Stress, the Catalase Issue. International journal of molecular sciences. 2020;21(23). doi: 10.3390/ijms21239149. PubMed PMID: 33266350; PubMed Central PMCID: PMC7731207.
54. Zhong Y, Caplan AI, Welter JF, Baskaran H. Glucose Availability Affects Extracellular Matrix Synthesis During Chondrogenesis *In vitro*. Tissue engineering Part A. 2021;27(19-20):1321-32. doi: 10.1089/ten.TEA.2020.0144. PubMed PMID: 33499734; PubMed Central PMCID: PMC8610032.
55. Yudoh K, Nguyen v T, Nakamura H, Hongo-Masuko K, Kato T, Nishioka K. Potential involvement of oxidative stress in cartilage senescence and development of osteoarthritis: oxidative stress induces chondrocyte telomere instability and downregulation of chondrocyte

function. Arthritis research & therapy. 2005;7(2):R380-91. doi: 10.1186/ar1499. PubMed PMID: 15743486; PubMed Central PMCID: PMC1065334.
56. Morgan AJ, Jacob R. Ionomycin enhances Ca2+ influx by stimulating store-regulated cation entry and not by a direct action at the plasma membrane. The Biochemical journal. 1994;300 (Pt 3):665-72. doi: 10.1042/bj3000665. PubMed PMID: 8010948; PubMed Central PMCID: PMC1138219.

CHAPTER 7: Engineering thicker scaffold-free neocartilage constructs with biomimetic properties using sequential seeding and deferoxamine

Abstract

The self-assembling process is a scaffold-free tissue-engineering approach that allows for the development of neocartilage with clinically relevant mechanical properties. However, methods to enhance the compressive and tensile properties of self-assembled constructs also tend to decrease neotissue thickness. Toward overcoming this tradeoff, we propose that sequential seeding can be used to increase the thickness of neocartilage formed using expanded and rejuvenated human chondrocytes without compromising mechanical properties. The objectives of this work were 1) to determine the appropriate seeding times that allowed for thicker hyaline-like tissue formation using passage 3 (P3) minipig costal chondrocytes, a relevant cell source for preclinical studies, 2) to evaluate the effects of deferoxamine stimulation toward increasing neocartilage thickness, and 3) to translate this methodology to extensively passaged (P7) human articular chondrocytes. This study employed a phased approach. In Phase I, sequential seeding did not increase construct thickness at any of the times tested, although performing the second seeding event at 2 hours was the only treatment to retain the round, flat gross morphology of the control group. In Phase II, a combination of sequential seeding and deferoxamine stimulation resulted in a 52% increase in thickness over unstimulated controls, formed using a single layer of 2M cells. Compared to DFO-stimulated neotissues formed using a single seeding with 4M cells, stimulated and sequentially seeded constructs exhibited a more desirable (flatter, homogeneous) morphology, higher ECM content, and higher compressive properties. In Phase III, sequential seeding with DFO-stimulated human articular chondrocytes resulted in constructs with a 90%

Chapter in preparation for submission as: Otarola, G.A., Kwon, H., Hu, J.C., Athanasiou, K.A. Engineering thicker scaffold-free neocartilage constructs with biomimetic properties using sequential seeding and deferoxamine.

significant increase in thickness over the control group, along with an 8% increase in the diameter, a 32% increase in DNA content, and retention of biochemical content and mechanical properties. This is the first time that DFO has been shown to increase cartilage thickness, and its use with sequential seeding provides a new strategy toward developing clinically relevant neocartilage constructs.

Introduction

Articular cartilage, which provides load bearing, load distribution, and a smooth surface to allow joint movement, does not heal after damage occurs, and a surgical strategy capable of producing a biomechanically fit repair tissue is still unavailable in the market. Osteochondral grafts provide a good alternative tissue that can serve as a replacement, but healthy donors are scarce, and graft failure has been reported in as much as 55% of patients after 10 years (1-3). An autologous approach, such as mosaicplasty, exposes the patient to donor site morbidity (4). Microfracture, considered the gold standard of cartilage repair, produces mechanically inferior fibrocartilage and is prone to revisions after 5 years (5, 6). Matrix-induced autologous chondrocyte implantation (MACI), a two-stage procedure which uses a patient's own chondrocytes, also provides inconsistent repair and fibrocartilage formation due, among other reasons, to the use of expanded cells on a collagen type I/III membrane (7, 8). Considering that over 30 million Americans suffer from osteoarthritis, new therapies capable of overcoming such limitations are needed.

The depth and symptomatology of the cartilage defect determine the treatment strategy to be used by clinicians. If asymptomatic, or successfully addressed using pain management, many partial thickness defects are left untreated due to the lack of a therapies capable of treating such indications (9-11). Full-thickness chondral lesions (defects that do not penetrate into the subchondral bone) and osteochondral lesions (defects that penetrate into the subchondral bone), on the other hand, tend to be symptomatic and typically require a donor tissue of equal size and thickness (e.g., osteochondral graft) or a treatment strategy capable of filling the defect with new

tissue (e.g., microfracture, MACI) (12). These strategies bring thickness-related complications. For example, the use of osteochondral grafts can result in superficial irregularities between the native tissue and the repair tissue due to difference in graft and host tissue thickness, compromising its outcome; surface disparities induce stress concentrations, delamination of the native tissue, and dislodging of the implant (13). Similar issues have been observed with MACI; a 60-month follow-up study of 65 patients treated with MACI determined that 18.5% of the patients presented disintegration of the tissue at the border with the surrounding tissue, likely due to stress- and/or shear-induced disintegration of the adjacent cartilage arising from mismatched thickness or surface irregularities (14). Thus, attaining implants with an appropriate thickness is relevant toward successful treatment.

Tissue engineered implants have emerged as a promising strategy toward overcoming current treatment limitations and providing off-the-shelf hyaline-like implants, although with their own set of challenges to solve. Over 10 tissue engineered cell-based products have entered preclinical and clinical studies toward FDA-approval (15). Most of these products utilize autologous articular chondrocytes (ACs) with 1-3 passages, and some form of scaffold. These approaches, however, require two surgeries to be performed because donor tissue needs to be collected in advance. Moreover, monolayer expansion of chondrocytes results in cell dedifferentiation. The self-assembling process, a scaffold-free approach, has the potential to overcome such limitations by using allogeneic expanded and rejuvenated chondrocytes that exhibit a chondrogenic phenotype (16-18). The process utilizes high-density culture, which allows the cells to interact and generate their own hyaline-like extracellular matrix (19). This methodology has been replicated with various cell types of clinical relevance, including articular and costal chondrocytes (CCs) (16, 18). In all cases, the biochemical and biomechanical properties of the resulting neotissue are comparable to those of native articular cartilage (20). Self-assembled neocartilage constructs exhibit tensile, compressive, and tribological properties on par with native articular cartilage, with Young's modulus of ~10MPa, ultimate tensile strength (UTS) of ~4MPa,

aggregate modulus of ~800kPa, and coefficient of friction of ~0.2 (21). Thus, self-assembled neocartilage has the potential of addressing clinical needs provided that the tissues can also be formed at appropriate thicknesses.

Treatment of articular lesions requires constructs capable of filling the full depth of a defect. Scaffold-based products such as CaReS and INSTRUCT report thicknesses of 4mm or more (15), and other examples can be found in the literature depending on the scaffold used. However, contractile remodeling often occurs during culture or after implantation due to cell metabolism and tissue maturation can disrupt the original shape and volume of the implant, generating surface disparities that can negatively impact clinical outcomes (22, 23). Contraction is not observed in self-assembled neocartilage, but current constructs tend to present thicknesses of ~0.5mm, as the stimuli used to increase their mechanical properties to native tissue-levels has come with a tradeoff in tissue thickness; TGF-β1 (24), tensile stimulation (25), and increases in construct area (26) result in constructs with smaller thicknesses. Toward clinical use, a scale-up of the self-assembling process is needed, and potential methods can include changes in how the cells are seeded and the use of chemical stimuli.

The self-assembling process can be disrupted by high cell density at the cell seeding stage. An increase of the cell seeding density is often associated with significant negative effects on the constructs' biochemical and biomechanical properties (27). As shown in a recent study, using high cell-seeding densities during the self-assembling process led to the development of constructs with a fluid-filled cavity devoid of cells and filled by water and matrix components (28). Increasing cell seeding density can also result in irregular shapes and surface abnormalities, and in lower biomechanical properties (27, 28). Thus, improvements on neocartilage thickness and cell numbers may require, among others, a sequence of separate cell seeding events.

The current self-assembling process involves the application of stimuli toward producing biomimetic tissues (24). Chemical treatments that stimulate chondrogenesis using ion modulation, such as ionomycin and deferoxamine (DFO), have been developed to improve tissue

properties (21). DFO, in particular, chelates iron and inhibits HIF1α degradation, triggering a hypoxic response shown to increase the PYR crosslink content and improve the tensile properties of neocartilage constructs (29). Evidence indicates that DFO promotes chondrogenesis (30) and enables the production of hyaline-like tissue (31). In addition, DFO has also been shown to induce expression of membrane proteins, including integrins. It has been found that the self-assembling process depends on integrin and cadherin function (32), and time-lapse imaging determined that chondrocytes form the cell-cell and cell-matrix interactions that give rise to the neocartilage construct within the first 4-8 hours after seeding (32). Thus, the expression of integrins and cadherins in the membrane of chondrocytes at the time of seeding is critical to the final morphology. Thus, DFO's influence on integrin expression has the potential to facilitate or promote self-assembling. Recently, DFO has been shown to reduce cartilage lesion development when administered to osteoarthritic joints (33), further motivating the examining of its potential in tissue engineering.

Lastly, the cell type and passage number used can influence the biomechanical properties of self-assembled constructs. Neocartilage constructs can be produced using primary or expanded chondrocytes (18, 34) obtained from various species including rabbit, sheep, and horse (28, 35-37). Recently, aiming to avoid donor site morbidity and producing an analog animal product for preclinical studies using the minipig model, expanded and rejuvenated minipig CCs have been used with success (21, 38). Importantly, using conservative chondrogenic passaging and aggregate rejuvenation, self-assembling can be achieved using extensively passages chondrocytes obtained from different tissues and species, and requiring fewer cells (18). Clinically, primary or low-passaged (P1-P3) human ACs remains the only cell type used for cartilage cell-based therapy products.

Toward the development of thicker constructs, without compromising functional and gross morphological features, the objectives of this study were 1) to determine the appropriate timing between seeding layers that allow construct formation using minipig CCs, 2) to increase construct

thickness by stimulating CCs with DFO before self-assembling, and 3) to translate this methodology to expanded and rejuvenated human ACs, the current cell source used to treat chondral defects, to produce neocartilage thicker than the current self-assembled standard, and with mechanical properties equivalent to those of single layer constructs.

This study employed a phased approach. First, using minipig CCs and considering the lack of success of obtaining thicker constructs by solely increasing cell density, Phase I tested the hypothesis that sequential seeding would yield constructs with a desirable gross morphology (e.g., comparable to the control group) using a higher cell density depending on the duration of time between the seeding events. Four different seeding time points were tested, using two volumes with 2M minipig CCs sequentially seeded, and compared to a (single-layer) 2M control group. An additional single-layer 4M group was included to re-evaluate the necessity of performing sequential seeding. The selection of minipig CCs follows current strategies aiming at developing neocartilage constructs with an alternate cell source from allogeneic rib cartilage. The selection criteria for Phase I was the maintenance of gross morphology and biochemical content. Using minipig CCs, Phase II tested the hypothesis that the use of DFO, alone or in combination with the sequential seeding as determined in Phase I, would produce thicker constructs. The groups were compared to an unstimulated control group formed using 2M cells. The selection criteria for Phase II were the increase of construct thickness and the maintenance of gross morphology. Using the sequential seeding time determined in Phase I and the DFO stimulation regime determined in Phase II, Phase III tested the hypothesis that extensively passaged human ACs treated with these regimes would yield thicker constructs. Human ACs were chosen for Phase III because they are currently the only cell type used in existing cell-based cartilage repair and also represent the majority of upcoming cell-based tissue engineering strategies for cartilage.

Methodology

Isolation and expansion of minipig costal chondrocytes

Juvenile porcine CCs were isolated from the unmineralized portion of floating ribs of two male and one female juvenile Yucatan minipigs obtained from Premier BioSource (California, USA) no later than 48 hours after slaughter. The rib cartilage was cleaned of all non-cartilaginous tissue, cut into 1mm^3 pieces, and washed three times with GlutaMAX Dulbecco's Modified Eagle Medium containing 4.5g/L glucose (DMEM; Gibco) and 1% (v/v) penicillin/streptomycin/fungizone (PSF; Lonza, Basel, Switzerland). The cartilage was then digested with 0.4% pronase (Sigma) in DMEM for 1 hour at 37°C, and then in 0.2% collagenase type II (Worthington Biochemical, Lakewood, NJ) in DMEM supplemented with 3% (v/v) fetal bovine serum (FBS; Atlanta Biologicals, Lawrenceville, GA) for 18 hours at 37°C. Cells were then strained through a 70µm strainer, washed with red blood cell lysis buffer (39) for 4 min, counted, and frozen in freezing medium containing 90% (v/v) FBS + 10% (v/v) DMSO (Sigma) in liquid nitrogen until use. For expansion, primary (P0) CCs were thawed and seeded in T225 flasks at a density of ~2.5 million cells per flask in chondrogenic medium (CHG) consisting of GlutaMAX DMEM, 1% (v/v) PSF, 1% (v/v) insulin-transferrin-selenium (BD Biosciences, San Jose, CA), 1% (v/v) non-essential amino acids (Thermo Fisher Scientific), 100mg/mL sodium pyruvate (Thermo Fischer Scientific), 50mg/mL ascorbate-2-phosphate (Sigma, St. Louis, MO), 40mg/mL L-proline (Sigma), and 100nM dexamethasone (Sigma). Throughout expansion, medium was supplemented with 2% (v/v) FBS, 1ng/mL TGF-β1 (Peprotech, Rocky Hills, NJ), 5ng/mL bFGF (PeproTech), and 10ng/mL PDGF (PeproTech). Cells were cultured at 37°C in 10% CO_2, and passaged to P3 at confluence using 0.05% trypsin-EDTA (Gibco) and 0.2% collagenase type II solutions.

Isolation and expansion of human articular chondrocytes

Chondrocytes were isolated from human knee articular cartilage of three donors without signs of musculoskeletal pathology. The donor tissues were obtained from the Musculoskeletal Transplant Foundation (Kansas City, MO) under an IRB exemption (the donor tissues were discarded samples from deidentified donors). These donors were a 43 year-old Caucasian male (donor 1), an 18 year-old Hispanic female (donor 2), and a 34 year-old Caucasian male (donor 3). Minced cartilage was digested in 0.2% collagenase type II (Worthington, Lakewood, NJ) solution containing 3% fetal bovine serum (FBS, Atlanta Biologicals, Lawrenceville, GA) for 18 h at 37°C, followed by filtration through a 70µm strainer. Isolated cells were counted, resuspended in freezing medium consisting of 90% (v/v) FBS + 10% (v/v) DMSO, and stored in liquid nitrogen until use. For expansion, a conservative chondrogenic passaging method was used, based on a previously reported chondrogenically tuned expansion [33]. Briefly, human ACs were seeded at 25,000 cells/cm^2 and expanded in chondrogenic culture medium (CHG), supplemented with 2% FBS, 1ng/ml TGF-β1, 5ng/ml bFGF, and 10ng/ml PDGF. Cells were passaged using 0.05% trypsin-EDTA, followed by 0.2% collagenase type II solution containing 3% FBS, and frozen at P6 in liquid nitrogen until use. After thawing, cells from these three donors were mixed and underwent one more passage, leading to P7.

Chondrogenic differentiation in aggregate rejuvenation

Passaged minipig CCs and human ACs were seeded at P3 or P7, respectively, on 1% (w/v) agarose-coated plates at a density of 750,000 cells/mL (30 mL total) per plate with CHG supplemented with 10 ng/ml TGF-β1, 100 ng/ml GDF-5, and 100 ng/ml BMP-2 (PeproTech) (18). Plates were placed on an orbital shaker at 50 rpm for 24 hours at 37°C in 10% CO_2, and then kept static, changing medium every 4 days. At 14 days (minipig CCs) or 7 days (human ACs) of aggregate rejuvenation, the aggregates were digested using 0.05% trypsin-EDTA for 45 min, and

then 0.2% collagenase type II for 1 hr. Cells were strained through a 70µm cell strainer, washed twice, and resuspended in CHG for counting and seeding.

DFO stimulation

DFO (Sigma) was applied to a final concentration of 100µM to cells in aggregate culture 24 hours before construct seeding. After 24 hours, DFO was washed at the moment of digestion and seeding.

Neocartilage self-assembling and sequential seeding

Construct formation via the self-assembling process was performed as previously described (19). For neocartilage control constructs, 2 million cells were seeded in a volume of 100µL in 5mm diameter non-adherent 2% (w/v) agarose wells at a density of 20 million cells/mL. To confirm the inability of forming thicker constructs by increasing cell density, a second group of constructs was seeded in the same way, but using 4 million cells at a density of 40 million cells/mL. For groups engineered using sequential seeding, 2 million cells were seeded in a volume of 50uL in 5mm diameter non-adherent 2% (w/v) agarose wells (at a density of 40 million cells/mL), followed by a second seeding of equal volume and cell density at 1, 2, 3, or 4 hrs (**Fig 1**). At 4 hours post initial seeding, additional 400µL of CHG supplemented with 10ng/ml TGF-β1 were added. This medium was replaced daily until unconfinement (at day 3 post initial seeding for ACs-derived constructs and day 6 post initial seeding for CCs-derived constructs), after which, constructs were kept in 2mL of medium, replaced every 2 days. All constructs were maintained in CHG medium supplemented with TGF-β1, chondroitinase ABC (c-ABC, Sigma Aldrich), and LOXL2 (SignalChem, Richmond, BC, Canada) as follows: TGF-β1 was applied at 10ng/ml after seeding and until day 28, c-ABC was applied at 2Units/mL for 4 hours in day 7, and LOXL2 was applied

at 0.15µg/mL between days 7 and 21 post self-assembling, together with 0.146µg/mL hydroxylysine (Sigma) and 1.6µg/mL copper sulfate (Sigma).

Histology

Samples were fixed in 10% neutral-buffered formalin, embedded in paraffin, and sectioned at a thickness of 6µm for histological evaluation. Sections were subsequently processed and stained with hematoxylin and eosin (H&E), safranin-O, and picrosirius red using standard protocols.

Mechanical testing

Tensile properties were determined using uniaxial tension in an Instron model 5565 (Instron, Canton, MA). Dog bone-shaped samples were obtained from every engineered cartilage construct with a gauge length of 1.55 mm. The dog bones were photographed to measure thickness and width in ImageJ. The ends of the dog-bone were fixed to paper with cyanoacrylate to increase the gripping area for testing. A strain rate of 1% of the gauge length per second was used until failure. The Young's modulus was obtained from the linear region of the stress-strain curve, and the ultimate tensile strength (UTS) was defined as the maximum stress obtained.

Compressive properties of the neocartilage constructs were determined by creep indentation testing. Briefly, 2.5mm punches obtained from every construct were submerged in PBS until equilibrium and indented with a flat porous 0.5mm diameter tip perpendicular to the surface of the sample to ~10% strain. The aggregate modulus (H_A), permeability (k), and shear modulus (μ_s) were obtained using a semi-analytical, semi-numerical, biphasic model and finite-element optimization (40).

Biochemical testing

Cartilage constructs were weighed to obtain wet weight, lyophilized for 3 days, and weighed again to obtain dry weight. Lyophilized samples were digested in 125μg/mL papain (Sigma) +5mM N-acetyl-L-cysteine +5mM EDTA in phosphate buffer pH 6.5 for 18 hours at 60°C. GAG content was quantified using a Blyscan glycosaminoglycan assay kit (Biocolor, Newtownabbey, Northern Ireland). Total collagen content was quantified using a modified chloramine-T hydroxyproline assay (41). DNA content was quantified with a picogreen assay (ThermoFisher Scientific). For the quantification of PYR crosslinks, separate tissue samples (~0.2-1mg) were weighed, lyophilized, and acid-digested for 12 hours in 6N HCl. After evaporation, the dried hydrolysates were resuspended in a 75%/25% (v/v) solution of 0.1% formic acid and acetonitrile. Samples were measured through mass spectrometry using a cogent diamond hydride column and a PYR standard (42).

Statistical analysis

All quantitative biochemical and biomechanical tests for Phases I-III were performed using n=6-8. All data are presented as means ± standard deviations. A single factor one-way ANOVA was employed in each phase of the study to assess differences among experimental groups. Multiple comparisons were performed using a Dunnett's *post hoc* test (Phase I and II) or a Tukey's *post hoc* test (Phase III). All statistical analyses were performed using GraphPad Prism version 8.4.1 for Windows (GraphPad Software, San Diego, California USA). Groups marked with * indicate that there are statistically significant differences compared to the control group ($p<0.05$) based on Dunnett's *post hoc* test. Group marked with different letters indicate that there are statistically significant differences among groups ($p<0.05$) based on Tukey's *post hoc* test.

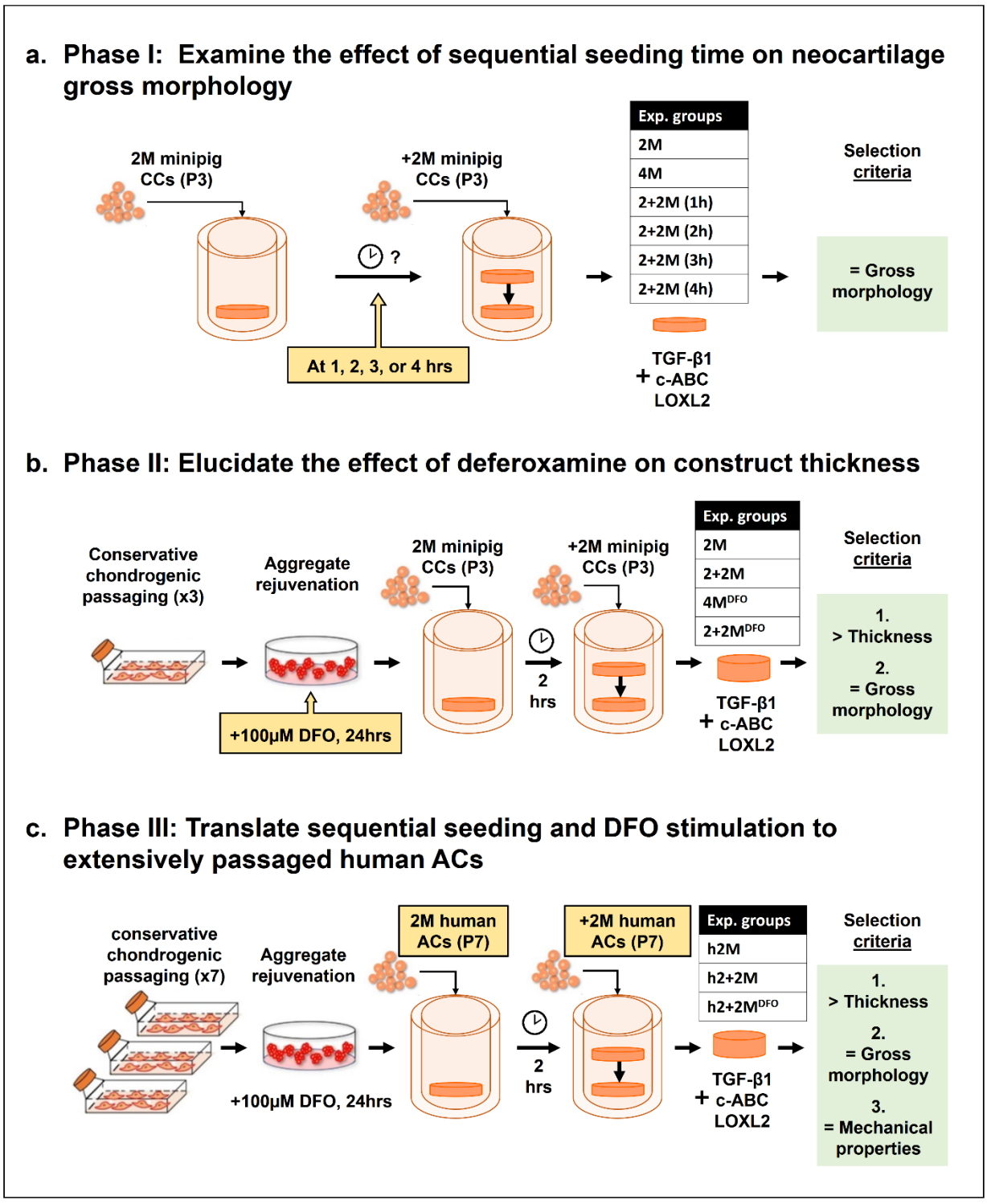

Figure 1. Schematic diagram of the study. (**a**) Phase I examined the effects of four different time points between the first and second seeding events on the gross morphology of neocartilage derived from expanded and rejuvenated minipig CCs. A 2M control group was defined as the

standard for a desirable gross morphology. A 4M group was added to confirm the damaging effects of using high cell density in the self-assembling process. All other experimental groups built using sequential seeding were labeled as 2+2M, indicating the two seeding events each with 2M cells. The time point between seedings is shown in parenthesis. Based on the results of this phase, the 2-hour time point was carried forward to the next phase. (**b**) Phase II tested the effects of the stimulation of chondrocytes with 100µM deferoxamine (DFO) during rejuvenation, 24 hours prior to cell seeding. A 2M control group was included, together with a sequential seeding group without DFO (2+2M), a high cell density group with DFO but without sequential seeding ($4M^{DFO}$), and a group that included both sequential seeding and DFO stimulation ($2+2M^{DFO}$). Based on the results and the selection criteria, the combined regime was carried to the last phase. (**c**) Phase III examined the translation of sequential seeding and DFO stimulation to extensively passaged (P7) human ACs. A human 2M control group (h2M) was included, alongside two experimental groups: sequential seeding (h2+2M) and sequential seeding with DFO stimulation ($h2+2M^{DFO}$). The final selection criteria toward future work were defined as an increase in thickness and the maintenance of the gross morphology and mechanical properties. All constructs included TGF-β1, c-ABC, and LOXL2.

Results

Phase I: Effect of time in sequential seeding using expanded and rejuvenated minipig CCs

Constructs from all minipig CC experimental groups exhibited thicknesses comparable to that of the control group (**Fig. 2A-B** and **Table 1**). The control group, seeded with 2M cells, exhibited a desirable gross morphology, i.e., flat, round, and with no irregular shapes, surface abnormalities, or cyst formation. A single seeding with 4M cells resulted in constructs with several abnormalities, including surface irregularities and heterogeneous thickness (**Fig. 2A**). Constructs built using sequential seeding, particularly with 3 and 4 hours between the first and second seeding, also

showed abnormalities in their gross morphology upon visual examination (e.g., surface irregularities and heterogeneous thickness), although not as severe as that of the 4M group. Constructs built with the second seeding applied at 1 and 2 hours showed the least negative impact on gross morphology based on a close examination of appearance. In particular, constructs built using a 2-hour time between seedings showed a gross morphology equivalent to that of the control group. Most groups showed significant differences in their total wet weight compared to the control group, indicating possible changes in the biochemical composition of the constructs (**Fig. 2C**).

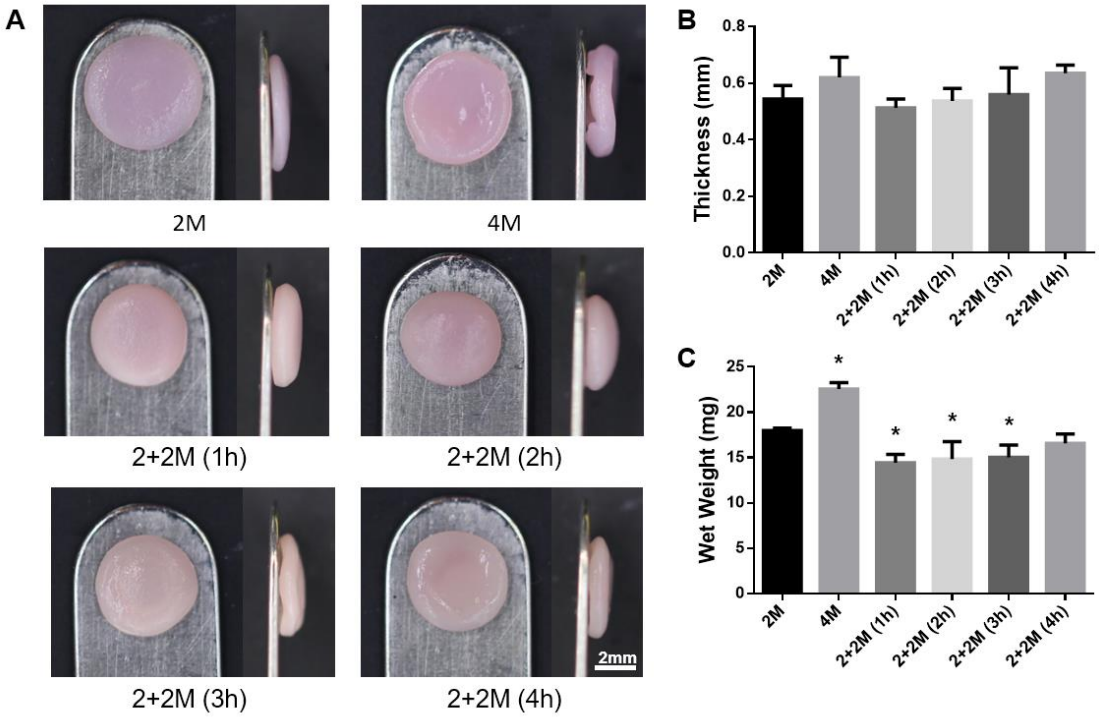

Figure 2. Gross morphology, thickness, and wet weight of minipig CC constructs built using sequential seeding. (A) Compared to the control group (2M), constructs built with 4M cells showed abnormalities in their gross morphology, including surface irregularities, heterogeneous thickness, cysts, and swelling, increasing its wet weight. (B, C) While sequential seeding did not result in increased thickness, constructs built with a 2-hour time between seedings retained gross

morphology similar to that of the control group. All the experimental groups with sequential seeding showed a decrease in wet weight. Asterisks denote significant differences ($p<0.05$) compared with the 2M control group based on Dunnett's *post hoc* test.

All experimental groups showed a higher water content compared to the control group (**Table 1**). The increase observed in hydration, however, was still within the normal ranges for cartilaginous tissues. More importantly, all experimental groups showed an increase in the DNA content. This was expected as the number of cells was doubled. The highest DNA content, observed in the groups in which the second seeding was applied 1 or 2 hours after the first layer, indicated higher cell retention (i.e., successful assembling into the construct) and/or cell survival. Additionally, several significant differences in the GAG and collagen content were observed. Of the experimental groups, constructs built with a 2-hour time between seedings showed no significant changes in GAG content and the least variation in collagen content compared to the 2M control group (**Table 1**).

In terms of mechanical properties, no significant changes were observed in the aggregate modulus or the shear modulus when sequential seeding was performed, compared to the control group (**Table 1**). Similarly, the Young's modulus was unaffected by the application of a second seeding. However, the values for UTS were inferior in all experimental groups, compared to the 2M control group, and a significant decrease was observe when the second layer was applied 1 or 2 hours after the first layer (**Table 1**).

Overall, considering the effects on gross morphology, DNA content, and GAG and collagen deposition, compared to the 2M control group, the group with a 2-hour window between the first and second seeding was selected and taken forward to Phase II.

Table 1. Gross morphology, biochemical, and biomechanical data of minipig CC constructs built using sequential seeding at different time points, presented as mean ± standard deviation. H_A, aggregate modulus. G, shear modulus. Ey, Young's modulus. Asterisks denote significant differences ($p<0.05$) compared with the 2M control group based on Dunnett's *post hoc* test.

	Thickness (mm)	Diameter (mm)	Wet Weight (mg)	Hydration (%)	DNA (µg/const.)	GAG/DW (%DW)	COL/DW (%DW)	H_A (kPa)	G (kPa)	Ey (MPa)	UTS (MPa)
2M	0.54±0.05	5.86±0.10	18.00±0.27	78.76±0.85	6.77±0.94	47.51±1.53	18.96±0.67	343±67	151±21	3.97±0.64	1.67±0.18
4M	0.62±0.07	5.65±0.12	**22.55±0.70***	81.34±1.45	11.85±2.96	44.57±3.57	**16.91±1.06***	148±83	70±36	2.79±1.05	1.36±0.25
2+2M (1h)	0.51±0.03	**5.18±0.12***	**14.44±0.92***	**82.49±2.12***	**14.86±3.33***	**35.06±4.55***	**13.21±1.15***	271±120	126±60	2.08±1.12	**0.82±0.30***
2+2M (2h)	0.54±0.04	**4.97±0.10***	**14.85±1.91***	**83.30±1.42***	**19.27±3.20***	44.23±4.46	**16.52±1.49***	359±185	166±89	2.80±1.43	**0.98±0.26***
2+2M (3h)	0.56±0.09	**5.20±0.18***	**15.03±1.35***	80.87±2.06	**15.30±2.48***	**35.67±3.66***	**15.00±1.27***	202±144	94±55	3.73±2.35	1.34±0.41
2+2M (4h)	0.64±0.03	**5.27±0.15***	16.58±1.03	**81.91±1.01***	**19.90±4.96***	**36.00±3.38***	**16.19±0.69***	265±256	80±52	2.31±0.80	1.41±0.15

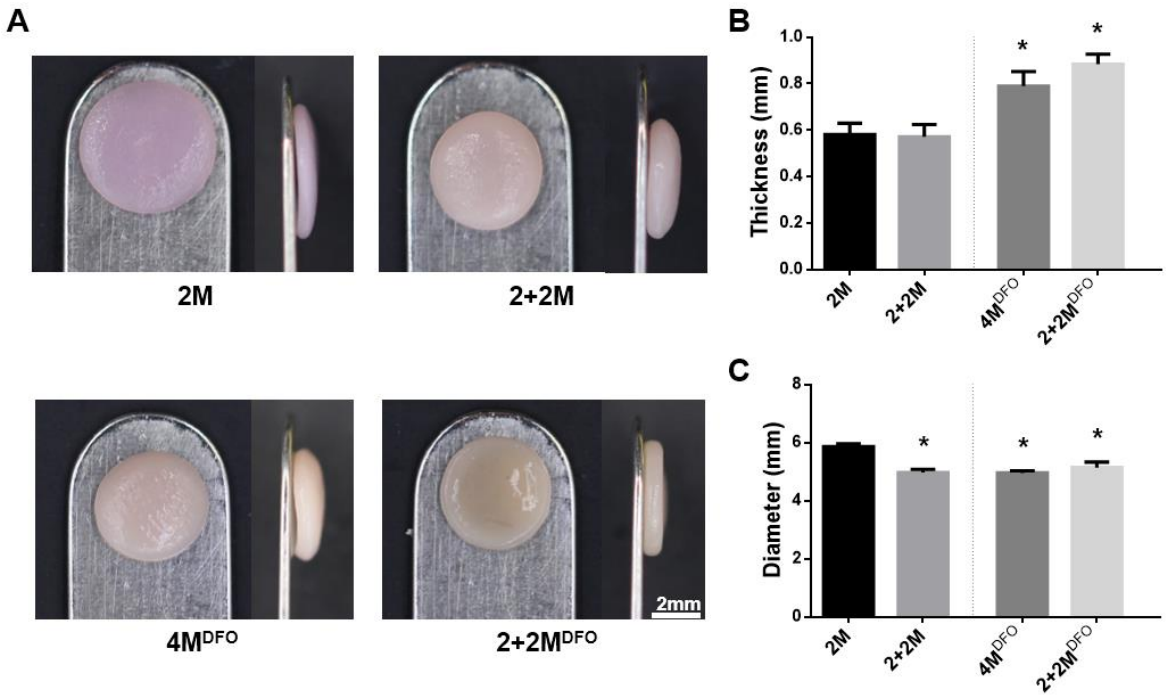

Figure 3. Gross morphology, thickness, and diameter of minipig CC constructs built using sequential seeding with and without DFO stimulation. (A) The combined use of DFO stimulation and sequential seeding produced constructs with normal flat, round gross morphology. (B, C) The stimulation of cells using DFO prior to the self-assembling process resulted in constructs with increased thickness and decreased diameter. Asterisks denote significant differences ($p<0.05$) compared with the 2M control group based on Dunnett's *post hoc* test.

Phase II: Effect of DFO stimulation and sequential seeding using expanded and rejuvenated minipig CCs

DFO stimulation of CCs was tested in Phase II toward increasing construct height. Neocartilage constructs derived from minipig CCs which were treated with DFO during rejuvenation, 24 hrs before seeding, showed a significant increase in thickness (**Fig. 3**). The 2M control group resulted in constructs with a desirable gross morphology (**Fig. 3A**). As in Phase I, constructs built using sequential seeding (2+2M) also showed a normal gross morphology, with a significant reduction in diameter and no increase in thickness (**Fig. 3B-C**). The stimulation of chondrocytes with DFO

resulted in the significant increase in the thickness of the constructs alone ($4M^{DFO}$), and in combination with sequential seeding ($2+2M^{DFO}$); these changes in thickness corresponded to 36% and 52% increases, compared to the 2M control group, respectively. While gross morphological abnormalities were found in the $4M^{DFO}$ group, including construct surface irregularities and heterogeneous thickness, constructs built using sequential seeding showed a flat, round gross morphology.

The biochemical content showed several differences among the Phase II conditions (**Table 2**). Doubling the cell number increases the water content compared to the 2M control group. This effect was also observed in Phase I. DNA content was also increased, and showed the highest values in the groups built with sequential seeding (**Table 2**). Of the groups that exhibited a significant increase in thickness ($4M^{DFO}$ and $2+2M^{DFO}$), the group that included both DFO and sequential seeding showed no significant differences in the GAG content, and the least decrease in collagen content compared to the control group (**Table 2**).

Table 2. Biochemical data of minipig CC constructs built using sequential seeding and DFO stimulation, presented as mean ± standard deviation. Asterisks denote significant differences ($p<0.05$) compared with the 2M control group based on Dunnett's *post hoc* test.

	Hydration (%)	**DNA (µg/construct)**	**GAG/DW (%DW)**	**COL/DW (%DW)**
2M	78.76±0.85	6.77±0.94	47.51±1.53	18.96±0.67
2+2M	**83.30±1.42***	**19.27±3.20***	44.23±4.63	**16.52±1.49***
$4M^{DFO}$	**82.53±1.46***	**17.15±1.84***	**40.34±3.34***	**13.91±0.51***
$2+2M^{DFO}$	**82.49±0.91***	**18.04±1.87***	41.94±2.81	**15.04±1.31***

The mechanical assessment showed that the application of DFO during rejuvenation ($4M^{DFO}$ and $2+2M^{DFO}$) had no effects on the compressive properties (**Fig. 4A-B**). In terms of tensile properties, the negative effects, as shown by a significant reduction in both the Young's modulus and UTS, are only observed in the group that underwent layered self-assembling (**Fig. 4C-D**). Based on the overall results obtained in Phase II, primarily the increase in thickness and then gross morphology, the sequential seeding with the DFO stimulation regime was taken forward to Phase III.

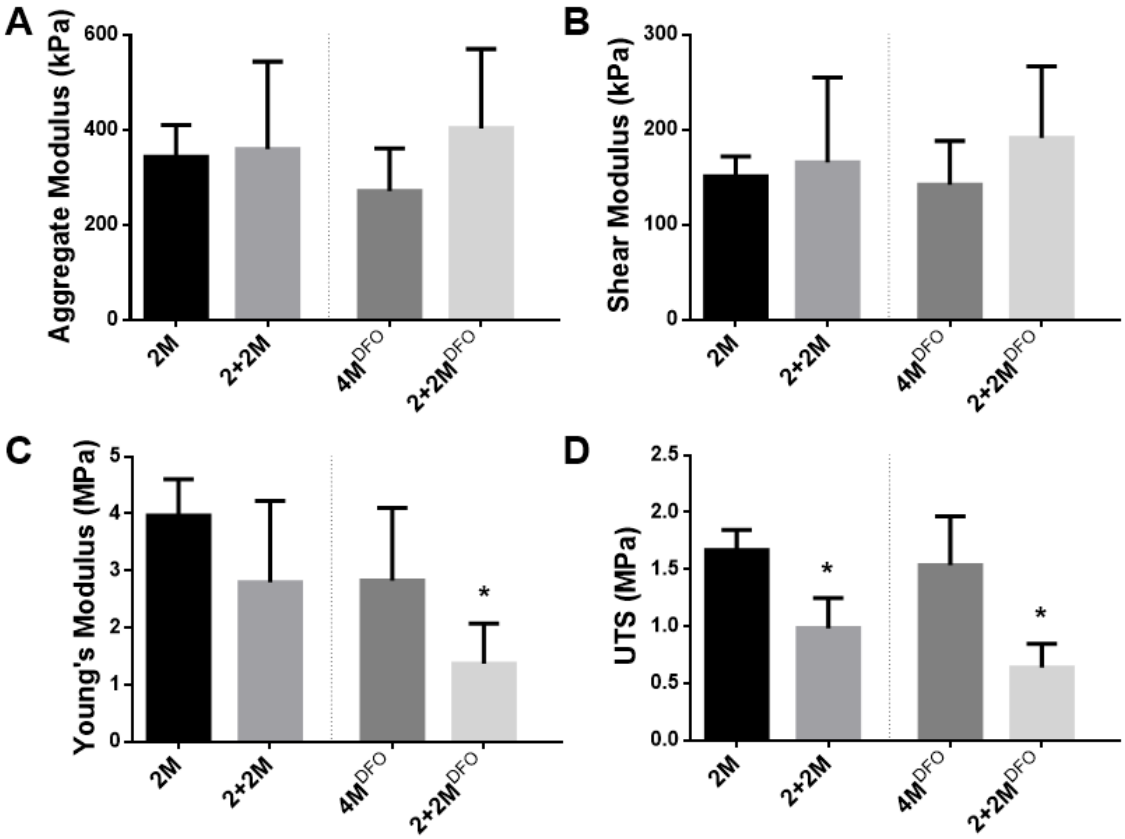

Figure 4. Mechanical data of minipig CC constructs built using sequential seeding with and without DFO stimulation. (A, B) The use of sequential seeding or DFO did not affect the aggregate and shear moduli of constructs. (C, D) Sequential seeding, however, induced a decrease in the Young's modulus and UTS. Asterisks denote significant differences ($p<0.05$) compared with the 2M control group based on Dunnett's *post hoc* test.

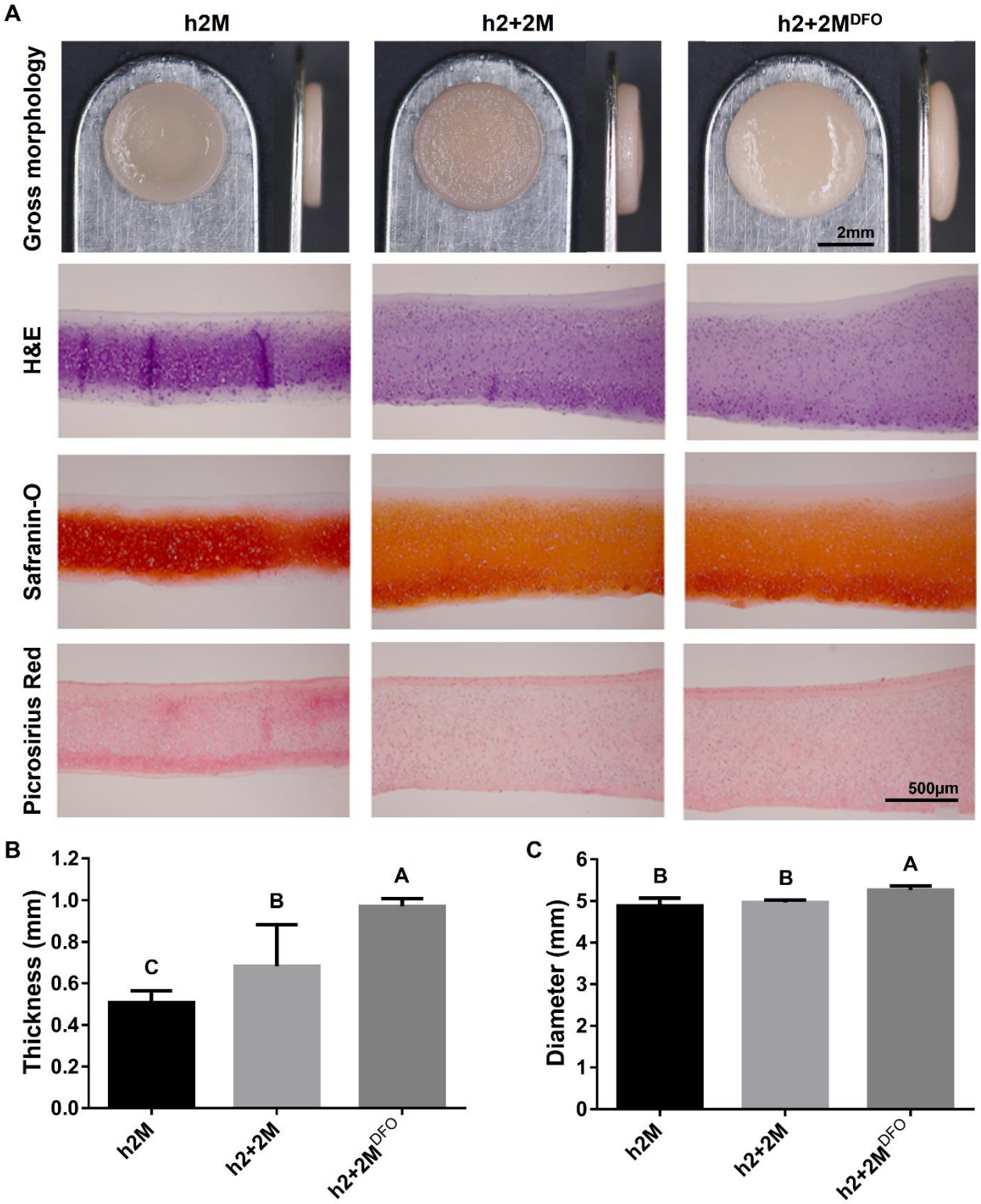

Figure 5. Gross morphology and histological analysis of human AC constructs built using sequential seeding and DFO stimulation. (A) Gross morphology of constructs built using sequential seeding showed an apparent increase in thickness compared to the 2M control group.

More importantly, the histology of constructs built using sequential seeding showed a homogeneous distribution of GAGs and collagens, with no internal boundary. (B) Quantification of construct thickness demonstrated the significant changes between the three groups demonstrating that DFO almost doubled neocartilage thickness. (C) DFO also increased construct diameter. Using connecting letters report, different uppercase letters over bars indicate statistical difference ($p<0.05$) among groups, based on Tukey's *post hoc* test.

Phase III: Sequential seeding using expanded, rejuvenated, and DFO-stimulated human ACs

All neocartilage constructs derived from human ACs showed a flat, round gross morphology, and the histological evaluation of the constructs showed a homogeneous distribution of cells, GAGs, and collagens, with no internal boundary within the constructs built using sequential seeding (**Fig. 5A**). Furthermore, constructs built using sequential seeding, with or without DFO during rejuvenation, were thicker compared to the human 2M control group (**Fig. 5B**). The thicknesses of constructs built with sequential seeding, with or without DFO stimulation, were 90% and 33% larger over the control group, respectively (**Table 3**). In addition, the diameter of the constructs treated with DFO showed an 8% increase over the human 2M control group (**Fig. 5C**, **Table 3**).

As observed in Phases I and II, the constructs built using sequential seeding showed a significant increase in DNA content (**Table 3**). In terms of biochemical composition, the sequential seeding alone induced a significant decrease in the GAG and collagen content. DFO stimulation, however, promoted the maintenance of GAG and collagen content, and the thicker DFO-treated constructs showed no significant differences compared to the control group. The PYR quantification showed that the control group had the highest amount of crosslinks per dry weight, followed by the DFO-treated constructs ($h2+2M^{DFO}$), and the untreated constructs (h2+2M) (**Table 3**). However, no significant changes are reported when calculating the amount of PYR crosslinks

per collagen content, indicating that the decrease of PYR crosslinks is associated with the decrease in collagen content.

Table 3. Biochemical data of human AC constructs built using sequential seeding and DFO stimulation, presented as mean ± standard deviation. DFO was found to increase construct thickness by 90%. Using connecting letters report, different uppercase letters over bars indicate statistical difference ($p<0.05$) among groups, based on Tukey's *post hoc* test.

	Thickness (mm)	Wet Weight (mg)	Hydration (%)	DNA (µg/ construct)	GAG/DW (%DW)	COL/DW (%DW)	PYR/DW (ng/mg)	PYR/COL (ng/mg)
h2M	0.51 ±0.06^{C}	10.93 ±0.67^{B}	86.82 ±1.23	19.81 ±0.79^{B}	23.25 ±1.71^{A}	10.45 ±1.78^{A}	153.04 ±22.67^{A}	14.93 ±2.83
h2+2M	0.68 ±0.20^{B}	15.37 ±3.02^{A}	87.62 ±1.22	25.20 ±5.40^{A}	18.91 ±2.98^{B}	8.11 ±1.44^{B}	104.11 ±21.42^{B}	12.90 ±1.97
h2+2M^{DFO}	0.97 ±0.04^{A}	16.56 ±1.24^{A}	87.81 ±0.37	26.29 ±1.28^{A}	25.21 ±1.77^{A}	8.57 ±0.95^{AB}	113.40 ±22.97^{B}	13.25 ±2.30

The mechanical properties of constructs built using sequential seeding differ depending on the use of DFO. The aggregate and shear moduli on constructs built using sequential seeding without DFO were 14% and 8% lower compared to the human 2M control group (**Fig. 6A-B**). Conversely, the stimulation of ACs with DFO during rejuvenation induced an increase in the compressive properties; the resulting aggregate and shear moduli of the DFO-stimulated group (h2+2M^{DFO}) group were 33% and 41% higher compared to the human 2M control group, respectively. Though both treatments did not differ significantly from the control group, the difference was significant between them. For the tensile properties, the use of sequential seeding without DFO reduced both the Young's modulus and UTS by 57% and 48%, respectively (**Fig. 6C-D**). However, the group stimulated with DFO did not exhibit a loss of tensile strength and stiffness, and no significant changes were observed between the control group and the group that underwent sequential seeding with DFO-stimulated human ACs.

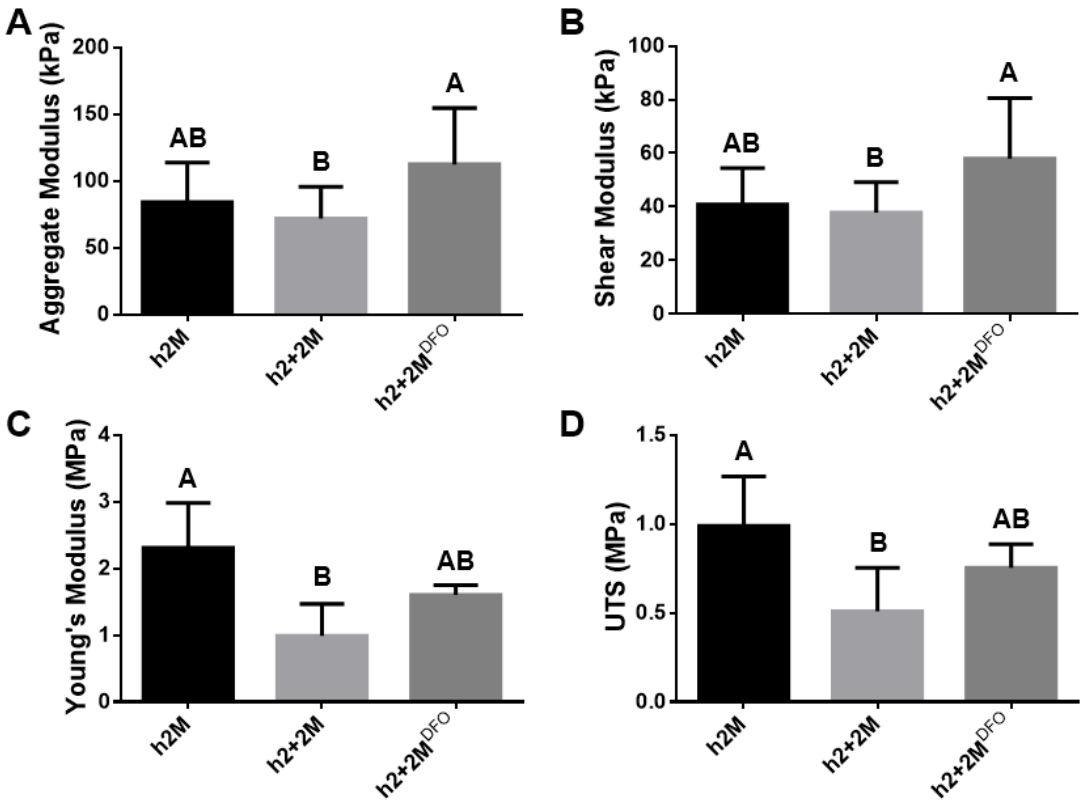

Figure 6. Mechanical data of human AC constructs built using sequential seeding and DFO stimulation. DFO had distinct effects on the compressive and tensile properties. (A, B) The combined use of sequential seeding with DFO increased the aggregate and shear moduli of constructs. (C, D) DFO maintained the Young's modulus and UTS in constructs built using sequential seeding. Using connecting letters report, different uppercase letters over bars indicate statistical difference ($p<0.05$) among groups, based on Tukey's *post hoc* test.

Discussion

The development of self-assembled neocartilage is emerging as a new solution for the treatment of articular cartilage lesions, however, the attainment of biomimetic properties has come with a tradeoff in the thickness of implants. This work's objective was to develop a new methodology to increase the thickness of self-assembled neocartilage, while retaining a desirable gross morphology and its mechanical properties.

In **Phase I**, it was hypothesized that sequential seeding would yield constructs with a desirable gross morphology using a higher cell density depending on the duration of time between the seeding events. Thickness of constructs derived from minipig CCs was unaffected, and three out of the five experimental groups showed disruptions in the self-assembling process, evidenced by the appearance of abnormalities in construct gross morphology (e.g., irregular surface, heterogeneous thickness, cysts). The 4M group, in which all cells were seeded at a single seeding event, showed the largest incidence of morphological abnormalities, followed by sequential seeding performed at 4 and 3 hours. Conversely, the experimental group with a 2-hour time between the seeding events (2+2M (2h)) showed a desirable gross morphology (i.e., round, flat) that resembled that of the 2M control group. Thus, toward developing thicker constructs that require a larger number of cells, the sequential seeding at a 2-hour time point was carried forward.

In **Phase II**, it was hypothesized that the use of DFO, alone or in combination with sequential seeding would produce thicker constructs. Indeed, the combination of DFO and sequential seeding (2+2M^{DFO}) yielded construct that were 52% thicker compared to the 2M control group, and retained a desirable gross morphology, comparable to that of the control. Treatment with DFO alone, with no sequential seeding (4M^{DFO}), induced a 36% increase in construct thickness, but yielded constructs with abnormalities in their gross morphology. In addition, the group that included DFO and sequential seeding showed a higher ECM content and higher compressive properties, compared to the group treated with DFO only. Thus, the combined regime, which included sequential seeding and DFO stimulation was carried forward to the last phase.

In **Phase III**, it was hypothesized that extensively passaged human ACs would yield thicker constructs when using sequential seeding and DFO stimulation. The results showed that the use of sequential seeding and DFO produced constructs derived from P7 human ACs that were 90% and 43% significantly thicker compared to the human 2M control group (h2M) and the sequentially seeded group without DFO (h2+2M), respectively. Moreover, the mechanical

properties of the constructs built using the combined regime were equal or superior compared to the control group and the constructs built using sequential seeding alone; the compressive properties (of the h2+2M^{DFO} group) trended higher compared to the 2M control group and were significantly higher compared to the sequential seeding alone (h2+2M) group; the tensile properties were not significantly lower compared to the h2M control group, whereas the group with sequential seeding only (h2+2M) saw a significant decrease in both Young's modulus and UTS, compared to the control. Lastly, constructs built with the combined regime displayed a homogeneous tissue with complete integration of the two seeding events, as shown in histology, an 8% increase in the diameter, and a 32% increase in DNA content compared to the 2M control group, and the retention of GAG and collagen content. This work represents the first evidence of DFO stimulation toward enhancing neocartilage thickness without a tradeoff in the mechanical properties.

This study demonstrated that sequential seeding performed at 1 or 2 hours allowed for tissue formation without disruption of gross morphology. The most evident disruption in the self-assembling process due to an increase in cell seeding was observed in the 4M group, which resulted in constructs with morphological abnormalities, including surface irregularities and heterogeneous construct thickness. These observations are largely comparable to results shown by others (27, 28), and indicate that neotissue scale-up, in terms of thickness, cannot be performed using a single seeding event. The most desirable gross morphology, established as a tissue with a round, flat gross morphology, without abnormalities, and comparable to that of the 2M control group, was attained using sequential seeding at the 1- and 2-hour time point. Of these groups, the latter showed higher DNA content, indicating higher cell retention and/or cell survival. Conversely, applying the second seeding at the 3- or 4-hour time points induced the appearance of construct abnormalities. A quantitative follow-up of the self-assembling process using a self-assembly index (which represents the degree of cell condensation into compact clusters) was used to determine that the process depends on cell-cell and cell-matrix interactions (32).

Importantly, the study also showed that the self-assembly index increased rapidly within the first 2 hours following cell seeding. After this, the index plateaued and reached steady date at 4 hours. These data suggest that a second seeding event must be added before maximum cell density that occurs 4 hours after seeding (32), thus, allowing us to consider a second seeding at 1, 2, 3, or 4 hours. Toward the scale-up of engineered self-assembled neocartilage, the results showed that a separate seeding event 2 hours after the initial seeding is required to retain a desirable gross morphology.

The combined use of DFO stimulation and sequential seeding resulted in increased construct thickness. The combined regime resulted in a 52% thickness increase in constructs derived from minipig CCs and a 90% thickness increase in constructs derived from human ACs, compared to their respective 2M controls. The human AC constructs achieved a thickness of ~1mm without compromising biomechanical properties, thus, allowing us to consider addressing at least partial thickness defects. With the inclusion of DFO stimulation, the process may be repeated, using more than two seeding events to obtain larger thicknesses.

For the first time, DFO stimulation was shown to work with the self-assembling process at higher cell density to achieve thicker and robust constructs. DFO seems to facilitate tissue formation, possibly by stimulating cell-cell interactions via its iron chelation characteristics. Iron chelation inhibits HIF1a degradation, inducing a hypoxic response (43, 44) that promotes chondrogenic phenotype (45, 46) and induces integrin and cadherin expression (47), necessary for cartilage self-assembly (32). The pharmacological induction of hypoxia in our study may have increased the expression of integrins, and therefore, cell adhesiveness (48). Lastly, it is significant that the effects of DFO follow a 24-hour treatment, which is short compared to the overall culture time. Similar findings have been reported by others; only 1-hour stimulations with DFO had significant chondrogenic effects in neocartilage, inducing tissue maturation by promoting the formation of collagen pyridinoline crosslinks (29). All together, these findings motivate additional examination as to how DFO facilitates neocartilage formation and how it may be more effective

at different time points and durations. Recent findings using intraarticular injection of DFO in an *in vivo* mouse osteoarthritis model indicated that DFO alleviated osteoarthritis by promoting the activation of nuclear factor E2–related factor 2 (Nrf2) antioxidant system and inhibiting erastin-induced chondrocyte death (49). The identification of a chemical treatment that can thicken cartilage by itself has clinical significance in terms of engineered tissues and pharmacological treatments of native tissues.

DFO stimulation enables the maintenance of the mechanical properties of human AC constructs undergoing sequential seeding. The stimulation of chondrocytes with DFO prior to sequential seeding resulted in a significant increase of the aggregate and shear moduli, compared to the non-stimulated sequentially seeded constructs. The resulting compressive properties of the group with the combined regime were also higher compared to the control group. The increase in the compressive properties may be attributed to the GAG content, which follows the same trend. In terms of tensile properties, the use of DFO avoided a significant loss in Young's modulus and UTS, which follows the same trend as the collagen content and the PYR crosslink content. Prior work showed the beneficial effects of using DFO during the tissue maturation phase, corresponding to weeks 2-4 of cartilage self-assembly (29). This, however, is the first evidence of DFO improving mechanical properties when applied during aggregate rejuvenation (before cartilage self-assembly). It may be instructive to consider DFO application both during chondrocyte preparation (i.e., conservative chondrogenic passaging or aggregate rejuvenation) and tissue formation (i.e., self-assembly) (21) toward further improving the mechanical properties of the neocartilage. The results obtained in this work enable the production of functional neocartilage implants of clinically relevant sizes toward preclinical and clinical studies.

The use of an allogeneic approach with CCs offers translational advantages over an autologous approach, yet autologous ACs remain the preferred cell type used clinically. Rib chondrocytes obtained from the unmineralized portion of floating ribs have proven to be a valuable cell source capable of producing constructs with indistinguishable biochemical and mechanical

properties to ACs (50). This is particularly significant when the scarcity of healthy donor cartilage and donor site morbidity of autologous approaches is considered. In addition, with an autologous approach patients much undergo two surgeries, and the quality of the donor chondrocytes is limited to the conditions and age of the patient. The use of an allogeneic approach does not require an additional surgery, avoids donor site morbidity, and allows for the identification of an optimal donor source. Indeed, following donor screening in accordance to the FDA, a well-characterized cell source can be used to produce constructs on demand, with known material properties, free of diseases, and with little biological variability.

Extensive passaging also offers translational advantages over using primary or P1-3 chondrocytes currently used for cell-based therapies. In Phase III, using conservative chondrogenic passaging and aggregate rejuvenation, extensively passaged (P7) human ACs were used to produce neocartilage that 1) showed a significant increase in construct thickness, 2) retained a desirable gross morphology, and 3) retained its mechanical properties. The expansion factor of human ACs undergoing conservative chondrogenic passaging at P7 is ~65,000 (18). This number corresponds to the final cell number divided by the initial cell number. Noteworthy, a recent work established an initial number of 5M cells harvested by MACI to develop one membrane (51); with an initial number of 5M cells, conservative chondrogenic passaging and aggregate rejuvenation would yield enough cells to seed over 80,000 4M constructs, such as the ones shown in our results. The level of cell expansion used in this work, followed by aggregate redifferentiation, is significant because human ACs, in spite of being the preferred cell type used clinically to repair cartilage lesions, are scarce and dedifferentiate upon monolayer expansion; the inability to maintain a chondrogenic phenotype during cell expansion jeopardizes the outcome of current and prospective cell-based therapies. Thus, conservative chondrogenic passaging and aggregate rejuvenation, as used in this study, together with DFO stimulation and sequential seeding, address the longstanding limitation of chondrocyte scarcity and dedifferentiation, and allow the scale-up of the production of neocartilage implants with clinical relevance.

Conclusion

This work examined the development of a novel methodology to produce thicker neocartilage constructs through sequential seeding as part of the self-assembling process, using expanded and rejuvenated chondrocytes, while preserving gross morphology and mechanical properties. It was determined that sequential seeding alone does not produce thicker neocartilage constructs derived from minipig CCs. However, with a time of 2 hours between the first and the second seeding events, CCs can form constructs with a flat, round morphology and smooth surface (Phase I). Stimulation of CCs with DFO during rejuvenation, in combination with sequential seeding, induced a 52% increase in construct thickness. Lastly, this work demonstrated the translational potential of the methodology using human ACs, the current cell used in cell-based cartilage therapies. With human ACs, sequential seeding, together with DFO stimulation, resulted in constructs with a 90% significant increase in construct thickness, an 8% increase in diameter, a 33% and a 41% increase in aggregate and shear modulus values, and the maintenance of the tensile properties, compared to the control group. The results of this work provide a new strategy toward developing clinically relevant neocartilage constructs.

REFERENCES

1. Demange M, Gomoll AH. The use of osteochondral allografts in the management of cartilage defects. Current reviews in musculoskeletal medicine. 2012;5(3):229-35. doi: 10.1007/s12178-012-9132-0. PubMed PMID: 22628178; PubMed Central PMCID: PMC3535086.
2. Jones KJ, Mosich GM, Williams RJ. Fresh Precut Osteochondral Allograft Core Transplantation for the Treatment of Femoral Cartilage Defects. Arthroscopy techniques. 2018;7(8):e791-e5. doi: 10.1016/j.eats.2018.03.016. PubMed PMID: 30167355; PubMed Central PMCID: PMC6111451.
3. Bentley G, Biant LC, Vijayan S, Macmull S, Skinner JA, Carrington RW. Minimum ten-year results of a prospective randomised study of autologous chondrocyte implantation versus mosaicplasty for symptomatic articular cartilage lesions of the knee. The Journal of bone and joint surgery British volume. 2012;94(4):504-9. doi: 10.1302/0301-620X.94B4.27495. PubMed PMID: 22434467.
4. Kwon H, Brown WE, Lee CA, Wang D, Paschos N, Hu JC, Athanasiou KA. Surgical and tissue engineering strategies for articular cartilage and meniscus repair. Nature reviews Rheumatology. 2019;15(9):550-70. doi: 10.1038/s41584-019-0255-1. PubMed PMID: 31296933.
5. Kreuz PC, Steinwachs MR, Erggelet C, Krause SJ, Konrad G, Uhl M, Sudkamp N. Results after microfracture of full-thickness chondral defects in different compartments in the knee. Osteoarthritis and cartilage. 2006;14(11):1119-25. doi: 10.1016/j.joca.2006.05.003. PubMed PMID: 16815714.
6. Goyal D, Keyhani S, Lee EH, Hui JH. Evidence-based status of microfracture technique: a systematic review of level I and II studies. Arthroscopy : the journal of arthroscopic & related surgery : official publication of the Arthroscopy Association of North America and the International Arthroscopy Association. 2013;29(9):1579-88. doi: 10.1016/j.arthro.2013.05.027. PubMed PMID: 23992991.
7. Migliorini F, Eschweiler J, Spiezia F, van de Wall BJM, Knobe M, Tingart M, Maffulli N. Arthroscopy versus mini-arthrotomy approach for matrix-induced autologous chondrocyte implantation in the knee: a systematic review. Journal of orthopaedics and traumatology : official journal of the Italian Society of Orthopaedics and Traumatology. 2021;22(1):23. doi: 10.1186/s10195-021-00588-6. PubMed PMID: 34152483; PubMed Central PMCID: PMC8217351.
8. Bartlett W, Skinner JA, Gooding CR, Carrington RW, Flanagan AM, Briggs TW, Bentley G. Autologous chondrocyte implantation versus matrix-induced autologous chondrocyte implantation for osteochondral defects of the knee: a prospective, randomised study. The Journal of bone and joint surgery British volume. 2005;87(5):640-5. doi: 10.1302/0301-620X.87B5.15905. PubMed PMID: 15855365.
9. Flanigan DC, Harris JD, Trinh TQ, Siston RA, Brophy RH. Prevalence of chondral defects in athletes' knees: a systematic review. Medicine and science in sports and exercise. 2010;42(10):1795-801. doi: 10.1249/MSS.0b013e3181d9eea0. PubMed PMID: 20216470.
10. Bezuglov EN, Lyubushkina AV, Khaitin VY, Tokareva AV, Goncharov EN, Gorinov AV, Sivakova EY, Sereda AP. Prevalence of Asymptomatic Intra-articular Changes of the Knee in Adult Professional Soccer Players. Orthopaedic journal of sports medicine.

2019;7(11):2325967119885370. doi: 10.1177/2325967119885370. PubMed PMID: 32010730; PubMed Central PMCID: PMC6967194.
11. Seo SS, Kim CW, Jung DW. Management of focal chondral lesion in the knee joint. Knee surgery & related research. 2011;23(4):185-96. doi: 10.5792/ksrr.2011.23.4.185. PubMed PMID: 22570833; PubMed Central PMCID: PMC3341803.
12. Makris EA, Gomoll AH, Malizos KN, Hu JC, Athanasiou KA. Repair and tissue engineering techniques for articular cartilage. Nature reviews Rheumatology. 2015;11(1):21-34. doi: 10.1038/nrrheum.2014.157. PubMed PMID: 25247412; PubMed Central PMCID: PMC4629810.
13. Rosa D, Di Donato SL, Balato G, D'Addona A, Smeraglia F, Correra G, Di Vico G. How to Manage a Failed Cartilage Repair: A Systematic Literature Review. Joints. 2017;5(2):93-106. doi: 10.1055/s-0037-1603900. PubMed PMID: 29114638; PubMed Central PMCID: PMC5672873.
14. \Basad E, Wissing FR, Fehrenbach P, Rickert M, Steinmeyer J, Ishaque B. Matrix-induced autologous chondrocyte implantation (MACI) in the knee: clinical outcomes and challenges. Knee surgery, sports traumatology, arthroscopy : official journal of the ESSKA. 2015;23(12):3729-35. doi: 10.1007/s00167-014-3295-8. PubMed PMID: 25218576.
15. Huang BJ, Hu JC, Athanasiou KA. Cell-based tissue engineering strategies used in the clinical repair of articular cartilage. Biomaterials. 2016;98:1-22. Epub 2016/05/14. doi: 10.1016/j.biomaterials.2016.04.018. PubMed PMID: 27177218; PubMed Central PMCID: PMCPMC4899115.
16. Huwe LW, Brown WE, Hu JC, Athanasiou KA. Characterization of costal cartilage and its suitability as a cell source for articular cartilage tissue engineering. Journal of tissue engineering and regenerative medicine. 2018;12(5):1163-76. doi: 10.1002/term.2630. PubMed PMID: 29286211; PubMed Central PMCID: PMC5948132.
17. Lavernia L, Brown WE, Wong BJF, Hu JC, Athanasiou KA. Toward tissue-engineering of nasal cartilages. Acta biomaterialia. 2019;88:42-56. doi: 10.1016/j.actbio.2019.02.025. PubMed PMID: 30794988.
18. Kwon H, Brown WE, O'Leary SA, Hu JC, Athanasiou KA. Rejuvenation of extensively passaged human chondrocytes to engineer functional articular cartilage. Biofabrication. 2021;13(3). doi: 10.1088/1758-5090/abd9d9. PubMed PMID: 33418542; PubMed Central PMCID: PMC8263804.
19. Athanasiou KA, Eswaramoorthy R, Hadidi P, Hu JC. Self-organization and the self-assembling process in tissue engineering. Annual review of biomedical engineering. 2013;15:115-36. doi: 10.1146/annurev-bioeng-071812-152423. PubMed PMID: 23701238; PubMed Central PMCID: PMC4420200.
20. Kwon H, O'Leary SA, Hu JC, Athanasiou KA. Translating the application of transforming growth factor-beta1, chondroitinase-ABC, and lysyl oxidase-like 2 for mechanically robust tissue-engineered human neocartilage. Journal of tissue engineering and regenerative medicine. 2019;13(2):283-94. doi: 10.1002/term.2791. PubMed PMID: 30557915.
21. Otarola G, Hu JC, Athanasiou KA. Intracellular Calcium and Sodium Modulation of Self-Assembled Neocartilage Using Costal Chondrocytes. Tissue engineering Part A. 2021. doi: 10.1089/ten.TEA.2021.0169. PubMed PMID: 34877888.
22. Visscher DO, Bos EJ, Peeters M, Kuzmin NV, Groot ML, Helder MN, van Zuijlen PP. Cartilage Tissue Engineering: Preventing Tissue Scaffold Contraction Using a 3D-Printed

Polymeric Cage. Tissue engineering Part C, Methods. 2016;22(6):573-84. doi: 10.1089/ten.TEC.2016.0073. PubMed PMID: 27089896.
23. Zhang L, Spector M. Comparison of three types of chondrocytes in collagen scaffolds for cartilage tissue engineering. Biomedical materials. 2009;4(4):045012. doi: 10.1088/1748-6041/4/4/045012. PubMed PMID: 19636108.
24. Makris EA, MacBarb RF, Paschos NK, Hu JC, Athanasiou KA. Combined use of chondroitinase-ABC, TGF-beta1, and collagen crosslinking agent lysyl oxidase to engineer functional neotissues for fibrocartilage repair. Biomaterials. 2014;35(25):6787-96. doi: 10.1016/j.biomaterials.2014.04.083. PubMed PMID: 24840619; PubMed Central PMCID: PMC4105108.
25. Lee JK, Huwe LW, Paschos N, Aryaei A, Gegg CA, Hu JC, Athanasiou KA. Tension stimulation drives tissue formation in scaffold-free systems. Nature materials. 2017;16(8):864-73. doi: 10.1038/nmat4917. PubMed PMID: 28604717; PubMed Central PMCID: PMC5532069.
26. Huang BJ, Brown WE, Keown T, Hu JC, Athanasiou KA. Overcoming Challenges in Engineering Large, Scaffold-Free Neocartilage with Functional Properties. Tissue engineering Part A. 2018;24(21-22):1652-62. doi: 10.1089/ten.TEA.2017.0495. PubMed PMID: 29766751; PubMed Central PMCID: PMC6238610.
27. Revell CM, Reynolds CE, Athanasiou KA. Effects of initial cell seeding in self assembly of articular cartilage. Annals of biomedical engineering. 2008;36(9):1441-8. doi: 10.1007/s10439-008-9524-x. PubMed PMID: 18574692; PubMed Central PMCID: PMC3164522.
28. Huang BJ, Huey DJ, Hu JC, Athanasiou KA. Engineering biomechanically functional neocartilage derived from expanded articular chondrocytes through the manipulation of cell-seeding density and dexamethasone concentration. Journal of tissue engineering and regenerative medicine. 2017;11(8):2323-32. doi: 10.1002/term.2132. PubMed PMID: 27138113.
29. Otarola G. Chapter 6. Ion Modulatory Treatments Toward Functional Self-Assembled Neocartilage. Doctoral dissertation, UC Irvine. 2022.
30. Huang Z, He G, Huang Y. Deferoxamine synergizes with transforming growth factor-beta signaling in chondrogenesis. Genetics and molecular biology. 2017;40(3):698-702. doi: 10.1590/1678-4685-GMB-2016-0324. PubMed PMID: 28810001; PubMed Central PMCID: PMC5596375.
31. Tchetina EV, Markova GA, Poole AR, Zukor DJ, Antoniou J, Makarov SA, Kuzin AN. Deferoxamine Suppresses Collagen Cleavage and Protease, Cytokine, and COL10A1 Expression and Upregulates AMPK and Krebs Cycle Genes in Human Osteoarthritic Cartilage. International journal of rheumatology. 2016;2016:6432867. doi: 10.1155/2016/6432867. PubMed PMID: 28042296; PubMed Central PMCID: PMC5155111 Poole who is a consultant to IBEX, Montreal, Canada, who manufacture and market the C1,2C ELISA assay.
32. Lee JK, Hu JC, Yamada S, Athanasiou KA. Initiation of Chondrocyte Self-Assembly Requires an Intact Cytoskeletal Network. Tissue engineering Part A. 2016;22(3-4):318-25. doi: 10.1089/ten.TEA.2015.0491. PubMed PMID: 26729374; PubMed Central PMCID: PMC4779322.
33. Burton LH, Afzali MF, Radakovich LB, Campbell MA, Culver LA, Olver CS, Santangelo KS. Systemic administration of a pharmacologic iron chelator reduces cartilage lesion development in the Dunkin-Hartley model of primary osteoarthritis. Free radical biology & medicine. 2022;179:47-58. doi: 10.1016/j.freeradbiomed.2021.12.257. PubMed PMID: 34923104; PubMed Central PMCID: PMC8760171.

34. Murphy MK, Huey DJ, Reimer AJ, Hu JC, Athanasiou KA. Enhancing post-expansion chondrogenic potential of costochondral cells in self-assembled neocartilage. PloS one. 2013;8(2):e56983. doi: 10.1371/journal.pone.0056983. PubMed PMID: 23437288; PubMed Central PMCID: PMC3578801.
35. Paschos NK, Makris EA, Hu JC, Athanasiou KA. Topographic variations in biomechanical and biochemical properties in the ankle joint: an *in vitro* bovine study evaluating native and engineered cartilage. Arthroscopy : the journal of arthroscopic & related surgery : official publication of the Arthroscopy Association of North America and the International Arthroscopy Association. 2014;30(10):1317-26. doi: 10.1016/j.arthro.2014.05.025. PubMed PMID: 25064757.
36. White JL, Salinas EY, Link JM, Hu JC, Athanasiou KA. Characterization of Adult and Neonatal Articular Cartilage From the Equine Stifle. Journal of equine veterinary science. 2021;96:103294. doi: 10.1016/j.jevs.2020.103294. PubMed PMID: 33349403.
37. Brown WE, Huang BJ, Hu JC, Athanasiou KA. Engineering large, anatomically shaped osteochondral constructs with robust interfacial shear properties. NPJ Regenerative medicine. 2021;6(1):42. doi: 10.1038/s41536-021-00152-0. PubMed PMID: 34362933; PubMed Central PMCID: PMC8346478.
38. Salinas EY, Donahue RP, Herrera JM, Hu JC, Athanasiou KA. The functionality and translatability of neocartilage constructs are improved with the combination of fluid-induced shear stress and bioactive factors. FASEB journal : official publication of the Federation of American Societies for Experimental Biology. 2022;36(4):e22225. doi: 10.1096/fj.202101699R. PubMed PMID: 35224777.
39. Brown WE, Hu JC, Athanasiou KA. Ammonium-Chloride-Potassium Lysing Buffer Treatment of Fully Differentiated Cells Increases Cell Purity and Resulting Neotissue Functional Properties. Tissue engineering Part C, Methods. 2016;22(9):895-903. doi: 10.1089/ten.TEC.2016.0184. PubMed PMID: 27553086; PubMed Central PMCID: PMC5035916.
40. Athanasiou KA, Niederauer GG, Schenck RC, Jr. Biomechanical topography of human ankle cartilage. Annals of biomedical engineering. 1995;23(5):697-704. doi: 10.1007/bf02584467. PubMed PMID: 7503470.
41. Cissell DD, Link JM, Hu JC, Athanasiou KA. A Modified Hydroxyproline Assay Based on Hydrochloric Acid in Ehrlich's Solution Accurately Measures Tissue Collagen Content. Tissue engineering Part C, Methods. 2017;23(4):243-50. doi: 10.1089/ten.tec.2017.0018. PubMed PMID: 28406755; PubMed Central PMCID: PMC5397204.
42. Bielajew BJ, Hu JC, Athanasiou KA. Methodology to Quantify Collagen Subtypes and Crosslinks: Application in Minipig Cartilages. Cartilage. 2021;13(2_suppl):1742S-54S. doi: 10.1177/19476035211060508. PubMed PMID: 34823380; PubMed Central PMCID: PMC8804780.
43. Wu LY, He YL, Zhu LL. Possible Role of PHD Inhibitors as Hypoxia-Mimicking Agents in the Maintenance of Neural Stem Cells' Self-Renewal Properties. Frontiers in cell and developmental biology. 2018;6:169. doi: 10.3389/fcell.2018.00169. PubMed PMID: 30619851; PubMed Central PMCID: PMC6297135.
44. Woo KJ, Lee TJ, Park JW, Kwon TK. Desferrioxamine, an iron chelator, enhances HIF-1alpha accumulation via cyclooxygenase-2 signaling pathway. Biochemical and biophysical research communications. 2006;343(1):8-14. doi: 10.1016/j.bbrc.2006.02.116. PubMed PMID: 16527254.

45. Makris EA, Hu JC, Athanasiou KA. Hypoxia-induced collagen crosslinking as a mechanism for enhancing mechanical properties of engineered articular cartilage. Osteoarthritis and cartilage. 2013;21(4):634-41. doi: 10.1016/j.joca.2013.01.007. PubMed PMID: 23353112; PubMed Central PMCID: PMC3670708.
46. Yodmuang S, Gadjanski I, Chao PH, Vunjak-Novakovic G. Transient hypoxia improves matrix properties in tissue engineered cartilage. Journal of orthopaedic research : official publication of the Orthopaedic Research Society. 2013;31(4):544-53. doi: 10.1002/jor.22275. PubMed PMID: 23203946; PubMed Central PMCID: PMC4136653.
47. Befani C, Liakos P. Hypoxia upregulates integrin gene expression in microvascular endothelial cells and promotes their migration and capillary-like tube formation. Cell biology international. 2017;41(7):769-78. doi: 10.1002/cbin.10777. PubMed PMID: 28418174.
48. Goggins BJ, Minahan K, Sherwin S, Soh WS, Pryor J, Bruce J, Liu G, Mathe A, Knight D, Horvat JC, Walker MM, Keely S. Pharmacological HIF-1 stabilization promotes intestinal epithelial healing through regulation of alpha-integrin expression and function. American journal of physiology Gastrointestinal and liver physiology. 2021;320(4):G420-G38. doi: 10.1152/ajpgi.00192.2020. PubMed PMID: 33470153.
49. Guo Z, Lin J, Sun K, Guo J, Yao X, Wang G, Hou L, Xu J, Guo J, Guo F. Deferoxamine Alleviates Osteoarthritis by Inhibiting Chondrocyte Ferroptosis and Activating the Nrf2 Pathway. Frontiers in pharmacology. 2022;13:791376. doi: 10.3389/fphar.2022.791376. PubMed PMID: 35359876; PubMed Central PMCID: PMC8964096.
50. Huwe LW, Sullan GK, Hu JC, Athanasiou KA. Using Costal Chondrocytes to Engineer Articular Cartilage with Applications of Passive Axial Compression and Bioactive Stimuli. Tissue engineering Part A. 2018;24(5-6):516-26. doi: 10.1089/ten.TEA.2017.0136. PubMed PMID: 28683690; PubMed Central PMCID: PMC5833255.
51. Zikria B, Hafezi-Nejad N, Patten I, Johnson A, Haj-Mirzaian A, Wilckens JH, Ficke JR, Demehri S. Image-Guided Chondrocyte Harvesting for Autologous Chondrocyte Implantation: Initial Feasibility Study with Human Cadaver and Pilot Clinical Experience. JB & JS open access. 2019;4(2):e0039. doi: 10.2106/JBJS.OA.18.00039. PubMed PMID: 31334460; PubMed Central PMCID: PMC6613850.

Supplementary material

Supplementary Table 1. Gross morphology and mechanical data of minipig CC constructs built using sequential seeding and DFO stimulation, presented as mean ± standard deviation. H_A, aggregate modulus. G, shear modulus. Ey, Young's modulus. Asterisks denote significant differences ($p<0.05$) compared with the 2M control group based on Dunnett's *post hoc* test.

	Thickness (mm)	Diameter (mm)	Wet Weight (mg)	H_A (kPa)	Shear Modulus (kPa)	Ey (MPa)	UTS (MPa)
2M	0.58±0.05	5.86±0.10	18.00±0.27	343±67	151±21	3.97±0.64	1.67±0.18
2+2M	0.57±0.05	**4.97±0.10***	**14.85±1.91***	359±185	166±89	2.80±1.43	**0.98±0.27***
$4M^{DFO}$	**0.79±0.06***	**4.95±0.07***	15.76±1.23	271±90	142±46	2.82±1.28	1.54±0.43
$2+2M^{DFO}$	**0.88±0.04***	**5.14±0.19***	**14.67±0.78***	403±167	191±76	**1.36±0.71***	**0.64±0.21***

Supplementary Table 2. Gross morphology and mechanical data of human AC constructs built using sequential seeding and DFO stimulation, presented as mean ± standard deviation. H_A, aggregate modulus. G, shear modulus. Ey, Young's modulus. Using connecting letters report, different uppercase letters over bars indicate statistical difference ($p<0.05$) among groups, based on Tukey's *post hoc* test.

	Thickness (mm)	Diameter (mm)	Wet Weight (mg)	H_A (kPa)	Shear Modulus (kPa)	Ey (MPa)	UTS (MPa)	k ($\times 10^{15}$ m^4/Ns)
h2M	$0.51±0.06^C$	4.88±0.19	$10.93±0.67^B$	$84±30^{AB}$	$41±14^{AB}$	$2.31±0.67^A$	$0.99±0.28^A$	6.73±4.70
h2+2M	$0.68.±0.20^B$	4.96±0.06	$15.37±3.02^A$	$72±24^B$	$38±11^B$	$0.99±0.48^B$	$0.51±0.24^B$	4.58±1.60
$h2+2M^{DFO}$	$0.97±0.04^A$	5.26±0.10	$16.56±1.24^A$	$112±42^A$	$58±23^A$	$1.60±0.15^{AB}$	$0.75±0.13^{AB}$	8.69±4.38

Conclusions

Despite the prevalence of cartilage related diseases such as osteoarthritis, which affects over 30 million people in the US alone, current surgical treatments fail to stop the progression of chondral degeneration. Tissue engineering has the potential to address the unmet need of long-term treatment of articular cartilage diseases. However, a number of limitations still hinder the translation of cell-based therapies such as self-assembled neocartilage constructs. With the intention of translating this technology from bench to bedside, this work aimed at overcoming two major limitations: 1) to produce biomimetic neocartilage using scalable, reproducible, low-cost exogenous agents toward translation, capable of withstanding the strenuous environment of the knee, and 2) to engineer thicker, biomimetic neocartilage. Throughout this work, expanded and rejuvenated chondrocytes were employed in the production of neocartilage, including human and minipig neocartilages, derived from articular cartilage and costal cartilage, and at low and high passages.

This objective was met by performing an assessment of the effects of storage time and storage temperature on the bulk and surface properties of cartilage explants, and the further development of a non-contact methodology to determine the mechanical properties of cartilage specimens, followed by a characterization of the material properties of young, healthy human native articular cartilage of the medial femoral condyle of the knee. With data on the values for the biochemical and biomechanical properties of human articular cartilage, including tribological, tensile, and compressive properties, ion modulation strategies were developed in order to improve the mechanical properties of neocartilage constructs based on two known chondrogenic stimuli, mechanotransduction and hypoxia. Finally, a new self-assembling methodology that uses sequential seeding and deferoxamine stimulation was developed to target, for the first time, the improvement of neocartilage construct thickness. The neocartilage that resulted from this work

represents significant improvements toward clinical translation, attaining both gross morphological features and biomechanical properties in the range of human native tissue values.

Tissue engineering relies on the assessment of native cartilage tissues toward defining target values of neocartilage biochemical and biomechanical characteristics. To assess such values, this work employed fresh and stored human and animal cartilage specimens. Because of this, and toward ensuring that all data gathered in this work truly reflected the native cartilage, a study of the effects of storage time and temperature on the mechanical properties, including assessment of tribology and topography, was performed. Of the storage conditions examined, including 37°C, 4°C, -20°C, and -80°C for 1 day, 1 week, and 1 month, a 49% decrease in coefficient of friction was observed at 1 week in -80°C, possibly caused by tissue damage induced by ice crystals, and not an improvement in function. Interestingly, prolonged storage and tissue culture of explants at 37°C resulted in up to an 83% increase in the compressive aggregate modulus after 1 month, with a corresponding increase in the glycosaminoglycan (GAG) content. Thus, proper storage conditions, namely at -20°C, were used to store cartilage tissues in the totality of this work to avoid reporting storage-induced variations. In addition, tribology showed frictional anisotropy, illustrated by a 53% increase in coefficient of friction in the mediolateral direction compared to the anteroposterior direction. For the first time, interferometry, a non-contact testing methodology, was used to show cartilage topographical anisotropy as seen in an anteroposterior striated pattern in the same direction as joint articulation. In addition to illustrating the differential effects of storage conditions on cartilage, the data obtained show that a bulk-only analysis of cartilage function is not sufficient or representative, and that non-destructive surface characterization assays enable improvement in cartilage functionality assessment by considering both surface and bulk cartilage properties.

Considering the utility of a non-contact, non-destructive methodology toward future cartilage research and tissue engineering endeavors, vibrometry was used to develop a fast, novel alternative to traditional mechanical assays (e.g., stress relaxation, creep indentation).

Finite-element models predicted tissue resonant frequencies and bending modes, which strongly correlated with experimental data (R^2=0.93). Vibrometry-based viscoelastic properties significantly correlated with moduli from stress relaxation and creep tests, with correlation strengths reaching up to 0.78 (Spearman ρ correlations). Loss modulus also strongly correlated with GAG content. Dynamic properties measured by vibrometry significantly differed among various knee cartilages, ranging between 6.1-56.4MPa. Interestingly, meniscus viscoelastic properties suggest that contrary to common belief, it may lack shock absorption abilities; instead, condylar hyaline cartilage may be a better shock absorber. These data demonstrate, for the first time, that vibrometry is a non-contact approach to dynamic mechanical characterization of hyaline cartilage and fibrocartilage, which correlates with outcomes of standard quasistatic mechanical testing and biochemical composition. Thus, with a single tool, vibrometry greatly facilitates the non-contact, non-destructive assessment of tissues, supporting translational efforts of cartilage tissue engineering.

Young and healthy human tissues represent the primary design criteria for the neocartilage developed throughout this work. Because of this, and toward understanding the association between regional variation in the mechanical properties and predisposition to injury, a topographical characterization of the histological, biochemical, tribological, tensile, and compressive properties of articular cartilage of the medial femoral condyle from young, healthy donors was performed. Surprisingly, unlike the bovine cartilage tissues examined in the vibrometry study (see previous paragraph), in young, healthy human cartilage, tribological anisotropy disappears, as evidenced by the coefficient of friction, which did not differ with regard to direction of articulation or region; it ranged between 0.22 and 0.26 throughout the medial condyle. This suggests tissue-engineered implants do not require direction-specific tribological properties. In contrast, topographical variations were observed in the tensile and compressive properties. The Young's modulus, ultimate tensile strength, aggregate modulus, and shear modulus in the posterior region were 1.0-fold, 2.8-fold, 1.1-fold, and 1.0-fold less than the values

in the anterior region, respectively. Although glycosaminoglycan content is thought to correlate with compressive properties, in this study, the aggregate and shear moduli correlated more robustly to the amount of pyridinoline crosslinks per collagen. Because of this, new structure-function relationships may need to be developed to account for the role of collagen crosslinks in the mechanical properties of cartilage. In addition, the lower tensile and compressive properties of the posterior medial condyle were found in the region with the highest incidence of chondral degeneration. This indicates that the lower mechanical properties may predispose the region to injury. Toward informing tissue engineering, these data provide comprehensive design criteria and highlight the importance of increasing the collagen crosslink content of neocartilage constructs toward improved mechanical properties.

Targeting the functional properties of young, healthy human articular cartilage, this work aimed to develop new strategies capable of improving the mechanical properties of neocartilage constructs. Treatment of neocartilage with ionomycin produced 61% and 115% increases in glycosaminoglycan and pyridinoline crosslink content, respectively. These changes directly influenced the mechanical properties of the construct. The treatment with the calcium ionophore resulted in a 45% increase of the aggregate modulus, and a 63% increase in the tensile Young's modulus, resulting in aggregate and Young's moduli of 567kPa and 8.43MPa, respectively. Similarly, constructs treated with 100μM of deferoxamine exhibited an 87% increase in pyridinoline crosslinks, a 57% increase in the Young's modulus, and a 112% increase in the ultimate tensile strength. Finally, the combined use of ionomycin and deferoxamine resulted in a 150% and 176% significant increase in the Young's modulus and ultimate tensile strength (UTS) of neocartilage constructs, respectively. The results obtained with this strategy are significant because neocartilage constructs achieved a Young's modulus of 11.76±3.29MPa and UTS of 4.20±1.24MPa, the highest reported for self-assembled constructs to date. Toward clinical translation, the use of ion modulators, as shown in this work, is a repeatable, efficient, and cost effective methodology which outperforms strategies that require bioactive factors and/or

bioreactors. The results shown here provide evidence that ion modulation can be employed to improve the biomechanical properties of engineered neotissues.

In a final effort to provide a biomimetic tissue toward the treatment and permanent alleviation of cartilage diseases, the development of a new strategy to increase the thickness of self-assembled tissues was examined. In Phase I, constructs derived from costal chondrocytes did not show an increase in thickness upon sequential seeding; however, the use of a 2-hour time between the first and second seeding events allowed for proper gross morphology (e.g., with no presence of bending, heterogeneous thickness, surface irregularities, or cyst formation) and high cell survival. In Phase II, the stimulation of constructs with deferoxamine during rejuvenation, in combination with sequential seeding, induced a 52% increase in thickness. In Phase III, sequential seeding with human articular chondrocytes stimulated with deferoxamine resulted in constructs with a 90% significant increase in thickness compared to the control group. Excitingly, the increase in thickness did not affect the compressive and tensile properties of human constructs. This work represents the first successful strategy in generating thicker constructs by manipulating the self-assembling process, and provides a new strategy toward developing clinically relevant neocartilage constructs. Future studies should aim at further utilizing this technique to create larger and thicker neocartilage, increasing the diameter and the number of layers. In addition, aiming toward translation, the safety and efficacy of the neocartilage constructs should be examined *in vivo*.

The tissue engineering field is closing in on creating a cogent therapy for cartilage diseases in the form of neocartilage, capable of providing a functional replacement tissue. In the 1990s, when the term tissue engineering came to denote the fabrication of tissues using cells, scaffolds, and bioactive signals, cartilage was predicted to be one of the first tissues to be successfully regenerated. However, the unique biochemical and mechanical properties of the tissue have shown to be far more complex than originally thought. As detailed in Chapter 1 of this work, the Food and Drug Administration (FDA) has made great efforts in providing guidance to

the field toward facilitating and motivating translation. Still, despite a wealth of basic science research within the field of cartilage repair and the clear clinical need for additional treatments, only one cell-based cartilage therapy product has obtained FDA approval to date. While persisting issues specific to the application of cartilage products hinder attempts of translation, such as the selection of a large animal model and reporting efficacy at a preclinical stage, other issues related to the development and production of cell-based products may be addressed beforehand, such as engineering methods that ensure reproducibility and technical feasibility upon scale-up. Based on guidance documents specific to knee cartilage or similar cell-based products, tissue-engineered self-assembled neocartilage will require well-designed preclinical studies to obtain approval of an investigational new drug (IND) application, followed by clinical studies and a successful biologics license application (BLA) before getting to market. The manufacturing compliance underlying this process is governed by the human cell, tissue, and cellular and tissue-based product (HCT/P) pathway, under Section 351 of the Public Health Service act. The research detailed in this work, in consideration of the regulatory needs for cartilage therapies that include HCT/Ps, provides concrete steps toward translation in accordance to the FDA guidance documents.

Ultimately, this work successfully achieved the objectives proposed: 1) A complete assessment of the biochemical and biomechanical properties of native cartilage was provided. First, a characterization of the tribological and topographical properties of articular cartilage was performed. This was followed by the development of a new non-contact, non-destructive methodology to determine the dynamic mechanical properties of cartilage tissues. Lastly, and most importantly, a comprehensive characterization of young, healthy donor tissues provided accurate and much needed data on the properties of healthy cartilage. 2) The development of new ion modulation treatments to achieve *in vitro* tissue maturation was presented. In particular, ionomycin and deferoxamine, two cost-effective, stable and easy to manipulate ion modulators, were employed as analogs of mechanotransduction and hypoxia. These analogs, through the

modulation of calcium and iron, allowed the presumable activation of the two known chondrogenic stimuli, without the use of bioreactors, resulting in some of the highest mechanical properties reported thus far for self-assembled tissue-engineered neocartilage. 3) A new strategy using sequential seeding was developed toward producing thicker neocartilage constructs while maintaining the biomimetic properties of the tissue and desirable gross morphological features toward translation. Altogether, the studies presented in this dissertation demonstrate the potential of self-assembled neocartilage as a therapy to treat hyaline articular cartilage defects. They also provide important tools that support translational efforts toward preclinical trials, clinical trials, and eventually, FDA approval. It is envisioned that, in the coming years, neocartilage implants will provide treatment solutions to the millions of people affected by the as-of-yet intractable cartilage diseases.

Appendix: *In vitro* effects of bupivacaine on the viability and mechanics of native and engineered cartilage grafts

Abstract

Background: Although the toxic effects of bupivacaine on chondrocyte monolayer culture have been well-described, its cellular and mechanical effects on native and engineered articular cartilage remain unclear. For the repair of articular cartilage defects, fresh autologous and allogeneic cartilage grafts are commonly used, and engineered cell-based therapies are emerging. The outcome of grafting therapies aimed at repairing damaged cartilage relies largely in maintaining proper viability and mechanical suitability of the donor tissues.

Hypothesis/Purpose: To investigate the *in vitro* effects of single bupivacaine exposure on the viability and mechanics of two cartilage graft types: native articular cartilage and engineered neocartilage

Study Design: Controlled Laboratory Study.

Methods: Articular cartilage explants were harvested from the bovine stifle femoral condyles, and neocartilage constructs were engineered from bovine stifle chondrocytes using the self-assembling process, a scaffold-free approach to engineer cartilage tissue. Both explants and neocartilage were exposed to chondrogenic medium containing a clinically relevant bolus of 0.5%, 0.25%, or 0% (control) bupivacaine for 1 hour, followed by fresh medium wash and exchange. Cell viability and matrix content (collagen and glycosaminoglycan [GAG]) were assessed at t=24 hours post-treatment, and compressive mechanical properties were assessed with creep indentation testing at t=5-6 days post-treatment.

Published as: Oyadomari, S., Brown, W.E., Kwon, H., Otarola, G.A., Athanasiou, K.A., Wang, D. *In Vitro* Effects of Bupivacaine on the Viability and Mechanics of Native and Engineered Cartilage Grafts. The American Journal of Sports Medicine 2021; 49(5): 1305-1312

Results: Single bupivacaine exposure was chondrotoxic in both explants and neocartilage, with 0.5% bupivacaine causing a significant decrease in chondrocyte viability compared to controls (55.0±13.4% vs. 71.9±13.5%; p<0.001)). Bupivacaine had no significant effect on matrix content for either tissue type. There was significant weakening of the mechanical properties in the neocartilage when treated with 0.5% bupivacaine compared to control with decreased aggregate modulus (415.8±155.1 vs 660.3±145.8 kPa; p=0.003), decreased shear modulus (143.2±14.0 vs 266.5±89.2 kPa; p=0.002), and increased permeability (14.7±8.1 vs 6.6±1.7 $10^{-15}m^4/Ns$; p=0.009). Bupivacaine exposure did not have a significant effect on the mechanical properties of native cartilage explants.

Conclusion: Single bupivacaine exposure resulted in significant chondrotoxicity in native explants and neocartilage and significant weakening of mechanical properties of neocartilage. The presence of abundant extracellular matrix does not appear to confer any additional resistance to the toxic effects of bupivacaine.

Clinical Relevance: Clinicians should be judicious regarding use of intra-articular bupivacaine in the setting of articular cartilage repair.

What is known about the subject: Many studies have shown that bupivacaine is toxic to chondrocytes in a time- and dose-dependent manner. However, the majority of these studies have been performed on monolayer culture. Some studies have suggested that the dense extracellular matrix of articular cartilage may confer a protective effect against the toxicity of these agents.

What this study adds to existing knowledge: The findings of this study indicate that the dense extracellular matrix of the cartilage tissue does not confer resistance against the chondrotoxic effects of bupivacaine. Additionally, although the cellular toxicity of local anesthetics has been well established, whether the mechanical properties of the articular cartilage are similarly affected

is unknown and not well studied to date. To our knowledge, this is the first study to demonstrate weakening of the mechanical properties of cartilaginous tissue induced by bupivacaine exposure, and this phenomenon may be dependent on tissue permeability.

Introduction

Local anesthetics are commonly used as intra-articular injections to reduce pain caused by acute injury, degenerative disease, or surgery (1, 2). Multiple studies have shown the deleterious effects of these anesthetics on chondrocyte viability with chondrotoxic effects occurring in a time- and dose-dependent manner (3-7). Historically, continuous infusion intra-articular pain pumps have been associated with frank chondrolysis (8). Subsequent investigations have reported that significant chondrocyte death can still occur after a short exposure period, raising concern about the potential detrimental effects of single-injection local anesthetics (4).

Despite concerning evidence demonstrating the chondrotoxicity of local anesthetics, there remains widespread clinical use of these agents for relief of symptoms due to the lack of obvious detrimental effects in the *in vivo* setting (9, 10). In both normal and anterior cruciate ligament (ACL)-transected knees of rats, weekly injections of 0.5% bupivacaine for five consecutive weeks did not induce any changes in chondrocyte viability compared to saline injection (9). However, unlike humans, rodents can exhibit spontaneous articular cartilage repair due to life-long open growth plates and thinner cartilage (11, 12). Another reason for the skepticism regarding the chondrotoxicity of anesthetics is that the majority of studies examining the toxic effects have been performed on monolayer culture, which does not adequately simulate *in vivo* conditions of chondrocytes embedded within the hyaline extracellular matrix (ECM). Some studies have suggested that an intact ECM may confer a protective effect against the toxicity of these agents (3, 9, 13). Even if chondrocyte viability diminishes, changes to the ECM may not occur, and therefore, the mechanical functionality of articular cartilage may remain intact. To date, the effects

of local anesthetics on the ECM and mechanical characteristics of articular cartilage have not been well studied.

The purpose of this study is to evaluate the *in vitro* effects of bupivacaine, one of the most commonly used anesthetics, on two types of mature, ECM-dense cartilage grafts: native articular cartilage explants and engineered neocartilage. Native articular cartilage explants are representative of fresh autografts and allografts, which are frequently used clinically to treat articular cartilage damage in patients. Bovine articular cartilage has historically been used to study the effects of medication exposure *in vitro* (4, 5, 14). There is extensive data on the histology and mechanical properties of the tissue, and it has been used as a model to study osteoarthritis pathogenesis (15, 16). Moreover, the large joint size allows for sufficient explant material. Cell-based engineered cartilaginous tissues are emerging as therapeutic alternatives. The scaffold-free, self-assembling process produces robust neocartilage with abundant extracellular matrix (17). This biomimetic neocartilage has histological, biochemical, and mechanical properties similar to native articular cartilage (tensile and compressive stiffness of 6.4 MPa and 326 kPa, respectively, and coefficient of friction of 0.04) (18, 19), and is a promising novel strategy being investigated for cartilage repair (17, 20, 21). To examine the effects of bupivacaine, native articular cartilage and engineered neocartilage underwent single exposure to bupivacaine followed by quantification of chondrocyte viability, biochemical content, and mechanical properties. It was hypothesized that single bupivacaine exposure would cause chondrotoxicity and decreased mechanical properties in both native explants and neocartilage.

Materials and Methods

Explant harvest

Full-thickness cartilage punches, 3 mm in diameter, were harvested from the femoral condyles of three juvenile bovine stifle joints (Research 87, Boston, MA) less than 36 hours after slaughter

using aseptic technique. All cadaveric specimens were grossly normal without any abnormalities of the articular cartilage. Punches were rinsed in Dulbecco's modified Eagle's medium (DMEM; Gibco) with high glucose/GlutaMAX™ and with 1% (v/v) penicillin/streptomycin/fungizone (PSF; BD Biosciences). Punches were trimmed to 1 to 2 mm thick, preserving the articular surface, superficial zone, and part of the middle zone. This was done with the intention to have the native cartilage be more comparable to the engineered neocartilage in terms of total exposed surface area and thickness of the graft. Explants were maintained in chondrogenic (CHG) medium (DMEM with high glucose/GlutaMAX™ containing 1% PSF, 1% (v/v) ITS+ premix, 1% (v/v) non-essential amino acids, 100 nM dexamethasone, 40 µg/mL L-proline, 50 µg/mL ascorbate-2-phosphate, 100 µg/mL sodium pyruvate; all from Sigma) and 3% (v/v) fetal bovine serum (FBS; Atlanta Biologicals) until bupivacaine exposure later that same day.

Neocartilage engineering

Articular cartilage was harvested from the femoral condyles and trochlea of juvenile bovine stifle joints (n=3; Research 87, Boston, MA) within 36 hours of slaughter. The cartilage was minced into 1-2 mm^3 pieces and digested in 0.2% (w/v) type II collagenase (Worthington, Lakewood, NJ) in DMEM with 1% PSF and 3% FBS for 18 hours on an orbital shaker at 37˚C. Following digestion, chondrocytes were filtered through 70 µm cell strainers, resuspended in DMEM, and frozen in cryovials in liquid nitrogen until use. After thawing, primary (P0) chondrocytes were resuspended in CHG medium, and neocartilage constructs were formed using the self-assembling process as previously described (17). Briefly, non-adherent self-assembly wells, 3 mm in diameter, were made from 2% (w/v) agarose and saturated with CHG medium for two days prior to construct seeding. Neocartilage constructs were seeded at a density of 1.62×10^6 P0 cells per construct in 50 µL of CHG medium into each 3 mm-diameter agarose well. Constructs were maintained at 37˚C and 10% CO_2. On day 7 constructs were unconfined from the self-assembly wells and

transferred to a 24-well plate. Medium was changed daily until construct unconfinement, after which medium was exchanged every other day for the remaining duration of the 28-day culture. Constructs were exposed to bupivacaine on day 28 of culture.

Bupivacaine exposure

Both native explants and neocartilage constructs (n=6 per group) were exposed to CHG medium supplemented with 0.5% (w/v) bupivacaine, 0.25% (w/v) bupivacaine, or 0% bupivacaine (control) for 1 hour at 37˚ C at 50 RPM on an orbital shaker. Bupivacaine doses were calculated based on a standard clinical 10 mL bolus injection of medication into an adult human knee and accounting for a dilution from 6.7 mL of synovial joint fluid (22). For example, a 10 mL bolus of 0.5% bupivacaine injected into a knee joint with 6.7 mL of synovial fluid yields a bupivacaine concentration of 3 mg/mL within the joint. Using this adjusted concentration, each group of native explants or constructs was placed in a well of a 12-well plate and incubated with 1.2 mL of appropriate bupivacaine-CHG medium dilution to allow for complete submersion of the tissues. Following bupivacaine exposure, explants and constructs were washed three times with CHG medium. Explants and constructs were then maintained in individual wells in a 24-well plate in CHG medium at 37˚C and 10% CO_2 until testing.

Viability assessment

Twenty-four hours after bupivacaine exposure, 1 mm thick, vertical cross sections were taken and incubated in 80 µL of CHG medium plus 80 µL of LIVE/DEAD reagent (calcein AM, ethidium homodimer-1; ThermoFisher) for 30 minutes. Sections were viewed with fluorescence microscopy using the Texas Red and GFP filters at 4x and 10x magnification. Images were analyzed with Image J. Three regions of interest (ROI) measuring 150 µm by 150 µm were taken from random,

non-overlapping areas at least 100 μm below the surface. A macro was created using the auto local threshold, watershed, and analyze particles functions to count live and dead cells in order to calculate viability. An average was taken from these three ROIs to yield one measurement of viability per explant or construct.

Histological evaluation

Twenty-four hours after exposure, samples from explants and constructs were fixed in 10% neutral buffered formalin and embedded in paraffin. Cross sections, 4 μm thick, were stained with Hematoxylin and Eosin to assess cellular morphology, Picrosirius Red to assess total collagen distribution, and Safranin O to assess glycosaminoglycan (GAG) distribution.

Quantitative biochemistry

Twenty-four hours after exposure, samples from explants and constructs were weighed to measure their wet weights (ww). Samples were then lyophilized and weighed again to measure their dry weights (dw). Water content of the tissues was determined from sample weights before and after lyophilization. Lyophilized tissue samples were digested in 125 μg/mL papain in phosphate buffer at 60˚C for 18 hours. Sulfated GAG content was measured using the Blyscan dimethyl methylene blue assay kit (Biocolor Ltd). Collagen content was quantified by a modified colorimetric chloramine-T hydroxyproline assay using a Sircol collagen assay standard (Biocolor Ltd) (23). DNA content was measured with a Picogreen cell proliferation assay (Quant-iT Picogreen dsDNA assay kit). Collagen and GAG content were normalized to wet weight, dry weight, and DNA.

Creep indentation testing

A compression indentation apparatus (24) was used to assess creep of explants and neocartilage on day 5 or 6 post-exposure. Sample thickness was determined prior to testing using ImageJ software. As previously described (17), a 0.55 mm-diameter, flat-ended, porous indenter tip was applied to the samples under a 2.5–3.5 g or 0.5–4.5 g load, and specimens were allowed to creep until reaching equilibrium, resulting in 5–18% or 8–15% strain for explants and constructs, respectively. A semi-analytical, semi-numerical, linear biphasic model and finite element analysis were used to obtain the aggregate modulus (H_A), shear modulus, and permeability (k) from the experimental data (25).

Statistical analysis

Statistical analyses were performed using GraphPad Prism 8. Sample size (n=6 per group) was determined based on prior study data (4) using viability as the primary outcome with alpha set at 0.05 and minimum power of 80%. For the mechanical data, all samples that experienced strains below 8% were excluded (n=3) to ensure conformity with the assumptions of the analytical model used. Statistical outliers were identified and removed before any statistical analyses were performed. A two-way analysis of variance (ANOVA) with Tukey's post-hoc tests were used to determine differences caused by bupivacaine dose within tissue type for all quantitative data. In figures and tables showing quantitative data, statistical significance ($p<0.05$) is indicated by groups marked with different letters. All data are presented as means ± standard deviations.

Results

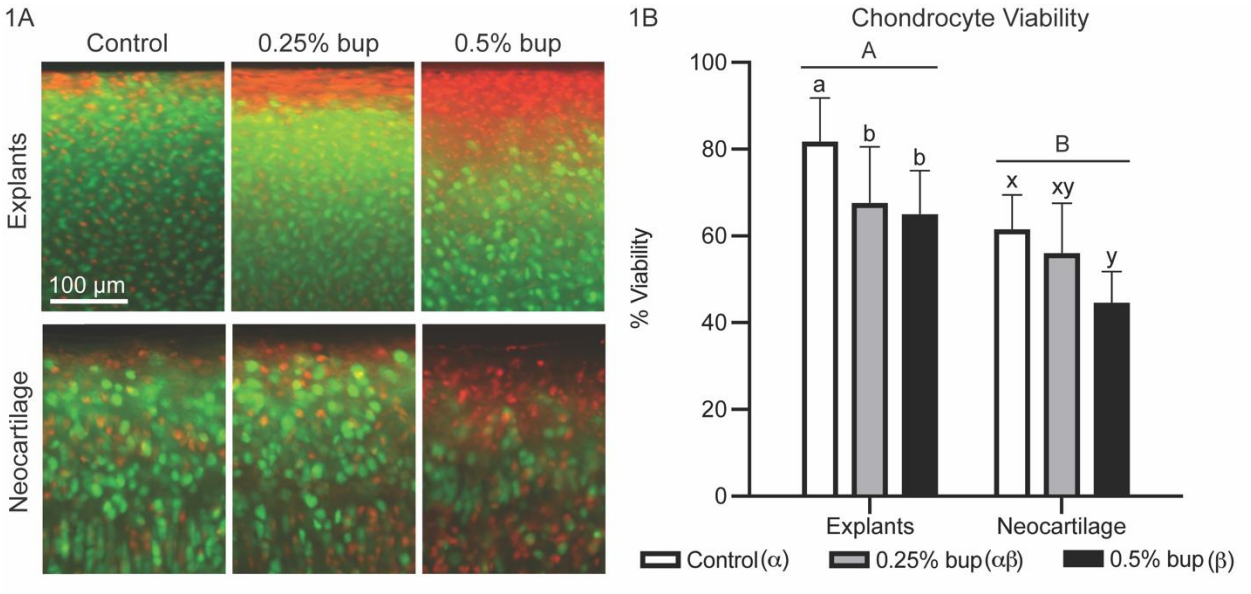

Figure 1. Chondrocyte viability in native explants and neocartilage constructs after bupivacaine exposure. (A) Top surface of cartilage tissue (10x). (B) Tissue type and bupivacaine exposure are significant sources of variation in chondrocyte viability. Statistical significance ($p<0.05$) is indicated by groups marked with different letters.

Chondrocyte viability

Overall, neocartilage had decreased chondrocyte viability compared to native explants (**Figure 1**). Histologically, chondrocyte death was localized at the tissue periphery in both groups (**Figure 1A**). Specimens exposed to bupivacaine exhibited reduced viability compared to control, irrespective of tissue type. Among all specimens (both explants and neocartilage), lower chondrocyte viability was observed in the 0.5% bupivacaine-treated specimens (55.0±13.4%; $p<0.001$) and 0.25% bupivacaine-treated specimens (62.0±13.0%; $p=0.054$) compared to controls (71.9±13.5%). Differences in mean chondrocyte viability between 0.5% and 0.25% bupivacaine-treated specimens were not significant. Both bupivacaine dose ($p=0.001$) and tissue type ($p<0.001$) were significant factors affecting chondrocyte viability with no significant

interaction between factors (**Figure 1B**). Among the native explant groups, chondrocyte viability was significantly decreased in 0.5% bupivacaine-treated specimens (65.2±9.9%; p=0.018) and 0.25% bupivacaine-treated specimens (67.8±12.8%; p=0.049) compared to the control (82.0±9.8%). Among the neocartilage groups, chondrocyte viability was significantly decreased in 0.5% bupivacaine-treated specimens compared to control (44.8±7.0% vs 61.7±7.7%; p=0.016).

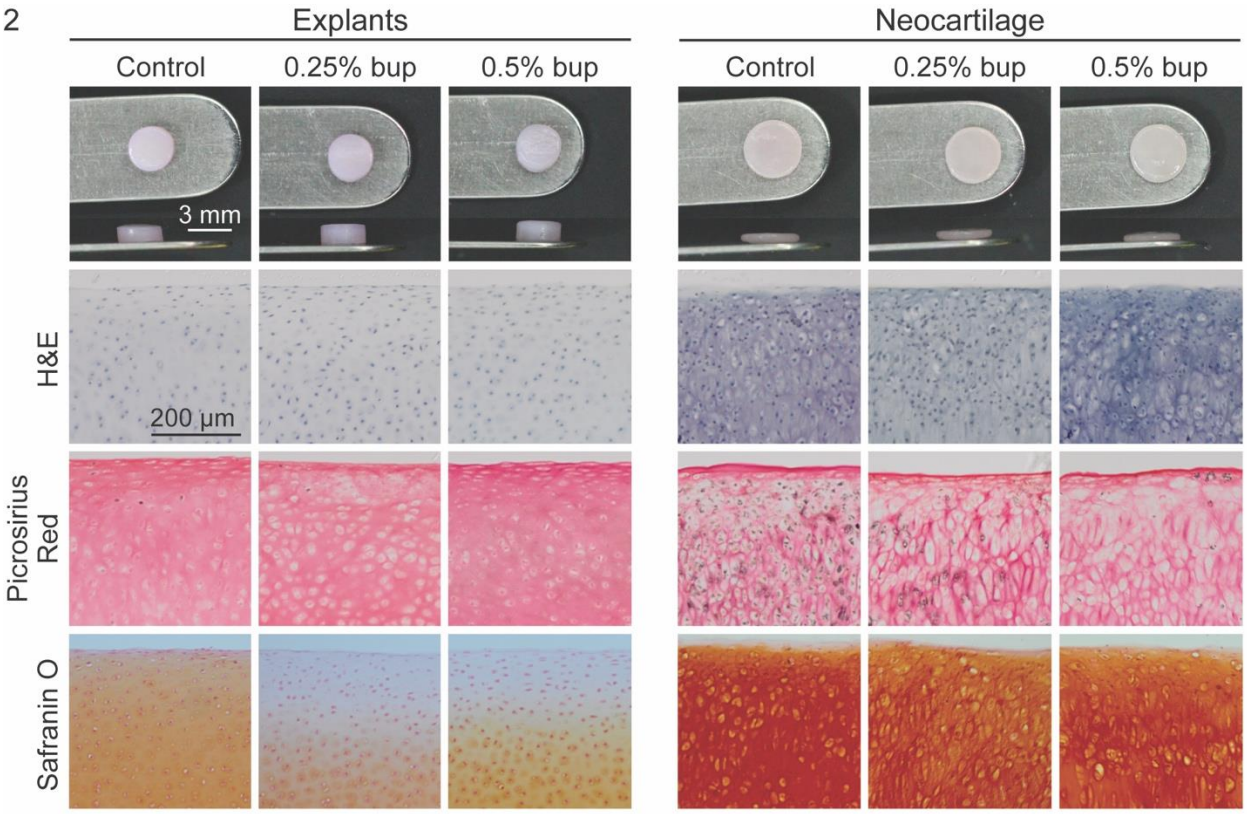

Figure 2. Gross and microscopic histology of native explants and neocartilage constructs after exposure to bupivacaine. H&E – hematoxylin and eosin.

Histology

Cell morphology in both the native explants and neocartilage constructs did not appear to be affected by bupivacaine treatment (**Figure 2**). This was evident by the presence of many cells within lacunae, with elongated cells in the superficial zone and a columnar arrangement of cells in the deep zone. Collagen distribution within the native explants and neocartilage constructs also

appeared unaffected by bupivacaine exposure (**Figure 2**). Among the native explants, collagen staining was more intense in the superficial and deep zones of all treatment groups. Among neocartilage constructs, collagen was homogeneously distributed throughout the tissue except for intense staining localized at the periphery in all treatment groups. In contrast, GAG distribution did appear to be affected by bupivacaine exposure (**Figure 2**). Among the native explants, GAG staining was less intense in the superficial and mid zones in the groups that received 0.25% and 0.5% bupivacaine treatment. Among the neocartilage constructs, GAG staining was less intense throughout the tissue treated with 0.25% and 0.5% bupivacaine.

Table 1. Biochemical composition of extracellular matrix. Data are presented as mean +/- SD. Biochemical composition was significantly different ($p<0.001$) between explants and neocartilage for all column measures.

	Bupivacaine Treatment	Hydration (%)	Col/ww (%)	Col/dw (%)	Col/DNA (μg/μg)	GAG/ww (%)	GAG/dw (%)	GAG/DNA (μg/μg)
Explants	Control	78.3 ±2.7	13.8 ±3.5	62.8 ±9.1	343.9 ±102.6	5.0 ±0.6	23.0 ±3.1	125.0 ±33.7
	0.25%	80.2 ±1.3	12.2 ±2.5	61.2 ±9.5	294.4 ±81.0	4.9 ±0.7	24.5 ±3.5	117.2 ±25.6
	0.5%	80.6 ±2.5	12.3 ±2.4	63.3 ±7.1	359.6 ±110.9	4.3 ±0.9	22.3 ±3.1	128.6 ±45.9
Neocartilage	Control	82.2 ±0.7	2.0 ±0.2	11.4 ±0.9	22.7 ±1.2	7.5 ±1.0	42.3 ±5.2	84.5 ±11.9
	0.25%	81.9 ±0.4	2.1 ±0.2	11.7 ±0.8	18.3 ±2.0	8.3 ±0.5	46.1 ±2.2	72.4 ±7.3
	0.5%	82.6 ±1.2	1.9 ±0.4	10.7 ±2.4	16.6 ±4.8	8.0 ±0.5	46.0 ±2.3	71.1 ±13.1

Quantitative biochemistry

Tissue type, but not bupivacaine dose, was a significant factor affecting tissue biochemical properties. Collagen/ww, collagen/dw, collagen/DNA, and GAG/DNA were greater in the explant groups compared to the neocartilage groups ($p<0.001$), while hydration, GAG/ww, and GAG/dw were greater in the neocartilage groups compared to the explant groups ($p<0.001$) (**Table 1**). Bupivacaine treatment did not have a significant effect on the biochemical content of both explants and neocartilage **(Figure 3)**.

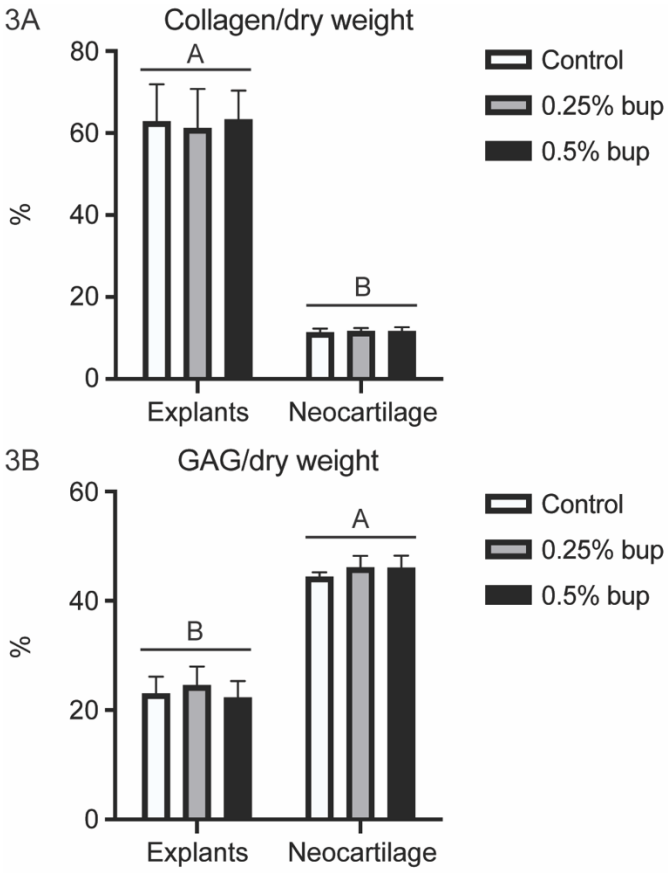

Figure 3. Biochemical composition of the extracellular matrix. Tissue type was a significant source of variation in (A) collagen per dry weight and (B) GAG per dry weight.

Compressive mechanical properties

Both bupivacaine dose ($p=0.021$) and tissue type ($p<0.001$) were significant factors affecting aggregate modulus, with no significant interaction between factors (**Figure 4A**). Among the self-assembled constructs, mean aggregate modulus for 0.5% bupivacaine-treated specimens (415.8±155.1 kPa) was significantly decreased compared to 0.25% bupivacaine-treated specimens (618.5±103.1 kPa; $p=0.012$) and controls (660.3±145.8 kPa; $p=0.003$). Bupivacaine dose did not have a significant effect on aggregate modulus among native explants.

Both bupivacaine dose ($p=0.015$) and tissue type ($p=0.011$) were significant factors affecting shear modulus, with no significant interaction between factors (**Figure 4B**). Among the self-assembled constructs, mean shear modulus for 0.5% bupivacaine-treated specimens (143.2±14.0 kPa) was significantly decreased compared to 0.25% bupivacaine-treated specimens (237.7±48.6 kPa; $p=0.018$) and controls (266.5±89.2 kPa; $p=0.002$). Bupivacaine dose did not have a significant effect on shear modulus among native explants.

Finally, both bupivacaine dose ($p=0.021$) and tissue type ($p=0.011$) were significant factors affecting permeability, with a significant interaction between factors ($p=0.021$) (**Figure 4C**). Among the self-assembled constructs, mean permeability for 0.5% bupivacaine-treated specimens (14.7±8.1 $10^{-15}m^4/Ns$) was significantly increased compared to 0.25% bupivacaine-treated specimens (4.4±1.8 $10^{-15}m^4/Ns$; $p=0.001$) and controls (6.6±1.7 $10^{-15}m^4/Ns$; $p=0.009$). Bupivacaine dose did not have a significant effect on permeability among native explants.

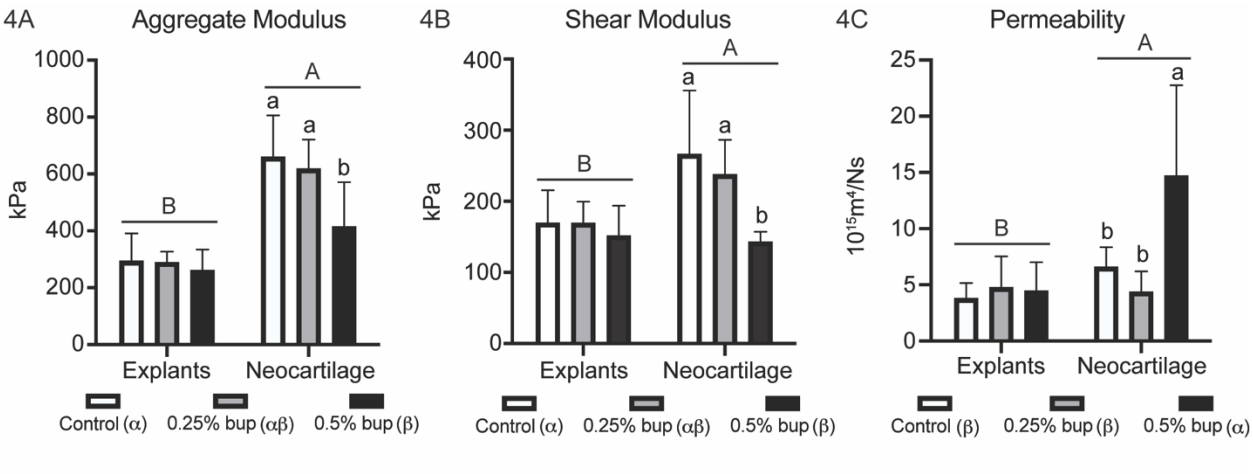

Figure 4. Compressive mechanical properties of native explants and neocartilage. Tissue type and bupivacaine exposure were significant sources of variation in (A) aggregate modulus and (B) shear modulus. (C) For permeability, there was a significant interaction between tissue type and bupivacaine exposure. Both factors were also significant sources of variation. Statistical significance ($p<0.05$) is indicated by groups marked with different letters.

Discussion

In this study, single exposure of native articular cartilage explants and neocartilage constructs to clinically relevant doses of bupivacaine resulted in significant chondrotoxicity and changes in tissue mechanics. The findings of this study suggest that the existence of abundant extracellular matrix within native cartilage and neocartilage tissue does not confer any additional resistance to the chondrotoxic effects of bupivacaine. However, the effect of bupivacaine on tissue mechanics may be less deleterious for native cartilage tissue compared to tissue-engineered neocartilage.

The chondrotoxic effect of bupivacaine is well known and has been the subject of study by a number of groups (3-7, 26). This effect is dose-dependent, with higher concentrations of bupivacaine exhibiting more chondrotoxicity (3, 26-30). Similar dose-dependent effects were observed in both cartilage tissue types in this study. Although the majority of prior studies have

been performed using monolayer cell culture, recent studies examining the effects of bupivacaine on intact tissue explants have found similar chondrotoxicity (26, 27, 31, 32). Sherman et al. found that 1-hour exposures of canine cartilage explants to 0.25% and 0.125% bupivacaine both had chondrotoxic effects with corresponding decreases in metabolic activity (26). In an *in vivo* rat study, Chu et al. demonstrated that a single intra-articular injection of 0.5% bupivacaine resulted in a reduction in chondrocyte density after six months (33). The outcomes of the present study support the growing body of literature which demonstrates that bupivacaine is chondrotoxic to cartilage, despite the presence of intact extracellular matrix.

The primary function of articular cartilage is to provide low-friction articulation and absorption of joint loads. Thus, it is critical that cartilage mechanics not be affected by the administration of anesthetics. Although the cellular toxicity of local anesthetics has been well established, whether the mechanical properties of the articular cartilage are similarly affected is unknown and not well studied to date. This study found that the aggregate modulus and shear modulus of neocartilage constructs was significantly diminished 5 to 6 days after single bupivacaine exposure, indicating a loss of load-bearing and energy dissipation capabilities of the tissue. It was also shown that 0.5% bupivacaine exposure resulted in an increase of neocartilage permeability compared to 0.25% bupivacaine or control. Furthermore, this study found that neocartilage was more susceptible to an increase in permeability from high-dose bupivacaine exposure compared to native explants. This increased permeability may contribute to the decrease in compressive mechanical properties observed among the neocartilage constructs, but not among native explants, as a result of fluid exudation. Importantly, human cartilage is more permeable than bovine cartilage and, therefore, may be further susceptible to bupivacaine-induced changes than those demonstrated by this study (34). Although this study did not find any significant changes in the compressive mechanical properties of native explants following bupivacaine exposure, a single measurement at 5 to 6 days after exposure may not have allowed

sufficient time for alterations in the matrix and tissue mechanics to develop. It is postulated that substantial chondrocyte death would initiate a cascade of decreased matrix production and consequently, loss of mechanical functionality over time. Therefore, longitudinal assessment of cartilage mechanics over a longer period of time after single bupivacaine exposure is warranted.

The findings of this study caution against the use of intra-articular bupivacaine, which is commonly administered during surgery to reduce postoperative pain, in the setting of articular cartilage repair. Cell-based approaches to cartilage repair, such as Matrix-induced Autologous Chondrocyte Implantation (MACI) are becoming commonly used, with many additional products in clinical development (35). The neocartilage constructs used in this study are fabricated using the cell-based, scaffold-free, self-assembling process that generates scaffold-free neocartilage with abundant extracellular matrix and compressive, tensile, and low-friction properties similar to those of native articular cartilage (17-19, 21, 36, 37). This neocartilage has been investigated for cartilage repair in the knee and temporomandibular joint and demonstrated outstanding healing and prevention of osteoarthritis compared to empty defect controls in preclinical animal models (21). This study showed that neocartilage was more susceptible to bupivacaine-induced reduction in mechanical properties. Compared to self-assembled neocartilage, MACI and other cell-based implants contain less mature matrix and are likely more permeable than the neocartilage tested in this study (38). Therefore, these implants may be even more susceptible to the chondrotoxic effects of bupivacaine and the corresponding deterioration of mechanical integrity. Additionally, most cartilage repair implants also lack a robust lamina splendens, which serves as a protective barrier to intra-articular elements (3). Cartilage changes associated with OA, such as fibrillation and increased hydration, may similarly make the tissue more susceptible to bupivacaine toxicity. Greater anesthetic-induced chondrotoxicity has been noted in osteoarthritic cartilage compared to intact cartilage (6, 29), and further weakening in the biomechanical properties of osteoarthritic cartilage may occur from bupivacaine exposure.

While this study presents compelling data demonstrating the negative effects of bupivacaine on chondrocyte viability and cartilage mechanics, there are several notable limitations. Biochemical measurement was performed once at 24 hours after bupivacaine exposure (concurrently with viability measurement) and was not performed at the same time as creep indentation testing, precluding correlation of biochemical and mechanical results. Second, this *in vitro* study may not have accurately represented *in vivo* conditions regarding bupivacaine exposure time, dosage, and clearance from the joint. The half-life of bupivacaine is longer than the exposure time used in this study, and this steady concentration of medication does not factor in the pharmacokinetics of the medication in the body (27, 39). During surgery, blood may further dilute the anesthetic bolus. Third, chondrocytes used to generate neocartilage were isolated from the femoral condyles and the trochlea, whereas the explants were only harvested from the femoral condyles. It has been shown that neocartilage generated from cells derived from different topographical areas within the bovine patellofemoral joint have different functional properties (40). Finally, native explants in this study only consisted of the superficial and middle zones and did not contain the deep zone, and bupivacaine sensitivity may differ among each zone of cartilage (13). Moreover, trimming the native explants to exclude the deep zone, calcified cartilage, and subchondral bone layer created a non-physiological interface that may have allowed for increased penetration of bupivacaine upon exposure. Despite these limitations, this study reports the effects of bupivacaine on both native and engineered cartilage tissues and encourages further, in-depth analyses of alterations in cartilage matrix composition and mechanical properties resulting from local anesthetic exposure.

Single bupivacaine exposure resulted in dose-dependent chondrotoxicity to native explants and neocartilage, both extracellular matrix-dense tissues. Additionally, single bupivacaine exposure significantly increased the permeability and weakened the compressive mechanical properties of neocartilage. The existence of abundant extracellular matrix does not

appear to confer any additional resistance to the chondrotoxic effects of bupivacaine. Furthermore, tissue permeability appeared to influence the susceptibility of the tissue to dose-dependent decreases in mechanical properties. Clinicians should be judicious regarding use of intra-articular bupivacaine in the setting of articular cartilage repair.

References

1. Eker HE, Cok OY, Aribogan A, Arslan G. The efficacy of intra-articular lidocaine administration in chronic knee pain due to osteoarthritis: A randomized, double-blind, controlled study. Anaesth Crit Care Pain Med. 2017;36(2):109-14. Epub 2016/08/04. doi: 10.1016/j.accpm.2016.05.003. PubMed PMID: 27485803.
2. Turnbull ZA, Sastow D, Giambrone GP, Tedore T. Anesthesia for the patient undergoing total knee replacement: current status and future prospects. Local Reg Anesth. 2017;10:1-7. Epub 2017/03/24. doi: 10.2147/LRA.S101373. PubMed PMID: 28331362; PubMed Central PMCID: PMCPMC5349500.
3. Chu CR, Izzo NJ, Coyle CH, Papas NE, Logar A. The *in vitro* effects of bupivacaine on articular chondrocytes. J Bone Joint Surg Br. 2008;90(6):814-20. Epub 2008/06/10. doi: 10.1302/0301-620X.90B6.20079. PubMed PMID: 18539679; PubMed Central PMCID: PMCPMC6548455.
4. Chu CR, Izzo NJ, Papas NE, Fu FH. *In vitro* exposure to 0.5% bupivacaine is cytotoxic to bovine articular chondrocytes. Arthroscopy. 2006;22(7):693-9. Epub 2006/07/18. doi: 10.1016/j.arthro.2006.05.006. PubMed PMID: 16843803.
5. Karpie JC, Chu CR. Lidocaine exhibits dose- and time-dependent cytotoxic effects on bovine articular chondrocytes *in vitro*. Am J Sports Med. 2007;35(10):1621-7. Epub 2007/08/01. doi: 10.1177/0363546507304719. PubMed PMID: 17664340.
6. Kreuz PC, Steinwachs M, Angele P. Single-dose local anesthetics exhibit a type-, dose-, and time-dependent chondrotoxic effect on chondrocytes and cartilage: a systematic review of the current literature. Knee Surg Sports Traumatol Arthrosc. 2018;26(3):819-30. Epub 2017/03/16. doi: 10.1007/s00167-017-4470-5. PubMed PMID: 28289821.
7. Seshadri V, Coyle CH, Chu CR. Lidocaine potentiates the chondrotoxicity of methylprednisolone. Arthroscopy. 2009;25(4):337-47. Epub 2009/04/04. doi: 10.1016/j.arthro.2009.01.003. PubMed PMID: 19341919; PubMed Central PMCID: PMCPMC6548446.
8. Hansen BP, Beck CL, Beck EP, Townsley RW. Postarthroscopic glenohumeral chondrolysis. Am J Sports Med. 2007;35(10):1628-34. Epub 2007/07/05. doi: 10.1177/0363546507304136. PubMed PMID: 17609526.
9. Iwasaki K, Sudo H, Kasahara Y, Yamada K, Ohnishi T, Tsujimoto T, Iwasaki N. Effects of Multiple Intra-articular Injections of 0.5% Bupivacaine on Normal and Osteoarthritic Joints in Rats. Arthroscopy. 2016;32(10):2026-36. Epub 2016/05/03. doi: 10.1016/j.arthro.2016.02.011. PubMed PMID: 27132778.
10. Sola M, Dahners L, Weinhold P, Svetkey van der Horst A, Kallianos S, Flood D. The viability of chondrocytes after an *in vivo* injection of local anaesthetic and/or corticosteroid: a laboratory study using a rat model. Bone Joint J. 2015;97-B(7):933-8. Epub 2015/07/02. doi: 10.1302/0301-620X.97B7.35398. PubMed PMID: 26130348.
11. Libbin RM, Rivera ME. Regeneration of growth plate cartilage induced in the neonatal rat hindlimb by reamputation. J Orthop Res. 1989;7(5):674-82. Epub 1989/01/01. doi: 10.1002/jor.1100070507. PubMed PMID: 2760739.

12. Watrin-Pinzano A, Ruaud JP, Cheli Y, Gonord P, Grossin L, Gillet P, Blum A, Payan E, Olivier P, Guillot G, Netter P, Loeuille D. T2 mapping: an efficient MR quantitative technique to evaluate spontaneous cartilage repair in rat patella. Osteoarthritis Cartilage. 2004;12(3):191-200. Epub 2004/02/20. doi: 10.1016/j.joca.2003.10.010. PubMed PMID: 14972336.
13. Syed HM, Green L, Bianski B, Jobe CM, Wongworawat MD. Bupivacaine and triamcinolone may be toxic to human chondrocytes: a pilot study. Clin Orthop Relat Res. 2011;469(10):2941-7. Epub 2011/03/09. doi: 10.1007/s11999-011-1834-x. PubMed PMID: 21384211; PubMed Central PMCID: PMCPMC3171524.
14. Lo IK, Sciore P, Chung M, Liang S, Boorman RB, Thornton GM, Rattner JB, Muldrew K. Local anesthetics induce chondrocyte death in bovine articular cartilage disks in a dose- and duration-dependent manner. Arthroscopy. 2009;25(7):707-15. Epub 2009/06/30. doi: 10.1016/j.arthro.2009.03.019. PubMed PMID: 19560633.
15. Mahmood H, Shepherd DET, Espino DM. Surface damage of bovine articular cartilage-off-bone: the effect of variations in underlying substrate and frequency. BMC Musculoskelet Disord. 2018;19(1):384. Epub 2018/10/26. doi: 10.1186/s12891-018-2305-2. PubMed PMID: 30355307; PubMed Central PMCID: PMCPMC6201575.
16. Riemenschneider PE, Rose MD, Giordani M, McNary SM. Compressive fatigue and endurance of juvenile bovine articular cartilage explants. J Biomech. 2019;95:109304. Epub 2019/08/27. doi: 10.1016/j.jbiomech.2019.07.048. PubMed PMID: 31447176.
17. Hu JC, Athanasiou KA. A self-assembling process in articular cartilage tissue engineering. Tissue Eng. 2006;12(4):969-79. Epub 2006/05/06. doi: 10.1089/ten.2006.12.969. PubMed PMID: 16674308.
18. Elder BD, Athanasiou KA. Synergistic and additive effects of hydrostatic pressure and growth factors on tissue formation. PloS one. 2008;3(6):e2341. doi: 10.1371/journal.pone.0002341. PubMed PMID: 18523560; PubMed Central PMCID: PMC2394656.
19. Elder BD, Athanasiou KA. Systematic assessment of growth factor treatment on biochemical and biomechanical properties of engineered articular cartilage constructs. Osteoarthritis Cartilage. 2009;17(1):114-23. Epub 2008/06/24. doi: 10.1016/j.joca.2008.05.006. PubMed PMID: 18571441; PubMed Central PMCID: PMCPMC2659617.
20. McNary SM, Athanasiou KA, Reddi AH. Transforming growth factor beta-induced superficial zone protein accumulation in the surface zone of articular cartilage is dependent on the cytoskeleton. Tissue Eng Part A. 2014;20(5-6):921-9. Epub 2013/10/15. doi: 10.1089/ten.TEA.2013.0043. PubMed PMID: 24116978; PubMed Central PMCID: PMCPMC3938930.
21. Vapniarsky N, Huwe LW, Arzi B, Houghton MK, Wong ME, Wilson JW, Hatcher DC, Hu JC, Athanasiou KA. Tissue engineering toward temporomandibular joint disc regeneration. Science translational medicine. 2018;10(446). doi: 10.1126/scitranslmed.aaq1802. PubMed PMID: 29925634.
22. Heilmann HH, Lindenhayn K, Walther HU. [Synovial volume of healthy and arthrotic human knee joints]. Z Orthop Ihre Grenzgeb. 1996;134(2):144-8. Epub 1996/03/01. doi: 10.1055/s-2008-1039786. PubMed PMID: 8779258.
23. Cissell DD, Link JM, Hu JC, Athanasiou KA. A Modified Hydroxyproline Assay Based on Hydrochloric Acid in Ehrlich's Solution Accurately Measures Tissue Collagen Content. Tissue engineering Part C, Methods. 2017;23(4):243-50. doi: 10.1089/ten.tec.2017.0018. PubMed PMID: 28406755; PubMed Central PMCID: PMC5397204.
24. Athanasiou KA, Agarwal A, Dzida FJ. Comparative study of the intrinsic mechanical properties of the human acetabular and femoral head cartilage. Journal of orthopaedic research : official publication of the Orthopaedic Research Society. 1994;12(3):340-9. doi: 10.1002/jor.1100120306. PubMed PMID: 8207587.

25. Athanasiou KA, Agarwal A, Muffoletto A, Dzida FJ, Constantinides G, Clem M. Biomechanical properties of hip cartilage in experimental animal models. Clin Orthop Relat Res. 1995(316):254-66. Epub 1995/07/01. PubMed PMID: 7634715.
26. Sherman SL, Khazai RS, James CH, Stoker AM, Flood DL, Cook JL. *In Vitro* Toxicity of Local Anesthetics and Corticosteroids on Chondrocyte and Synoviocyte Viability and Metabolism. Cartilage. 2015;6(4):233-40. Epub 2015/10/02. doi: 10.1177/1947603515594453. PubMed PMID: 26425261; PubMed Central PMCID: PMCPMC4568732.
27. Dragoo JL, Braun HJ, Kim HJ, Phan HD, Golish SR. The *in vitro* chondrotoxicity of single-dose local anesthetics. Am J Sports Med. 2012;40(4):794-9. Epub 2012/01/31. doi: 10.1177/0363546511434571. PubMed PMID: 22287644.
28. Grishko V, Xu M, Wilson G, Pearsall AWt. Apoptosis and mitochondrial dysfunction in human chondrocytes following exposure to lidocaine, bupivacaine, and ropivacaine. J Bone Joint Surg Am. 2010;92(3):609-18. Epub 2010/03/03. doi: 10.2106/JBJS.H.01847. PubMed PMID: 20194319.
29. Breu A, Rosenmeier K, Kujat R, Angele P, Zink W. The cytotoxicity of bupivacaine, ropivacaine, and mepivacaine on human chondrocytes and cartilage. Anesth Analg. 2013;117(2):514-22. Epub 2013/06/12. doi: 10.1213/ANE.0b013e31829481ed. PubMed PMID: 23749443.
30. Baker JF, Walsh PM, Byrne DP, Mulhall KJ. *In vitro* assessment of human chondrocyte viability after treatment with local anaesthetic, magnesium sulphate or normal saline. Knee Surg Sports Traumatol Arthrosc. 2011;19(6):1043-6. Epub 2011/02/19. doi: 10.1007/s00167-011-1437-9. PubMed PMID: 21331650.
31. Farkas B, Kvell K, Czompoly T, Illes T, Bardos T. Increased chondrocyte death after steroid and local anesthetic combination. Clin Orthop Relat Res. 2010;468(11):3112-20. Epub 2010/08/12. doi: 10.1007/s11999-010-1443-0. PubMed PMID: 20700677; PubMed Central PMCID: PMCPMC2947661.
32. Piper SL, Kim HT. Comparison of ropivacaine and bupivacaine toxicity in human articular chondrocytes. J Bone Joint Surg Am. 2008;90(5):986-91. Epub 2008/05/03. doi: 10.2106/JBJS.G.01033. PubMed PMID: 18451389.
33. Chu CR, Coyle CH, Chu CT, Szczodry M, Seshadri V, Karpie JC, Cieslak KM, Pringle EK. *In vivo* effects of single intra-articular injection of 0.5% bupivacaine on articular cartilage. J Bone Joint Surg Am. 2010;92(3):599-608. Epub 2010/03/03. doi: 10.2106/JBJS.I.00425. PubMed PMID: 20194318; PubMed Central PMCID: PMCPMC6882542.
34. Athanasiou KA, Rosenwasser MP, Buckwalter JA, Malinin TI, Mow VC. Interspecies comparisons of in situ intrinsic mechanical properties of distal femoral cartilage. Journal of orthopaedic research : official publication of the Orthopaedic Research Society. 1991;9(3):330-40. doi: 10.1002/jor.1100090304. PubMed PMID: 2010837.
35. Kwon H, Brown WE, Lee CA, Wang D, Paschos N, Hu JC, Athanasiou KA. Surgical and tissue engineering strategies for articular cartilage and meniscus repair. Nature reviews Rheumatology. 2019;15(9):550-70. doi: 10.1038/s41584-019-0255-1. PubMed PMID: 31296933.
36. Lee JK, Link JM, Hu JCY, Athanasiou KA. The Self-Assembling Process and Applications in Tissue Engineering. Cold Spring Harbor perspectives in medicine. 2017;7(11). doi: 10.1101/cshperspect.a025668. PubMed PMID: 28348174; PubMed Central PMCID: PMC5666628.
37. MacBarb RF, Makris EA, Hu JC, Athanasiou KA. A chondroitinase-ABC and TGF-beta1 treatment regimen for enhancing the mechanical properties of tissue-engineered fibrocartilage. Acta Biomater. 2013;9(1):4626-34. Epub 2012/10/09. doi: 10.1016/j.actbio.2012.09.037. PubMed PMID: 23041782; PubMed Central PMCID: PMCPMC3518537.
38. Griffin DJ, Bonnevie ED, Lachowsky DJ, Hart JC, Sparks HD, Moran N, Matthews G, Nixon AJ, Cohen I, Bonassar LJ. Mechanical characterization of matrix-induced autologous chondrocyte implantation (MACI(R)) grafts in an equine model at 53 weeks. J Biomech.

2015;48(10):1944-9. Epub 2015/04/30. doi: 10.1016/j.jbiomech.2015.04.010. PubMed PMID: 25920896.
39. Burm AG. Clinical pharmacokinetics of epidural and spinal anaesthesia. Clin Pharmacokinet. 1989;16(5):283-311. Epub 1989/05/01. doi: 10.2165/00003088-198916050-00002. PubMed PMID: 2663301.
40. Paschos NK, Lim N, Hu JC, Athanasiou KA. Functional properties of native and tissue-engineered cartilage toward understanding the pathogenesis of chondral lesions at the knee: A bovine cadaveric study. Journal of orthopaedic research : official publication of the Orthopaedic Research Society. 2017;35(11):2452-64. doi: 10.1002/jor.23558. PubMed PMID: 28294398.